

Conductive Filler Modified Polymers for Structural Health Monitoring Applications

By

Amirhossein Biabangard Oskouyi

A thesis submitted in partial fulfillment of the requirements for the degree of

Doctor of Philosophy

Department of Mechanical Engineering
University of Alberta

© Amirhossein Biabangard Oskouyi, 2015

ABSTRACT

In this thesis, a novel three-dimensional continuum percolation model based on Monte Carlo simulation approach was developed and employed to investigate the percolation behavior of the electrically insulating matrix reinforced with conductive nanoplatelet fillers such as graphene. The conductivity behavior of composites rendered conductive by randomly dispersed conductive platelets was modeled by developing a three-dimensional finite element resistor network. Parameters related to the percolation threshold and a power-law describing the conductivity behavior were determined. The piezoresistivity behavior of conductive composites was studied employing a reoriented resistor network emulating a conductive composite subjected to mechanical strain. The effects of the governing parameters, i.e., electron tunneling distance, conductive particle aspect ratio and size effects on conductivity behavior were examined. In this thesis, a numerical modeling approach was used to investigate the current-voltage behavior of conductive nanoplatelet based nanocomposites. A nonlinear finite element based model was developed to evaluate the electrical behavior of the nanocomposite for different levels of the applied electric field. Furthermore, the effect of filler loading on nonlinear conductivity behavior of nanocomposites was investigated. The validity of the developed model was verified through qualitative comparison of the simulation results with results obtained from experimental works. The effect of temperature on electrical conductivity of polymer nanocomposites with carbon nanotube and graphene nanoplatelet fillers was investigated. Other aspects such as polymer tunneling and filler resistivities were also considered as.

These models were applied in a method based on electrical impedance tomography to detect wear and abrasion in composite pipes. In order to utilize electrical impedance tomography for polymeric structures, the polymer phase is made conductive through dispersing graphene nanoplatelets. A finite element analysis was conducted to predict the response of the degraded structure to the input electrical signal.

PREFACE

Chapter 3 of this thesis has been published as A. B. Oskouyi and P. Mertiny, “Monte Carlo model for the study of percolation thresholds in composites filled with circular conductive nano-disks,” *Procedia Engineering*, vol. 10, 403-408. Chapter 4 of this thesis has been published as A. B. Oskouyi, U. Sundararaj, P. Mertiny , “Tunneling Conductivity and Piezoresistivity of Composites Containing Randomly Dispersed Conductive Nano-Platelets,” *Journal of Materials*, vol. 7, issue 4, 2501-2521. Chapter 5 of this thesis has been published as A. B. Oskouyi, U. Sundararaj, P. Mertiny , “Current-voltage characteristics of nanoplatelet-based conductive nanocomposites,” *Journal of Nanoscale Research Letters* 2014, 9:369. Chapter 6 of this thesis has been published as A. B. Oskouyi, U. Sundararaj, P. Mertiny , “A Numerical Model to Study the Effect of Temperature on Electrical Conductivity of Polymer-CNT Nanocomposites,” *ASME 2013 International Mechanical Engineering Congress and Exposition*. American Society of Mechanical Engineers, 2013.

All authors contributed to the development of the aforementioned papers. I conducted the modeling work under the supervision and guidance of Dr. Pierre Mertiny. He contributed as principal research supervisor. Dr. Uttandaraman Sundararaj contributed toward this research with manuscript composition, scientific support and concept formation.

ACKNOWLEDGMENT

I would like to express my gratitude to my supervisor Dr. Pierre Mertiny for his appreciable inspiration and support during my PhD studies. I would not have been able to complete my research work without his guidance, support and helpful suggestions. Also, I am using the opportunity to express my warm thanks to Dr. Uttandaraman Sundararaj for his invaluable instructions, guidance and generous support as my thesis co-advisor through the course of this research work.

I would also like to acknowledge funding provided by Syncrude Canada Ltd, Rosen Swiss AG and Alberta Innovates Technology Futures.

For last but not least, I would like to convey my gratitude to my mother and father for their continued, endless and unconditional support throughout of my life. This list would be deficient without expressing my deepest, heartfelt appreciation to my sister.

TABLE OF CONTENTS

LIST OF TABLES	xi
LIST OF FIGURES	xii
CHAPTER 1 INTRODUCTION	1
1.1 Background and Motivation	1
1.2 Organization and Outlines of the Research	2
1.3 Bibliography	5
CHAPTER 2 A REVIEW ON THE ELECTRICAL BEHAVIOR OF CARBON ALLOTROPE MODIFIED POLYMERS	7
2.1 Introduction.....	7
2.1 CNT Based Conductive Composites:	10
2.1.1 Carbon Nanotubes.....	10
2.2 Synthesis Methods for Carbon Nanotubes.....	11
2.2.1 Arc Discharge	12
2.2.2 Laser Ablation.....	13
2.2.3 Chemical Vapor Deposition.....	13
2.3 Electrical Behavior of CNT/Polymer Composites.....	14
2.4 Graphene Based Conductive Composites.....	20
2.4.1 Graphene.....	20
2.5 Synthesis Methods for Graphene Nanoplatelets.....	21
2.5.1 Exfoliation of Intercalated Graphite	21
2.5.2 Reduction of Graphite Oxide	22

2.5.3	Chemical Vapor Deposition.....	22
2.5.4	Epitaxial Growth on Silicon Carbide.....	23
2.5.5	Preparation of Graphene by Electrochemical Methods.....	23
2.6	Electrical Behavior of Graphene-Polymer Composites.....	23
2.7	Carbon Black Based Conductive Composites.....	36
2.1	Conclusion.....	41
2.2	Bibliography.....	41
CHAPTER 3 NUMERICAL APPROACH FOR PERCOLATION PROBLEM: METHODOLOGY AND FORMULATION.....		51
3.1	Introduction.....	51
3.1.1	Motivation and Background.....	51
3.1.2	Monte Carlo Method in Percolation Problems.....	52
3.1.2.1	Percolation of Rod-Shaped and Spherical Inclusions.....	52
3.1.2.2	Percolation of Platelet Shaped Inclusions.....	53
3.2	Percolation Theory.....	56
3.3	Methodology and Formulation.....	58
3.3.1	Random Nanoplatelet Generation.....	58
3.3.2	Electrical Conductivity, Cluster and Percolation Network.....	60
3.4	Results and Discussion.....	62
3.4.1	RVE Size Effect.....	62
3.4.2	Conductivity Criterion.....	63
3.4.3	Critical Volume Fraction.....	64
3.4.4	Dimensional Analysis.....	64
3.4.5	Percolation of Polydispersed Particles.....	66
3.5	Conclusion.....	70
3.6	Bibliography.....	70

CHAPTER 4 ELECTRICAL CONDUCTIVITY AND PIEZORESISTIVITY OF THE NANOCOMPOSITE	73
4.1 Introduction.....	73
4.2 Electrical Conductivity, Clusters and Percolation Network	74
4.3 Piezoresistivity Effects	77
4.3.1 Formulation.....	78
4.3.2 Piezoresistivity Coefficients of Nanocomposite.....	80
4.3.3 Finite Element Modeling	80
4.4 Results and Discussion	82
4.4.1 Effective Electron Tunneling Distance.....	82
4.4.2 Effect of Matrix Electrical Properties on Nanocomposite Conductivity	83
4.4.3 Percolation Threshold and Electrical Conductivity	84
4.4.4 Piezoresistivity of Nanoplatelet Nanocomposites	92
4.5 Conclusions.....	98
4.6 Bibliography	98
CHAPTER 5 CURRENT-VOLTAGE CHARACTERISTICS OF NANOPATELET BASED CONDUCTIVE NANOCOMPOSITES.....	102
5.1 Introduction.....	102
5.2 Methodology and Formulation	103
5.2.1 Monte Carlo Modeling.....	103
5.2.1 Finite Element Modeling	107
5.3 Results and Discussion	108
5.3.1 Effect of Electrical Field on the Nanocomposite Conductivity	108
5.3.2 Comparison with Experimental Data.....	110
5.3.3 Characterization of Resistivity Behavior	112
5.1 Conclusions.....	114

5.2	Bibliography	114
CHAPTER 6 EFFECT OF TEMPERATURE ON ELECTRICAL CONDUCTIVITY OF CNT AND GNP NANOCOMPOSITES		116
6.1	Introduction.....	116
6.2	Modeling Procedure.....	118
6.2.1	Initial Model Generation using MC Approach	118
6.2.2	Modeling Electrical Connection Between Filler Particles.....	119
6.2.3	Model Completion using Finite Element Method	122
6.3	Results and Discussion	125
6.3.1	Effect of Temperature on Conductivity of CNT Nanocomposites	125
6.3.1	Effect of Temperature on Conductivity of GNP Nanocomposites	128
6.4	Conclusions.....	132
6.5	Bibliography	132
CHAPTER 7 STRUCTURAL HEALTH MONITORING OF COMPOSITE PIPING USING ELECTRICAL IMPEDANCE TOMOGRAPHY		135
7.1	Introduction.....	135
7.2	Theoretical Approach	139
7.2.1	Finite Element Modeling	139
7.2.1	Electrical Impedance Tomography.....	141
7.1	Simulation Results and Discussion.....	143
7.2	Conclusion	148
7.3	Bibliography	149
CHAPTER 8 CONCLUSIONS AND RECOMMENDATIONS		152
8.1	Findings and Contributions.....	152
8.2	Future Research Work	154
BIBLIOGRAPHY.....		155

APPENDIX A	SAMPLE DEVELOPED COMPUTER ROUTINES	171
A.1	Routine to Generate 3D Circular Nanodisk and Form MC Model.....	171
A.2	Finite Element Code Developed to Evaluate the Conductivity of the 3D Resistor Network	188

LIST OF TABLES

Table 2-1 Electrical and mechanical properties of CNT [25-29].....	11
Table 2-2 Electrical properties of some of the CNT based conductive nanocomposites.....	15
Table 2-3 Electrical and mechanical properties of graphene.	21
Table 2-4: Different preparation methods and graphene sheets oxygen content (table adapted from [142]).	31
Table 2-5 Some of the electrical properties reported for graphene based conductive nanocomposites.....	34
Table 3-1 Percolation threshold for different lattice [201].	57
Table 3-2 Best fit coefficients (mse: mean square error).....	69
Table 3-3 Comparison of Monte Carlo and proposed equation.	69

LIST OF FIGURES

Figure 2-1: Change in electrical conductivity of a nanocomposite with MWCNT content [23]. Reproduced with permission.	10
Figure 2-2: Schematic representation of SWCNT and MWCNT [30]. Reproduced with permission.	11
Figure 2-3: Different synthesis methods for CNTs. Figure adapted from [31].	12
Figure 2-4: Influence of CNT filler alignment on percolation threshold. Figure adapted from [46].	18
Figure 2-5: Influence of CNT filler aggregation on percolation threshold. Figure adapted from [46].	19
Figure 2-6: Effect of waviness and aspect ratio on percolation threshold [90]. (λ is a parameter indicating the waviness of the nanotube, see [90] for details). Figure adapted from reference [90].	20
Figure 2-7: Conductivity of graphene vs graphite nanocomposite. (Figure has been adapted from reference [125]).	24
Figure 2-8: Illustration of procedure to fabricate graphene/polyvinylidene fluoride conductive nanocomposite Special permission is obtained from [133] to re-print.	26
Figure 2-9: Electrical conductivity vs. graphene loading for one-step (circle) and two-step (square) prepared nanocomposite. Figure has been adapted from reference [136].	27
Figure 2-10: SEM images of two-step graphene/UHMWPE powders. The selected regions in (a) shows graphene sheets. Two step (a and b) and one-step (c and d) derived composite powder. Dashed line shows the boundary of graphene. Permission is obtained from [136] to re-print.	28
Figure 2-11: TEM images of (a) 0.5 wt% composite and (b) 2wt% composite Special permission is obtained from [137] to re-print.	29
Figure 2-12: In-plane and through-the -thickness conductivity of composite versus filler loading. Figure has been adapted from reference [137].	29

Figure 2-13: Conductivity-filler concentration of functionalized and non-functionalized graphene oxide nanocomposite. Figure has been adapted from reference [140].	30
Figure 2-14: SEM images for composites with 2.67 vol% graphene content (a) graphene 13.2, (b) graphene 9.6, (c) graphene 5.0. Special permission is obtained from [142] to re-print.	32
Figure 2-15: Conductivity-filler content of composites reinforced by graphene sheets with different surface chemistry. Figure has been adapted from reference [142]	32
Figure 2-16: Effect of surfactant on dispersion quality of GNS dispersion in WPU matrix. 1 vol% (a) P-GNS/WPU, (b) S-GNS/WPU. Special permission is obtained from [143] to re-print.	33
Figure 2-17: Conductivity-filler loading curves for S-GNS/WPU and P-GNS/WPU (Figure has been adapted from reference [143]).	33
Figure 2-18: Electrical conductivity of CB/ABS composite vs. filler concentration for alternative/direct current. Figure has been adapted from reference [165].	37
Figure 2-19: Electrical conductivity of CB/ polyisoprene composite versus filler concentration for different mixing methods (red: ultrasound-mixed, blue: mechanically mixed, green: roll-mixed). Figure has been adapted from reference [175].	40
Figure 3-1: a) Schematic of site percolation concept for square lattice, b) Schematic of bond percolation concept for square lattice.	56
Figure 3-2. a) Triangular lattice, b) Honey-comb lattice, c) Bethe lattice, d) Rectangular lattice (Figures adapted from [201])	57
Figure 3-3: Parameter definition for disks intersection problem	59
Figure 3-4: Schematic of cluster (gray) and percolation network (white).	60
Figure 3-5: Schematic of tunneling resistance and electron hopping.	61
Figure 3-6: Illustration of the algorithm employed to determine the shortest distance between two disks	62
Figure 3-7: Effect of the RVE size on percolation threshold.	63
Figure 3-8: Percolation threshold based on different criteria ($d_t=75$ nm).	64
Figure 3-9: Percolation threshold vs. nanodisk size and tunneling distance.	65
Figure 3-10: Percolation threshold vs. dimensionless variable.	66

Figure 3-11: Effect of R_{max}/R_{min} on percolation threshold V_p	67
Figure 3-12: Effect of tunneling distance on percolation threshold V_p	68
Figure 3-13: Effect of minimum particle size R_{min} on percolation threshold V_p	68
Figure 4-1: Tunneling conductivity vs. tunneling distance for electrons passing through an insulator matrix for different insulator barrier heights λ	75
Figure 4-2: Schematic of representative volume element with individual nanoplatelets (gray), and platelets forming clusters (white) and a percolation network (black).	76
Figure 4-3: Schematic of three-dimensional percolation network modeled by tunneling resistors (A).....	77
Figure 4-4: Schematic of nanoplatelet composite subjected to tensile strain.	78
Figure 4-5: Orientation vector of the nanoplatelet and related parameter definition	79
Figure 4-6: Schematic for the conductivity mechanism in nanocomposites with conductive platelet inclusions.	81
Figure 4-7: Effect of tunneling cut-off distance (1 nm, 2 nm and 3 nm) on the resistivity of nanoplatelet composites for an insulator barrier height of $\lambda = 0.5\text{eV}$ and a platelet diameter of $D = 10\text{ nm}$	83
Figure 4-8: Effect of insulator barrier height λ on the resistivity of conductive nanoplatelet composites plotted vs. filler volume fraction for a platelet diameter of $D = 10\text{ nm}$	84
Figure 4-9: Graph defining the percolation region depicted as nanoplatelet composite resistivity vs. filler volume fraction.	85
Figure 4-10: Deviation of nanoplatelet composite resistivity from a universal power-law description with $s=2$ for increasing filler content.	86
Figure 4-11: Nanoplatelet composite resistivity vs. filler volume fraction and best-fit curves for post-percolation power-law description for filler concentration near the percolation threshold ($V_p, 1.4V_p$).	87
Figure 4-12: Nanocomposite resistivity vs. filler volume fraction and best-fit curves for a post-percolation power-law description (percolation region and erratic points are considered data outlier).....	88
Figure 4-13: Values for the critical exponent, s , for data in the percolation region.	89
Figure 4-14: Graph depicting filler volume fraction at the percolation threshold V_p vs. nanoplatelet diameter D	90

Figure 4-15: Percolation threshold of oblates of revolution as a function of aspect ratio and ratio of soft shell thickness to the major axis. The dashed line depicts the percolation threshold trend when b and d are constant. (adapted from [195]).	90
Figure 4-16: Percolation threshold of oblates of revolution as a function of aspect ratio. The soft shell volume was deducted in order to make the data analogous to a tunneling percolation problem with platelet based nanocomposites. (adapted from [195]).	91
Figure 4-17: Percolation threshold for 2D disks dispersed in a 2D domain. (adapted from [230]).	92
Figure 4-18: Resistivity vs. filler volume fraction demonstrating the response of an unconstrained nanoplatelet composite to applied tensile strain ϵ for a platelet diameter of $D=70$ nm.	93
Figure 4-19: Erratic piezoresistivity behavior for low filler loadings	93
Figure 4-20: Piezoresistivity behavior for $V_f=7.5\%$;	94
Figure 4-21: Piezoresistivity graph with plateau region for $V_f=8.8\%$	95
Figure 4-22: Piezoresistivity behavior for $V_f= 11\%$.	95
Figure 4-23: Piezoresistivity behavior and critical strain for a CNT-graphene nanoplatelet hybrid composite. (adapted from [234]).	96
Figure 5-1: Schematic of a RVE containing individually dispersed nanoplatelets (black), platelets forming an electrically connected cluster (white), and particles creating a percolation network (grey).	104
Figure 5-2: Illustration of tunneling resistors for simulating electron tunneling through the insulator matrix and the formation of a percolation network.	104
Figure 5-3: Resistivity per unit area of polymer with 4 nm thickness and a quantum tunneling barrier height λ of 1 eV, with respect to the normalized voltage eV/λ .	106
Figure 5-4: Tunneling resistivity versus insulator thickness	107
Figure 5-5: Conductivity of nanocomposite with respect to filler loading of conductive nanodisks	109
Figure 5-6: Electric current density of nanocomposites with 100 nm diameter nanoplatelets versus the applied electrical field.	109
Figure 5-7: Normalized resistivity of nanocomposites with 100 nm nanodisks as a function of the applied electrical field	110

Figure 5-8: Normalized resistivity data versus applied electrical field from experiments with nanographene/epoxy samples.....	111
Figure 5-9: Resistivity of nanocomposites with 100 nm circular nanoplatelets as a function of electric power.....	113
Figure 5-10: Value of α as a function of filler volume fraction for nanocomposites with 100 nm circular nanoplatelets.....	113
Figure 6-1: Schematic of periodic boundary conditions (elements in red color indicate CNTs crossing the RVE boundary).....	119
Figure 6-2: Tunneling conductivity versus insulator thickness for $\lambda = 1.5$	121
Figure 6-3: Schematic for the formation of a percolation network at the percolation threshold.....	121
Figure 6-4: Schematic of the electron tunneling mechanism in CNT and GNP based conductive nanocomposites.	123
Figure 6-5: Schematic of the conductivity mechanism in conjunction with a percolation network.	124
Figure 6-6: Electrical conductivity of a CNT nanocomposite with $\rho_{\text{CNT}} = 0.5\text{E-}6 \Omega\text{m}$, $\lambda = 0.5 \text{ ev}$	126
Figure 6-7: Qualitative comparison of experimental data [264, 281] with simulation results for a CNT nanocomposite with $\rho_{\text{CNT}} = 0.5\text{E-}6 \Omega\text{m}$, $\lambda = 0.5 \text{ ev}$, $V_f = 1\%$	127
Figure 6-8: Effect of polymer electrical properties on the resistivity-temperature behavior for a CNT nanocomposite with $V_f = 1\%$ and $\rho_{\text{CNT}} = 0.5\text{E-}6 \Omega\text{m}$	128
Figure 6-9: Effect of CNT resistivity on the resistivity-temperature behavior of CNT nanocomposites with $\lambda = 0.5 \text{ ev}$	129
Figure 6-10: Normalized resistivity as a function of the temperature, from simulations with 100 nm nanodisks and $\lambda = 0.5 \text{ ev}$	130
Figure 6-11: Fitting of GNP nanocomposite resistivity data according to the VRH model proposed by Mott [266, 282]	131
Figure 6-12: Fitting of CNT nanocomposite resistivity data according to the VRH model proposed by Mott [266, 282]. ($\lambda = 1 \text{ ev}$, $V_f = 0.65\%$).	131
Figure 7-1: EIT application example for lung imaging. Lung image is reproduced with permission from [317].	141
Figure 7-2: Schematic of the proposed technique for SHM in polymer composite piping.	142

Figure 7-3: Modeling of the sensing electrodes on the outer surface of the pipeline segment.	143
Figure 7-4: Corrosion in pipe represented by ellipsoid.	143
Figure 7-5: Conductivity of the conductive nanocomposite as a function of the electrical field.....	144
Figure 7-6: Electrode configuration schematic for the sensing array and current injection patterns.	145
Figure 7-7: EIT measurements based on scheme one.	146
Figure 7-8: EIT measurements based of scheme.	147
Figure 7-9: Comparison of the EIT measurements for the damaged and undamaged pipe based on scheme one.	147
Figure 7-10: Comparison of the EIT measurements for the damaged and undamaged pipe based on scheme 2.....	148

CHAPTER 1

INTRODUCTION

1.1 Background and Motivation

Excellent mechanical and physical properties of reinforced polymers such as light weight, high mechanical strength and corrosion resistance have provided a wide range of applications for these materials [1]. Conversely, properties such as low thermal conductivity and the lack of electrical conductivity also pose restriction on the application of reinforced polymers. Polymer based composite pressure vessels and piping are commonly used components in industrial facilities like refineries, petrochemical complexes and power plants. Hazards and potential risks associated with structural defects in composite structures necessitate employing effective structural health monitoring (SHM) strategies to assure their safety and integrity [2]. In addition to the drawbacks listed for polymeric structures, employing conventional SHM techniques for composite structures is usually associated with considerable shortcomings. Acoustic and ultrasonic methods have shown excellent efficacy in monitoring structures made from conventional (metallic) material; however, their practicality for fiber reinforced and layered composite structures with multiple interfaces is questionable [3]. Short embedded sensing elements, such as piezoelectric films, may comprise locations for stress concentration and crack initiation. Moreover, these sensing systems are not capable of detecting defects and flaws with insufficient proximity to the sensing elements. Furthermore, similar to short fibrous sensors, long fiber sensors such as piezoelectric filaments and optical fibers with Bragg gratings have shown insignificant sensitivity to damage initiating in the polymer matrix [3].

The development and availability of nanoscale conductive particles, such as carbon black, carbon nanotubes and graphene nanoplatelets, has motivated researchers to consider the feasibility of employing these materials in developing electrically conductive

polymers [4-6]. Imparting electrical behavior to polymers through dispersing conductive fillers can extend their range of applications to include e.g. electrostatic dissipation, magnetic interface shielding and wave absorption [7-9]. Besides these applications, promising findings have been reported in the technical literature on utilizing conductive nanocomposites for structural health monitoring purposes [10-12]. In particular graphene nanoplatelets (GNP) have emerged as a promising nanoparticle filler for industrial applications. In addition to exceptional electrical and mechanical properties, GNP is favorable due to the development of low cost and large-scale production methods in recent years [13].

The evaluation of the electrical behavior of conductive nanoplatelet-based composites has been the subject of a considerable number of experimental studies [4, 5, 14]. However, the technical literature has been scarce on work simulating the electrical conductivity of nanoplatelets-based nanocomposites.

The promise that nanoplatelet-based conductive composites hold for industrial applications, the limited expertise in modeling these materials, and aforementioned shortcomings in SHM techniques for polymeric composite structures motivated the present author to conduct a numerical study to investigate the electrical conductivity behavior of polymers made conductive through the dispersion of nanoplatelets. The objective of this study is therefore the evaluation of nanoplatelet-based polymer composite electrical behavior, including electrical conductivity, piezoresistivity, and effects of temperature and electric field intensity.

1.2 Organization and Outlines of the Research

A numerical methodology was proposed and developed to achieve the aforementioned research objectives. Subsequent to the present chapter the thesis document describing the undertaken research is outlined as follows:

Chapter 2: On the electrical behavior of carbon allotrope modified polymers

An extensive literature review was conducted on the electrical behavior of polymeric composites, including a brief review of different synthesis methods for carbon fillers. The

effects of different filler synthesizing and composite preparation methods on conductivity and percolation behavior were studied. As such, the important role of composite preparation and filler dispersion techniques on the electrical behavior of polymeric conductive nanocomposites was underlined. Other determining factors, such as filler geometry, size and aspect ratio that govern the electrical behavior of conductive composites are also discussed in the review. The review of the technical literature highlights the necessity of conducting further experimental, analytical and numerical studies to fully appreciate the effects of governing parameters, such as filler type, surface treatment and manufacturing method, on the electrical behavior of conductive nanocomposites, enabling their behavior to be tailored for specific industrial applications.

Chapter 3: Numerical approach for percolation behavior investigation

In the first phase of the study a three-dimensional continuum Monte Carlo model was developed to evaluate the percolation behavior of circular nanoplatelets that are randomly distributed in a cubic representative volume element. A computer code was created in the FORTRAN programming language for execution on a general purpose Linux Cluster to study percolation problems. The developed model was employed to predict the critical volume fraction, that is, the percolation threshold, for composites filled with conductive circular nanodisks. Geometry aspects of the problem include representative volume element size effects, particle size distribution, and quantum mechanical electron tunneling distance.

Chapter 4: Nanocomposite electrical conductivity and piezoresistivity

The aforementioned three-dimensional continuum percolation model provides information on the percolation behavior of an electrically insulating polymer matrix rendered conductive by randomly dispersed conductive platelets. The broader conductivity behavior of such composites was modeled by developing a three-dimensional finite element resistor network. Parameters related to the percolation threshold and the conductivity behavior were thus determined. Further, the piezoresistivity behavior of conductive composites was studied employing a reoriented resistor network emulating a conductive composite subjected to mechanical strain. The

effects of governing parameters, i.e., electron tunneling distance, conductive particle aspect ratio and size, on conductivity behavior were examined.

Chapter 5: Nanocomposite current-voltage characteristics

In order to be able to employ conductive nanocomposites for sensing applications, the conductivity behavior of nanocomposites for different stimulating voltage levels should be well determined. This phase of the research was devoted to the investigation of nonlinear electrical conductivity behavior of platelet-based polymers nanocomposites. Studying the current-voltage behavior was again based on the three-dimensional continuum Monte Carlo modeling approach. A nonlinear finite element model technique was implemented to evaluate the electrical behavior of the nanocomposite for different levels of the applied electric field. The validity of the developed model was verified through qualitative comparison of the simulation results with results obtained from experimental works.

Chapter 6: Effect of temperature on nanocomposite electrical conductivity

In addition to temperature sensing applications, understanding the effect of the temperature on the nanocomposite is essential for temperature compensation. A numerical study was conducted to evaluate the effect of temperature on the electrical resistivity of nanoparticle filled polymers, i.e., carbon nanotube and graphene nanoplatelet composites. As such, the three-dimensional Monte Carlo modeling approach was expended to study the percolation behavior of stick-shaped nanofillers in addition to nanoplatelet systems. The study was carried out investigating the temperature-resistivity behavior of nanocomposites for a range of parameters, including carbon nanotube electrical conductivity, quantum tunneling barrier height of the polymer matrix, and filler volume loading. The developed model was validated comparing the modeling results with available experimental works.

Chapter 7: SHM of composite piping using electrical impedance tomography

Different aspects of the nanocomposite such conductivity, piezoresistivity, non-ohmic effect and temperature compensation was comprehensively investigated in the previous chapter. In this chapter a study was performed to investigate the feasibility of employing

the developed conductive nanocomposite for industrial applications. As the final phase of this research, a study was conducted to evaluate the feasibility of employing conductive nanocomposites in SHM applications. A novel concept based on electrical impedance tomography was explored to detect wear and abrasion damage in composite piping. A SHM concept was thus developed based on electrical impedance tomography for detecting material loss in polymeric piping modified with graphene nanoplatelets.

Chapter 8: Conclusions and recommendations

The last chapter of this thesis summarizes the key results of the research work. Significant findings from the thesis work are highlighted, and a set of conclusions was drawn from the conducted study. Moreover, several recommendations were made to extend the current work toward exploring a wider scope of nanoplatelets-based conductive nanocomposites.

1.3 Bibliography

- [1] J. S. Hwang, "Carbon black filled electrospun fiberweb: Electrical and mechanical properties," PhD, North Carolina State University Raleigh, NC, 2006.
- [2] J. H. Lee and S. J. Lee, "Application of laser-generated guided wave for evaluation of corrosion in carbon steel pipe," *Ndt & E International*, vol. 42, pp. 222-227, Apr 2009.
- [3] L. M. Gao, E. T. Thostenson, Z. G. Zhang, and T. W. Chou, "Coupled carbon nanotube network and acoustic emission monitoring for sensing of damage development in composites," *Carbon*, vol. 47, pp. 1381-1388, Apr 2009.
- [4] S. G. Miller, J. L. Bauer, M. J. Maryanski, P. J. Heimann, J. P. Barlow, J. M. Gosau, *et al.*, "Characterization of epoxy functionalized graphite nanoparticles and the physical properties of epoxy matrix nanocomposites," *Composites Science and Technology*, vol. 70, pp. 1120-1125, Jul 2010.
- [5] W. Thongruang, R. J. Spontak, and C. M. Balik, "Correlated electrical conductivity and mechanical property analysis of high-density polyethylene filled with graphite and carbon fiber," *Polymer*, vol. 43, pp. 2279-2286, Apr 2002.
- [6] H. Koerner, W. D. Liu, M. Alexander, P. Mirau, H. Dowty, and R. A. Vaia, "Deformation-morphology correlations in electrically conductive carbon nanotube thermoplastic polyurethane nanocomposites," *Polymer*, vol. 46, pp. 4405-4420, May 26 2005.
- [7] M. H. Al-Saleh and U. Sundararaj, "Electromagnetic interference (EMI) shielding effectiveness of PP/PS polymer blends containing high structure carbon black (vol 298, pg 621, 2008)," *Macromolecular Materials and Engineering*, vol. 293, pp. 789-789, Sep 12 2008.
- [8] P. Saini, V. Choudhary, B. P. Singh, R. B. Mathur, and S. K. Dhawan, "Polyaniline-MWCNT nanocomposites for microwave absorption and EMI shielding," *Materials Chemistry and Physics*, vol. 113, pp. 919-926, Feb 15 2009.
- [9] X. S. Yi, G. Z. Wu, and Y. Pan, "Properties and applications of filled conductive polymer composites," *Polymer International*, vol. 44, pp. 117-124, Oct 1997.
- [10] N. D. Alexopoulos, C. Bartholome, P. Poulin, and Z. Marioli-Riga, "Structural health monitoring of glass fiber reinforced composites using embedded carbon nanotube (CNT) fibers," *Composites Science and Technology*, vol. 70, pp. 260-271, Feb 2010.

- [11] L. Boeger, M. H. G. Wichmann, L. O. Meyer, and K. Schulte, "Load and health monitoring in glass fibre reinforced composites with an electrically conductive nanocomposite epoxy matrix," *Composites Science and Technology*, vol. 68, pp. 1886-1894, Jun 2008.
- [12] V. Eswaraiah, K. Balasubramaniam, and S. Ramaprabhu, "Functionalized graphene reinforced thermoplastic nanocomposites as strain sensors in structural health monitoring," *Journal of Materials Chemistry*, vol. 21, pp. 12626-12628, 2011.
- [13] K. R. Paton, E. Varrla, C. Backes, R. J. Smith, U. Khan, A. O'Neill, *et al.*, "Scalable production of large quantities of defect-free few-layer graphene by shear exfoliation in liquids," *Nature materials*, vol. 13, pp. 624-630, 2014.
- [14] L. L. Wu, X. Lv, and C. C. Zhang, "Effect of modified graphene addition on the electrical properties of epoxy resin composite," *Advanced Materials, Pts 1-4*, vol. 239-242, pp. 55-58, 2011.

CHAPTER 2

A REVIEW ON THE ELECTRICAL BEHAVIOR OF CARBON ALLOTROPE MODIFIED POLYMERS

SYNOPSIS- This chapter provides an extensive literature review on research devoted to enhancing the electrical conductivity of polymers through the addition of carbon based nanoparticles. Included in this review are the most common methods for synthesizing nanoparticles, as well as experimental and numerical research on the electrical behavior of conductive nanocomposites. The present study mainly focuses on the effect of nanoscale carbon fillers on nanocomposite conductivity, percolation threshold and piezoresistivity. In recent years a great deal of research on polymeric nanocomposites has been conducted for carbon nanotube and graphene nanoplatelet based composites. However, this chapter also includes a review on carbon black based conductive nanocomposites. In addition, the effects of different composite preparation parameters, such as employing surfactants, mixing techniques, morphology of nanoparticles, particle dispersion methods, on the electrical behavior of nanocomposites are discussed.

2.1 Introduction

Polymeric materials and their composites have numerous industrial applications. Polymers are generally considered electrically insulating materials; however, for some industrial applications, polymers with some level of the electrical conductivity are desired. Intrinsically conductive polymers (ICP) such as Polyaniline (PAni) and Polypyrrole (PPy) have poor mechanical properties, restricting their employment for industrial application [15]. Poor electrical characteristics of polymers and poor mechanical properties of ICPs limit their broader industrial use. The addition of conductive particles into these materials is a widely used technique to improve their electrical conductivity. Enhancing the electrical conductivity of polymer based materials extends their range of possible applications and may even enable multifunctionality.

These materials may be utilized for strain sensors, embedded structural health monitoring systems, electromagnetic interference (EMI) shielding, electrostatic discharge (ESD) protection and the like [15]. Employing the conductive filler modified polymers for ESD protection and EMI shielding applications have been the subject of great number of research projects in recent years. Metal particles were the earliest fillers used in developing conductive polymeric composites and electrically conductive adhesives (ECA). In 1956, Wolfson and Elliott [16] patented a method to develop conductive cement containing silver and epoxy resin. Following their method, several research works have been performed on conductive nanocomposites based on silver flakes and silver nanoparticles based conductive composites [17-19]. Employing copper flakes to render the epoxy resin electrically conductive was patented by Marshall and Agarwal in 1974 [20]. In recent years, copper nanowires (CuNW) with high aspect ratio have been utilized to enhance the electrical properties of polymers has been paid attention in recent years. As an example, Lin et al. [21] explored the mechanical and electrical properties of polystyrene/CuNW nanocomposites. In another work, Al-Saleh et al. reported exceptional EMI shielding effectiveness for the CuNW/styrene nanocomposites [22].

Recent advances in synthesis of nanoscale carbon structures, such as graphene platelets (GNP) and carbon nanotubes (CNT), provide new opportunities for the use of these unique multi-functional materials in a broad range of applications. Their outstanding mechanical and electrical properties may be utilized to enhance the mechanical and electrical properties of polymers. CNT, GNP and carbon black (CB) particles are three commonly used carbon allotropes for improving the electrical conductivity of polymeric composites.

In this chapter, common production methods and properties of CNT, GNP, and CB are discussed, the electrical behavior of polymers modified through addition of these fillers is outlined, and effects of different processing procedures and parameters (such as the composite processing method, particle size and polymer material) on the conductivity of carbon filler modified polymers is investigated. Particular attention was paid to the percolation threshold as it is a key characteristic of conductive nanocomposites. Advances in synthesis techniques for CNT and GNP and their unique electrical

conductivity and geometry, such as a high aspect ratio, has made these materials a prevalent choice for researchers in the field of conductive polymeric nanocomposites. Arguably, attention to CB for conductive nanocomposite applications has diminished over the years. Nevertheless, as CB is one of the earliest conductive fillers used in polymeric nanocomposite, a review of CB-nanocomposites has been included in this work to comprehensively elucidate the evolution of carbon allotrope based conductive nanocomposites.

In general, conductivity of nanocomposites increases as the amount of added carbon filler increases. **Figure 2-1** shows an example of the increase in conductivity of a nanocomposite as a function of the of multiwall carbon nanotubes (MWCNT) content. Here, a sharp increase in conductivity is observed exceeding a critical volume fraction. For **Figure 2-1**, this critical volume fraction was identified as 0.28 wt% [23]. Percolation theory has widely been used to describe the conductivity mechanism of conductive particle based nanocomposites. According to this theory, a conductive path is formed by conductive inclusions through which an electrical current can pass, making the nanocomposite conductive. The aforementioned critical volume fraction is known as the percolation threshold. The conductivity of nanocomposites with filler loadings higher than the percolation threshold can generally be described by a power-law expression, i.e.

$$\sigma = \sigma_0 (\phi - \phi_c)^t \quad \text{Eq. 2-1}$$

where σ , σ_0 , ϕ , ϕ_c , t are the conductivity of the composite, a constant, the filler loading, the percolation threshold and a universal constant known as the critical exponent [23].

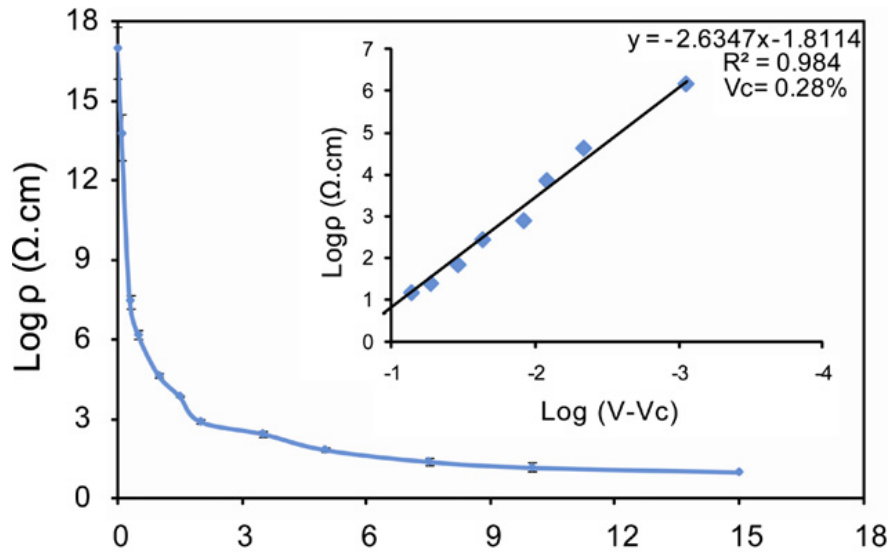


Figure 2-1: Change in electrical conductivity of a nanocomposite with MWCNT content [23]. Reproduced with permission.

2.1 CNT Based Conductive Composites:

2.1.1 Carbon Nanotubes

Discovery of CNTs, as one of the allotropes of carbon, was first reported by Iijima in 1991 [24]. CNTs were synthesized using an arc-discharge evaporation method. The exceptional mechanical and electrical properties of CNTs have attracted broad attention from researchers since CNTs can be used to improve the electrical and mechanical properties of polymers and composites. CNTs can be sub-categorized into three main forms: single wall carbon nanotubes (SWCNT), double walled carbon nanotubes (DWCNT) and multiwall carbon nanotubes (MWCNT). Since research on the application of DWCNT for conductive polymeric composites has been scarce in the technical literature, the focus of the present review was placed on SWCNTs and MWCNTs. As shown schematically in **Figure 2-2**, SWCNTs are composed of cylindrical single graphene sheets while MWCNTs are composed of several coaxial SWCNTs. General electrical and mechanical properties for SWCNTs and MWCNTs are summarized in **Table 2-1**.

Table 2-1 Electrical and mechanical properties of CNT [25-29]

CNT type	Specific Gravity (g/cm ³)	Electrical Conductivity (S/cm)	Tensile Strength (GPa)	Modulus of Elasticity (TPa)
MWCNT	1.8	10 ³ -10 ⁵	1.7	1.7-2.4
SWCNT	0.8	10 ² -10 ⁶	13-52	2.8-3.6

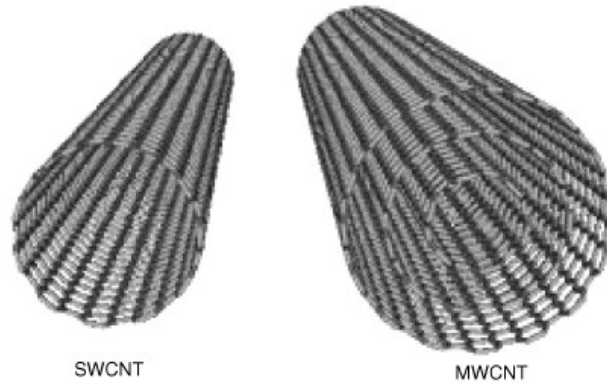


Figure 2-2: Schematic representation of SWCNT and MWCNT [30]. Reproduced with permission.

2.2 Synthesis Methods for Carbon Nanotubes

Since the discovery of CNTs, several synthesis methods have been developed. Among these, arc discharge, laser ablation and chemical vapor deposition are the most commonly employed CNT production methods. A detailed review on carbon nanotube synthesis methods is illustrated by **Figure 2-3** [31, 32]. In this chapter a brief explanation on the most commonly employed synthesizing methods is provided.

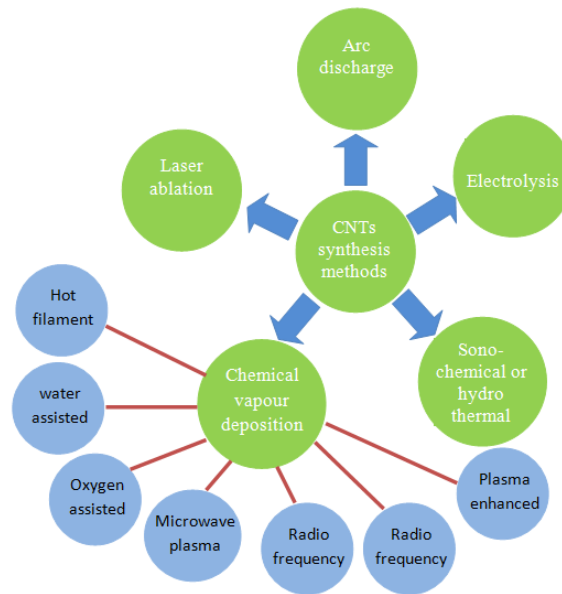


Figure 2-3: Different synthesis methods for CNTs. Figure adapted from [31].

2.2.1 Arc Discharge

The earliest method used for synthesizing CNTs is the arc-discharge technique, which is a high temperature method suitable for large-scale production, providing particles with very few defects [28]. In this technique, an arc is discharged between two graphite electrodes in a gaseous environment. The quality and characteristics of the obtained MWCNT is governed by the synthesizing parameters that include type and pressure of the filling gas and intensity of the arc current. For example, Zhao et al. [28, 33] reported that employing helium gas provides a more uniform product in comparison to methane (CH₄) gas. In another work it was observed that using hydrogen (H₂) gas yields high grade MWCNTs and produces less smoke [28, 34]. Single-pulse arc discharge has also been employed by some researches to produce CNT [28, 35, 36]. They showed that employing pulses with different length results in CNTs with different characteristics, which has advantages in comparison with other technologies, such as the absence of a process chamber. Using the arc discharge method without a catalyst mostly produces MWCNTs [28]. SWCNTs are typically produced when a metal catalyst is utilized. For SWCNTs, the anode electrode is made of graphite with metal as a catalyst. Similar to MWCNTs, the specification of the produced SWCNT is governed and controlled by the

process parameters, such as the type of gas, pressure and the choice of catalyst. For example, Saito et al. [37] showed that SWCNTs with higher aspect ratio are grown from Ni particles, and a lanthanide catalyst yields short and thick SWCNTs.

2.2.2 *Laser Ablation*

Kroto et al. were one of the earliest researchers who utilized laser ablation or laser evaporation technique to produce fullerene, [38]. In this method a laser beam is focused onto a graphite target located in a tubular chamber with high temperature while a flow of inert gas (e.g. helium, argon) sweeps away the particles produced by laser ablation [38]. The properties of CNTs produced by this technique are again affected by the process parameters. These parameters can be listed as laser power, excitation wavelength, composition of the target material, the pressure and type of the inert gas, and chamber temperature [28, 39]. For example, Kusaba and Tsunawaki [40] carried out the synthesis of SWCNTs using a XeCl excimer laser with a wavelength of 308 nm at different chamber temperatures (1273 K, 1373 K, 1473 K and 1623 K) in argon atmosphere. They found that laser ablation at 1623 K yielded the highest amount of SWCNTs.

2.2.3 *Chemical Vapor Deposition*

Chemical vapor deposition (CVD) for synthesizing CNTs has been the topic of a large number of research works. Joseyacamán et al. [41] reported production of microtubules with fullerene like structure by chemical vapor deposition of acetylene on iron in 1993. They obtained carbon microtubules via decomposition of acetylene over Fe particles. Ni, Co and Fe are the most commonly used catalysts in CVD processes [31, 42]. The role of the catalyst is the decomposition of the feeding gas through plasma irradiation known as plasma-enhanced radiation or heat in thermal CVD [28]. Methane, ethanol, acetone, xylene and acetylene are some hydrocarbons reported in the literature that are used as feeding gases. Stainless steel, silicon dioxide (SiO₂), nickel (Ni), silicon (Si), copper (Cu) are some of the material used as substrates [31]. Inami et al. [43] showed that the feeding gas, temperature, and catalyst all play an important role in SWCNT growth.

2.3 Electrical Behavior of CNT/Polymer Composites

The electrical properties of CNT based nanocomposites have widely been investigated experimentally and theoretically since the discovery of CNTs. A large number of parameters have been identified to affect the electrical properties (particularly the percolation threshold, ϕ_c) of these materials. The most important ones can be listed as the type and aspect ratio (l/d) of the filler, filler treatment (e.g. applying surfactants), dispersion techniques and the type of solvent used in the nanocomposite preparation. **Table 2-2** summarizes the findings of some notable experimental research published in the technical literature on the effects of CNTs on nanocomposite electrical conductivity. As shown in **Table 2-2**, the results reported in the technical literature cover a wide range of percolation thresholds varying from 0.0025 to 3.4 wt%. As stated earlier, the percolation threshold is governed by various different parameters. The review of the technical literature did not reveal any controlled study that is devoted to evaluating the individual effects of the governing parameters on the percolation behavior. For example, the electrical behavior of conductive nanocomposites based on CNTs synthesized using different techniques has been the subject of several publications; however, the composite preparation procedures like mixing, curing and dispersion were not identical in all of these studies. Hence, it is not possible to evaluate and fully appreciate the role of the CNT synthesis method on the electrical behavior of nanocomposites using the current literature. On the other hand, numerical predictive models, such as continuum Monte Carlo based studies, have been reported to successfully predict percolation thresholds [44-48]. For example, Oskouyi et al. [49] predicted a value of 0.6 vol% (approximately 0.3 wt%, calculated using $X \text{ vol\%} = 2X \text{ wt\%}$ for MWCNT composites) for the percolation threshold using a thorough uniform dispersion assumption of MWCNTs (with length of 5 μm and diameter of 50 nm).

Table 2-2 Electrical properties of some of the CNT based conductive nanocomposites.

Ref	Filler			Polymer	Treatment	Solution	l/d	Φ_c (¹)	t	Mixing	Conductivity (S/cm)
	Type	Synthesis Method ²	Supplier								
[50]	MWCNT	Chemical vapor grown method	Jeio Ltd	Polycarbonate	-	THF	-	0.4 wt%	-	Sonication	4.68E-1@3wt%
[51]	MWCNT	-	Nanostructured & Amorphous	Epoxy	-	-	-	0.9 wt%* (1.8 vol%)	-	Stirring	1.15E-4@2vol%
[51]	MWCNT	-	Nanostructured & Amorphous	Epoxy	-	acetone	-	0.75 wt%* (1.5 vol%)	-	Stirring	2.59E-4@2vol%
[51]	MWCNT	-	Nanostructured & Amorphous	Epoxy	-	-	-	0.5 wt%* (1 vol%)	-	Sonication/stirring	7.71E-4@2vol%
[51]	MWCNT	-	Nanostructured & Amorphous	Epoxy	-	acetone	-	0.24 wt%* (0.48 vol%)	1.8	Sonication/stirring	1.725E-4@2vol%
[52]	MWCNT	thermally assisted CVD	N/A	polystyrene	-	toluene	-	0.21 wt%	1.95	Sonication	1E-2@3wt%
[53]	MWCNT	-	Nanolab Inc.	-	hyperbranched polyethylene	THF	-	0.91 wt%	2.8	sonication/stirring	6.60E-5 S/m@5wt%
[53]	MWCNT	-	Sigma Aldrich	-	-	THF	-	0.91 wt%	2.4	-	1.45E-4 S/m@5wt%
[54]	MWCNT	catalytic CVD-the fixed bed method	N/A	polyamide 6.6	-	-	-	0.81 wt.%	2	Melt mixing	-
[55]	MWCNT	CVD	Shenzhen Nanotech Port	PP/EPDM	-	-	-	3.5 wt%* (7 vol%)	4.5	Melt mixing	2.6 E-7@7vol%
[56]	MWCNT	Aligned CVD	-	bisphenol-A resin	-	-	340	0.0025 wt%	1.2	Stirring	1E-5@0.005wt%
[57]	MWCNT	CCVD	-	epoxy	-	-	3300	0.011 wt%	-	Stirring	1E-5@0.1wt%
[58]	MWCNT	CVD	-	polypropylene	-	-	1000	0.3 wt%* (0.6 vol%)	4.5	Melt mixing	-
[59]	MWCNT	-	Nanocyl	3-hexylthiophene	-	chloroform	100	0.1 wt%	1.68	Sonication	1E-4@10wt%
[60]	SWCNT	Arc discharge method	Carbolex	3-octylthiophene	-	chloroform	-	11 wt%	2	Sonication	1E-6@18wt%
[61]	MWCNT	CVD	ILJIN Nanotech	vinyl ester	-	-	-	0.1 wt.%	-	Calendering	1E-6@10wt%

¹ Φ_c (Percolation threshold) was converted to wt% when it is stated in term of vol% in the original reference using (vol%=2 wt% for MWCNT composites) approximation. The original value is presented in parenthesis.

² The synthesizing method of the CNT is provided in the parenthesis if reported. Supplier is reported in the following if the CNT has not synthesized by the author.

Filler				Polymer	Treatment	Solution	l/d	Φ_c (*)	t	Mixing	Conductivity (S/cm)
Ref	Type	Synthesis Method ¹	Supplier								
[62]	MWCNT	CVD	Organic Chemical Ltd	p-phenylene sulfide	-	-	-	5 wt%	-	Melt mixing	1E-8@7.5wt%
[62]	MWCNT	-	-	methyl methacrylate	dodecyl sulfate sodium	toluene	-	0.6 wt%	-	Stirring/sonication	1E0@1wt%
[63]	MWCNT	CVD	-	unsaturated polyester	-	-	160	0.026wt%	2.55	Stirring	1E-4@1wt%
[64]	MWCNT	-	Cheap Tubes Inc.	polypropylene	-	-	51	2.11 wt%	2.99	Melt mixing	1E-2@7.5wt%
[64]	MWCNT	-	Cheap Tubes Inc.	polypropylene	-	-	51	2.11 wt%	2.99	Melt mixing	1E-2@7.5wt%
[64]	MWCNT	-	Cheap Tubes Inc.	polypropylene	-	-	84	1.57 wt%	3.10	Melt mixing	1E-2@7wt%
[64]	MWCNT	-	Cheap Tubes Inc.	polypropylene	-	-	167	0.74 wt%	3.05	Melt mixing	1E-3@3wt%
[65]	MWCNT	catalytic pyrolysis of propylene	-	ethylene terephthalate	-	-	-	-	5.5	Extrusion	1E-3@4 wt%
[66]	MWNT	-	Nanostructured and Amorphous Materials Inc.	Polypropylene	-	-	-	3.0 wt%	-	Melt mixing	3E-6@2wt%
[67]	MWCNT	CVD	Hyperion Catalysis International	polyamide-6	-	-	-	5.0 wt%	-	Extrusion	4.2E-5@8wt%
[68]	MWNT	-	Shenzhen Nanotech Port Co.	ethylene terephthalate	-	phenol	-	0.9 wt%	2.2	Sonication/stirring	1E-4@2.0 wt%,
[68]	SWCNT	-	HiPCO	polyethylene	SDS	H ₂ O	-	3.4 wt%	-	Sonication/spraying/extrusion	1E-3@5wt%
[69]	MWCNT	CVD	Nanocyl S.A.	polystyrene	SDS	H ₂ O	-	0.81 wt%	-	Sonication/stirring	4.6E-3@2wt%
[69]	SWCNT	CVD	Nanocyl S.A.	polystyrene	SDS	H ₂ O	-	0.55 wt%	-	Sonication/stirring	9E-2@2wt%
[69]	MWCNT	CVD	Nanocyl S.A.	isotactic polypropylene	SDS	H ₂ O	-	0.1 wt%	-	Sonication/stirring	6.8E-3@2wt%
[69]	SWCNT	CVD	Nanocyl S.A.	isotactic polypropylene	SDS	H ₂ O	-	0.04 wt%	-	Sonication/stirring	7E-2@2wt%
[70]	MWCNT	-	Arkema	diglycidyl ether of bisphenol-A	-	diamine	-	0.06 wt%	-	Sonication/stirring(Fibers alligned by electrical field)	1E-6@0.12wt%
[70]	MWCNT	-	Arkema	diglycidyl ether of bisphenol-A	-	diamine	-	0.5 wt%	-	Sonication/shear mixing	1E-6@0.5wt%
[71]	MWCNT	-	NANOCYL	ether sulfone	NH ₂	-	<105	1.25 wt%	-	Melt mixing	1E-4@1.5wt%
[71]	MWCNT	-	NANOCYL	ether sulfone	-	-	<105	0.37 wt%	-	Melt mixing	1E-1@4wt%
[71]	MWCNT	-	NANOCYL	ether sulfone	-	-	158	0.57 wt%	-	Melt mixing	1E-3@0.8wt%
[72]	MWCNT	fluidized bed catalytic CVD	-	polystyrene	-	-	72	0.15 wt%	3.5	Melt mixing	1E-7@1.2wt%
[73]	MWCNT	-	Arkema	styrene-butadiene	-	tetrahydrofuran	-	0.67wt%	-	Sonication/rotation-revolution	6E-3@3.35wt%
[74]	MWCNT	-	Nanostructured & Amorphous Materials	polyurethane	-COOH	N-dimethyl formamide	-	0.49 wt% 0.98 vol%	2	Sonication/stirring	1E-6@2 vol%

Filler				Polymer	Treatment	Solution	l/d	Φ_c (*)	t	Mixing	Conductivity (S/cm)
Ref	Type	Synthesis Method ¹	Supplier								
[75]	SWCNT	laser ablated	Rice University	polyimide	-	DMF	-	0.05wt% (0.05 vol%)	1.5	Sonication/stirring	1.6E-8@ 0.1 vol%
[76]	MWCNT	-	Shenzhen Dynanonic Co	vinylidene fluoride	-	-	-	0.039wt% (0.078vol%)	1.038	Stirring	1e-2@0.14 vol%
[77]	MWCNT	-	Nanostructured and Amorphous Materials Inc.	Polypropylene	-	-	-	0.11 wt% (0.22 vol%)	-	Melt mixing	1E-3@2.1 vol%
[78]	MWCNT	CVD	TMS-Petsmash	polyvinylchloride	-	ethanol	1000	0.0225wt% (0.045 vol%)	3.5	Sonication/grinding	1E-6@0.22 vol%
[79]	MWCNT	-	Sigma-Aldrich	polypropylene	Octadecylamine	xylene	10-1000	0.12wt% (0.24 vol.%)	2	Sonication/stirring	-
[79]	MWCNT	-	Sigma-Aldrich	polypropylene	-	-	10-1000	0.12wt% (0.24 vol.%)	2	Melt mixing	-
[80]	SWCNT	laser ablation	-	paraphenylene vinylene	-	sulfonium polyelectrolyte	-	1.8 wt%	2	Sonication	1E-3@9 wt%
[81]	MWCNT	-	Aldrich	polystyrene	vinyl pyrrolidone	ethyl alcohol	-	1.8 wt%	2.25	Stirring	-
[82]	MWNT	catalytic decomposition	Hyperion Co. Ltd,	polyimide	N,N-dimethylacetamide	-	-	0.07wt% (0.15 vol%)	1.56	Sonication/stirring	3.3@1.5 vol%
[83]	SWCNT	Arc discharge	-	Polyimide	-	toluene	-	0.33wt% (0.33 vol%)	2.15	Sonication	1E-1@vol 6%
[84]	MWCNT	CVD	Iljin Nanotech Ltd.	epoxy	Ozone+UV	acetone	-	0.0048 wt%	1.2	Sonication-DC field applied during curing	1E-5@0.05 wt%
[6]	MWCNT	Arc discharge	-	Polyurethane	-	THF	-	0.005 wt%	3.1	Stirring	10@0.12 wt%
[55]	MWCNT	CVD	Shenzhen Nanotech Port	polypropylene	-	-	-	0.035wt% (0.07 vol%)	4.5	Melt mixing	1E-3@0.09 vol%
[85]	SWCNT	-	Thomas Swan and Co. Ltd.	epoxy	-	-	-	0.23 wt%	-	Stirring	1E-3@0.28 wt%
[85]	SWCNT	-	Thomas Swan and Co. Ltd.	epoxy	sodium hydroxide	ethanol	-	0.05 wt%	-	Stirring/sonication	1E-5@0.1 wt%
[85]	MWCNT	CVD	-	epoxy	-	-	-	0.0025 wt%	-	Stirring	1E-5@0.5 wt%
[86]	MWCNT	CCVD	-	epoxy	-	ethanol	-	0.3 wt%	1.6	Sonication/stirring	1E-4@2.5 wt%
[87]	MWCNT	-	Carbolex	polystyrene	Sodium dodecyl sulfate	H ₂ O	-	0.28 wt%	1.58	Sonication	1E-3 @ 1.5 wt%
[88]	MWCNT	CCVD	-	vinylester	-	-	-	0.5 wt%	-	Sonication/stirring	4E-4@2wt%
[89]	MWCNT	-	Shenzhen Nanport	Bisphenol Acyanate ester	H ₂ SO ₄ /HNO ₃	dichloromethane	500-1500	-	-	Sonication/stirring	3.89 @1 wt%

The percolation threshold values reported in **Table 2-2** are in certain cases several orders higher or lower than those predicted by numerical and statistical studies. This discrepancy may be attributed to the dispersion quality during sample preparation in the experimental studies. Hu et al. [46] discussed that alignment and aggregation are two important parameters that govern the percolation threshold of CNT based nanocomposites. As illustrated by **Figure 2-4**, the percolation threshold decreases with decreasing CNT alignment (characterized by the maximum angle between CNTs). In **Figure 2-5**, aggregation is characterized by an intensity parameter δ , i.e. a uniform filler distribution is provided as δ is approaching unity. The data depicted in **Figure 2-5** indicates an initial decrease in percolation threshold with increasing aggregation (i.e. diminishing δ); then, beyond a certain threshold, the percolation threshold rises sharply.

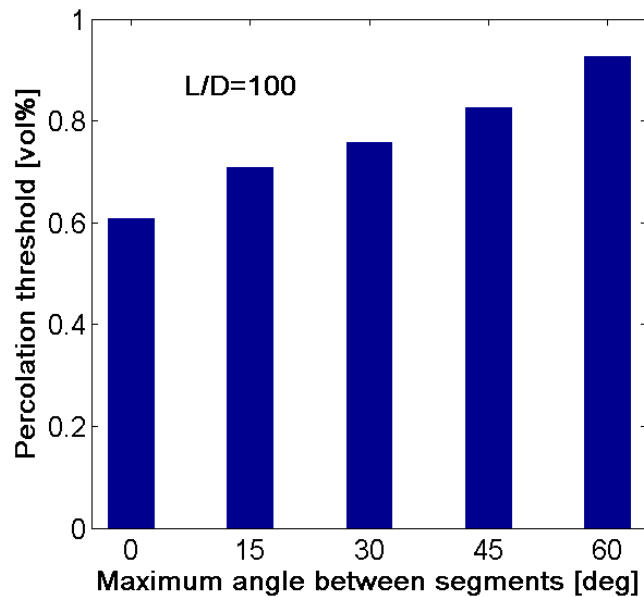


Figure 2-4: Influence of CNT filler alignment on percolation threshold. Figure adapted from [46].

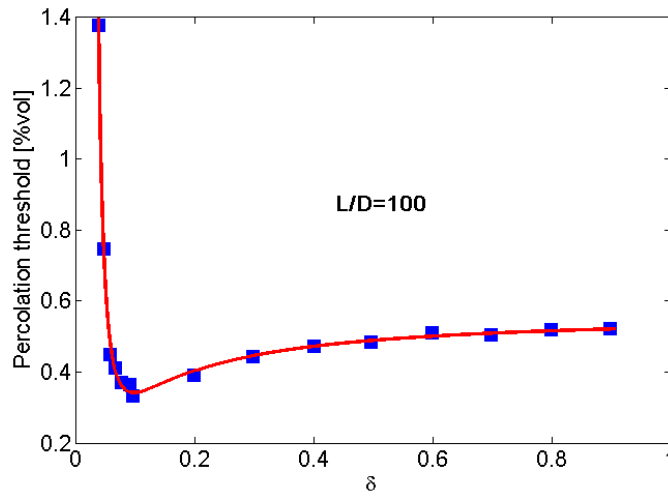


Figure 2-5: Influence of CNT filler aggregation on percolation threshold. Figure adapted from [46].

Percolation thresholds reported for MWCNTs with different aspect ratios show that the percolation threshold decreases as the tube aspect ratio increases [64]. This finding is in agreement with results obtained from numerical studies [46, 90, 91]. It was further observed that molding and curing of CNT/polymers under an electrical field also lowers the percolation threshold [70], which possibly indicates percolation threshold reductions with CNT alignment. A similar behavior was reported by the predictive study in [84]. Some of the extremely low percolation thresholds reported in the technical literature were for nanocomposites prepared by mechanical techniques for dispersing CNT filler in polymer, e.g. shear stirring and melt mixing without sonication. Hence, it may be argued that comparatively low values reported for composite prepared employing mechanical mixing techniques, resulted from a poor dispersion quality. It is further probable to find diminished mechanical properties of these composites due to relatively large agglomerations in the matrix that may act as stress concentrations.

Li et al. [92] studied another aspect of CNT nanocomposites, that is, they conducted a numerical study on the effect of fiber waviness on the percolation threshold. They reported an increase in percolation threshold with increasing waviness. Based on [46], increasing the aspect ratio leads to lower percolation thresholds; yet, increasing the aspect ratio also increases the susceptibility to waviness, which then plays a role in less

favorable (higher) percolation thresholds. Shown in **Figure 2-6**, Li and Chou [90] also evaluated the influence of waviness and aspect ratio on the percolation threshold for a stick-like filler conductive polymeric composite.

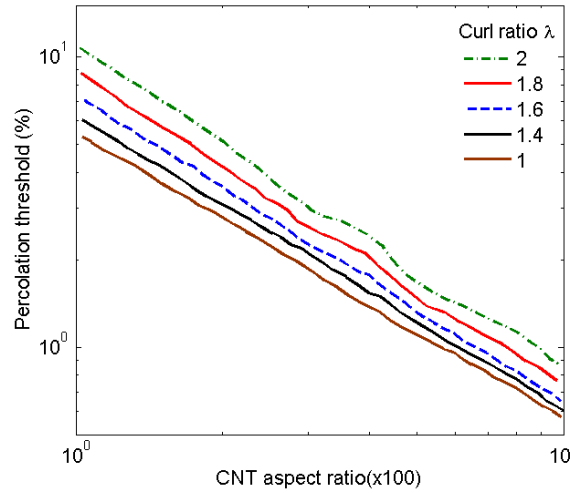


Figure 2-6: Effect of waviness and aspect ratio on percolation threshold [90]. (λ is a parameter indicating the waviness of the nanotube, see [90] for details). Figure adapted from reference [90].

One other important parameter used in investigating these nanocomposites is the critical exponent, t , as indicated in **Table 2-2** values of the critical exponent vary between 1.03 and 5.5 in the experimental studies. On the other hand, a range of t values are also reported in numerical works, varying from 1.17 to 3.1 [49, 90-95]. Hu et al. [46] showed that t is not sensitive to the aspect ratio. Also they showed that fiber curviness does not play a significant role in magnitude of t . For example Li et al. [92] obtained 2.06, 1.88, 1.83 for curl ratios, λ , of 1, 1.43 and 2.03, respectively. ($\lambda = L_{CNT}/L_{effective}$).

2.4 Graphene Based Conductive Composites

2.4.1 Graphene

Graphene, composed of single layer s-p² hybridization of carbon atoms[96], has attracted massive attention from researchers in recent years due to its highly desirable mechanical and electrical properties. Development of new and low cost graphene production techniques have enabled the potential use of this material in mass-produced commercial

applications. Consequently, researchers have started to concentrate on utilization of graphene to improve the electrical and mechanical properties of polymers. In the technical literature different values have been reported as electrical and mechanical characteristics of the GNP. **Table 2-3** provides some of the electrical and mechanical properties of graphene nanosheet (GNS). Electrical mobility and carrier density of GNS is 20 m²/v.s and 10¹² cm⁻², respectively [97]. The corresponding conductivity can be calculated using electrical mobility/conductivity relation, $\sigma = n.e.\mu_e$, where n , e and μ_e are the carrier density, electron charge and electrical mobility, respectively.

Table 2-3 Electrical and mechanical properties of graphene.

Specific surface area m ² g ⁻¹	Electrical Conductivity (S/m)	Tensile Strength GPa	Modulus of Elasticity (TPa)	Electrical mobility (m ² /v.s)	carrier density (cm ⁻²)
2630 [98]	10 ⁸	130 [99]	1 [99]	20[97]	10 ¹² [97]

Several GNS production and synthesis methods have been developed since its discovery in 2004 [100]. Following is a brief review on the different preparation methods that are currently available.

2.5 Synthesis Methods for Graphene Nanoplatelets

2.5.1 Exfoliation of Intercalated Graphite

Graphene nanoplatelets are composed of small numbers of stacked graphene sheets which are widely used in polymeric conductive nanocomposites. Exfoliation of graphite is a common method to produce graphene nanoplatelets. Generally, at first stage, the bonding between the graphene layers is weakened and the interlayer space is increased through intercalation of the graphite. Chemical intercalation of graphite is one of the techniques employed to weaken the interlayer bonding in graphite. This forms a product known as graphite intercalation compound (GIC). As an example, Chen et al. [101] exposed graphite to nitric and sulfuric acid as intercalating agents and expanded graphite is obtained through heating the intercalated graphite. Subsequently, it was sonicated while immersed in alcohol.

2.5.2 *Reduction of Graphite Oxide*

Reduction of the graphene oxide is one of the earliest methods employed to synthesize graphene. Different methods have been developed to produce graphene oxide from graphite. For instance, in Hummers and Offeman's method [102] the graphite is exposed to a combination of sodium nitrate, potassium permanganate and sulfuric acid. It is predicted that hydroxyl and epoxy groups are formed on the surface of the graphene planes and carboxylic groups are formed on the edge of the graphene sheets [103]. The interlayer distance in the graphite oxide is increased in comparison with the graphite. Currently, the graphite oxide can be expanded by employing different methods such as thermal shocking [104]. Subsequently, the expanded graphite oxide is exfoliated by mechanical stirring or sonication leading to formation of graphene oxide. In order to obtain pristine graphene with superior electrical and mechanical properties graphene oxide should be exposed to a reducing agent. Stankovich et al. [105] employed hydrazine hydrate as reducing agent. A wide range of reductants has been employed by researcher to synthesize graphene from graphene oxide. Park et al. [106] have conducted a comprehensive literature review on chemical methods developed for production of graphene nanoplatelets. Some of the reduction methods listed in their review article can be found in [107-109]. As an innovative method, Eswaraiah et al. produced graphene from graphene oxide by using focused solar radiation [110].

2.5.3 *Chemical Vapor Deposition*

Kim et al. [111] synthesized graphene by chemical vapor deposition growth on nickel substrate on a silicon wafer. Isolated graphene sheets are obtained by etching the nickel substrate using a strong acid such as nitric acid. During this process, hydrogen bubbles produced through exposure of the nickel to the acid may potentially damage the graphene sheets; therefore, as an alternative method, they used aqueous ferric chloride (FeCl_3) as etchant agent solution to remove the nickel substrate. Several other researchers have also reported on synthesis of graphene nanosheets using chemical vapor deposition method [112-116].

2.5.4 *Epitaxial Growth on Silicon Carbide*

In this method, Shivaraman et al. [117] heated single crystal silicon carbide (SiC) up to 1200°C to 1600°C under vacuum. Considering the high sublimation rate of silicon in comparison with that of carbon, the Si is sublimated and carbon atoms are left on the substrate forming a graphene coating. They developed and employed a wet etching technique to isolate the formed graphene sheet.

2.5.5 *Preparation of Graphene by Electrochemical Methods*

Zhou et al. [118] have reported preparation of few layers graphene nanoplatelets by electrochemical exfoliation of graphite. They used graphite rods as anode and cathode electrodes and the electrolyte solution is composed of thionin acetate, water, NaCl and dimethyl sulfoxide. Passing the electrical current through the electrolyte, yields edge-exfoliated graphite. They obtained graphene by filtering solution and sonicating the edge-exfoliated graphite. Their structural studies indicate that the thickness of the nanoplatelets is about 3 nm. Synthesizing the graphene nanoplatelets by employing the electrochemical techniques also has been reported in several other research works [119, 120]. For example, Zhang et al. [121], developed an electrochemical based method to reduce the graphite oxide. They carried out electrochemical reduction in KOH aqueous solution.

In addition to the most common methods explained above, several other methods such as arc discharge method [122], unzipping carbon nanotube [123] and sonication of graphite [124] have been employed to synthesize graphene nanosheets.

2.6 **Electrical Behavior of Graphene-Polymer Composites**

Several different polymerization methods such as *in situ* polymerization and melt or dry compounding have been employed by the researchers to prepare graphene based conductive nanocomposites. Zhang et al. [125] prepared polyethylene terephthalate/graphene nanocomposite by melt compounding at 285 °C. They obtained graphene nanosheets by thermal exfoliation and reduction of graphite oxide. **Figure 2-7** compares the effect of exfoliation of the graphite on conductivity behavior of nanocomposite. As can be seen from this figure, the percolation threshold significantly

decreases for the exfoliated fillers. This results in a sharp increase in conductivity. It was shown that the percolation threshold (ϕ_c) was 0.47 vol% and the critical exponent (t) was 4.22 for the best fitting (Eq. 2-1 above).

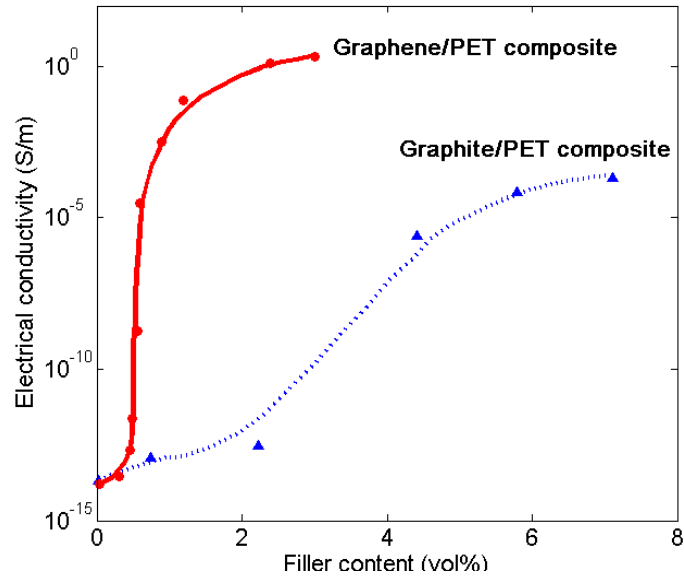


Figure 2-7: Conductivity of graphene vs graphite nanocomposite. (Figure has been adapted from reference [125]).

Stankovich et al. [126] showed that treatment of graphene oxide with organic isocyanates can improve its dispersion in solvent N, N-dimethylformamide through reducing its hydrophilic character. This enables a homogeneous and stable dispersion with thickness ~ 1 nm in the solvent, and solvent eventually facilitates mixing of graphene oxide with polymers. Then polystyrene is added to the solution and graphene oxide is reduced chemically. The authors reported 0.1 vol% and 2.74 for percolation threshold and critical exponent, respectively.

Pang et al. [127] employed Hummers and Offeman's method [102] to obtain graphene oxide. In their method graphene oxide is sonicated in water solution and polyethylene particles and ethanol added to the system undergoing a stirring and sonication. Graphene oxides were reduced with hydrazine. The powder cured under pressure after evaporating the solvent. The percolation threshold and critical exponent were evaluated as 0.07 vol% and 1.26, respectively.

Araby et al. [128] synthesized graphene nanoplatelets by heat treatment of graphite intercalated compound followed by sonication in acetone and in the following acetone was removed by filtration. Styrene butadiene rubber and graphene nanoplatelets were mixed using a roll mill and curing agent was added to the mixture and vulcanized at 150°C. Values of 16.5 vol% and 3 are reported for percolation threshold and critical exponent, respectively.

Du et al. [129] compared the properties of CNT and graphene nanosheet based composites. Composite powders were prepared by sonication of filler and polyethylene in alcohol solution. Then the composite was molded under pressure and elevated temperature of 170 °C. They reported a critical exponent value of 1.67 and 1.08 for MWCNT and graphene nanosheets, respectively. Also, percolation threshold values of 1.67 and 1.08 for MWCNT and graphene nanosheets, respectively. Also, percolation threshold values of 0.14 and 0.95 vol% were reported for MWCNT and graphene nanosheet composites, respectively.

Kujawski et al [130] employed microwave exfoliation method developed by Falcao et al. [131] and Wei et al. [132] to exfoliate the acid washed graphite. The exfoliated graphite is dispersed in hexane and sonicated. Then polydimethylsiloxane was added to the solution that was followed by sonication. The air bubbles and solvent were removed by vacuuming and the mixture and the compound was cured. They reported a sharp drop in resistivity versus filler concentration graph of the composite at 3 wt.%. In a similar work, Shang et al. [133] prepared polyvinylidene fluoride/graphene nanocomposite by *in situ* reduction of the graphene oxide. The schematic given in **Figure 2-8** illustrates the fabrication procedure. They obtained graphene oxide by following the procedure developed by Hummers and Offeman [102]. They reported 1.29 vol% and 0.51 for dielectric constant percolation threshold and critical exponent, respectively.

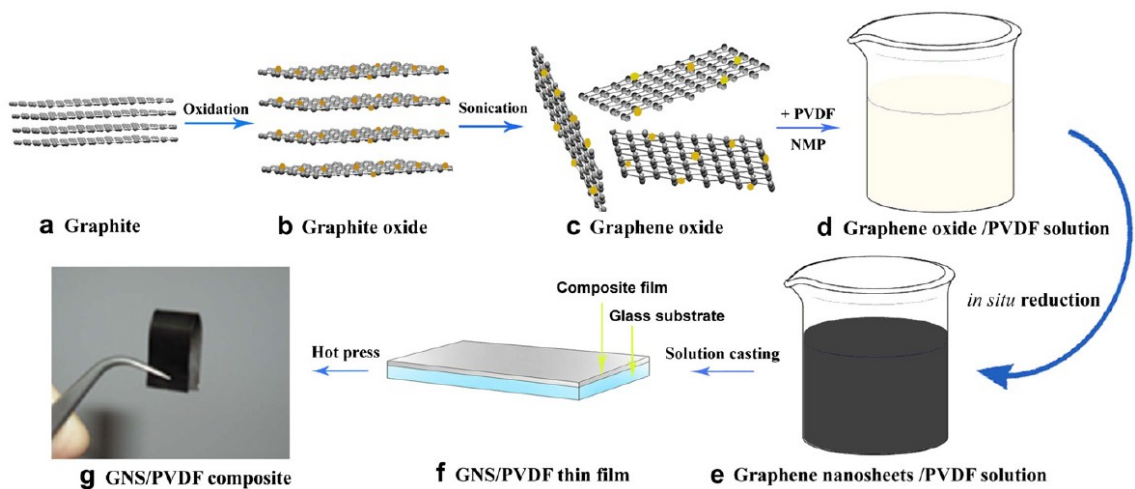


Figure 2-8: Illustration of procedure to fabricate graphene/polyvinylidene fluoride conductive nanocomposite Special permission is obtained from [133] to re-print.

Vadukumpully et al. [134] sonicated graphite in cetyltrimethylammonium bromide (CTAB) and acetic acid and then heated in inert atmosphere and washed graphene sheets. Graphene was dispersed in DMF and Polyvinyl Chloride (PVC) was dissolved in DMF. Later, PVC solution was added to the graphene mixture undergoing a sonication. The mixture was cured at 120°C. Electrical resistivity measurements revealed a sharp increase in the conductivity when filler concentration increased from 0.6 to 1.3 vol%.

Mahmoud [135] investigated the effect of two different fabrication methods on electrical properties of graphene reinforced polyethylene oxide (PEO) nanocomposites. In this study, graphite oxide was prepared using Hummers and Offeman's method [102]. Then graphite oxide was exfoliated by rapid heating. Acetonitrile was used as reducing agent to obtain graphene from graphene oxide. First, graphene was dispersed in distilled water through sonication and similarly polyethylene oxide were dispersed and solved in distilled water undergoing a sonication at elevated temperature, and then the solutions were mixed and cured at 60°C. In the second method, polyethylene oxide powder and graphene were mixed using mixer and the compound was molded under high temperature and pressure. Conductivity measurement analysis for different volume fractions showed that solvent based fabrication method yields a lower percolation threshold than the blending method, but the maximum conductivity is approximately same for the both

methods. Percolation threshold was reported as 0.5 and 0.3 vol% for blending and solvent based method, respectively. Critical exponent, t , was estimated to be 1.2 for solvent and 3.6 for blending based methods.

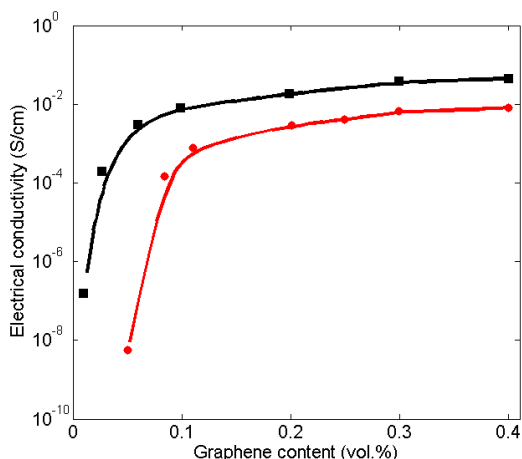


Figure 2-9: Electrical conductivity vs. graphene loading for one-step (circle) and two-step (square) prepared nanocomposite. Figure has been adapted from reference [136].

Hu et al. [136] developed a two-step method to prepare graphene/polymer nanocomposites. In first step graphene oxide sheets produced by Hummers method [102] were coated with ultrahigh molecular weight polyethylene (UHMWPE). Graphene oxide was dispersed in diluted ethanol and sonicated. Subsequently, polymer powder was added to the solution and stirred. The solvent was removed from the system by heating and vacuuming. In second step, the graphene oxide coated with polymer was reduced by adding to hydrazine. As a reference, another sample was prepared by employing a one-step method. Graphene oxide and polymer powders dispersed in ethanol/water solution undergoing sonication. In the following hydrazine was added to the solvent. The polymer coated graphenes were isolated by filtration. Filtered and water washed compound was dried and cured at 200 °C in pressed mold. **Figure 2-9** illustrates the conductivity versus filler loading curves of the one-step and two-step methods utilized to produce nanocomposites. A percolation threshold of 0.028 vol.% and 0.085 vol.% was estimated for two step and one step derived nanocomposites, respectively. **Figure 2-10** shows the scanning electron microscopy (SEM) images for 0.1 vol.% graphene-polymer powders. As illustrated by **Figure 2-10.a** and **Figure 2-10.b**, they found that two-step method

yields a superior exfoliation and dispersion of graphene in polymer powder. **Figure 2-10.c** and **10.d** indicate the agglomeration of graphene sheets and some polymer rich regions with no graphene. Conductivity test results and SEM images indicate the superiority of the two-step preparation method.

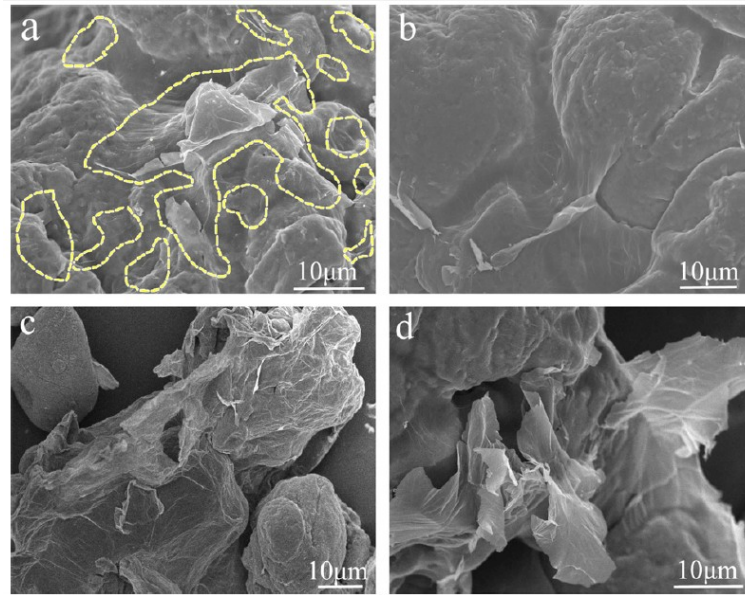


Figure 2-10: SEM images of two-step graphene/UHMWPE powders. The selected regions in (a) shows graphene sheets. Two step (a and b) and one-step (c and d) derived composite powder. Dashed line shows the boundary of graphene. Permission is obtained from [136] to re-print.

Yousefi et al. [137] studied the self-alignment of fibers in epoxy/graphene nanocomposites and its effect on the anisotropy and electrical behavior of the prepared nanocomposites. Polymer/graphene was prepared through *in situ* polymerization and reduction of the graphene oxide. Graphene oxide was synthesized using the method described in [138, 139]. Graphene oxide was dispersed in aqueous emulsion of epoxy by stirring and then graphene oxide was reduced by adding hydrazine as to the solution reductant. Solvent was removed from the mixture and hardener was added and the compound cured in the oven. **Figure 2-11.a** and **Figure 2-11.b** are the transmission electron microscope (TEM) images of the composite for two different filler loadings, 0.5 wt% and 2wt%, respectively. They observed that the arrangement of GNPs in the polymer is governed by the filler loading. In **Figure 2-11.a** reduced graphene sheets are

randomly dispersed in the polymer, meanwhile in **Figure 2-11.b** fillers are aligned into a layered structure.

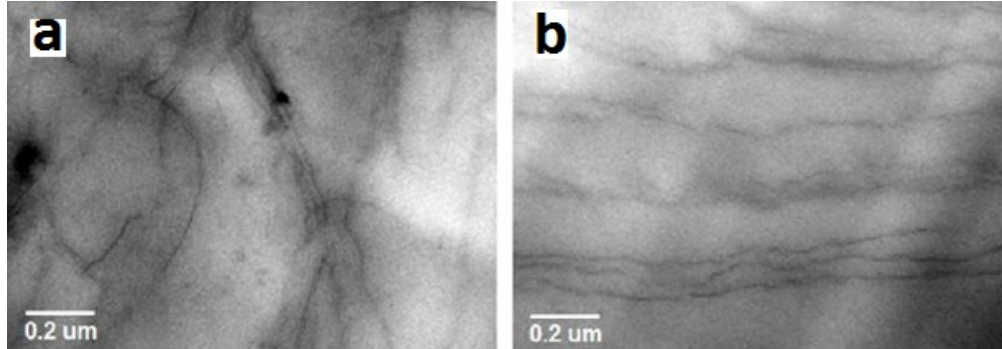


Figure 2-11: TEM images of (a) 0.5 wt% composite and (b) 2wt% composite. Special permission is obtained from [137] to re-print.

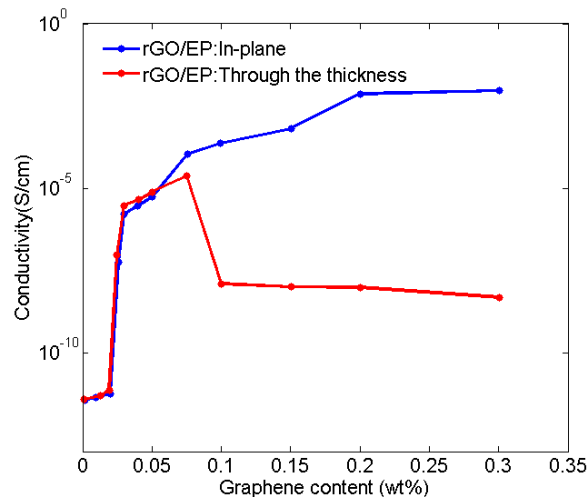


Figure 2-12: In-plane and through-the -thickness conductivity of composite versus filler loading. Figure has been adapted from reference [137].

Figure 2-12 shows the in-plane and through-the-thickness electrical conductivity measurements versus filler loading. It can be observed that for low filler loadings, the composite samples show almost identical electrical behavior in both directions and directionality is insignificant. The anisotropy appears as filler mass fraction increases, which is in agreement with the finding from TEM images. They reported a value of 0.12

vol.% as percolation threshold obtained through fitting the power-law description to the acquired data.

Li et al. [140] reduced and functionalized graphene oxide by refluxing with octadecylamine. They employed the technique presented in [140, 141] to oxidize natural graphite. Graphene oxide was dispersed in deionized water by sonication. Graphite oxide suspension and octadecylamine solved in ethanol was mixed in three neck flask and the solution was refluxed through mechanical stirring. The graphene oxide-octadecylamine (GO-ODA) was isolated by filtration and rinsing in ethanol and dispersed and exfoliated in tetrahydrofuran (THF) by ultrasonication. Polystyrene was added to the suspension and mixed by stirring. Functionalizing by octadecylamine converts the hydrophilic graphene oxide to hydrophobic; hence, increasing their solubility in tetrahydrofuran. GO-ODA sheets are electrically conductive while graphene oxide is insulator. The solvent was removed and the mixture was compression molded and cured under vacuum. **Figure 2-13** depicts the conductivity of the functionalized and non-functionalized graphene oxide nanocomposite versus filler loading. Lower percolation threshold of GO-ODA (0.45 vol.%), in comparison with that of GO composite, proves the high dispersion quality of functionalized graphene oxide. Higher conductivity of GO-ODA nanocomposite indicates the superior conductivity of the octadecylamine treated GO.

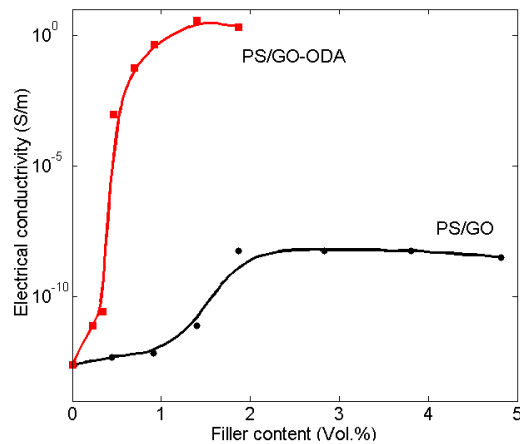


Figure 2-13: Conductivity-filler concentration of functionalized and non-functionalized graphene oxide nanocomposite. Figure has been adapted from reference [140].

Zhang et al. [142] studied the effect of graphene sheet chemistry on the electrical characteristics of graphene nanocomposites. Graphene nanosheets were prepared through reduction of the graphene oxide. As listed in **Table 2-4**, employing different preparation methods provides graphene sheets with different oxygen contents. Thermal exfoliation at different temperatures and ambient pressure gives graphene sheets with different oxygen/carbon ratios. In this study, composite samples were prepared by blending. Graphene sheets were dispersed in methylene dichloride by sonication and polymethyl methacrylate was added to the solution and blended by mechanical stirring. The solvent was evaporated by vacuuming and composite was hot pressurized to molds.

Table 2-4: Different preparation methods and graphene sheets oxygen content (table adapted from [142]).

Sample	Temperature (°C)	Atmosphere	BET surface area (m ² /g)	C/O ratio
Graphene-13.2	1050	Air	700	13.2
Graphene-9.6	145	Vacuum	660	9.6
Graphene-5.0	135	Vacuum	758	5.0

Using the SEM images given in **Figure 2-14**, authors [142] concluded that the quality of dispersion is governed by the surface chemistry of graphene sheets. Quality of dispersion suffers as oxygen content on the surface of graphene sheets increasing. This conclusion can be verified through considering the conductivity versus filler loading graphs for polymers reinforced by graphene sheets with different surface chemistries given in **Figure 2-15**. Percolation threshold decreases as the oxygen content at the surface of the graphene sheets is decreasing, but saturated conductivity is approximately the same for all of the samples. This may indicate the conductivity of the composite is dominated by the tunneling conductivity.

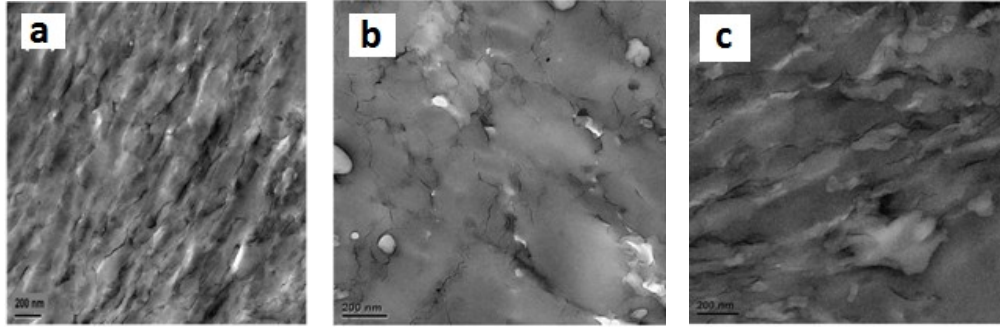


Figure 2-14: SEM images for composites with 2.67 vol% graphene content (a) graphene 13.2, (b) graphene 9.6, (c) graphene 5.0. Special permission is obtained from [142] to re-print.

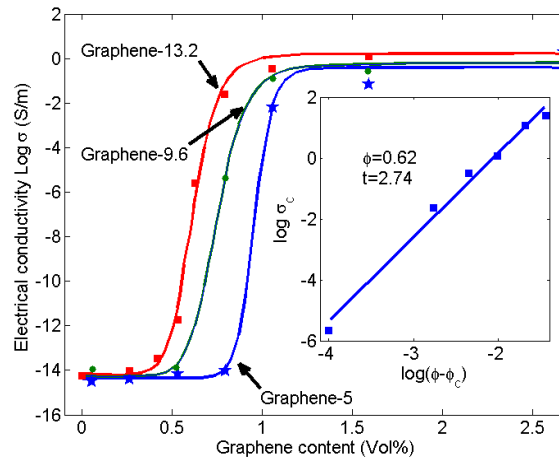


Figure 2-15: Conductivity-filler content of composites reinforced by graphene sheets with different surface chemistry. Figure has been adapted from reference [142]

Hsiao et al. [143] investigated the effect of surfactant and surface treatment on electromagnetic interference performance and electrical conductivity of graphene nanosheet (GNS)/water-borne polyurethane (WPU) composites. The authors reported that GNS synthesized by using NaBH_4 as reducing agent, were employed. In order to obtain surface treated graphene nanosheets, stearyl trimethyl ammonium chloride was adsorbed on the surface of the graphene oxides before applying the reducing agent. Surface treated graphene sheets (S-GNS) and pristine graphene sheets (P-GNS) were mixed with polymer by solution mixing and molded and dried in oven. **Figure 2-16** shows the SEM

images of P-GNS/WPU and S-GNS/WPU nanocomposites. P-GNS/WPU nanocomposites show a poor quality of the dispersion of the filler in the polymer matrix. The red arrows in **Figure 2-16.a** indicate the poor compatibility of the P-GNS with WPU polymer. On the other hand, **Figure 2-16.b** shows the high quality of the S-GNS dispersion in WPU polymer.

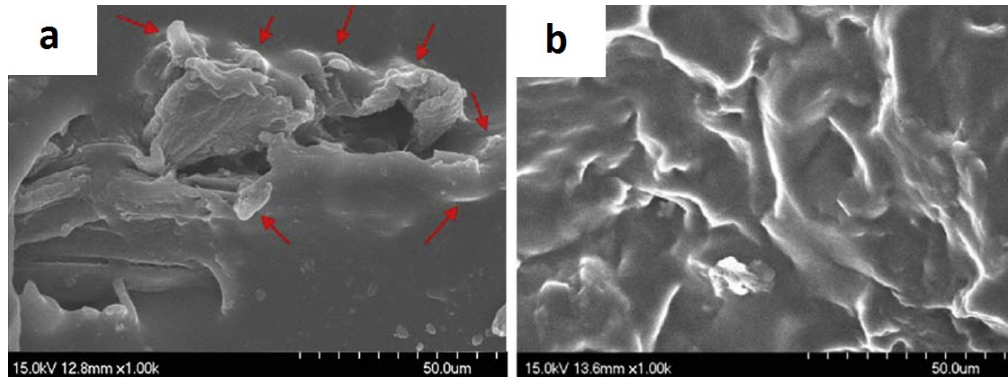


Figure 2-16: Effect of surfactant on dispersion quality of GNS dispersion in WPU matrix. 1 vol% (a) P-GNS/WPU, (b) S-GNS/WPU. Special permission is obtained from [143] to re-print.

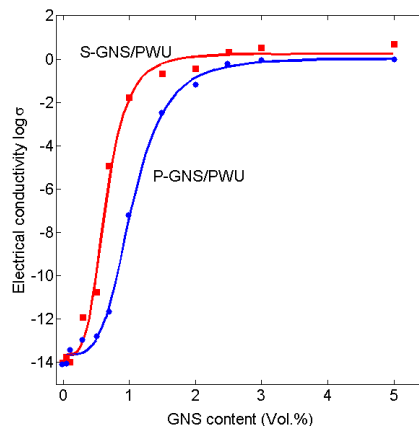


Figure 2-17: Conductivity-filler loading curves for S-GNS/WPU and P-GNS/WPU (Figure has been adapted from reference [143]).

Table 2-5 Some of the electrical properties reported for graphene based conductive nanocomposites.

Filler				Polymer	Treatment	Solution	Aspect ratio	thickness	ϕ_c	t	Mixing	Conductivity (S/cm)
Ref	Type	Synthesis Method ¹	Supplier									
[125]		Thermal expansion and reduction of GO	-	polyethylene terephthalate	-	-	146	1.57 nm	0.47 vol%	4.22	Melt compounding	1E-3 @1.25 vol%
[126]	-	In situ reduction of graphite oxide	-	polystyrene	phenyl isocyanate	DMF	-	-	0.1 vol.%	2.74	Solution mixing	1E-2@2.5 vol.%.
[127]	-	In situ reduction of graphite oxide	-	polyethylene	-	water/ethanol	455	1.1 nm	0.07 vol%,	1.26	Solution mixing/sonication	1E-4@0.31 vol%
[128]	-	Rapid heating of GIC and sonication	-	Styrene butadiene rubber	-	-	-	3.55 nm	16.5 vol%	3	Roll mill mixing	1E-7 @ 32 vol%
[129]	-	Arc discharge exfoliation of graphite oxide	-	high density polyethylene	-	Alcohol	-	-	0.95 vol%	1.08	Solution dispersion and hot press molding	1E-6@1.6 vol%
[130]	-	Microwave irradiation exfoliation	-	polydimethylsiloxane	-	hexane	50-1000	10-200 nm	3 wt%	3	Solution based sonication	0.1 @15 wt.%
[137]	-	In situ reduction of GO	-	epoxy	-	-	-	-	0.12 vol.%	-	Stirring in aqueous solution	1E-2@2wt%
[142]	Graphene C/O ratio: 13.2	Thermal exfoliation of GO at 1050 °C/Air	-	polymethylmethacrylate	-	Methylene dichloride	-	-	0.62 vol.%	-	Solution blending/sonication	2.38E-2@0.78 vol.%
[142]	Graphene C/O ratio: 9.6	Thermal exfoliation of GO at 145 °C/vacuum	-	polymethylmethacrylate	-	Methylene dichloride	-	-	0.77 vol.%	-	Solution blending/sonication	3.93E-6@0.78 vol.%,
[142]	Graphene C/O ratio: 5.0	Thermal exfoliation of GO at 135 °C/Vacuum	-	polymethylmethacrylate	-	Methylene dichloride	-	-	0.92 vol.%	-	Solution blending/sonication	1E-14@0.78 vol.%,
[143]	-	Reduction of GO by NaBH ₄	-	water-borne polyurethane	-	Hexamethylene diisocyanate	-	-	0.7 vol%	-	Solution mixing	5.1 E-2 @5 vol.%
[143]	-	Reduction of GO by NaBH ₄	-	water-borne polyurethane	Stearyl trimethyl ammonium chloride	Hexamethylene diisocyanate	-	-	0.5 vol%	-	Solution mixing	1 E-2 @3.5 vol.%
[144]	-	Reduction of GO	-	Poly vinylidene fluoride	-	DMF	-	1.2 nm	1.9 wt %	-	Solution mixing and sonication	1E-7@20 vol%
[145]	-	-	Vorbeck™	Polyurethane acrylate	-	tetrahydrofuran	-	-	0.07 vol%	5.17	Solution based sonication/ Cured	-
[145]	-	-	Vorbeck™	Polyurethane acrylate	-	tetrahydrofuran	-	-	0.23 vol%	-	Solution based sonication/ un-Cured	-

Figure 2-17 shows the surfactant effect on the conductivity and percolation behavior of GNS/WPU composites. Composites prepared with surface treated GNS shows a lower percolation threshold ($\sim 0.5\text{vol.}\%$) and higher conductivity due to good quality of dispersion. **Table 2-5** gives a summary of the electrical characteristics of the discussed graphene/polymer composites.

As it is listed in **Table 2-5**, values of critical exponent have been reported to vary in a wide range, from 1.08 to 5.17. Based on statistical percolation theory, value of t is expected to be governed by the geometry and dimension of the problem. Composite preparation method and quality of dispersion play an important role in value of t , for example [135] reported two different values for t . Analyzing the conductivity test measurements for melt compounding and solvent mixing technique gives values of 1.2 and 3.6, respectively. Oskouyi et al [146] predicted a mean value of 2.01 for t , by developing Monte Carlo and finite element based model for 2D circular disks uniformly dispersed in 3D space.

One of the interesting characteristics of the conductive polymer/graphene nanocomposites that allows them to be considered for strain sensing applications is their piezoresistivity behavior. Piezoresistive materials show changes in their resistivity when subjected to strain due to mechanical loading. Several studies have investigated the piezoresistivity of the graphene/polymer nanocomposites [147-151].

As it is outlined, a considerable number of publications have been devoted to investigate the electrical behavior of graphene/polymer nanocomposites. To the best of the author's knowledge, all of the research in this field have been limited to the electrical properties of nanoplatelet based nanocomposites with filler sizes varying from a few microns to several hundreds of micron and thickness varies from a few nm to several nm. Investigating the electrical conductivity of polymers with single layer graphene is lacking in the literature. It is important to develop a data-base on the percolation and electrical behavior of polymers reinforced with actual single-layer graphene sheets. Developing methods to synthesize small size graphene nanosheets, known as graphene nanoribbons,

such as lithographic [152], chemical [124], solution-based oxidative method [153], and chemical vapor deposition [154], necessitate conducting research on submicron size graphene/polymer nanocomposite. There are a few experimental work conducted to investigate the mechanical properties of small size graphene/polymer composites and to the best of the author's knowledge there is no report on electrical and percolation behavior of polymers reinforced by submicron graphene sheets. Oskouyi et al. [146, 155, 156] investigated the electrical and percolation behavior of these materials by developing a numerical 3D continuum model based on Monte Carlo method. In [157] author studied the effect of particle size and tunneling distance on percolation threshold. In another study, [146], they developed a model based on Monte Carlo and finite element method to predict the piezoresistivity behavior of graphene/polymer nanocomposites.

2.7 Carbon Black Based Conductive Composites

Carbon black is a material widely employed in a broad range of industries such as paints, inks, pigments and rubbers [158, 159]. It is a product of incomplete combustion of petroleum derivatives [160]. CB has been commonly used to improve the mechanical properties of polymers. An example is its use to enhance the mechanical properties of styrene-butadiene in tire manufacturing industry [161, 162]. Also it was one of the earliest conductive fillers employed for conductive nanocomposite applications. They can be used to improve the electrical properties and electromagnetic shielding effectiveness of insulator polymers [163, 164]. Low cost of carbon black can be considered as the main reason behind its wide industrial applications. Percolation threshold for CNT and graphene based nanocomposites is much lower than polymers made conductive by CB particles. Considering the lower percolation threshold, higher conductivity and superior mechanical properties of CNT, graphene based composites, researchers in the field of conductive composites have focused their effort on these type of conductive composites in recent years. In the following some of the research works on the CB/polymer composites are listed as example.

Ou et al. [165] assessed the electrical behavior of acrylonitrile-co-butadiene-co-styrene (ABS) polymer made conductive through dispersion of CB particles. The composite was prepared by twin-screw extrusion at 200-240°C. They evaluated the conductivity of the

samples for AC and DC currents. Some of the ABS/CB samples were chopped and fed to the screw extruder. As shown in **Figure 2-18**, there is a sharp increase in the conductivity of twice extruded samples between 8 and 10 vol% of fillers. Poor electrical performance is reported for one-time extruded samples that can be explained by existence of non-uniform dispersion of CB particles as well as pore and voids in the one-time extruded samples.

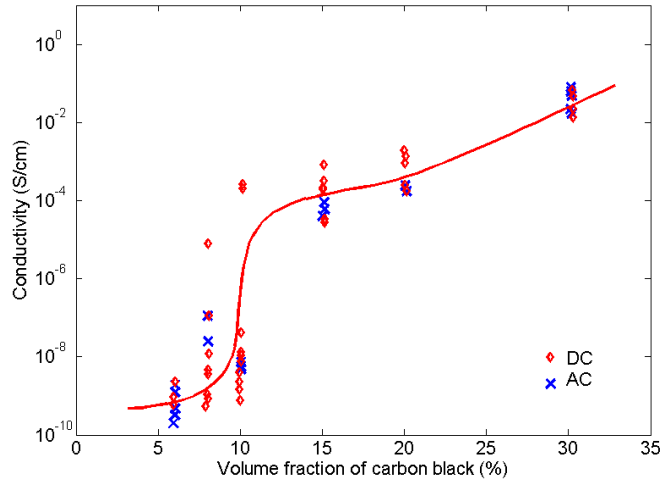


Figure 2-18: Electrical conductivity of CB/ABS composite vs. filler concentration for alternative/direct current. Figure has been adapted from reference [165].

Li et al. [166] developed a CB based polymeric composite for gas sensing applications. CB/styrene was prepared by *in-situ* polymerization method. Electrical conductivity/filler concentration graphs showed a singularity at 10 vol%. Samples showed a 10^5 to 10^6 times increase in resistivity when they are exposed to tetrahydrofuran, moreover the developed sensors showed a good repeatability during the test.

Katada et al. [167] investigated the electrical conductivity of poly (methyl methacrylate) (PMMA) filled with CB particles. CB and PMMA were mixed in a two-roll mill and compound was molded under pressure and elevated temperature and followed by cold water quenching. It was found that critical volume fraction for the samples was 6 vol% and value of $1000 \Omega \cdot \text{cm}$ was reported as resistivity of the samples at 10 vol% of CB.

Koysuren et al. [168] investigated the effect of two different preparing methods on conductivity of nylon 6/CB composites. Samples prepared by Masterbatch dilution method showed better conductivity in comparison with those prepared by melt mixing method; however, the difference in the conductivity was not significant for higher filler concentration.

Hwang et al. [169] prepared CB based conductive nanofiber composites by electrospinning method. CB particles were dispersed in N, N-dimethyl formamide/chloroform solvent and sonicated for 1.5 hr. Then polyurethane was added to the CB solution. Applied 25 kV electrical field accelerated the polymer towards the collecting drum. Prepared samples showed percolation behavior at filler loadings between 5.54 and 6.02 vol%. Fitting the exponential equation to the conductivity-volume fraction measurements gave a value of 2.165 for critical exponent.

Ma et al. [170] investigated the electrical and percolation behavior of epoxy/polyetherimide/carbon black composite system. The composite samples were prepared employing solution blending method. Epoxy and polyetherimide were dissolved in dichloromethane, and subsequently, CB particles were dispersed in the solution by ultrasonication. Curing agent was added to the solution after removing the solvent, and the molded samples were cured at elevated temperature. Volume resistivity versus CB content graph shows a sharp decrease in resistivity when filler concentration reaches 0.5 wt%.

Ji et al. [171] evaluated the current-voltage and piezoresistivity behavior of epoxy resin filled with conductive CB and sprayed CB particles that are hollow and solid spheres, respectively. Volume resistivity of conductive CB samples was reported to decrease monotonically with no percolation behavior while sprayed CB filled resin showed percolation behavior. Volume resistivity of samples filled with conductive CB fluctuated as mechanical strain increased. Resistivity of sprayed CB based samples decreased monotonically as compressive mechanical load was increased. Piezoresistivity effect declined as CB concentration was increasing. According to the authors, evaluation of the resistivity of conductive CB based samples for different levels of the applied electrical

field indicated the non-ohmic behavior of the prepared samples. Electrical resistivity decreased as intensity of the applied electric field was increasing. Non-ohmic behavior was not observed for the epoxy resin filled with spray CB particles.

Liu et al. [172] evaluated the electrical characteristics of CB/Polyvinyl chloride samples prepared by melt-mixing method. In this study, a sharp drop in the resistivity of samples was observed when filler loading exceeded 4 wt%. Evaluation of resistivity at different temperatures indicated that resistivity decreased as temperature was increasing. Resistivity of samples gradually decreased up to around 150~180°C. Trend of resistivity decrease was reported to change around 150~180°C and resistivity dropped sharply as temperature was further elevated.

Yacubowicz et al. [173] studied the electrical percolation and conductivity of CB/Polyethylene systems. Samples were prepared by dry mixing of the CB and polyethylene followed by compression molding at 190-200°C. Two different types of polyethylene, Lupolen Z and ultrahigh molecular weight polyethylene (UHMWPE), were used with average particle sizes of 500 and 100 μm , respectively. Authors used three different CB particles with different sizes i.e. 300, 180 and 5000 \AA . Electrical conductivity measurements showed a resistivity of 10 $\Omega\cdot\text{m}$ at 1 vol%. Samples prepared through dispersion of different types of CB particles in polyurethane showed that samples filled with smaller particles have a lower percolation threshold.

H. Zois et al. [174] studied the percolation behavior in CB filled polypropylene composites. CB and polypropylene were mixed in a mixing chamber and the compound was cured under applied pressure. Investigations show that insulator-to-conductive transition occurs at 6.2 wt%. Best fitting gives a value of 1.79 for critical exponent. Authors commented that the electrical resistivity measurements indicate that electrical conductivity of samples was governed by the electrical current frequency. Electrical conductivity increased as frequency was increasing. Frequency effect on the conductivity was reported to be more deterministic for composites with lower volume fraction, and dependence of conductivity on frequency declined as CB loading was decreasing.

Zavickis et al. [175] investigated the effect of different manufacturing techniques on electrical behavior of polyisoprene natural rubber made conductive through dispersion of high-structure carbon black particles by roll-mixing, solvent based mixing with mechanical and ultrasonication mixing. The correlation between the conductivity and filler concentration shown in **Figure 2-19** indicates the importance of mixing method on conductivity of CB/polyisoprene conductive composites. Ultrasound-mixed samples showed the lowest percolation threshold that is around 3.3 parts per hundred rubber, (p.h.r). Percolation threshold occur around 7.6 and 8.1 p.h.r for mechanically-mixed and roll-mixed samples, respectively. Values of 4.1, 5.65 and 6.6 are reported as critical exponent for ultrasound mixed, mechanically mixed and roll-mixed samples, respectively; however, the value of saturated conductivity shows no meaningful difference for samples prepared by different mixing methods. Values of 4.1, 6.6 and 5.65 are reported as critical exponents for ultrasound-mixed, mechanically-mixed and roll-mixed samples, respectively.

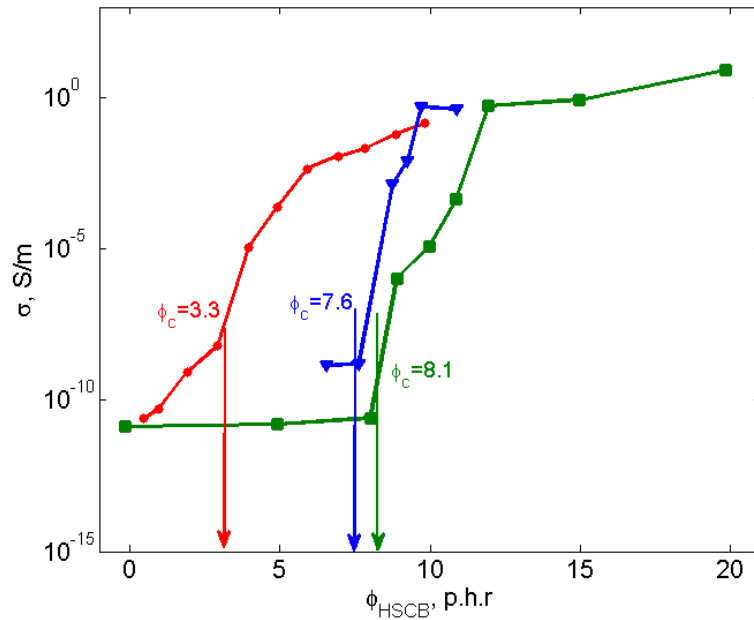


Figure 2-19: Electrical conductivity of CB/ polyisoprene composite versus filler concentration for different mixing methods (red: ultrasound-mixed, blue: mechanically mixed, green: roll-mixed). Figure has been adapted from reference [175].

2.1 Conclusion

In this chapter about 160 papers on electrical behavior of polymeric composites made conductive through dispersion of carbon based additives, i.e. CNT, graphene nanoplatelets and CB, were investigated. A review on different synthesis methods for these carbon fillers is outlined. Effects of different filler synthesizing and composite preparing methods on conductivity and percolation threshold were investigated. The important role of composite preparation and filler dispersion techniques on percolation threshold of polymeric conductive nanocomposites was underlined. The other deterministic factors, such as filler geometry, aspect ratio and size that govern the electrical behavior of conductive composites are also included in the review. Several papers devoted to numerical and analytical study of conductive nanocomposites were reviewed to provide an understanding on governing parameters; such as, fiber alignment, agglomeration, aspect ratio and waviness, for percolation behavior of conductive composites. The feasibility of employing the conductive nanocomposites for sensor application was evaluated through reviewing the papers on electro-mechanical behavior (i.e. piezoresistivity effect) and electro-thermal behavior (i.e. temperature-resistivity correlation) of conductive nanocomposites. This review article highlights the necessity of conducting further experimental, analytical and numerical studies to evaluate the effect of governing parameters, such as filler type, surface treatment, manufacturing method, on electrical behavior of conductive nanocomposites to tailor their behavior for specific industrial applications.

2.2 Bibliography

- [6] H. Koerner, W. D. Liu, M. Alexander, P. Mirau, H. Dowty, and R. A. Vaia, "Deformation-morphology correlations in electrically conductive carbon nanotube thermoplastic polyurethane nanocomposites," *Polymer*, vol. 46, pp. 4405-4420, May 26 2005.
- [15] M. Al-Saleh, "Nanostructured Conductive Polymeric Materials," PhD, Chemical and Materials Engineering, University of Alberta, Edmonton, Alberta, Canada, 2009.
- [16] W. Henry and E. George, "Electrically conducting cements containing epoxy resins and silver," ed: Google Patents, 1956.
- [17] J. P. Franey, T. E. Graedel, G. J. Gualtieri, G. W. Kammlot, J. Kelber, D. L. Malm, *et al.*, "The morphology and corrosion resistance of a conductive silver-epoxy paste," *Journal of Materials Science*, vol. 16, pp. 2360-2368, 1981/09/01 1981.
- [18] H. Jiang, K.-s. Moon, Y. Li, and C. Wong, "Surface functionalized silver nanoparticles for ultrahigh conductive polymer composites," *Chemistry of Materials*, vol. 18, pp. 2969-2973, 2006.

- [19] A. J. Lovinger, "Development of electrical conduction in silver-filled epoxy adhesives," 1979.
- [20] D. W. Marshall and J. C. Agarwal, "Copper filled conductive epoxy," ed: Google Patents, 1976.
- [21] B. Lin, G. A. Gelves, J. A. Haber, and U. Sundararaj, "Electrical, rheological, and mechanical properties of polystyrene/copper nanowire nanocomposites," *Industrial & engineering chemistry research*, vol. 46, pp. 2481-2487, 2007.
- [22] M. H. Al-Saleh, G. A. Gelves, and U. Sundararaj, "Copper nanowire/polystyrene nanocomposites: lower percolation threshold and higher EMI shielding," *Composites Part A: Applied Science and Manufacturing*, vol. 42, pp. 92-97, 2011.
- [23] M. Arjmand, M. Mahmoodi, G. A. Gelves, S. Park, and U. Sundararaj, "Electrical and electromagnetic interference shielding properties of flow-induced oriented carbon nanotubes in polycarbonate," *Carbon*, vol. 49, pp. 3430-3440, 2011.
- [24] S. Iijima, "Helical Microtubules of Graphitic Carbon," *Nature*, vol. 354, pp. 56-58, Nov 7 1991.
- [25] O. Lourie and H. D. Wagner, "Evaluation of Young's modulus of carbon nanotubes by micro-Raman spectroscopy," *Journal of Materials Research*, vol. 13, pp. 2418-2422, Sep 1998.
- [26] M. B. Nardelli, B. I. Yakobson, and J. Bernholc, "Brittle and ductile behavior in carbon nanotubes," *Physical Review Letters*, vol. 81, pp. 4656-4659, Nov 23 1998.
- [27] D. A. Walters, L. M. Ericson, M. J. Casavant, J. Liu, D. T. Colbert, K. A. Smith, *et al.*, "Elastic strain of freely suspended single-wall carbon nanotube ropes," *Applied Physics Letters*, vol. 74, pp. 3803-3805, Jun 21 1999.
- [28] G. J. W. D. Qian, W.K. Liu, M.F. Yu, R. S. Ruoff, G. J. Wagner, W. K. Liu, "Mechanics of carbon nanotubes," *Appl. Mech. Rev.*, vol. 55, pp. 495-533, 2005
- [29] P. C. Ma, N. A. Siddiqui, G. Marom, and J. K. Kim, "Dispersion and functionalization of carbon nanotubes for polymer-based nanocomposites: A review," *Composites Part a-Applied Science and Manufacturing*, vol. 41, pp. 1345-1367, Oct 2010.
- [30] M. Scarselli, P. Castrucci, and M. De Crescenzi, "Electronic and optoelectronic nano-devices based on carbon nanotubes," *Journal of Physics: Condensed Matter*, vol. 24, p. 313202, 2012.
- [31] J. Prasek, J. Drbohlavova, J. Chomoucka, J. Hubalek, O. Jasek, V. Adam, *et al.*, "Methods for carbon nanotubes synthesis-review," *Journal of Materials Chemistry*, vol. 21, pp. 15872-15884, 2011.
- [32] J. Liu, S. S. Fan, and H. J. Dai, "Recent advances in methods of forming carbon nanotubes," *Mrs Bulletin*, vol. 29, pp. 244-250, Apr 2004.
- [33] X. L. Zhao, M. Wang, M. Ohkohchi, and Y. Ando, "Morphology of carbon nanotubes prepared by carbon arc," *Japanese Journal of Applied Physics Part I-Regular Papers Short Notes & Review Papers*, vol. 35, pp. 4451-4456, Aug 1996.
- [34] X. Zhao, M. Ohkohchi, M. Wang, S. Iijima, T. Ichihashi, and Y. Ando, "Preparation of high-grade carbon nanotubes by hydrogen arc discharge," *Carbon*, vol. 35, pp. 775-781, 1997.
- [35] N. Parkansky, R. L. Boxman, B. Alterkop, I. Zontag, Y. Lereah, and Z. Barkay, "Single-pulse arc production of carbon nanotubes in ambient air," *Journal of Physics D-Applied Physics*, vol. 37, pp. 2715-2719, Oct 7 2004.
- [36] Y. Y. Tsai, J. S. Su, C. Y. Su, and W. H. He, "Production of carbon nanotubes by single-pulse discharge in air," *Journal of Materials Processing Technology*, vol. 209, pp. 4413-4416, May 1 2009.
- [37] Y. Saito, M. Okuda, and T. Koyama, "Carbon nanocapsules and single-wall nanotubes formed by arc evaporation," *Surface Review and Letters*, vol. 3, pp. 863-867, Feb 1996.
- [38] H. W. Kroto, J. R. Heath, S. C. O'Brien, R. F. Curl, and R. E. Smalley, "C-60 - Buckminsterfullerene," *Nature*, vol. 318, pp. 162-163, 1985.
- [39] T. Guo, P. Nikolaev, A. G. Rinzler, D. Tomanek, D. T. Colbert, and R. E. Smalley, "Self-Assembly of Tubular Fullerenes," *Journal of Physical Chemistry*, vol. 99, pp. 10694-10697, Jul 6 1995.

- [40] M. Kusaba and Y. Tsunawaki, "Production of single-wall carbon nanotubes by a XeCl excimer laser ablation," *Thin Solid Films*, vol. 506, pp. 255-258, May 26 2006.
- [41] M. Joseyacaman, M. Mikiyoshida, L. Rendon, and J. G. Santiesteban, "Catalytic Growth of Carbon Microtubules with Fullerene Structure," *Applied Physics Letters*, vol. 62, pp. 202-204, Jan 11 1993.
- [42] O. Lee, J. Jung, S. Doo, S. S. Kim, T. H. Noh, K. I. Kim, *et al.*, "Effects of temperature and catalysts on the synthesis of carbon nanotubes by chemical vapor deposition," *Metals and Materials International*, vol. 16, pp. 663-667, Aug 2010.
- [43] N. Inami, M. A. Mohamed, E. Shikoh, and A. Fujiwara, "Synthesis-condition dependence of carbon nanotube growth by alcohol catalytic chemical vapor deposition method," *Science and Technology of Advanced Materials*, vol. 8, pp. 292-295, May 2007.
- [44] H. M. Ma and X. L. Gao, "A three-dimensional Monte Carlo model for electrically conductive polymer matrix composites filled with curved fibers," *Polymer*, vol. 49, pp. 4230-4238, Sep 9 2008.
- [45] W. S. Bao, S. A. Meguid, Z. H. Zhu, and M. J. Meguid, "Modeling electrical conductivities of nanocomposites with aligned carbon nanotubes," *Nanotechnology*, vol. 22, Dec 2 2011.
- [46] N. Hu, Y. Karube, C. Yan, Z. Masuda, and H. Fukunaga, "Tunneling effect in a polymer/carbon nanotube nanocomposite strain sensor," *Acta Materialia*, vol. 56, pp. 2929-2936, Aug 2008.
- [47] L. Berhan and A. M. Sastry, "Modeling percolation in high-aspect-ratio fiber systems. II. The effect of waviness on the percolation onset," *Physical Review E*, vol. 75, Apr 2007.
- [48] N. Hu, Y. Karube, M. Arai, T. Watanabe, C. Yan, Y. Li, *et al.*, "Investigation on sensitivity of a polymer/carbon nanotube composite strain sensor," *Carbon*, vol. 48, pp. 680-687, Mar 2010.
- [49] A. Oskouyi, U. Sundararaj, and P. Mertiny, "A numerical model to study the effect of temperature on electrical conductivity of polymer-CNT nanocomposite," in *ASME International Mechanical Engineering Congress & Exposition, IMECE2013*, 2013.
- [50] M. S. Han, Y. K. Lee, C. H. Yun, H. S. Lee, C. J. Lee, and W. N. Kim, "Bent-shape effects of multi-walled carbon nanotube on the electrical conductivity and rheological properties of polycarbonate/multi-walled carbon nanotube nanocomposites," *Synthetic Metals*, vol. 161, pp. 1629-1634, Aug 2011.
- [51] L. X. He and S. C. Tjong, "Carbon nanotube/epoxy resin composite: Correlation between state of nanotube dispersion and Zener tunneling parameters," *Synthetic Metals*, vol. 162, pp. 2277-2281, Dec 31 2012.
- [52] R. Bhatia, V. Prasad, and R. Menon, "Characterization, electrical percolation and magnetization studies of polystyrene/multiwall carbon nanotube composite films," *Materials Science and Engineering B-Advanced Functional Solid-State Materials*, vol. 175, pp. 189-194, Dec 15 2010.
- [53] O. Osazuwa, K. Petrie, M. Kontopoulou, P. Xiang, Z. B. Ye, and A. Docoslis, "Characterization of non-covalently, non-specifically functionalized multi-wall carbon nanotubes and their melt compounded composites with an ethylene-octene copolymer," *Composites Science and Technology*, vol. 73, pp. 27-33, Nov 23 2012.
- [54] B. Krause, M. Ritschel, C. Taschner, S. Oswald, W. Gruner, A. Leonhardt, *et al.*, "Comparison of nanotubes produced by fixed bed and aerosol-CVD methods and their electrical percolation behaviour in melt mixed polyamide 6.6 composites," *Composites Science and Technology*, vol. 70, pp. 151-160, Jan 2010.
- [55] Z. M. Dang, K. Shehzad, J. W. Zha, A. Mujahid, T. Hussain, J. Nie, *et al.*, "Complementary percolation characteristics of carbon fillers based electrically percolative thermoplastic elastomer composites," *Composites Science and Technology*, vol. 72, pp. 28-35, Dec 6 2011.
- [56] J. K. W. Sandler, J. E. Kirk, I. A. Kinloch, M. S. P. Shaffer, and A. H. Windle, "Ultra-low electrical percolation threshold in carbon-nanotube-epoxy composites," *Polymer*, vol. 44, pp. 5893-5899, Sep 2003.
- [57] J. Z. Kovacs, B. S. Velagala, K. Schulte, and W. Bauhofer, "Two percolation thresholds in carbon nanotube epoxy composites," *Composites Science and Technology*, vol. 67, pp. 922-928, Apr 2007.

- [58] E. Logakis, E. Pollatos, C. Pandis, V. Peoglos, I. Zuburtikudis, C. G. Delides, *et al.*, "Structure-property relationships in isotactic polypropylene/multi-walled carbon nanotubes nanocomposites," *Composites Science and Technology*, vol. 70, pp. 328-335, Feb 2010.
- [59] A. W. Musumeci, G. G. Silva, J. W. Liu, W. N. Martens, and E. R. Waclawik, "Structure and conductivity of multi-walled carbon nanotube/poly(3-hexylthiophene) composite films," *Polymer*, vol. 48, pp. 1667-1678, Mar 8 2007.
- [60] I. A. E. Kymakis, G.A.J. Amaratunga, "Single-walled carbon nanotube-polymer composites: electrical, optical and structural investigation," *Synth. Met.*, vol. 127, pp. 59-62, 2002.
- [61] E. T. Thostenson, S. Ziaee, and T. W. Chou, "Processing and electrical properties of carbon nanotube/vinyl ester nanocomposites," *Composites Science and Technology*, vol. 69, pp. 801-804, May 2009.
- [62] J. H. Yang, T. Xu, A. Lu, Q. Zhang, H. Tan, and Q. Fu, "Preparation and properties of poly (p-phenylene sulfide)/multiwall carbon nanotube composites obtained by melt compounding," *Composites Science and Technology*, vol. 69, pp. 147-153, Feb 2009.
- [63] A. Battisti, A. A. Skordos, and I. K. Partridge, "Percolation threshold of carbon nanotubes filled unsaturated polyesters," *Composites Science and Technology*, vol. 70, pp. 633-637, Apr 2010.
- [64] Y. Z. Pan and L. Li, "Percolation and gel-like behavior of multiwalled carbon nanotube/polypropylene composites influenced by nanotube aspect ratio," *Polymer*, vol. 54, pp. 1218-1226, Feb 5 2013.
- [65] Z. F. Li, G. H. Luo, F. Wei, and Y. Huang, "Microstructure of carbon nanotubes/PET conductive composites fibers and their properties," *Composites Science and Technology*, vol. 66, pp. 1022-1029, Jun 2006.
- [66] G. D. Liang, S. P. Bao, and S. C. Tjong, "Microstructure and properties of polypropylene composites filled with silver and carbon nanotube nanoparticles prepared by melt-compounding," *Materials Science and Engineering B-Solid State Materials for Advanced Technology*, vol. 142, pp. 55-61, Sep 25 2007.
- [67] O. Meincke, D. Kaempfer, H. Weickmann, C. Friedrich, M. Vathauer, and H. Warth, "Mechanical properties and electrical conductivity of carbon-nanotube filled polyamide-6 and its blends with acrylonitrile/butadiene/styrene," *Polymer*, vol. 45, pp. 739-748, Feb 1 2004.
- [68] G. J. Hu, C. G. Zhao, S. M. Zhang, M. S. Yang, and Z. G. Wang, "Low percolation thresholds of electrical conductivity and rheology in poly(ethylene terephthalate) through the networks of multi-walled carbon nanotubes," *Polymer*, vol. 47, pp. 480-488, Jan 2006.
- [69] H. E. Miltner, N. Grossiord, K. B. Lu, J. Loos, C. E. Koning, and B. Van Mele, "Isotactic polypropylene/carbon nanotube composites prepared by latex technology. Thermal analysis of carbon nanotube-induced nucleation," *Macromolecules*, vol. 41, pp. 5753-5762, Aug 12 2008.
- [70] M. Felisberto, A. Arias-Duran, J. A. Ramos, I. Mondragon, R. Candal, S. Goyanes, *et al.*, "Influence of filler alignment in the mechanical and electrical properties of carbon nanotubes/epoxy nanocomposites," *Physica B-Condensed Matter*, vol. 407, pp. 3181-3183, Aug 15 2012.
- [71] S. Chakraborty, J. Pionteck, B. Krause, S. Banerjee, and B. Voit, "Influence of different carbon nanotubes on the electrical and mechanical properties of melt mixed poly(ether sulfone)-multi walled carbon nanotube composites," *Composites Science and Technology*, vol. 72, pp. 1933-1940, 10/12/ 2012.
- [72] M. S. de Luna, L. Pellegrino, M. Dagheta, C. V. Mazzocchia, D. Acierno, and G. Filippone, "Importance of the morphology and structure of the primary aggregates for the dispersibility of carbon nanotubes in polymer melts," *Composites Science and Technology*, vol. 85, pp. 17-22, Aug 21 2013.
- [73] K. Tsuchiya, A. Sakai, T. Nagaoka, K. Uchida, T. Furukawa, and H. Yajima, "High electrical performance of carbon nanotubes/rubber composites with low percolation threshold prepared with a rotation-revolution mixing technique," *Composites Science and Technology*, vol. 71, pp. 1098-1104, May 31 2011.
- [74] K. Wongtimnoi, B. Guiffard, A. Bogner-Van de Moortele, L. Seveyrat, and J. Y. Cavaille, "Electrostrictive thermoplastic polyurethane-based nanocomposites filled with carboxyl-functionalized

multi-walled carbon nanotubes (MWCNT-COOH): Properties and improvement of electromechanical activity," *Composites Science and Technology*, vol. 85, pp. 23-28, Aug 21 2013.

[75] Z. Ounaies, C. Park, K. E. Wise, E. J. Siochi, and J. S. Harrison, "Electrical properties of single wall carbon nanotube reinforced polyimide composites," *Composites Science and Technology*, vol. 63, pp. 1637-1646, Aug 2003.

[76] Q. M. Liu, J. C. Tu, X. Wang, W. X. Yu, W. T. Zheng, and Z. D. Zhao, "Electrical conductivity of carbon nanotube/poly(vinylidene fluoride) composites prepared by high-speed mechanical mixing," *Carbon*, vol. 50, pp. 339-341, Jan 2012.

[77] S. C. Tjong, G. D. Liang, and S. P. Bao, "Electrical behavior of polypropylene/multiwalled carbon nanotube nanocomposites with low percolation threshold," *Scripta Materialia*, vol. 57, pp. 461-464, Sep 2007.

[78] Y. P. Mamunya, V. V. Levchenko, A. Rybak, G. Boiteux, E. V. Lebedev, J. Ulanski, *et al.*, "Electrical and thermomechanical properties of segregated nanocomposites based on PVC and multiwalled carbon nanotubes," *Journal of Non-Crystalline Solids*, vol. 356, pp. 635-641, Apr 1 2010.

[79] C. C. Chu, K. L. White, P. Liu, X. Zhang, and H. J. Sue, "Electrical conductivity and thermal stability of polypropylene containing well-dispersed multi-walled carbon nanotubes disentangled with exfoliated nanoplatelets," *Carbon*, vol. 50, pp. 4711-4721, Oct 2012.

[80] H. Aarab, M. Baitoul, J. Wery, R. Almairac, S. Lefrant, E. Faulques, *et al.*, "Electrical and optical properties of PPV and single-walled carbon nanotubes composite films," *Synthetic Metals*, vol. 155, pp. 63-67, Oct 15 2005.

[81] S. Kara, E. Arda, F. Dolastir, and O. Pekcan, "Electrical and optical percolations of polystyrene latex-multiwalled carbon nanotube composites," *Journal of Colloid and Interface Science*, vol. 344, pp. 395-401, Apr 15 2010.

[82] X. W. Jiang, Y. Z. Bin, and M. Matsuo, "Electrical and mechanical properties of polyimide-carbon nanotubes composites fabricated by in situ polymerization," *Polymer*, vol. 46, pp. 7418-7424, Aug 23 2005.

[83] O. Chauvet, J. M. Benoit, and B. Corraze, "Electrical, magneto-transport and localization of charge carriers in nanocomposites based on carbon nanotubes," *Carbon*, vol. 42, pp. 949-952, 2004.

[84] S. U. Khan, J. R. Pothnis, and J.-K. Kim, "Effects of carbon nanotube alignment on electrical and mechanical properties of epoxy nanocomposites," *Composites Part A: Applied Science and Manufacturing*, vol. 49, pp. 26-34, 6// 2013.

[85] A. Moisala, Q. Li, I. A. Kinloch, and A. H. Windle, "Thermal and electrical conductivity of single- and multi-walled carbon nanotube-epoxy composites," *Composites Science and Technology*, vol. 66, pp. 1285-1288, Aug 2006.

[86] S. Barrau, P. Demont, A. Peigney, C. Laurent, and C. Lacabanne, "DC and AC conductivity of carbon nanotubes-polyepoxy composites," *Macromolecules*, vol. 36, pp. 5187-5194, Jul 15 2003.

[87] O. Regev, P. N. B. ElKati, J. Loos, and C. E. Koning, "Preparation of conductive nanotube-polymer composites using latex technology," *Advanced Materials*, vol. 16, pp. 248+, Feb 3 2004.

[88] O. Gryshchuk, J. Karger-Kocsis, R. Thomann, Z. Konya, and I. Kiricsi, "Multiwall carbon nanotube modified vinylester and vinylester - based hybrid resins," *Composites Part a-Applied Science and Manufacturing*, vol. 37, pp. 1252-1259, 2006.

[89] Q. Lin, L. Qu, B. Luo, C. Fang, and K. Luo, "Preparation and properties of multiwall carbon nanotubes/carbon foam composites," *Journal of Analytical and Applied Pyrolysis*, vol. 105, pp. 177-182, 1// 2014.

[90] C. Y. Li, E. T. Thostenson, and T. W. Chou, "Dominant role of tunneling resistance in the electrical conductivity of carbon nanotube-based composites," *Applied Physics Letters*, vol. 91, Nov 26 2007.

[91] Y. Yu, G. Song, and L. Sun, "Determinant role of tunneling resistance in electrical conductivity of polymer composites reinforced by well dispersed carbon nanotubes," *Journal of Applied Physics*, vol. 108, Oct 15 2010.

- [92] C. Li, E. T. Thostenson, and T. W. Chou, "Effect of nanotube waviness on the electrical conductivity of carbon nanotube-based composites," *Composites Science and Technology*, vol. 68, pp. 1445-1452, May 2008.
- [93] F. Dalmas, R. Dendievel, L. Chazeau, J.-Y. Cavaillé, and C. Gauthier, "Carbon nanotube-filled polymer composites. Numerical simulation of electrical conductivity in three-dimensional entangled fibrous networks," *Acta Materialia*, vol. 54, pp. 2923-2931, 6// 2006.
- [94] B. E. Kilbride, J. N. Coleman, J. Fraysse, P. Fournet, M. Cadek, A. Drury, *et al.*, "Experimental observation of scaling laws for alternating current and direct current conductivity in polymer-carbon nanotube composite thin films," *Journal of Applied Physics*, vol. 92, pp. 4024-4030, Oct 1 2002.
- [95] M. Foygel, R. D. Morris, D. Anez, S. French, and V. L. Sobolev, "Theoretical and computational studies of carbon nanotube composites and suspensions: Electrical and thermal conductivity," *Physical Review B*, vol. 71, Mar 2005.
- [96] M. J. Allen, V. C. Tung, and R. B. Kaner, "Honeycomb Carbon: A Review of Graphene," *Chemical Reviews*, vol. 110, pp. 132-145, Jan 2010.
- [97] J. H. Chen, C. Jang, S. D. Xiao, M. Ishigami, and M. S. Fuhrer, "Intrinsic and extrinsic performance limits of graphene devices on SiO₂," *Nature Nanotechnology*, vol. 3, pp. 206-209, Apr 2008.
- [98] Y. W. Zhu, S. Murali, W. W. Cai, X. S. Li, J. W. Suk, J. R. Potts, *et al.*, "Graphene and Graphene Oxide: Synthesis, Properties, and Applications (vol 22, pg 3906, 2010)," *Advanced Materials*, vol. 22, pp. 5226-5226, Dec 7 2010.
- [99] C. Lee, X. D. Wei, J. W. Kysar, and J. Hone, "Measurement of the elastic properties and intrinsic strength of monolayer graphene," *Science*, vol. 321, pp. 385-388, Jul 18 2008.
- [100] A. K. Geim and K. S. Novoselov, "The rise of graphene," *Nature Materials*, vol. 6, pp. 183-191, Mar 2007.
- [101] G. Chen, D. Wu, W. Weng, and C. Wu, "Exfoliation of graphite flake and its nanocomposites," *Carbon*, vol. 41, pp. 619-621, // 2003.
- [102] W. S. Hummers and R. E. Offeman, "Preparation of Graphitic Oxide," *Journal of the American Chemical Society*, vol. 80, pp. 1339-1339, 1958.
- [103] D. R. Dreyer, S. Park, C. W. Bielawski, and R. S. Ruoff, "The chemistry of graphene oxide," *Chem Soc Rev*, vol. 39, pp. 228-40, Jan 2010.
- [104] Y. Xu, H. Bai, G. Lu, C. Li, and G. Shi, "Flexible graphene films via the filtration of water-soluble noncovalent functionalized graphene sheets," *J Am Chem Soc*, vol. 130, pp. 5856-7, May 7 2008.
- [105] S. Stankovich, D. A. Dikin, R. D. Piner, K. A. Kohlhaas, A. Kleinhammes, Y. Jia, *et al.*, "Synthesis of graphene-based nanosheets via chemical reduction of exfoliated graphite oxide," *Carbon*, vol. 45, pp. 1558-1565, Jun 2007.
- [106] S. Park and R. S. Ruoff, "Chemical methods for the production of graphenes (vol 4, pg 217, 2009)," *Nature Nanotechnology*, vol. 5, pp. 309-309, Apr 2010.
- [107] J. R. Lomeda, C. D. Doyle, D. V. Kosynkin, W. F. Hwang, and J. M. Tour, "Diazonium Functionalization of Surfactant-Wrapped Chemically Converted Graphene Sheets," *Journal of the American Chemical Society*, vol. 130, pp. 16201-16206, Dec 3 2008.
- [108] V. C. Tung, M. J. Allen, Y. Yang, and R. B. Kaner, "High-throughput solution processing of large-scale graphene," *Nature Nanotechnology*, vol. 4, pp. 25-29, Jan 2009.
- [109] G. X. Wang, J. Yang, J. Park, X. L. Gou, B. Wang, H. Liu, *et al.*, "Facile synthesis and characterization of graphene nanosheets," *Journal of Physical Chemistry C*, vol. 112, pp. 8192-8195, Jun 5 2008.
- [110] V. Eswaraiyah, S. S. J. Aravind, and S. Ramaprabhu, "Top down method for synthesis of highly conducting graphene by exfoliation of graphite oxide using focused solar radiation," *Journal of Materials Chemistry*, vol. 21, pp. 6800-6803, 2011.
- [111] K. S. Kim, Y. Zhao, H. Jang, S. Y. Lee, J. M. Kim, K. S. Kim, *et al.*, "Large-scale pattern growth of graphene films for stretchable transparent electrodes," *Nature*, vol. 457, pp. 706-710, Feb 5 2009.

- [112] L. Brown, R. Hovden, P. Huang, M. Wojcik, D. A. Muller, and J. Park, "Twinning and Twisting of Tri- and Bilayer Graphene," *Nano Letters*, vol. 12, pp. 1609-1615, Mar 2012.
- [113] G. Nandamuri, S. Roumimov, and R. Solanki, "Chemical vapor deposition of graphene films," *Nanotechnology*, vol. 21, Apr 9 2010.
- [114] A. Malesevic, R. Vitchev, K. Schouteden, A. Volodin, L. Zhang, G. Van Tendeloo, *et al.*, "Synthesis of few-layer graphene via microwave plasma-enhanced chemical vapour deposition," *Nanotechnology*, vol. 19, Jul 30 2008.
- [115] E. Dervishi, Z. R. Li, F. Watanabe, A. Biswas, Y. Xu, A. R. Biris, *et al.*, "Large-scale graphene production by RF-cCVD method," *Chemical Communications*, pp. 4061-4063, 2009.
- [116] A. Reina, X. T. Jia, J. Ho, D. Nezich, H. B. Son, V. Bulovic, *et al.*, "Large Area, Few-Layer Graphene Films on Arbitrary Substrates by Chemical Vapor Deposition," *Nano Letters*, vol. 9, pp. 30-35, Jan 2009.
- [117] S. Shivaraman, R. A. Barton, X. Yu, J. Alden, L. Herman, M. V. S. Chandrashekar, *et al.*, "Free-Standing Epitaxial Graphene," *Nano Letters*, vol. 9, pp. 3100-3105, Sep 2009.
- [118] M. Zhou, J. Tang, Q. Cheng, G. Xu, P. Cui, and L.-C. Qin, "Few-layer graphene obtained by electrochemical exfoliation of graphite cathode," *Chemical Physics Letters*, vol. 572, pp. 61-65, 2013.
- [119] C.-Y. Su, A.-Y. Lu, Y. Xu, F.-R. Chen, A. N. Khlobystov, and L.-J. Li, "High-quality thin graphene films from fast electrochemical exfoliation," *Acs Nano*, vol. 5, pp. 2332-2339, 2011.
- [120] G. Wang, B. Wang, J. Park, Y. Wang, B. Sun, and J. Yao, "Highly efficient and large-scale synthesis of graphene by electrolytic exfoliation," *Carbon*, vol. 47, pp. 3242-3246, 2009.
- [121] X. Zhang, D. Zhang, Y. Chen, X. Sun, and Y. Ma, "Electrochemical reduction of graphene oxide films: Preparation, characterization and their electrochemical properties," *Chinese Science Bulletin*, vol. 57, pp. 3045-3050, 2012.
- [122] Z. S. Wu, W. C. Ren, L. B. Gao, J. P. Zhao, Z. P. Chen, B. L. Liu, *et al.*, "Synthesis of Graphene Sheets with High Electrical Conductivity and Good Thermal Stability by Hydrogen Arc Discharge Exfoliation," *Acs Nano*, vol. 3, pp. 411-417, Feb 2009.
- [123] A. Hirsch, "Unzipping Carbon Nanotubes: A Peeling Method for the Formation of Graphene Nanoribbons," *Angewandte Chemie-International Edition*, vol. 48, pp. 6594-6596, 2009.
- [124] Y. Hernandez, V. Nicolosi, M. Lotya, F. M. Blighe, Z. Y. Sun, S. De, *et al.*, "High-yield production of graphene by liquid-phase exfoliation of graphite," *Nature Nanotechnology*, vol. 3, pp. 563-568, Sep 2008.
- [125] H. B. Zhang, W. G. Zheng, Q. Yan, Y. Yang, J. W. Wang, Z. H. Lu, *et al.*, "Electrically conductive polyethylene terephthalate/graphene nanocomposites prepared by melt compounding," *Polymer*, vol. 51, pp. 1191-1196, Mar 2 2010.
- [126] S. Stankovich, D. A. Dikin, G. H. B. Dommett, K. M. Kohlhaas, E. J. Zimney, E. A. Stach, *et al.*, "Graphene-based composite materials," *Nature*, vol. 442, pp. 282-286, Jul 20 2006.
- [127] H. Pang, T. Chen, G. M. Zhang, B. Q. Zeng, and Z. M. Li, "An electrically conducting polymer/graphene composite with a very low percolation threshold," *Materials Letters*, vol. 64, pp. 2226-2229, Oct 31 2010.
- [128] S. Araby, L. Q. Zhang, H. C. Kuan, J. B. Dai, P. Majewski, and J. Ma, "A novel approach to electrically and thermally conductive elastomers using graphene," *Polymer*, vol. 54, pp. 3663-3670, Jun 2013.
- [129] J. H. Du, L. Zhao, Y. Zeng, L. L. Zhang, F. Li, P. F. Liu, *et al.*, "Comparison of electrical properties between multi-walled carbon nanotube and graphene nanosheet/high density polyethylene composites with a segregated network structure," *Carbon*, vol. 49, pp. 1094-1100, Apr 2011.
- [130] M. Kujawski, J. D. Pearse, and E. Smela, "Elastomers filled with exfoliated graphite as compliant electrodes," *Carbon*, vol. 48, pp. 2409-2417, Aug 2010.
- [131] E. H. L. Falcao, R. G. Blair, J. J. Mack, L. M. Viculis, C. W. Kwon, M. Bendikov, *et al.*, "Microwave exfoliation of a graphite intercalation compound," *Carbon*, vol. 45, pp. 1367-1369, May 2007.

- [132] T. Wei, Z. J. Fan, G. L. Luo, C. Zheng, and D. S. Xie, "A rapid and efficient method to prepare exfoliated graphite by microwave irradiation," *Carbon*, vol. 47, pp. 337-339, Jan 2009.
- [133] J. W. Shang, Y. H. Zhang, L. Yu, B. Shen, F. Z. Lv, and P. K. Chu, "Fabrication and dielectric properties of oriented polyvinylidene fluoride nanocomposites incorporated with graphene nanosheets," *Materials Chemistry and Physics*, vol. 134, pp. 867-874, Jun 15 2012.
- [134] S. Vadukumpully, J. Paul, N. Mahanta, and S. Valiyaveetil, "Flexible conductive graphene/poly(vinyl chloride) composite thin films with high mechanical strength and thermal stability," *Carbon*, vol. 49, pp. 198-205, 1// 2011.
- [135] W. E. Mahmoud, "Morphology and physical properties of poly(ethylene oxide) loaded graphene nanocomposites prepared by two different techniques," *European Polymer Journal*, vol. 47, pp. 1534-1540, Aug 2011.
- [136] H. L. Hu, G. Zhang, L. G. Xiao, H. J. Wang, Q. S. Zhang, and Z. D. Zhao, "Preparation and electrical conductivity of graphene/ultrahigh molecular weight polyethylene composites with a segregated structure," *Carbon*, vol. 50, pp. 4596-4599, Oct 2012.
- [137] N. Yousefi, X. Y. Lin, Q. B. Zheng, X. Shen, J. R. Pothnis, J. J. Jia, *et al.*, "Simultaneous in situ reduction, self-alignment and covalent bonding in graphene oxide/epoxy composites," *Carbon*, vol. 59, pp. 406-417, Aug 2013.
- [138] Q. Zheng, W. H. Ip, X. Lin, N. Yousefi, K. K. Yeung, Z. Li, *et al.*, "Transparent conductive films consisting of ultralarge graphene sheets produced by Langmuir-Blodgett assembly," *ACS Nano*, vol. 5, pp. 6039-51, Jul 26 2011.
- [139] Y. Geng, S. J. Wang, and J. K. Kim, "Preparation of graphite nanoplatelets and graphene sheets," *J Colloid Interface Sci*, vol. 336, pp. 592-8, Aug 15 2009.
- [140] W. J. Li, X. Z. Tang, H. B. Zhang, Z. G. Jiang, Z. Z. Yu, X. S. Du, *et al.*, "Simultaneous surface functionalization and reduction of graphene oxide with octadecylamine for electrically conductive polystyrene composites," *Carbon*, vol. 49, pp. 4724-4730, Nov 2011.
- [141] F. Yavari, M. A. Rafiee, J. Rafiee, Z. Z. Yu, and N. Koratkar, "Dramatic Increase in Fatigue Life in Hierarchical Graphene Composites," *Acs Applied Materials & Interfaces*, vol. 2, pp. 2738-2743, Oct 2010.
- [142] H. B. Zhang, W. G. Zheng, Q. Yan, Z. G. Jiang, and Z. Z. Yu, "The effect of surface chemistry of graphene on rheological and electrical properties of polymethylmethacrylate composites," *Carbon*, vol. 50, pp. 5117-5125, Nov 2012.
- [143] S. T. Hsiao, C. C. M. Ma, H. W. Tien, W. H. Liao, Y. S. Wang, S. M. Li, *et al.*, "Using a non-covalent modification to prepare a high electromagnetic interference shielding performance graphene nanosheet/water-borne polyurethane composite," *Carbon*, vol. 60, pp. 57-66, Aug 2013.
- [144] R. K. Layek, S. Samanta, D. P. Chatterjee, and A. K. Nandi, "Physical and mechanical properties of poly(methyl methacrylate) -functionalized graphene/poly(vinylidene fluoride) nanocomposites Piezoelectric beta polymorph formation," *Polymer*, vol. 51, pp. 5846-5856, Nov 12 2010.
- [145] K.-H. Liao, Y. Qian, and C. W. Macosko, "Ultralow percolation graphene/polyurethane acrylate nanocomposites," *Polymer*, vol. 53, pp. 3756-3761, 2012.
- [146] A. Oskouyi, U. Sundararaj, and P. Mertiny, "Tunneling conductivity and piezo-resistivity of composites containing randomly dispersed conductive nano-platelets," *Journal of materials*, vol. Article in press, 2014.
- [147] F. R. Al-Solamy, A. A. Al-Ghamdi, and W. E. Mahmoud, "Piezoresistive behavior of graphite nanoplatelets based rubber nanocomposites," *Polymers for Advanced Technologies*, vol. 23, pp. 478-482, Mar 2012.
- [148] S. Y. Qu and S. C. Wong, "Piezoresistive behavior of polymer reinforced by expanded graphite," *Composites Science and Technology*, vol. 67, pp. 231-237, Feb 2007.
- [149] Y. Hou, D. R. Wang, X. M. Zhang, H. Zhao, J. W. Zha, and Z. M. Dang, "Positive piezoresistive behavior of electrically conductive alkyl-functionalized graphene/polydimethylsilicone nanocomposites," *Journal of Materials Chemistry C*, vol. 1, pp. 515-521, 2013.

- [150] J. R. Lu, X. F. Chen, W. Lu, and G. H. Chen, "The piezoresistive behaviors of polyethylene/foliated graphite nanocomposites," *European Polymer Journal*, vol. 42, pp. 1015-1021, May 2006.
- [151] L. M. Chiacchiarelli, M. Rallini, M. Monti, D. Puglia, J. M. Kenny, and L. Torre, "The role of irreversible and reversible phenomena in the piezoresistive behavior of graphene epoxy nanocomposites applied to structural health monitoring," *Composites Science and Technology*, vol. 80, pp. 73-79, May 17 2013.
- [152] M. Y. Han, B. Ozyilmaz, Y. B. Zhang, and P. Kim, "Energy band-gap engineering of graphene nanoribbons," *Physical Review Letters*, vol. 98, May 18 2007.
- [153] D. V. Kosynkin, A. L. Higginbotham, A. Sinitskii, J. R. Lomeda, A. Dimiev, B. K. Price, *et al.*, "Longitudinal unzipping of carbon nanotubes to form graphene nanoribbons," *Nature*, vol. 458, pp. 872-U5, Apr 16 2009.
- [154] J. Campos-Delgado, J. M. Romo-Herrera, X. T. Jia, D. A. Cullen, H. Muramatsu, Y. A. Kim, *et al.*, "Bulk production of a new form of sp(2) carbon: Crystalline graphene nanoribbons," *Nano Letters*, vol. 8, pp. 2773-2778, Sep 2008.
- [155] A. Oskouyi, U. Sundararaj, and P. Mertiny, "Electrical conductivity of polymers with variable-sized conductive nanoplatelets," presented at the 6th ECCOMAS Conference on Smart Structures and Materials, SMART2013, Politecnico di Torino, 2013.
- [156] A. Oskouyi, U. Sundararaj, and P. Mertiny, "Current-voltage characteristics of nanoplatelet based conductive nano-composites," presented at the The 19th international conference on composite materials, Montreal, Canada.
- [157] A. B. Oskouyi and P. Mertiny, "Monte Carlo model for the study of percolation thresholds in composites filled with circular conductive nano-disks," *11th International Conference on the Mechanical Behavior of Materials (Icm11)*, vol. 10, 2011.
- [158] K. U. Lee, K. J. Park, O. J. Kwon, and J. J. Kim, "Carbon sphere as a black pigment for an electronic paper," *Current Applied Physics*, vol. 13, pp. 419-424, Mar 2013.
- [159] A. I. Medalia and L. W. Richards, "Tinting Strength of Carbon-Black," *Journal of Colloid and Interface Science*, vol. 40, pp. 233-&, 1972.
- [160] W. Zhang, R. S. Blackburn, and A. A. Dehghani-Sani, "Effect of carbon black concentration on electrical conductivity of epoxy resin-carbon black-silica nanocomposites," *Journal of Materials Science*, vol. 42, pp. 7861-7865, Sep 2007.
- [161] S. Praveen, P. K. Chattopadhyay, P. Albert, V. G. Dalvi, B. C. Chakraborty, and S. Chattopadhyay, "Synergistic effect of carbon black and nanoclay fillers in styrene butadiene rubber matrix: Development of dual structure," *Composites Part a-Applied Science and Manufacturing*, vol. 40, pp. 309-316, Mar 2009.
- [162] M. Mohsen, M. H. Abd-El Salam, A. Ashry, A. Ismail, and H. Ismail, "Positron annihilation spectroscopy in carbon black-silica-styrene butadiene rubber (SBR) composites under deformation," *Polymer Degradation and Stability*, vol. 87, pp. 381-388, Mar 2005.
- [163] S. R. Mahapatra, V. Sridhar, and D. K. Tripathy, "Impedance analysis and electromagnetic interference shielding effectiveness of conductive carbon black reinforced microcellular EPDM rubber vulcanizates," *Polymer Composites*, vol. 29, pp. 465-472, May 2008.
- [164] N. C. Das, T. K. Chaki, D. Khastgir, and A. Chakraborty, "Electromagnetic interference shielding effectiveness of conductive carbon black and carbon fiber-filled composites based on rubber and rubber blends," *Advances in Polymer Technology*, vol. 20, pp. 226-236, Fal 2001.
- [165] R. Q. Ou, R. A. Gerhardt, C. Marrett, A. Moulart, and J. S. Colton, "Assessment of percolation and homogeneity in ABS/carbon black composites by electrical measurements," *Composites Part B-Engineering*, vol. 34, pp. 607-614, 2003.
- [166] J. R. Li, J. R. Xu, M. Q. Zhang, and M. Z. Rong, "Carbon black/polystyrene composites as candidates for gas sensing materials," *Carbon*, vol. 41, pp. 2353-2360, 2003.

- [167] A. Katada, Y. Konishi, T. Isogai, Y. Tominaga, S. Asai, and M. Sumita, "Dynamic percolation phenomenon of poly(methyl methacrylate)/surface fluorinated carbon black composite," *Journal of Applied Polymer Science*, vol. 89, pp. 1151-1155, Jul 25 2003.
- [168] O. Koysuren, S. Yesil, and G. Bayram, "Effect of composite preparation techniques on electrical and mechanical properties and morphology of nylon 6 based conductive polymer composites," *Journal of applied polymer science*, vol. 102, pp. 2520-2526, 2006.
- [169] J. Hwang, J. Muth, and T. Ghosh, "Electrical and mechanical properties of carbon-black-filled, electrospun nanocomposite fiber webs," *Journal of Applied Polymer Science*, vol. 104, pp. 2410-2417, May 15 2007.
- [170] C. G. Ma, D. Y. Xi, and M. Liu, "Epoxy resin/polyetherimide/carbon black conductive polymer composites with a double percolation structure by reaction-induced phase separation," *Journal of Composite Materials*, vol. 47, pp. 1153-1160, Apr 2013.
- [171] X. Y. Ji, H. Li, D. Hui, K. T. Hsiao, J. P. Ou, and A. K. T. Lau, "I-V characteristics and electro-mechanical response of different carbon black/epoxy composites," *Composites Part B-Engineering*, vol. 41, pp. 25-32, Jan 2010.
- [172] X. Q. Liu, H. Q. Xing, L. L. Zhao, and X. S. Chen, "Study on NTC Electrical Behavior of Carbon Black/PVC Composite," *Proceedings of the 2nd International Conference on Electronic & Mechanical Engineering and Information Technology (Emeit-2012)*, vol. 23, 2012.
- [173] M. N. J. YACUBOWICZ, L. BENGUIGUI, "Electrical and Dielectric Properties of Segregated Carbon Black-Polyethylene Systems," *POLYMER ENGINEERING AND SCIENCE*, vol. 30, pp. 459-468, 1990.
- [174] L. A. H. Zois, M. Omastova, "Electrical Properties and Percolation Phenomena in Carbon Black Filled Polymer Composites," presented at the 10th International Symposium on Electrets, 1999.
- [175] A. L. Juris Zavickis, Maris Knite, "The downshift of the electrical percolation threshold in polyisoprene-nanostructured carbon composites," *ENERGETIKA*, vol. 57, pp. 44-49, 2011.

CHAPTER 3

NUMERICAL APPROACH FOR PERCOLATION PROBLEM: METHODOLOGY AND FORMULATION ¹

SYNOPSIS- The subject of the study described in this chapter is the percolation threshold of composites with conductive nanoscale fillers. Specifically, a three-dimensional continuous Monte Carlo algorithm was developed to determine the percolation threshold of polymers filled with two-dimensional conductive circular nanodisks. The Monte Carlo simulation provides the threshold value of the filler loading when at least one percolation network is formed. A scaling study was carried out to determine the minimum dimension of the representative unit volume that ensures a percolation threshold that is independent of the unit cell size. The effect of the aspect ratio of the nanoparticles and the tunneling distance on the percolation threshold was investigated employing the developed model.

3.1 Introduction

3.1.1 Motivation and Background

The development of nanoscale electrically conductive fillers and associated low cost fabrication methods has stimulated considerable interest in employing such particles to render otherwise insulating polymers conductive. Conductive nanofillers, such as graphene platelets and exfoliated graphite, were found to impart significant conductivity and piezoresistivity behavior to polymers, which makes such material systems an excellent choice for electrical applications, such as strain sensors. Nanoplatelet based conductive polymers have been the subject of a number of experimental studies [4, 5, 14, 126, 127, 135, 148, 176, 177].

¹ A modified version of this chapter was published as: Oskouyi, A. B., & Mertiny, P. Monte Carlo model for the study of percolation thresholds in composites filled with circular conductive nano-disks. *Procedia Engineering*, 2011, 10, 403-408.

Generally, the aforementioned works and works reviewed in CHAPTER 2 were devoted to the development of efficient fabrication methods and the evaluation of the conductivity and critical filler volume fraction at which a composite exhibits a transition from insulating to conductive behavior.

Percolation theory has been a successful tool to describe the transient behavior of the insulator polymers filled with the conductive inclusions [10, 11, 178-180]. Based on the percolation theory, there is a volume fraction where a percolation network is formed and the composite shows conductive behavior. This critical volume fraction is called percolation threshold, which signifies the onset of the formation of a percolation network that makes the polymer electrically conductive [46].

3.1.2 Monte Carlo Method in Percolation Problems

Monte Carlo simulation is one of the most commonly employed techniques to study the percolation behavior of polymers with randomly dispersed conductive inclusions. A large number of numerical and analytical investigations have been devoted to insulating polymers filled with spherical and stick-shaped conductive inclusions.

3.1.2.1 Percolation of Rod-Shaped and Spherical Inclusions

Pike and Seager [181] can be listed as pioneers who employed the Monte Carlo technique in conductive polymeric composites. Employing the Monte Carlo technique, they investigated the percolation threshold for a two-dimensional system of conductive sticks with a single size that are randomly dispersed in a matrix. Balberg and Binenbaum [182] extended Pike and Seager's work to study the percolation threshold in a two-dimensional anisotropic conductive sticks system. They considered the effect of macroscopic anisotropy and size distribution on percolation threshold by developing a Monte Carlo based model. Natsuki et al. [183] studied the percolation behavior for a 2D stick resistors network. They investigated the effect of the aspect ratio and fiber orientation on percolation threshold through a Monte Carlo simulation. Ma and Gao [44], developed a three-dimensional Monte Carlo model to predict the electrical conductivity and critical volume fraction for polymers filled with curved fibers. They evaluated the electrical conductivity of the composites by employing percolation theory. Dalmas et al. [184]

developed a three dimensional modeling procedure to simulate the electrical conductivity for a continuous entangled fibrous network. Li and Chou [185] proposed a Monte Carlo based method to investigate the percolation threshold of composites filled with fibers with arbitrary shapes. They assumed the conductive fibers to be polygons. Li et al. [90] studied the effect of the contact resistance on the electrical conductivity of carbon nanotube based composites. They carried out Monte Carlo simulations to investigate the role of tunneling resistance on electrical conductivity of composites. Wang and Ogale [186] studied the percolation behavior of composites with spherical inclusions. They employed the Monte Carlo method to predict the critical volume fraction when spherical conductive particles form a percolating resistor network.

3.1.2.2 *Percolation of Platelet Shaped Inclusions*

Some researchers used Monte Carlo simulation techniques to evaluate the conductivity of platelet based conductive polymers. Hicks et al. [187] developed a Monte Carlo-based computational model to predict the tunneling percolation behavior of a resistor network formed by rectangular conductive sheets that are oriented parallel to a substrate. Li and Morris [188] developed a two-dimensional (2D) computational percolation model to investigate the critical filler content and conductivity behavior for an adhesive filled with conductive flakes. They assumed the inclusions to be rectangular plates that are dispersed in a 2D space.

Yi and Tawerghi [189] carried out a numerical Monte Carlo based study to evaluate the percolation threshold for 2D interpenetrating plates, i.e., circular, elliptical, square, and triangular plates dispersed in three-dimensional (3D) space. It was shown that noncircular geometries tend to produce higher percolation thresholds. The percolation behavior of penetrable disks has been the subject of several other studies [190-192]. Vovchenko and Vovchenko [193], for example, predicted the percolation threshold of composites filled with intersecting circular disks. Otten and Schoot [194] developed an analytical approach to investigate the percolation behavior of polydisperse nanofillers, specifically focusing on conductivity of needle-like filler nanocomposites. They also briefly investigated the percolation behavior of platelet-based composites. However, their modeling approach was subject to certain limitations, that is, the platelet thickness and the so-called

tunneling decay length have to be of the same order of magnitude, and the diameter of disk-like fillers needs to be much larger than the disk thickness (tunneling decay length corresponds to inverse of the square root of the insulator barrier height in the present study). For monodisperse cases their model predicts the percolation threshold to be proportional to the ratio of filler thickness to decay length; interestingly, the percolation threshold was independent of the filler diameter. Ambrosetti et al. [195] conducted a numerical study to investigate the percolative properties of a system of hard oblate ellipsoids of revolution surrounded with soft penetrable shells. For higher aspect ratios, oblates approach a disk-like geometry but still deviate from an ideal circular disk. As described in a latter part of the present thesis (Chapter 4), data from [195] was employed for comparison to platelet filler based tunneling percolation problems. In a later work by Ambrosetti et al. [196], their initial study was expanded to evaluate the conductivity of percolation networks formed by ellipsoids of revolution dispersed in an insulating matrix.

Mathew et al. [197] conducted a Monte Carlo study on the percolation of hard platelets in a 3D continuum system. They represented the hard platelets by cut-spheres, which vary in shape from platelet geometry. In their model, platelet-like geometries were generated through intersecting a sphere with two parallel planes at equal distance from the equatorial plane. Their findings indicate that lower aspect ratios are associated with a lower percolation threshold. Note that the majority of related works neglected the condition of impenetrable disks, and only a few studies in the technical literature are devoted to the percolation behavior of impenetrable hard disk-like inclusions. To the best of the author's knowledge, research on this subject matter is limited to the last four studies mentioned above, which focus mainly on the percolation properties. Conductivity behavior in terms of a critical exponent describing post-percolation behavior and, more importantly, piezoresistivity behavior have been out of their scope.

Moreover, in these studies, circular disks were approximated by ellipsoids or cut-spheres. Hence, studies on the tunneling percolation behavior of impenetrable circular disks in 3D space are lacking.

Although Monte Carlo technique is the mostly employed method in numerical studies of the conductive nanocomposites problems, a few analytical studies have been conducted on the percolation problem of conductive nanocomposites. The excluded volume method is another techniques employed for studying the percolation threshold of conductive platelet based composites. Xia and Thorpe [198], for example, investigated the percolation behavior of overlapping ellipses randomly located in a plane using the excluded volume method. Modeling based on the excluded volume method however has its limitations as it is unable to predict the effect of tunneling distance on the critical volume fraction. Consequently, for cases in which tunneling distance plays an important role in the conductivity behavior of composites, excluded volume method based modeling is no longer efficient and cannot be employed to study the tunneling conductivity in conductive composites. Li and Kim [199] developed an analytical method based on the interparticle distance concept to predict the percolation threshold for polymers reinforced with circular conductive disks. They carried out a parametric study to investigate the contribution of aspect ratio and tunneling distance on the formation of percolating cluster.

The majority of works related to conductive composites with platelet fillers has been experimental. Thus far, the study of the percolation threshold of composites with circular fillers such as graphene nanoplatelets has only received scarce attention in the technical literature, and available works are mostly limited to two-dimensional problems or experimental investigations. The limited quantity of published works related to the modeling of platelet based conductive polymers, and limitations associated with the employed techniques motivated the author to conceive an alternative approach for modeling the electrical behavior of polymers filled with conductive nanoplatelet fillers. Published research on the electrical properties of nanoplatelet based nanocomposites has further been limited to studying the electrical conductivity of polymers with exfoliated sheets with in-plane dimensions varying from a few to several hundred micrometer and thicknesses ranging from a few to several nanometers. To achieve further enhancements in composite properties the synthesis of submicron size single layer graphene sheets may be an attractive proposition, and information on the percolation and electrical behavior of such reinforced polymers is therefore desirable. The latter aspects are also addressed in the next chapter.

3.2 Percolation Theory

Percolation theory can be explained as connectivity of clusters and formation of spanning cluster or “open path” [200] known as percolation network. The concept of the percolation theory in mathematics is illustrated by **Figure 3-1**. Each site in the lattice is occupied with the probability p . Considering a random number r , generated in a unit interval $0 < r < 1$, a site is occupied if r is less than p [201]. The sites that are connected to each other are called cluster. Based on percolation theory there is a critical probability, p_c , for the existence of a spanning or percolation network approaching unity. The spanning cluster or percolation network is a cluster that extends from one side of the lattice to the other side. The probability for this to occur is called percolation threshold. Several exact analytical solutions have been developed to predict the percolation threshold for different lattice percolation problems. Some of the lattice networks with their exact percolation threshold are provided by **Figure 3-2** and **Table 3-1**, respectively. It should be noted that exact solutions were developed for a limited number of lattice percolation problems where the possible position of each site in the lattice is well defined, and for continuous percolation problems the current solutions are limited to numerical and statistical approaches.

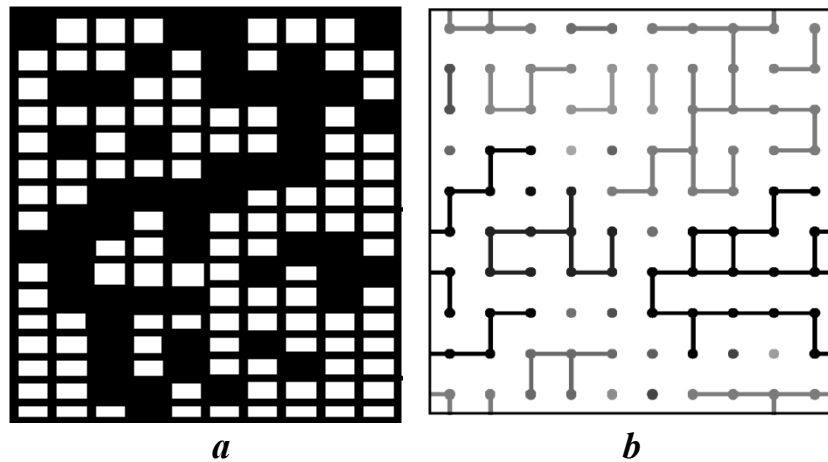


Figure 3-1: a) Schematic of site percolation concept for square lattice, b) Schematic of bond percolation concept for square lattice.

Monte Carlo method is a very general expression and it can be described as a probabilistic computational technique based on random sampling [202]. Monte Carlo modeling has been found an effective tool in dealing with problems in different fields, such as mathematical, engineering, physics and multidisciplinary problems that are involve a high degree of freedoms or uncertainties. The Monte Carlo method is further described in the subsequent section by explaining the application of the Monte Carlo method in percolation threshold assessment of nanoplatelet based composites.

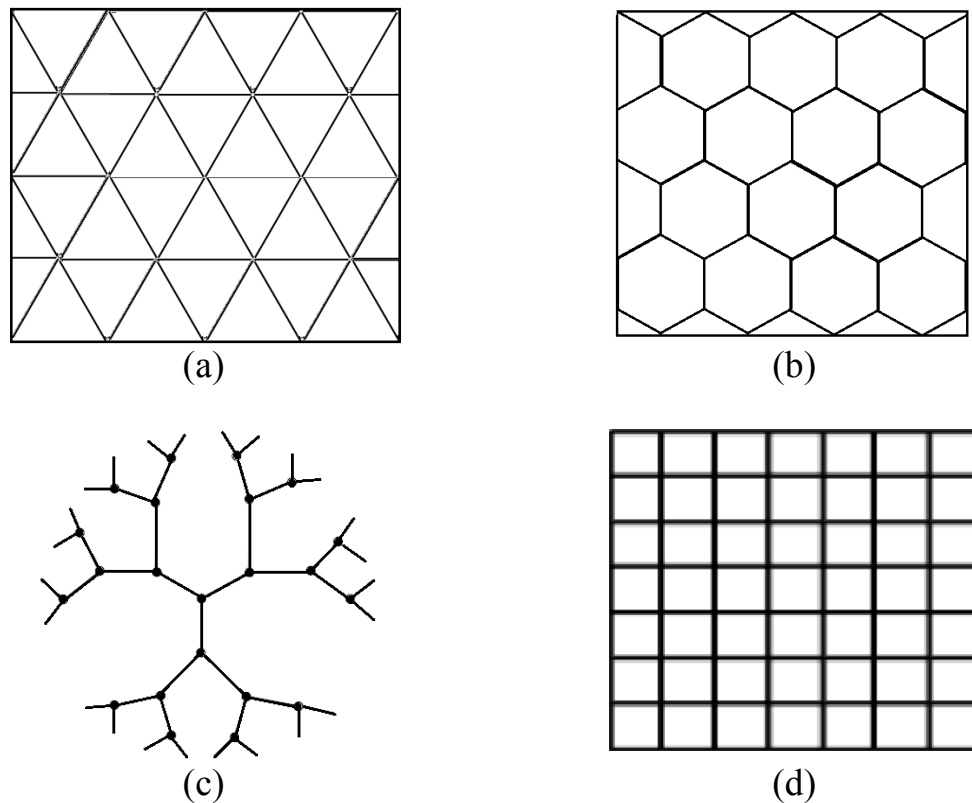


Figure 3-2. a) Triangular lattice, b) Honey-comb lattice, c) Bethe lattice, d) Rectangular lattice (Figures adapted from [201])

Table 3-1 Percolation threshold for different lattice [201].

Laattice	Bond Percolation	Site Percolation
1-D	1	1
Bethe	1/2	1/2
2-D Square	1/2	0.5927
2-D Honeycomb	$1 - 2 \sin(\pi/18)$	0.6962
Triangular	$2 \sin(\pi/18)$	1/2

3.3 Methodology and Formulation

3.3.1 Random Nanoplatelet Generation

To investigate the conductivity and percolation behavior of the composites filled with conductive nanoplatelets, a three dimensional (3D) continuum Monte Carlo (MC) model was developed. In continuum percolation modeling the location of points are not restricted to predefined location in the lattice and they are positioned in a continuous 3D space. Conductive inclusions were randomly dispersed inside a cubic representative volume element (RVE) with dimensions L . Conductive platelets are assumed to be impenetrable circular disks of radius R and thickness t . Circular disks were randomly generated and uniformly dispersed inside the RVE. Three random numbers (x_c, y_c, z_c) were chosen from the interval $(0, L)$ which indicate the coordinates of the center of the disks. Random numbers were generated using the Mersenne Twister (MT) random number generator algorithm developed by Matsumoto and Nishimura [203] which has a long period $(2^{19937}-1)$. Cornejo Diaz et al. [204] proved the suitability of this algorithm for Monte Carlo applications. In order to determine the normal of the plane containing the circular disk, a point from the surface of a unit sphere was chosen employing the method presented by Cook [205]. This point indicates the end point of the normal vector, which starting point is located at the center of the disk. In some of the Monte Carlo simulations [44, 46, 206], the orientation vectors (which origins and end points are located in the center and span to the surface of a unit sphere respectively) were obtained by generating elevation angles θ and inclination angles ψ , which correspondingly are bound in a spherical coordinate systems by $[-\pi/2, \pi/2]$ and $[0, 2\pi]$. These angles are bound in a spherical coordinate systems correspondingly by $[-\pi/2, \pi/2]$ and $[0, 2\pi]$. It should be noted that an elevation angle that is uniformly distributed in $[-\pi/2, \pi/2]$ does not provide a uniform distribution of points on the surface of a unit sphere. In fact, a uniform distribution on the unit sphere surface is achieved if θ is chosen as a weighted distribution between $-\pi/2$ and $\pi/2$ where the weight of the distribution is $\sin(\theta)$ [207].

In the present study a different algorithm presented by Cook [205] was employed to generate points that are uniformly distributed on a unit sphere. First, four random

numbers $\alpha_1, \alpha_2, \alpha_3$ and α_4 are chosen on $(-1, 1)$ that satisfy the requirement $V = (\alpha_1)^2 + (\alpha_2)^2 + (\alpha_3)^2 + (\alpha_4)^2 < 1$. The normal vector is then given by **Eq. 3-1**.

$$\mathbf{n}: (2(\alpha_2 \alpha_4 + \alpha_1 \alpha_3)/V, 2(\alpha_3 \alpha_4 - \alpha_1 \alpha_2)/V, (\alpha_1^2 + \alpha_4^2 - \alpha_2^2 - \alpha_3^2)/V) \quad \text{Eq. 3-1}$$

The point thus selected represents the end point of the normal vector with origin located at the center of the disk. Since nanoplatelets were assumed to be impenetrable rigid disks in the present study, the geometric feasibility of any generated disk needed to be validated so that only those disks were added to the RVE that have no intersection with existing disks. The intersection of two intersecting disks is a segment of a line, which is determined by the cross product of the normal vectors of the disk planes ($\mathbf{L} = \mathbf{n}_1 \times \mathbf{n}_2$). The procedure and the definition of the parameters are provided by **Figure 3-3**. Consequently, two disks (i and j) are intersecting when the following inequality is satisfied:

$$\sqrt{R^2 - \overline{o_i p_i}^2} + \sqrt{R^2 - \overline{o_j p_j}^2} \leq \overline{p_i p_j} \quad \text{Eq. 3-2}$$

where o_i is the center of the i^{th} disk and p_i is a point on the line \mathbf{L} that is corresponding to the shortest distance of o_i from line \mathbf{L} .

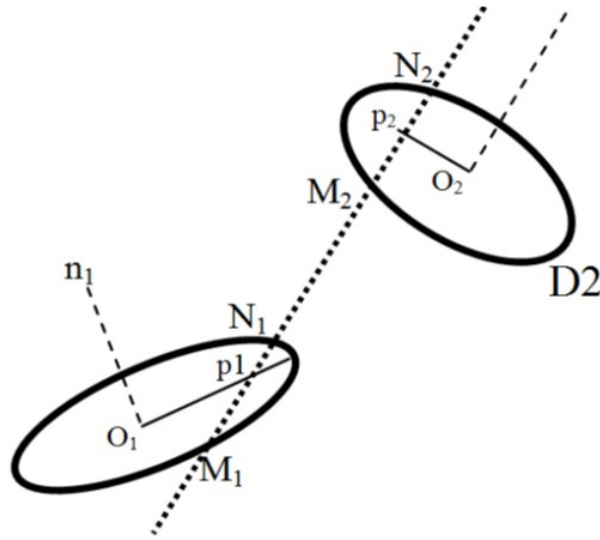


Figure 3-3: Parameter definition for disks intersection problem

3.3.2 Electrical Conductivity, Cluster and Percolation Network

It is herein assumed that two conductive inclusions dispersed in an insulator matrix are electrically connected by a resistor formed by the matrix. Nanoplatelets with distance shorter than the tunneling distance are labeled as a cluster and a cluster that connects the two parallel faces of the RVE is called a percolation network which allows electrical current to flow through and make the nanocomposite conductive. In Chapter 4, a comprehensive discussion is given on the value and concept of tunneling distance. **Figure 3-4** illustrates the concept of a cluster and percolation network in conductive nanocomposites. The volume fraction of the conductive particles at the onset of the percolation network is called the percolation threshold.

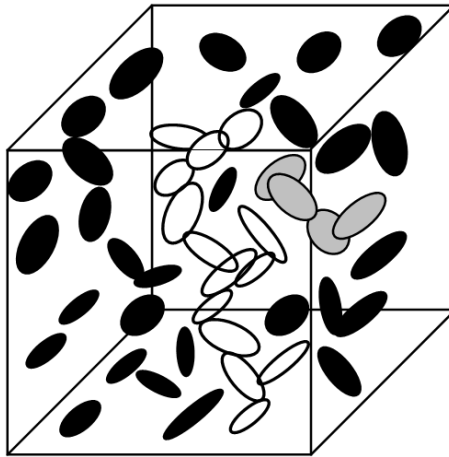


Figure 3-4: Schematic of cluster (gray) and percolation network (white).

As illustrated by the schematic in **Figure 3-5**, it was assumed that electrical current flow between two conductive inclusions would occur along the shortest possible path in between them. It is therefore necessary to determine the shortest distance between the inclusions. The algorithm developed by Almohamad and Selim [208] was employed in the present modeling approach to compute the shortest distance between two circular disks in 3D space. The algorithm is described geometrically by **Figure 3-6**. In order to calculate the shortest distance between two disks, a point on disk 2 corresponding to the

shortest distance of the center of disk 1 from disk 2 is determined. The procedure is repeated for disk 2, so that points p_1 and p_2 are found. In the next step the points corresponding to shortest distance of p_1 from disk 1 and p_2 from disk 2 are determined (q_1 and q_2). The shortest distance is the minimum of the $\overline{p_1q_1}$ and $\overline{p_2q_2}$.

In addition to the effective length of the tunneling paths, their effective cross section should be determined in order to model tunneling resistivity using electrical equivalent resistors. In other studies devoted to the investigation of conductivity of polymers rendered electrically conductive by dispersed CNTs, the CNT diameter was assumed to be the effective diameter of the tunneling path, even though this assumption is associated with uncertainties when two CNTs are not perpendicular to each other. As it is discussed in CHAPTER 4, the resistivity of graphene is negligible in comparison with that of the polymer matrix. Since the overall resistivity of graphene reinforced polymers thus arises solely from the resistivity of the tunneling paths, the effective area of the tunneling path plays qualitatively no role in the electrical and electromechanical behavior of the nanocomposite, i.e. the percolation threshold, piezoresistivity behavior, nonlinearity behavior and conductivity trend. In this study the tunneling resistivity of the polymers was therefore represented by cylindrical resistors with a diameter set at 1nm. It should be noted that for both CNT and graphene nanocomposites, the effective tunneling area can be tuned by correlating numerical and experimental results to also agree quantitatively.

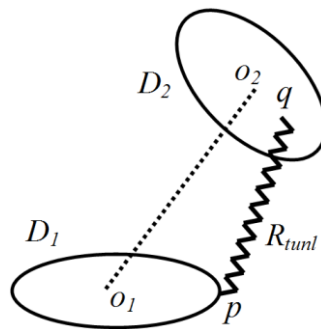


Figure 3-5: Schematic of tunneling resistance and electron hopping.

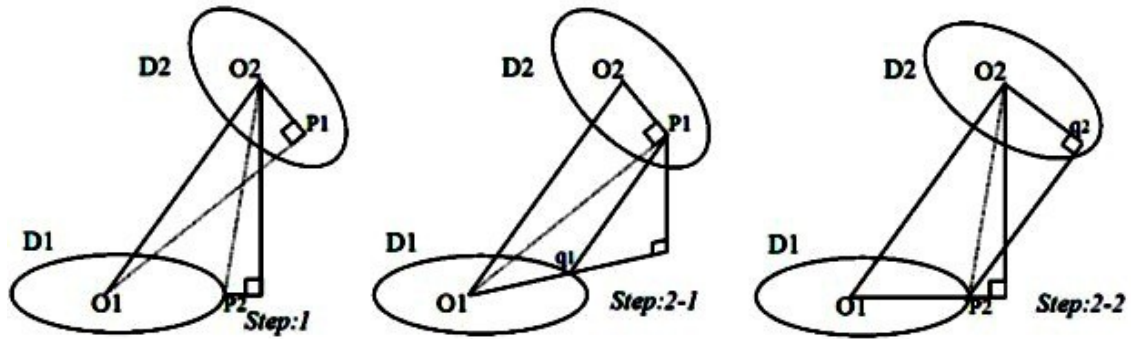


Figure 3-6: Illustration of the algorithm employed to determine the shortest distance between two disks

3.4 Results and Discussion

Monte Carlo methods are known to be computationally expensive modeling techniques. Tackling the high computational cost is a major challenge for researchers employing this method in their research. Owing to a rapid development of computing technology in recent years, high performance computing (hpc) facilities are now generally accessible to researchers in academia while just a few years ago their availability was restricted to researchers in prestigious research institutions. For the present study, a general purpose Linux Cluster provided by WestGrid (supercomputing resources platform) was employed that enables the usage of several processors and a large amount of memory.

A computer code developed in the FORTRAN programming language was run on this computing cluster to study percolation problems for circular nanodisks and the effect of different control parameters including the size of nanodisks, tunneling distance and RVE size. Moreover, scaling effects were examined through Monte Carlo simulations. The Monte Carlo code developed to form a network of circular nanodisks dispersed in a 3D RVE is provided in A.1.

3.4.1 RVE Size Effect

From a strict mathematically point-of-view the percolation threshold should be evaluated for an infinite lattice. However, computational limitations make it impossible to solve the problem in such a manner. Nevertheless, the size of a RVE should be large enough to

minimize any finite effect. Several simulations were carried out for different RVE sizes to determine the scale at which results are no longer dependent on the RVE size. For all simulations in this study the disk thickness t was fixed to 0.34 nm (graphite interlayer distance) [209], which corresponds to the thickness of graphene nanoplatelets. Corresponding results are illustrated in **Figure 3-7**. The RVE must have a large enough size so that the effect of the RVE boundary is negligible and simulation results can be generalized to larger samples. These results led to the approximation that the percolation threshold is independent of the RVE size when the ratio of L/d_t is greater than 35.

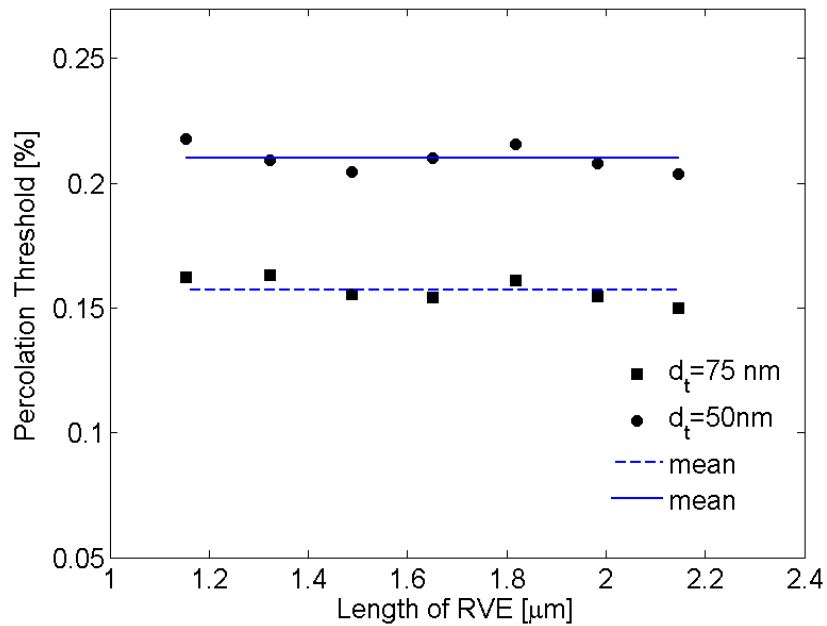


Figure 3-7: Effect of the RVE size on percolation threshold.

3.4.2 Conductivity Criterion

The conductivity criterion described thus far is the existence of a percolation network connecting two parallel sides of the RVE. In this case, electrical current can pass through the sample in this one direction, whereas between other parallel sides the RVE still acts as an insulator. In other words, the RVE properties are not homogenous. An alternative conductivity criterion may be defined, i.e. filler is added to the RVE until all parallel faces are mutually connected by percolation clusters. The resulting RVE would be

conductive in all directions. **Figure 3-8** shows a comparison of percolation thresholds based on both possible criteria. It can be observed that differences in percolation threshold between the two different criteria are diminutive.

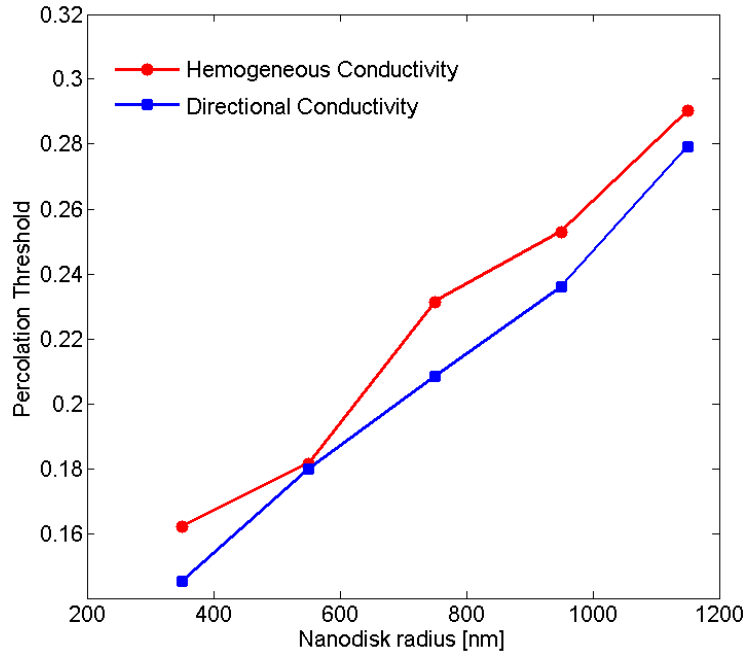


Figure 3-8: Percolation threshold based on different criteria ($d_t=75$ nm).

3.4.3 Critical Volume Fraction

Figure 3-9 shows the percolation threshold with respect to the nanodisk size. This simulation was carried out for different tunneling distances. The data indicates that the percolation threshold increases monotonically with increasing particles size. Consequently, nanodisks with smaller radii produce lower percolation thresholds. Furthermore, polymers with greater tunneling distance need less filler volume to become conductive.

3.4.4 Dimensional Analysis

A dimensional analysis was carried out to identify a dimensionless parameter that plays a dominant role in attaining a critical volume fraction. The percolation threshold is a

function of the various geometric variables, i.e. $V_f=f(R, d_t, t)$. As shown in **Figure 3-10**, the percolation threshold was found to be a linear function of the dimensionless parameter $t.R.d_t^{-2}$.

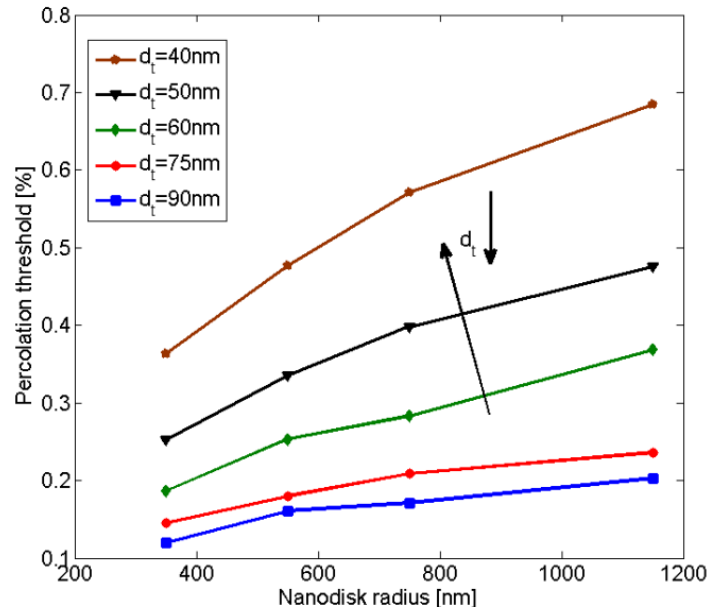


Figure 3-9: Percolation threshold vs. nanodisk size and tunneling distance.

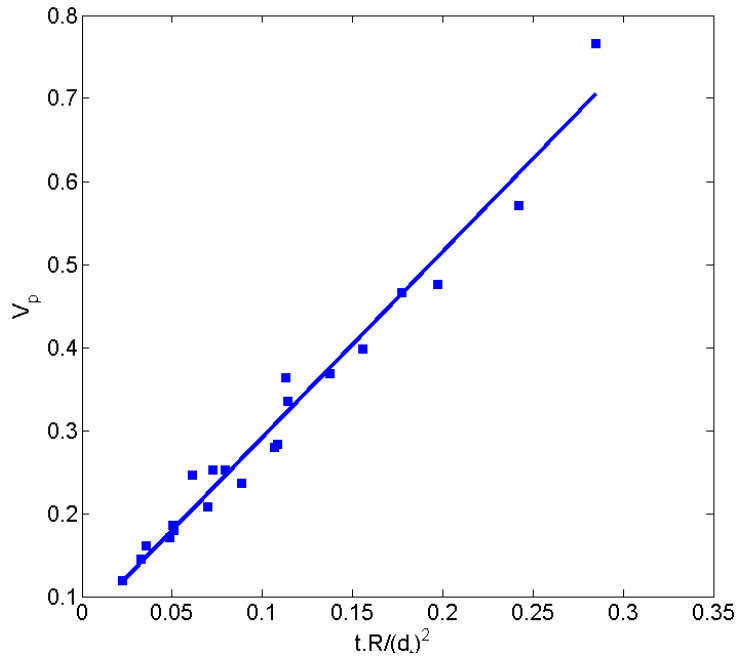


Figure 3-10: Percolation threshold vs. dimensionless variable.

3.4.5 *Percolation of Polydispersed Particles*

In practice the size of nanoscale particles employed for the enhancement of electrical or mechanical properties is not constant but varies from a minimum to a maximum value. An appropriate continuum percolation model was developed using Monte Carlo simulation. This model considers circular nanoplatelets to be randomly dispersed inside a cubic RVE, which was used to evaluate the critical volume fraction at which the composite exhibits a transition from non-conducting to conductive behavior. A parametric study was carried out to investigate the effect of critical parameters on the percolation threshold. These parameters are the tunneling distance, d_t , the smallest particle size contained in the RVE, R_{min} , and the ratio between the radii of the largest and the smallest particles R_{max}/R_{min} . Finally, an equation was developed that correlates the percolation threshold to the parameters considered in this problem.

Monte Carlo modeling was carried out for a range of parameters. The tunneling distance was varied from 2 to 40 nm. Four values for R_{max}/R_{min} were selected, i.e. 2, 4, 6 and 8, while 5, 10, 15, 25 and 35 nm were set for the minimum particle size R_{min} .

Figure 3-11 shows the variation of the percolation threshold with R_{max}/R_{min} . It is shown that the percolation threshold increases approximately linearly with increasing R_{max}/R_{min} .

Figure 3-12 indicates clearly that the percolation threshold decreases monotonically with rising tunneling distance. Conversely, the critical volume fraction becomes larger for increasing R_{min} , see **Figure 3-13**.

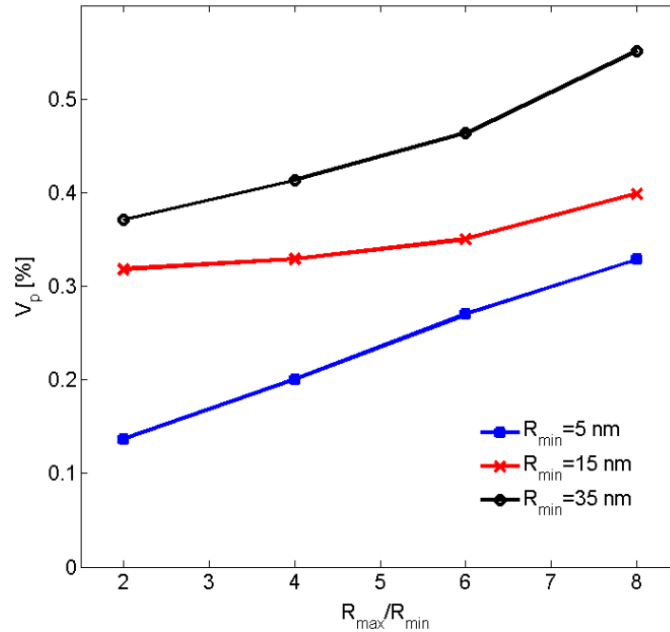


Figure 3-11: Effect of R_{max}/R_{min} on percolation threshold V_p .

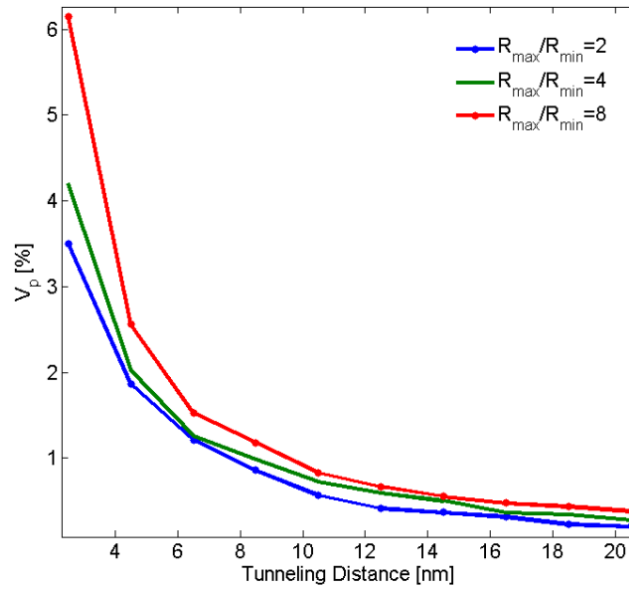


Figure 3-12: Effect of tunneling distance on percolation threshold V_p .

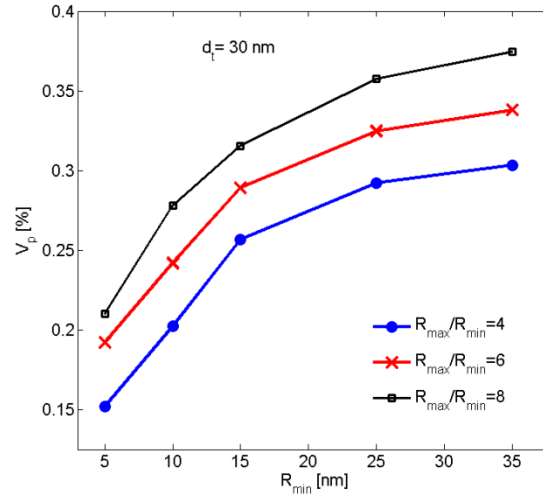


Figure 3-13: Effect of minimum particle size R_{min} on percolation threshold V_p .

In an effort to relate the results illustrated by **Figure 3-11** to **Figure 3-13** the following equation can be offered that correlates the percolation threshold to the involved parameters.

$$V_p = \left(\alpha_1 (R_{max}/R_{min})^{\beta_1} + \alpha_2 R_{min}^{\beta_2} \right) d_t^{\beta_3} \quad \text{Eq. 3-3}$$

The unknown coefficients and exponents in **Eq. 3-3** were evaluated through fitting the proposed equation to the Monte Carlo simulation results. A genetic algorithm (GA) method was employed to minimize the fitting error through finding the optimum coefficients and exponents. From a total of 366 sets of simulation results 300 were used to fit the equation and 66 sets of data were utilized to evaluate the performance and reliability of the developed fitting equation. Considering the randomness of GA solutions, results obtained from the GA optimization method were not expected to be unique, and the algorithm was employed several times providing different outputs. A subset of best fit results is shown in **Table 3-2**. A comparison of results obtained from Monte Carlo simulations and the developed correlation equation (**Eq. 3-3**) are listed in **Table 3-3**. **Table 3-2** shows that exponents, β_1 and β_2 are close to unity, indicating that the percolation threshold is approximately a linear function of R_{max}/R_{min} and R_{min} .

Table 3-2 Best fit coefficients (mse: mean square error).

	α_1	α_2	β_1	β_2	β_3	MSE
1	2.51	1.47	0.93	0.85	-1.37	2.13
2	2.81	1.29	0.92	0.91	-1.42	2.24
3	2.58	1.10	0.96	0.95	-1.39	2.54
4	2.37	2.22	0.95	0.75	-1.42	1.74
5	1.94	1.56	1.08	0.87	-1.41	2.40
6	2.47	1.29	0.97	0.90	-1.39	2.36
7	1.63	1.26	1.20	0.95	-1.42	2.99
8	3.00	1.49	0.86	0.85	-1.40	1.92
9	2.52	1.30	0.96	0.90	-1.39	2.32
10	2.16	1.79	1.00	0.81	-1.39	2.02
mean	2.40	1.48	0.98	0.87	-1.40	2.27

Table 3-3 Comparison of Monte Carlo and proposed equation.

d_c [nm]	R_{min} [nm]	R_{max}/R_{min}	V_p [%] MC	V_p [%] fitting	Error [%]
24	25	8	0.444	0.450	1.1
20	25	2	0.433	0.428	1.0
4	5	6	2.369	2.428	2.4
14	10	8	0.685	0.668	2.4
26	35	8	0.472	0.466	1.3
28	5	4	0.160	0.163	1.9
8	5	8	1.181	1.160	1.8
14	10	8	0.685	0.668	2.4
26	25	6	0.377	0.374	0.9
34	5	4	0.123	0.126	2.3

3.5 Conclusion

In this study a three dimensional continuum Monte Carlo model was developed to evaluate the percolation behavior of polymer composites filled with circular conductive nanodisks. A scaling study confirmed that the representative volume element chosen for this study was of appropriate dimensions to give reliable results independent of its size. A comprehensive study was conducted to evaluate the effect of parameters that affect conductivity properties. Simulations were carried out, and corresponding results were discussed, for a range of input parameters such as tunneling distance and particle dimensions. Finally, an equation was developed to correlate the percolation threshold to the given input parameters. An evaluation of the proposed relationship for selected test data confirmed its aptness for percolation threshold predictions.

3.6 Bibliography

- [4] S. G. Miller, J. L. Bauer, M. J. Maryanski, P. J. Heimann, J. P. Barlow, J. M. Gosau, *et al.*, "Characterization of epoxy functionalized graphite nanoparticles and the physical properties of epoxy matrix nanocomposites," *Composites Science and Technology*, vol. 70, pp. 1120-1125, Jul 2010.
- [5] W. Thongruang, R. J. Spontak, and C. M. Balik, "Correlated electrical conductivity and mechanical property analysis of high-density polyethylene filled with graphite and carbon fiber," *Polymer*, vol. 43, pp. 2279-2286, Apr 2002.
- [10] N. D. Alexopoulos, C. Bartholome, P. Poulin, and Z. Marioli-Riga, "Structural health monitoring of glass fiber reinforced composites using embedded carbon nanotube (CNT) fibers," *Composites Science and Technology*, vol. 70, pp. 260-271, Feb 2010.
- [11] L. Boeger, M. H. G. Wichmann, L. O. Meyer, and K. Schulte, "Load and health monitoring in glass fibre reinforced composites with an electrically conductive nanocomposite epoxy matrix," *Composites Science and Technology*, vol. 68, pp. 1886-1894, Jun 2008.
- [14] L. L. Wu, X. Lv, and C. C. Zhang, "Effect of modified graphene addition on the electrical properties of epoxy resin composite," *Advanced Materials, Pts 1-4*, vol. 239-242, pp. 55-58, 2011.
- [44] H. M. Ma and X. L. Gao, "A three-dimensional Monte Carlo model for electrically conductive polymer matrix composites filled with curved fibers," *Polymer*, vol. 49, pp. 4230-4238, Sep 9 2008.
- [46] N. Hu, Y. Karube, C. Yan, Z. Masuda, and H. Fukunaga, "Tunneling effect in a polymer/carbon nanotube nanocomposite strain sensor," *Acta Materialia*, vol. 56, pp. 2929-2936, Aug 2008.
- [90] C. Y. Li, E. T. Thostenson, and T. W. Chou, "Dominant role of tunneling resistance in the electrical conductivity of carbon nanotube-based composites," *Applied Physics Letters*, vol. 91, Nov 26 2007.
- [126] S. Stankovich, D. A. Dikin, G. H. B. Dommett, K. M. Kohlhaas, E. J. Zimney, E. A. Stach, *et al.*, "Graphene-based composite materials," *Nature*, vol. 442, pp. 282-286, Jul 20 2006.
- [127] H. Pang, T. Chen, G. M. Zhang, B. Q. Zeng, and Z. M. Li, "An electrically conducting polymer/graphene composite with a very low percolation threshold," *Materials Letters*, vol. 64, pp. 2226-2229, Oct 31 2010.
- [135] W. E. Mahmoud, "Morphology and physical properties of poly(ethylene oxide) loaded graphene nanocomposites prepared by two different techniques," *European Polymer Journal*, vol. 47, pp. 1534-1540, Aug 2011.

- [148] S. Y. Qu and S. C. Wong, "Piezoresistive behavior of polymer reinforced by expanded graphite," *Composites Science and Technology*, vol. 67, pp. 231-237, Feb 2007.
- [176] W. G. Zheng, S. C. Wong, and H. J. Sue, "Transport behavior of PMMA/expanded graphite nanocomposites," *Polymer*, vol. 43, pp. 6767-6773, Dec 2002.
- [177] W. Lu, J. X. Weng, D. J. Wu, C. L. Wu, and G. H. Chen, "Epoxy resin/graphite electrically conductive nanosheet nanocomposite," *Materials and Manufacturing Processes*, vol. 21, pp. 167-171, 2006.
- [178] E. T. Thostenson and T. W. Chou, "Real-time in situ sensing of damage evolution in advanced fiber composites using carbon nanotube networks," *Nanotechnology*, vol. 19, May 28 2008.
- [179] K. J. Loh, J. P. Lynch, and N. A. Kotov, "Passive wireless sensing using SWNT-based multifunctional thin film patches," *International Journal of Applied Electromagnetics and Mechanics*, vol. 28, pp. 87-94, 2008.
- [180] K. J. Loh, T. C. Hou, J. P. Lynch, and N. A. Kotov, "Carbon Nanotube Sensing Skins for Spatial Strain and Impact Damage Identification," *Journal of Nondestructive Evaluation*, vol. 28, pp. 9-25, Mar 2009.
- [181] G. E. Pike and C. H. Seager, "Percolation and Conductivity - Computer Study .1.," *Physical Review B*, vol. 10, pp. 1421-1434, 1974.
- [182] I. Balberg and N. Binenbaum, "Cluster structure and conductivity of three-dimensional continuum systems," *Physical Review A*, vol. 31, p. 1222, 1985.
- [183] T. Natsuki, M. Endo, and T. Takahashi, "Percolation study of orientated short-fiber composites by a continuum model," *Physica a-Statistical Mechanics and Its Applications*, vol. 352, pp. 498-508, Jul 15 2005.
- [184] F. Dalmas, R. Dendievel, L. Chazeau, J. Y. Cavaille, and C. Gauthier, "Carbon nanotube-filled polymer of electrical conductivity in composites. Numerical simulation three-dimensional entangled fibrous networks," *Acta Materialia*, vol. 54, pp. 2923-2931, Jun 2006.
- [185] C. Y. Li and T. W. Chou, "Continuum percolation of nanocomposites with fillers of arbitrary shapes," *Applied Physics Letters*, vol. 90, Apr 23 2007.
- [186] S. F. Wang and A. A. Ogale, "Continuum Space Simulation and Experimental Characterization of Electrical Percolation Behavior of Particulate Composites," *Composites Science and Technology*, vol. 46, pp. 93-103, 1993.
- [187] J. Hicks, A. Behnam, and A. Ural, "A computational study of tunneling-percolation electrical transport in graphene-based nanocomposites," *Applied Physics Letters*, vol. 95, Nov 23 2009.
- [188] L. Li and J. E. Morris, "Electrical conduction models for isotropically conductive adhesive joints," *Ieee Transactions on Components Packaging and Manufacturing Technology Part A*, vol. 20, pp. 3-8, Mar 1997.
- [189] Y. B. Yi and E. Tawerghi, "Geometric percolation thresholds of interpenetrating plates in three-dimensional space," *Physical Review E*, vol. 79, Apr 2009.
- [190] J. A. Quintanilla and R. M. Ziff, "Asymmetry in the percolation thresholds of fully penetrable disks with two different radii," *Physical Review E*, vol. 76, Nov 2007.
- [191] J. Quintanilla, "Measurement of the percolation threshold for fully penetrable disks of different radii," *Physical Review E*, vol. 63, pp. art. no.-061108, Jun 2001.
- [192] J. Quintanilla, S. Torquato, and R. M. Ziff, "Efficient measurement of the percolation threshold for fully penetrable discs," *Journal of Physics a-Mathematical and General*, vol. 33, pp. L399-L407, Oct 27 2000.
- [193] L. Vovchenko and V. Vovchenko, "Simulation of percolation threshold in composites filled with conducting particles of various morphologies," *Materialwissenschaft Und Werkstofftechnik*, vol. 42, pp. 70-74, Jan 2011.
- [194] R. H. J. Otten and P. van der Schoot, "Connectivity percolation of polydisperse anisotropic nanofillers," *Journal of Chemical Physics*, vol. 134, Mar 7 2011.

- [195] G. Ambrosetti, N. Johner, C. Grimaldi, A. Danani, and P. Ryser, "Percolative properties of hard oblate ellipsoids of revolution with a soft shell," *Physical Review E*, vol. 78, Dec 2008.
- [196] G. Ambrosetti, C. Grimaldi, I. Balberg, T. Maeder, A. Danani, and P. Ryser, "Solution of the tunneling-percolation problem in the nanocomposite regime," *Physical Review B*, vol. 81, Apr 15 2010.
- [197] M. Mathew, T. Schilling, and M. Oettel, "Connectivity percolation in suspensions of hard platelets," *Physical Review E*, vol. 85, Jun 20 2012.
- [198] W. Xia and M. F. Thorpe, "Percolation Properties of Random Ellipses," *Physical Review A*, vol. 38, pp. 2650-2656, Sep 1 1988.
- [199] J. Li and J. K. Kim, "Percolation threshold of conducting polymer composites containing 3D randomly distributed graphite nanoplatelets," *Composites Science and Technology*, vol. 67, pp. 2114-2120, Aug 2007.
- [200] G. R. Grimmett, "Percolation (Grundlehren der mathematischen Wissenschaften)," ed: Springer: Berlin, Germany, 2010.
- [201] M. Sahini and M. Sahimi, *Applications of percolation theory*: CRC Press, 1994.
- [202] T. Cazenave, "Nested Monte-Carlo Expression Discovery," in *ECAI*, 2010, pp. 1057-1058.
- [203] M. Matsumoto and T. Nishimura, "Mersenne twister: a 623-dimensionally equidistributed uniform pseudo-random number generator," *ACM Transactions on Modeling and Computer Simulation (TOMACS)*, vol. 8, pp. 3-30, 1998.
- [204] N. C. Diaz, A. V. Gil, and M. J. Vargas, "Assessment of the suitability of different random number generators for Monte Carlo simulations in gamma-ray spectrometry," *Applied Radiation and Isotopes*, vol. 68, pp. 469-473, Mar 2010.
- [205] J. Cook, "Rational formulae for the production of a spherically symmetric probability distribution," *Mathematics of Computation*, vol. 11, pp. 81-82, 1957.
- [206] A. A. Ogale and S. F. Wang, "Simulation of the Percolation Behavior of Quasi and Transversely Isotropic Short-Fiber Composites with a Continuum Model," *Composites Science and Technology*, vol. 46, pp. 379-388, 1993.
- [207] Z. Neda, R. Florian, and Y. Brechet, "Reconsideration of continuum percolation of isotropically oriented sticks in three dimensions," *Physical Review E*, vol. 59, pp. 3717-3719, Mar 1999.
- [208] H. A. Almohamad and S. Z. Selim, "An algorithm for computing the distance between two circular disks," *Applied Mathematical Modelling*, vol. 27, pp. 115-124, Feb 2003.
- [209] K. I. Bolotin, K. Sikes, Z. Jiang, M. Klima, G. Fudenberg, J. Hone, *et al.*, "Ultrahigh electron mobility in suspended graphene," *Solid State Communications*, vol. 146, pp. 351-355, 2008.

CHAPTER 4

ELECTRICAL CONDUCTIVITY AND PIEZORESISTIVITY OF THE NANOCOMPOSITE ¹

SYNOPSIS- In this chapter, a three-dimensional continuum percolation model developed based on a Monte Carlo simulation approach was employed to investigate the percolation behavior of an electrically insulating matrix reinforced with conductive nanoplatelet fillers. The conductivity behavior of composites rendered conductive by randomly dispersed conductive platelets was modeled by developing a three-dimensional finite element resistor network. Parameters related to the percolation threshold and a power-law describing the conductivity behavior were determined. The piezoresistivity behavior of conductive composites was studied employing a reoriented resistor network emulating a conductive composite subjected to mechanical strain. The effects of the governing parameters, *i.e.*, electron tunneling distance, conductive particle aspect ratio and size effects on conductivity behavior were examined.

4.1 Introduction

Chapter 3 of this thesis was devoted to study the percolation behavior of a system of nanoplatelets from a mathematical point-of-view. The present chapter is devoted to exploring the conductivity behavior of polymers rendered conductive through the dispersion of conductive nanoplatelets. The 3D Monte Carlo model developed in the previous chapter was employed to study the percolation, conductivity and piezoresistive behavior of composites filled with randomly dispersed impenetrable conductive nanodisks. The Monte Carlo model was first utilized to form a representative volume element filled with randomly dispersed nanoplatelet conductive inclusions. In a second stage a 3D finite element based resistors network model was used to analyze the

¹ A version of this chapter has been published as: Oskouyi, A.B.; Sundararaj, U.; Mertiny, P. Tunneling Conductivity and Piezoresistivity of Composites Containing Randomly Dispersed Conductive Nano-Platelets. *Materials* 2014, 7, 2501-2521.

conductivity behavior of nanoplatelet based conductive polymers. Previous studies have shown that conductivity of such polymers for volume fractions greater than the percolation threshold can be described by a power-law expression [210], i.e.:

$$\rho \propto (V - V_p)^s \quad \text{Eq. 4-1}$$

where V_p is the percolation threshold, V is the volume fraction of the dispersed inclusions, and ρ and s are the resistivity and a critical exponent respectively. Parameters in **Eq. 4-1** were determined through curve fitting using the results obtained from finite element modeling. The resistor network model was also used to study the piezoresistive behavior for reoriented and updated conductive platelets when a conductive composite is subjected to mechanical strain.

4.2 Electrical Conductivity, Clusters and Percolation Network

Electrical connection between two conductive inclusions arises from two different mechanisms, i.e.,

- (i) mechanical contact between conductive particles.
- (ii) electron tunneling effects.

Based on quantum mechanical tunneling theory, electrical current can flow under certain conditions through an insulator material. In other words, it can be assumed that a pair of conductive inclusions dispersed in an insulator matrix is electrically connected by a resistor formed by the matrix so that electrons can passage from one inclusion to the adjacent one. It was shown in different studies that tunneling conductivity plays the dominant role in the conductivity of insulating polymers filled with conductive inclusions [90]. For strongly conductive fillers the intrinsic filler conductivity has no appreciable contribution toward the nonlinear current-voltage behavior of nanocomposites, with nonlinearity arising from tunneling effects. Experimental research works devoted to studying the current-voltage behavior of carbon nanotubes based [75, 211] and graphene nanoplatelet based [212, 213] conductive nanocomposites indicate that nonlinear current-voltage behavior is more pronounced for disk-shaped fillers. The significant dependency of conductivity on voltage in circular disks indicates that conductivity is indeed governed by tunneling mechanisms. As shown by Simmons [214], electron tunneling resistivity can

be described by **Eq. 4-2** for a low-voltage range when $e\Delta V \ll \lambda$, where ΔV is the electrical potential, e is the quantum of electricity and λ is the barrier height of the insulator.

$$\rho_{tunnel} = \frac{h^2}{e^2 \sqrt{2m\lambda}} \exp\left(\frac{4\pi d}{h} \sqrt{2m\lambda}\right) \quad \text{Eq. 4-2}$$

where h is Planck constant, m is the mass of an electron and d is the tunneling distance.

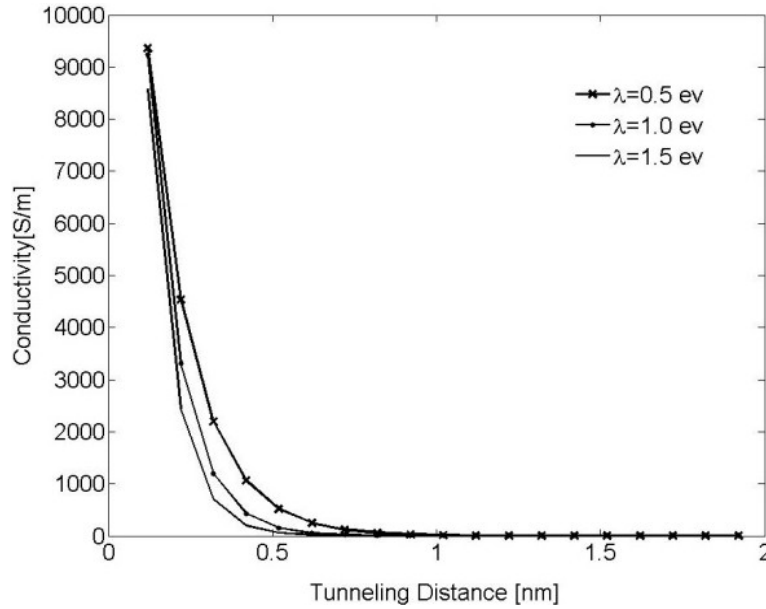


Figure 4-1: Tunneling conductivity vs. tunneling distance for electrons passing through an insulator matrix for different insulator barrier heights λ .

Eq. 4-2 was numerically evaluated for different values of λ ($\lambda = 0.5, 1.0$ and 1.5 eV) and results are illustrated in **Figure 4-1**. It can be observed that tunneling conductivity (i.e., the inverse of resistivity) drastically decreases for an increasing tunneling distance. It can, thus, be concluded that a cut-off distance can be approximated at which resistors with length greater than this distance have no appreciable contribution to the overall conductivity of the nanocomposite. This cut-off distance is called electron-tunneling distance. In the developed model, nanoplatelets with neighboring distance less than the tunneling distance are labeled a cluster. A cluster connecting two parallel faces of the RVE is called

a percolation network, which enables electrical current to flow through the RVE, thus, rendering the nanocomposite conductive.

The volume fraction of the conductive particles at the onset of the percolation network is called the percolation threshold. This concept is illustrated by the schematic shown in **Figure 4-2**. It was assumed that current flow between two conductive inclusions would occur along the shortest possible path in between them. It is therefore necessary to determine the shortest distance between the inclusions. As it was explained in the previous chapter in details, the algorithm developed by Almohamad and Selim [208] was employed in the present modeling approach to compute the shortest distance between two circular disks in 3D space.

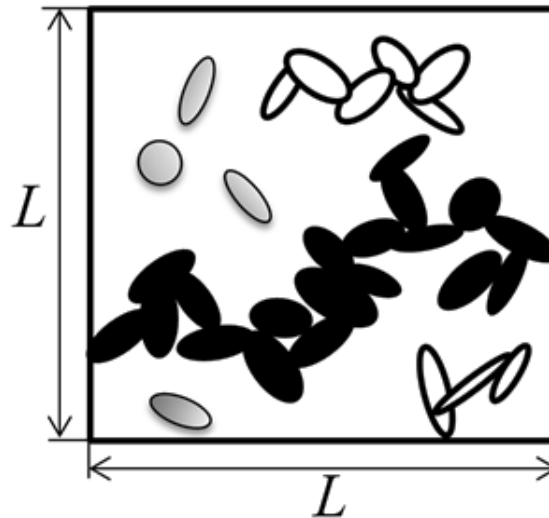


Figure 4-2: Schematic of representative volume element with individual nanoplatelets (gray), and platelets forming clusters (white) and a percolation network (black).

In order to estimate the conductivity of a conductive composite a 3D network of resistors was formed (see schematic in **Figure 4-3**). As such, randomly dispersed conductive nanoplatelets were modeled as circular disks generated and randomly dispersed inside the RVE using the methods described above, and disks in clusters were mutually connected by tunneling resistors which resistivity was approximated using **Eq. 4-2**. Disks were assumed to be in contact with each other when the shortest distance between their center planes is

less than the thickness of the disks. Finite element modeling was employed to evaluate the conductivity of a resistor network representing the nanocomposite.

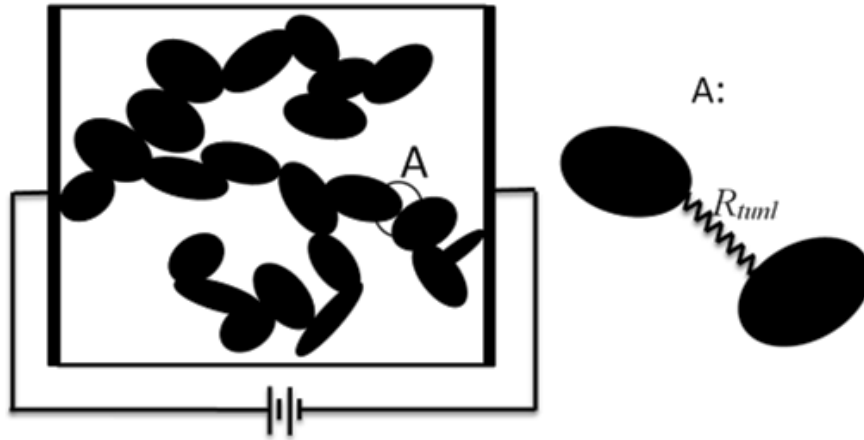


Figure 4-3: Schematic of three-dimensional percolation network modeled by tunneling resistors (A)

4.3 Piezoresistivity Effects

Subjecting a polymer with conductive inclusions to mechanical strain, as shown in **Figure 4-4**, is often accompanied by a change in resistivity. This behavior is known as the piezoresistivity effect, which is an interesting characteristic of conductive nanocomposites rendering them good candidates for sensor applications. Generally, there are two main reasons for piezoresistive behavior of nanocomposites, i.e.,

- i. changes in interparticular distance.
- ii. reorientation of conductive particles.

Piezoresistivity of nanocomposites with conductive inclusions has been the subject of several numerical and analytical works [46, 187, 215, 216]. In the present study, the described framework of Monte Carlo simulation and finite element modeling were employed to evaluate the piezoresistive behavior of conductive composites with nanoplatelets. Most conductive nanofillers have superior mechanical properties in comparison to the matrix. As a consequence their deformation was neglected for a nanocomposite being subjected to mechanical strain, and conductive nanoplatelets were assumed to undergo rigid body motion only. Note that nanoplatelets such as graphene may

be wrinkled or crumpled when dispersed in a host polymer. The probability of being non-planar increases as the size of the nanodisk is increasing. Since this study was conducted for small-size nanodisks, it was assumed that disks remain planar during dispersion and mechanical loading. Further work may be conducted to evaluate the effect of wrinkling and bending on the nanocomposite electrical behavior. The new position and orientation of the nanoplatelets in the deformed matrix (for uniaxial tensile strain) were determined using affine transformation utilizing the formulation developed by Pham [216]. Filler reorientation and displacement inside the polymer matrix is also governed by lateral mechanical strain, which is induced by Poisson's ratio effects. For numerical simulations the Poisson's ratio was set at 0.33, which was found to be the mean value reported in the literature for the Poisson's ratio of nanoplatelet based conductive composites. A 3D resistor network was then re-developed for the updated nanoplatelet structure, and aforementioned finite element modeling was employed to evaluate the conductivity of the strained nanocomposite.

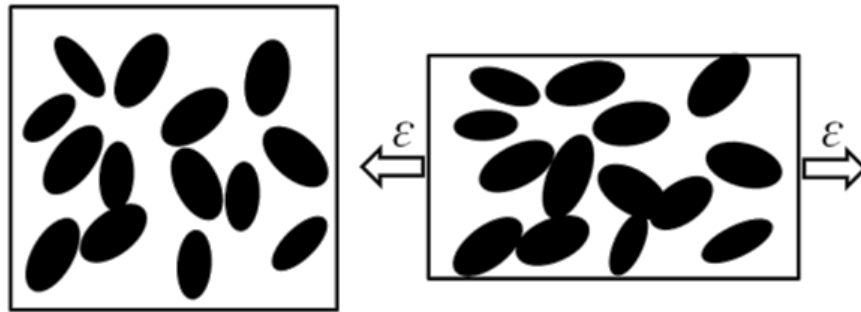


Figure 4-4: Schematic of nanoplatelet composite subjected to tensile strain.

4.3.1 Formulation

Figure 4-5 illustrates the orientation of the circular nanodisk in 3D space. XYZ is the global coordinate system and the X'Y'Z' indicates the local coordinate system where the normal vector of the nanodisk's plane in the local coordinate system is (0,0,1).

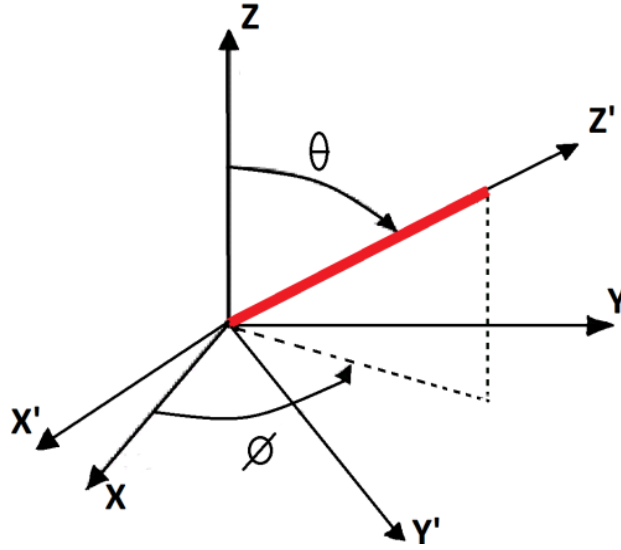


Figure 4-5: Orientation vector of the nanoplatelet and related parameter definition

The nanocomposite undergoes a mechanical strain where the strain tensor in global coordinate system is ε . The strain tensor in term of local coordinate system is given by the following equation [216]:

$$\varepsilon'_{ij} = T_{ki} T_{lj} \varepsilon_{kl} \quad \text{Eq. 4-3}$$

where, T is the transformation matrix. Changes in the angle θ due to the mechanical strain can be written as [216]:

$$\frac{\partial \theta}{\partial \varepsilon_{ij}} = \frac{\partial \theta}{\partial \varepsilon'_{13}} \frac{\partial \varepsilon'_{13}}{\partial \varepsilon_{ij}} \quad \text{Eq. 4-4}$$

Since $\frac{\partial \theta}{\partial \varepsilon'_{13}} = 1$ and using **Eq. 4-4**, it can be rewritten as [216]:

$$\frac{\partial \theta}{\partial \varepsilon_{ij}} = \frac{\partial \varepsilon'_{13}}{\partial \varepsilon_{ij}} = \frac{\partial (T_{i1} T_{j3} \varepsilon_{ij})}{\partial \varepsilon_{ij}} = T_{i1} T_{j3} \quad \text{Eq. 4-5}$$

Similarly the changes in the angle Φ , can be obtained as [216]:

$$\frac{\partial \Phi}{\partial \varepsilon_{ij}} = T_{i1} T_{j2} \quad \text{Eq. 4-6}$$

4.3.2 Piezoresistivity Coefficients of Nanocomposite

In order to employ the conductive nanocomposite as embedded sensor for structural health monitoring application, the piezoresistivity behaviour of the nanocomposite should be well determined. Considering the generalized Ohm's law the electrical field (E) can be evaluated as:

$$E_i = \rho_{ij} J_j \quad \text{Eq. 4-7}$$

where J is the electrical current density and ρ is the resistivity tensor. The resistivity change of piezoresistive material with cubic symmetry, induced by mechanical stress can be written as [217]:

$$\begin{bmatrix} \Delta\rho_1/\rho_0 \\ \Delta\rho_2/\rho_0 \\ \Delta\rho_3/\rho_0 \\ \Delta\rho_4/\rho_0 \\ \Delta\rho_5/\rho_0 \\ \Delta\rho_6/\rho_0 \end{bmatrix} = \begin{bmatrix} \pi_{11} & \pi_{12} & \pi_{12} & 0 & 0 & 0 \\ \pi_{12} & \pi_{11} & \pi_{12} & 0 & 0 & 0 \\ \pi_{12} & \pi_{12} & \pi_{11} & 0 & 0 & 0 \\ 0 & 0 & 0 & \pi_{44} & 0 & 0 \\ 0 & 0 & 0 & 0 & \pi_{44} & 0 \\ 0 & 0 & 0 & 0 & 0 & \pi_{44} \end{bmatrix} \begin{bmatrix} \sigma_1 \\ \sigma_2 \\ \sigma_3 \\ \sigma_4 \\ \sigma_5 \\ \sigma_6 \end{bmatrix} \quad \text{Eq. 4-8}$$

Considering uniaxial loading condition, it can be concluded that:

$$\begin{aligned} \pi_{11} &= (\Delta\rho_1/\rho_0)(1/\sigma_1) \\ \pi_{12} &= (\Delta\rho_2/\rho_0)(1/\sigma_1) \end{aligned} \quad \text{Eq. 4-9}$$

where, ρ_0 is the strain-free resistivity of nanocomposite and σ is the applied mechanical strain. In this study, the change in the resistivity of nanocomposite in both lateral and transverse directions are determined through finite element analysis. So, coefficients π_{11} and π_{12} can be obtained using **Eq. 4-9**, and from the isotropic condition the third piezoresistivity coefficient can be determined as: $\pi_{44} = \pi_{11} - \pi_{12}$ [218].

4.3.3 Finite Element Modeling

As mentioned earlier, it was assumed that two particles with a shortest distance between them of less than the cut-off distance are electrically connected through a tunneling resistor. The concept of a tunneling resistor was mathematically modeled as an electrical resistor connecting the adjacent nanoplatelets where its resistance is governed by **Eq. 4-2**.

The electrical resistivity of the network was evaluated developing a three-dimensional finite element model. The concept of a three-dimensional resistor network and resulting electrical conductivity is depicted in the schematic in **Figure 4-6**.

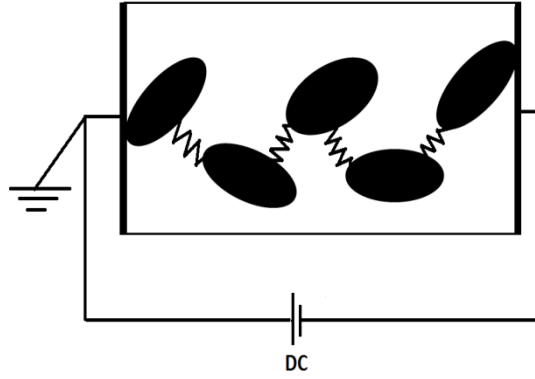


Figure 4-6: Schematic for the conductivity mechanism in nanocomposites with conductive platelet inclusions.

Considering the significantly higher conductivity of conductive nanoplatelets (e.g. $\sigma_{graphene} = 10^8$ S/m), the electrical potential drop across nanoplatelets was assumed to be negligible in comparison with the tunneling resistivity. Consequently, conductive inclusions were not taken into account when evaluating the resistivity of the nanocomposite. Applying the finite element formulation to the electrical resistors yields the following expression:

$$\begin{Bmatrix} I_{ij} \\ -I_{ij} \end{Bmatrix} = \begin{bmatrix} (R_{ij})^{-1} & -(R_{ij})^{-1} \\ -(R_{ij})^{-1} & (R_{ij})^{-1} \end{bmatrix} \begin{Bmatrix} V_i \\ V_j \end{Bmatrix} \quad \text{Eq. 4-10}$$

where R_{ij} is the resistance of the element between the i^{th} and j^{th} node, I_{ij} is the electrical current passing between nodes i and j , and V_i is the voltage at the i^{th} node with respect to ground. The system of equations determining the nanocomposite electrical behavior was obtained by assembling the governing equations for the individual elements. It was assumed that a known electrical current passes through the RVE, and that one of the RVE electrode nodes is grounded (see **Figure 4-6**). According to Kirchhoff's current law, $\Sigma I = 0$ at each node except for the electrode nodes. Defining a conductivity matrix, K , the voltages at the nodes can thus be given as:

$$\{V\} = \text{inv}[K]\{I\} \quad \text{Eq. 4-11}$$

Each element, i.e. the tunneling resistors and the pristine resistivity of the CNTs, were represented by a single element and for each case the number of the elements is fixed and equal to the number of the resistors in the network. Note that this model does not constitute a finite elements model as it is commonly presented for mechanical or thermal analysis, that is, with meshing of the matrix and filler particles

4.4 Results and Discussion

The computational code for the Monte Carlo simulation was developed in the FORTRAN language to numerically investigate the 3D continuum percolation problem of conductive nanodisks. Considering the high computational cost of the Monte Carlo simulation, multiple processors was employed to allow for rapid code execution on a Linux cluster.

The developed model was evaluated numerically considering a polymer matrix such as epoxy containing conductive nanodisk filler comprised of graphene platelets. Hence a constant nanodisk thickness of 0.34 nm was assumed, which is equal to the thickness of a single graphene layer (graphite interlayer distance) [219]. Considering the high conductivity of graphene predicted by experimental and numerical studies [220], it can reasonably be said that tunneling resistance dominates the conductivity properties of graphene nanocomposites. Hence, the electrical potential difference across graphene sheets was herein assumed negligible compared to the potential drop in the tunneling resistors. Ignoring the resistivity of the nanodisks in the present model also resulted in a considerable decrease in computational cost. The RVE size was set to be eight times $2R+d_t$, which was found large enough to minimize any errors introduced by finite size effects (d_t and R are the tunneling cut-off distance and nanodisk radius, respectively).

4.4.1 Effective Electron Tunneling Distance

As discussed earlier, a cut-off distance can be assumed at which the effect of tunneling resistors with length greater than this distance is negligible. The conductivity of nanocomposites was evaluated for different values of electron tunneling distance. Considering the results shown in **Figure 4-7** it was concluded that for a barrier height of 0.5eV (for epoxy polymer [46]), tunneling resistors with length greater than 2 nm have no

appreciable contribution to the conductivity of the nanocomposite. In the present study the tunneling distance was, thus, assumed to be 2.5 nm. This value is conservatively larger than values given in the literature (e.g., 1.4 nm in [221]), ensuring that essentially all tunneling paths that may contribute toward nanocomposite conductivity have been taken into account.

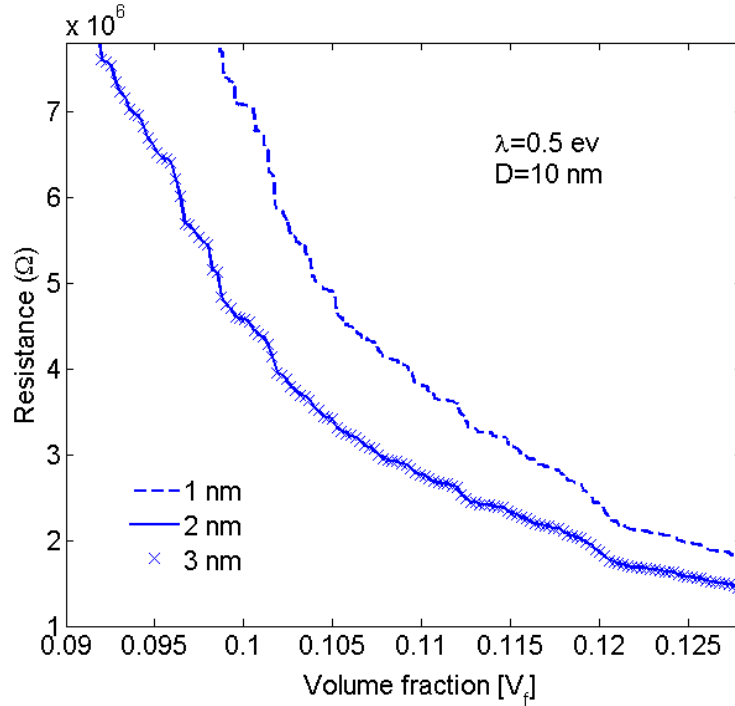


Figure 4-7: Effect of tunneling cut-off distance (1 nm, 2 nm and 3 nm) on the resistivity of nanoplatelet composites for an insulator barrier height of $\lambda = 0.5\text{eV}$ and a platelet diameter of $D = 10\text{ nm}$

4.4.2 Effect of Matrix Electrical Properties on Nanocomposite Conductivity

It was stated previously that the polymer matrix chiefly affects the electrical resistivity of a nanocomposite, especially for lower filler volume fractions. As such, the contribution of matrix electrical properties, i.e., the barrier height λ should be investigated. Electrical resistivity was evaluated for three different barrier heights, i.e., 0.5, 1.5 and 2.5 eV, representing typical values reported as height of barrier for epoxy [46] filled with randomly dispersed nanoplatelets. Results illustrated by **Figure 4-8** indicate that the matrix barrier height strongly affects the nanocomposite conductivity. For example, for a

filler volume fraction of 7.5% the electrical resistivity of a nanocomposite with $\lambda=1.5$ eV is more than two orders of magnitude greater than for a matrix with $\lambda=0.5$ eV.

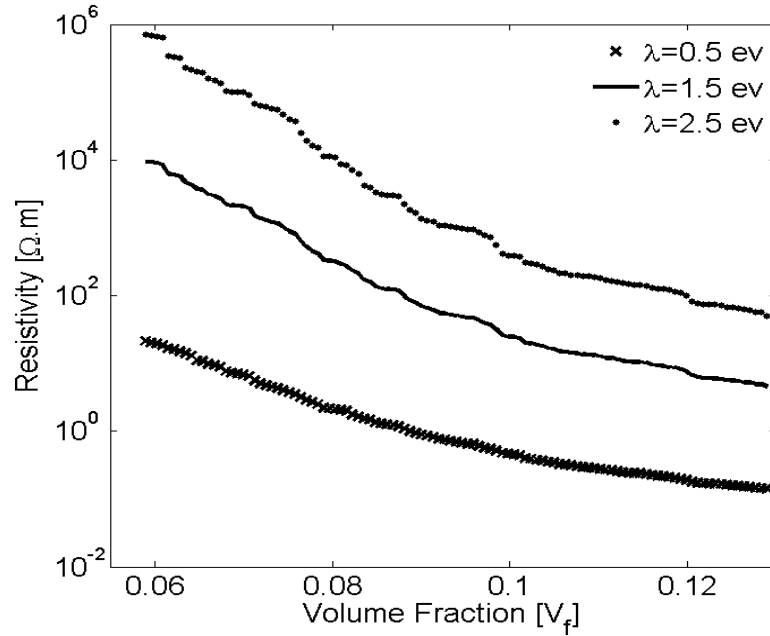


Figure 4-8: Effect of insulator barrier height λ on the resistivity of conductive nanoplatelet composites plotted vs. filler volume fraction for a platelet diameter of $D=10$ nm.

4.4.3 Percolation Threshold and Electrical Conductivity

Figure 4-9 illustrates the resistivity of nanocomposites with respect to changes in nanodisks volume fraction. A critical volume fraction is recognizable at which a sharp drop in nanocomposite resistivity occurs. This region was considered the formation of a percolation network.

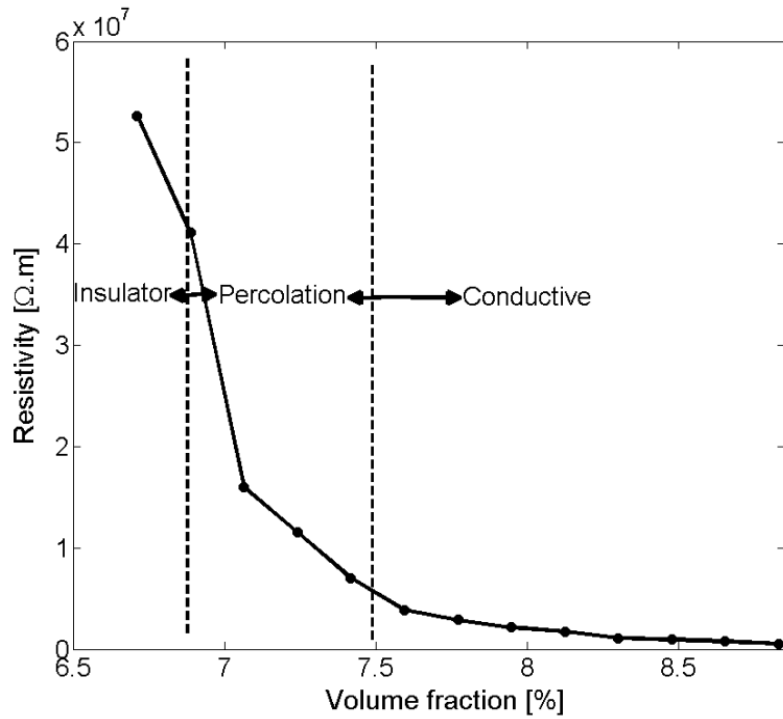


Figure 4-9: Graph defining the percolation region depicted as nanoplatelet composite resistivity vs. filler volume fraction.

Balberg et al. [222] showed that tunneling percolation conductivity yields a staircase effect in both lattice and continuum percolation systems. They also reported that the existence of the staircase percolation behavior is validated by experimental data [57, 127, 222-227]. Based on these findings the resistivity/filler-loading curves cannot be described by a single percolation threshold and critical exponent. In other words, **Eq. 4-1** cannot adequately describe any given set of resistivity/volume-fraction data, and each subset of data should be described with different values of s and V_p . The present study confirmed that a single expression with specific values of s and V_p is insufficient to represent the entire nanocomposite conductivity and percolation behavior. This is illustrated in **Figure 4-10**, where the power-law description with a universal value of s ($s_u=2$) was fitted to the resistivity data for nanocomposites with filler diameter of 20 nm. For low volume fractions the data points deviate little from the universal description, while the deviation increases with filler concentration. Interestingly, a threshold can be inferred from the curve at which the critical exponent regime changes. Findings illustrated in **Figure 4-11**

are results obtained from fitting **Eq. 4-1** to a data subset with interval of $(V_p, 1.4V_p)$. **Figure 4-12** shows the power-law approximation for higher filler volume fractions. As illustrated by **Figure 4-13**, fitting **Eq. 4-1** to the dilute region of the curve yields values of s with small deviation from s_u . Employing the power-law equation to describe the composite behavior for higher volume fractions, on the other hand, yields a mean value of 5.56 for the critical exponent, i.e., s deviates strongly from s_u .

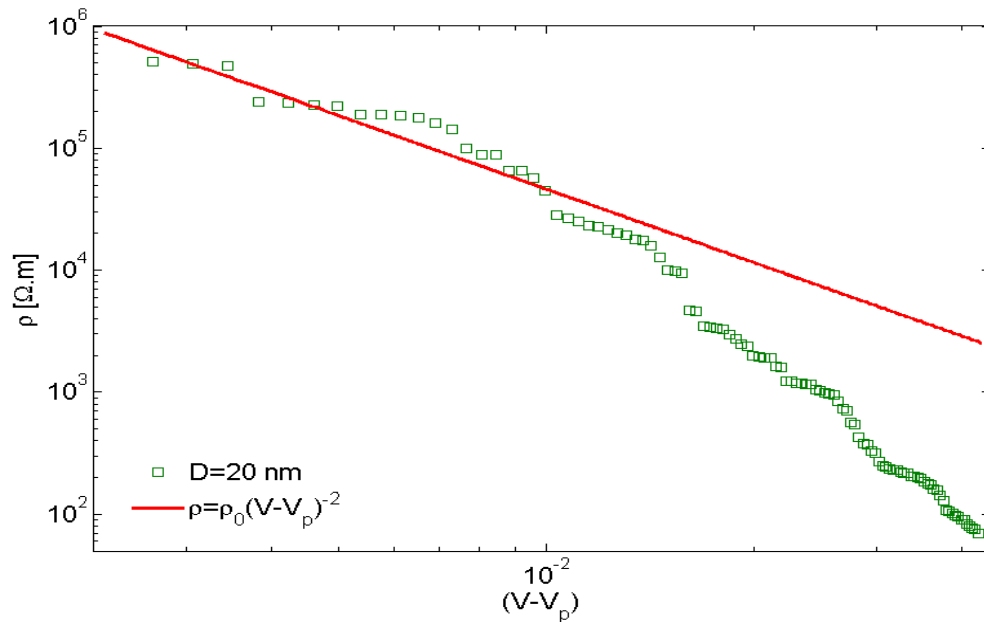


Figure 4-10: Deviation of nanoplatelet composite resistivity from a universal power-law description with $s=2$ for increasing filler content.

Comparing **Figure 4-11** and **Figure 4-12** reveals that the conductivity/filler-loading curves describe a rather smooth behavior for volume fractions well above the percolation region, while a somewhat “erratic” behavior can be observed near the percolation threshold. Assuming a single expression for the description of nanocomposite conductivity may necessitate ignoring the percolation neighborhood and considering its data outliers. As mentioned in [222, 228], close agreement between s and s_u is expected to be restricted to a small region near the percolation threshold, and non-universal percolation behavior becomes dominant as the filler volume fraction is increasing. Based on the above considerations, results obtained in the present study for conductive circular nanodisks indicate a critical exponent that is filler content dependent and converges toward

the universal value with filler loading approaching the percolation threshold. This conclusion is congruent with findings from Johner et al. [229]. Data for different nanodisk sizes given in **Figure 4-11**, **Figure 4-12** and **Figure 4-14** further indicate an increasing percolation threshold and electrical conductivity with increasing nanodisks size. Note that the trendline shown in **Figure 4-14** only illustrates the data trend.

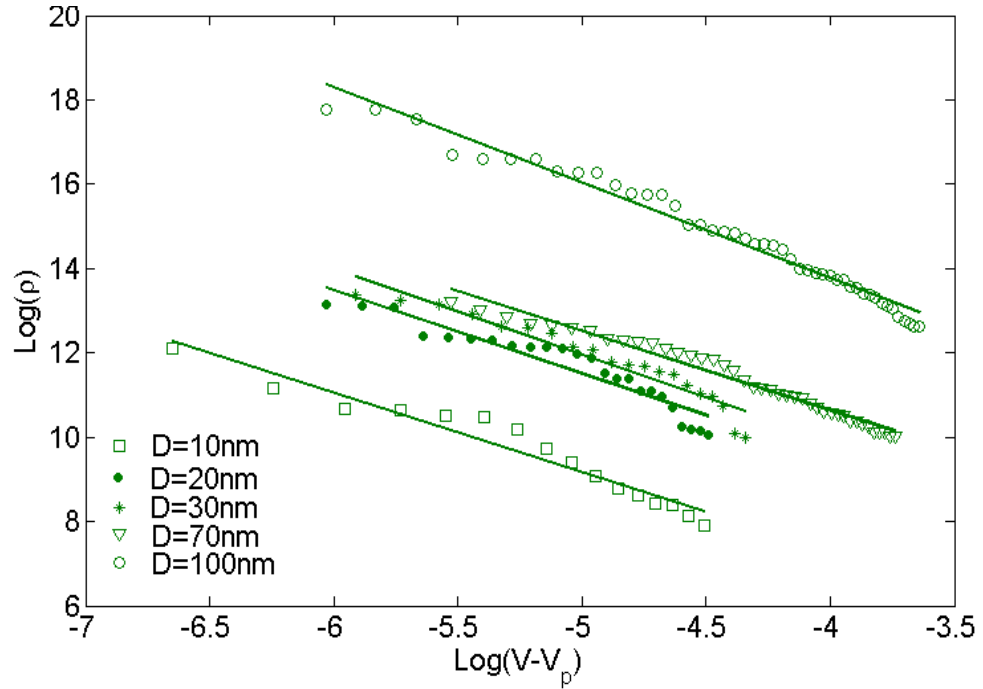


Figure 4-11: Nanoplatelet composite resistivity vs. filler volume fraction and best-fit curves for post-percolation power-law description for filler concentration near the percolation threshold ($V_p, 1.4V_p$).

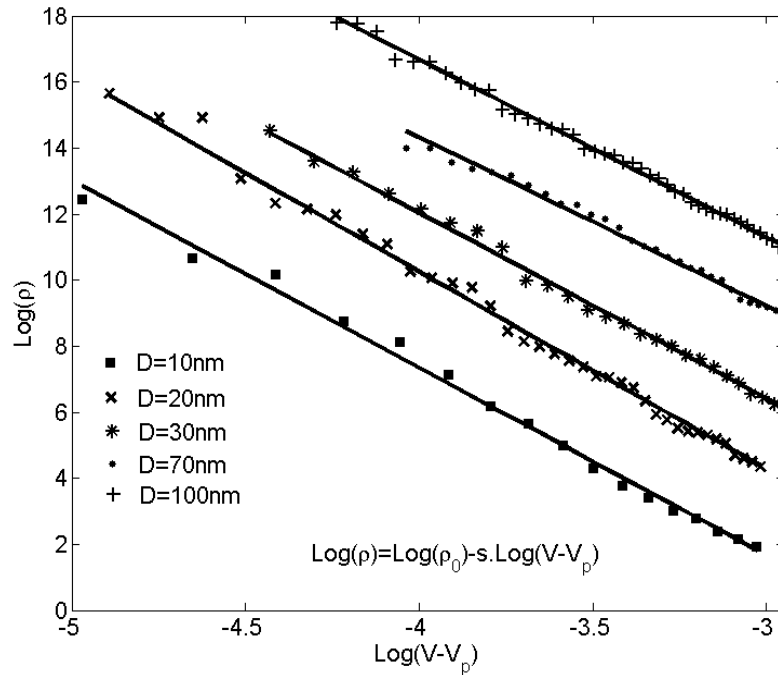


Figure 4-12: Nanocomposite resistivity vs. filler volume fraction and best-fit curves for a post-percolation power-law description (percolation region and erratic points are considered data outlier)

Ambrosetti et al. [195] studied the percolation threshold for hard oblate ellipsoids of revolution surrounded by a penetrable soft shell, which is analogous to the electron tunneling concept employed in the present study. Nanodisks can be assumed as spheroids where the major axis a is much larger than the minor axis b (axis of symmetry). In [195], it was shown that the percolation threshold is governed by the ratio of the major axis to the minor axis, a/b , and the ratio of the soft shell thickness d to the major axis, d/a . In the present study, parameters a , b and d are equivalent to the nanodisk radius, thickness and tunneling distance, respectively. As illustrated in **Figure 4-15**, percolation thresholds for different oblate radii (i.e., 1.25, 1.88, 2.92, 5.00, 7.10, 11.25 nm) were computed keeping b and d constant at 0.17 nm (disk thickness/2) and 1.25 nm (tunneling distance/2), respectively. Disk radii were chosen to correspond to percolation thresholds provided in [195]. Critical volume fractions provided in **Figure 4-15** include the volume of the soft penetrable shell surrounding the hard oblates. As explained previously, the soft shell is equivalent to tunneling distance concept in this study, so the volume of the soft shell has

been deduced from the volume fraction provided by **Figure 4-15** using the correction factor $a^2b/((a + d)^2(b + d))$. Resulting percolation thresholds are given in **Figure 4-16**, which indicates an increasing percolation threshold for an increasing oblate major axis (tunneling distance and oblates thickness are constant). It worth noting that in the present study the percolation threshold was evaluated for circular nanodisks, while in [195] the percolation threshold of oblates was investigated, and results from [195] are provided herein to illustrate the qualitative agreement between trends.

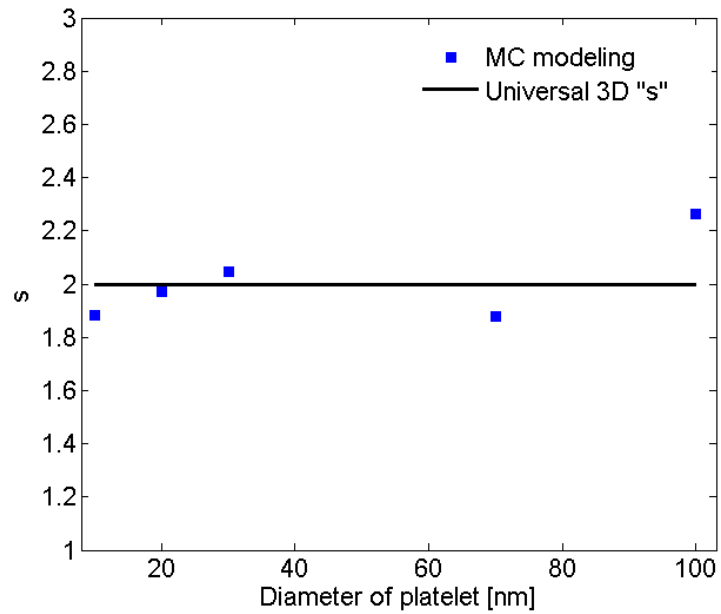


Figure 4-13: Values for the critical exponent, s , for data in the percolation region.

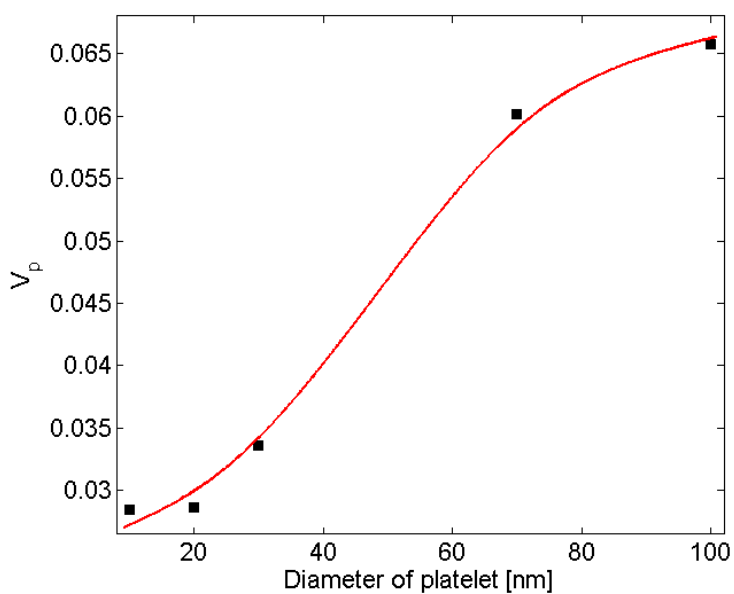


Figure 4-14: Graph depicting filler volume fraction at the percolation threshold V_p vs. nanoplatelet diameter D .

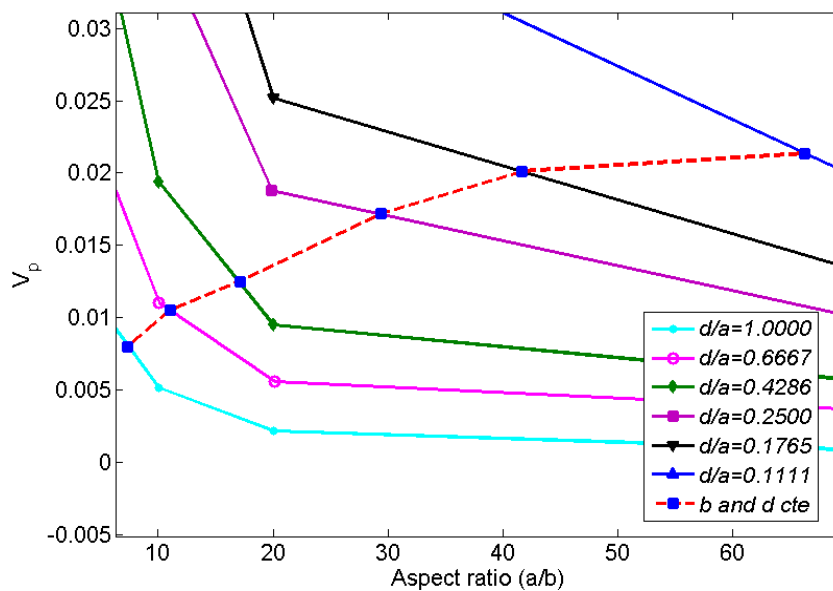


Figure 4-15: Percolation threshold of oblates of revolution as a function of aspect ratio and ratio of soft shell thickness to the major axis. The dashed line depicts the percolation threshold trend when b and d are constant. (adapted from [195]).

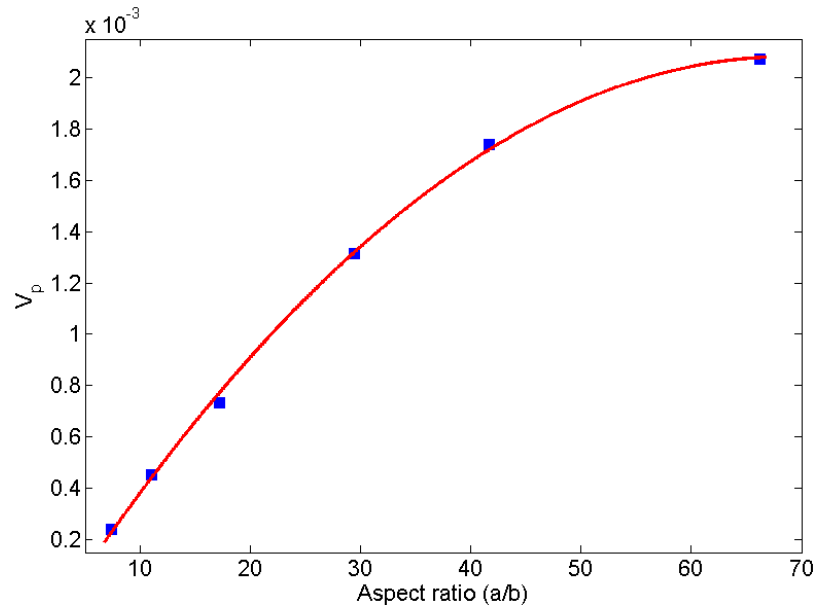


Figure 4-16: Percolation threshold of oblates of revolution as a function of aspect ratio. The soft shell volume was deducted in order to make the data analogous to a tunneling percolation problem with platelet based nanocomposites. (adapted from [195]).

In another work, Lee and Torquato [230] evaluated the critical area fraction for 2D circular disks with impenetrable radius of λR surrounded by a penetrable shell with thickness $(1 - \lambda)R$, dispersed in a 2D domain. Similar to Ambrosetti's work [195], $(1 - \lambda)R$ is equivalent to the tunneling distance used in the present study. In [230] the critical area fraction is given in term of λ . In **Figure 4-17** percolation thresholds are replotted *versus* $\lambda/(1 - \lambda)$, a parameter representing the ratio of disk diameter to tunneling distance. Values for the percolation threshold were multiplied by λ^2 to exclude the area of the penetrable shell that is equivalent to the tunneling distance. As illustrated by **Figure 4-17**, the percolation threshold increases as the ratio of disk size to the tunneling distance is increasing. Furthermore, Mathew et al. [197] showed that the dependency of platelet based conductive composite percolation threshold on the aspect ratio is in contradiction with that of needle-like fillers [231-233]. In other words, trends obtained for the relation between aspect ratio and percolation threshold of needle-like fillers cannot be generalized to a platelet-like filler percolation problem.

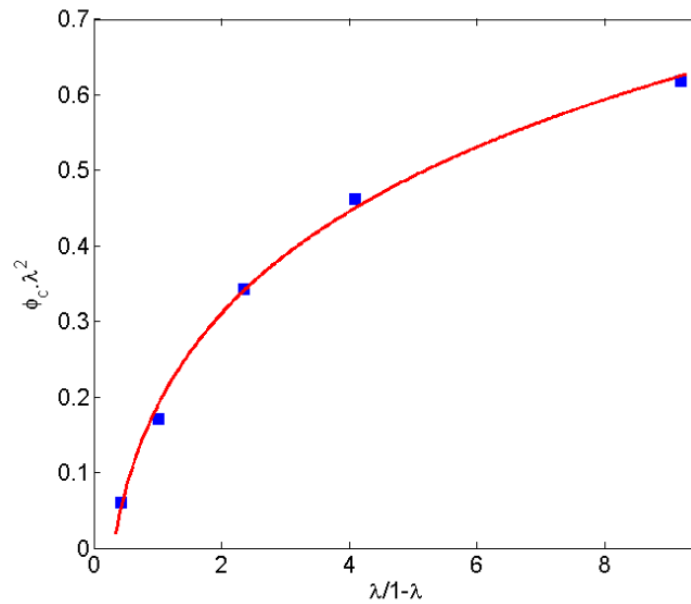


Figure 4-17: Percolation threshold for 2D disks dispersed in a 2D domain. (adapted from [230]).

4.4.4 Piezoresistivity of Nanoplatelet Nanocomposites

Employing the methods described in section 4.3, the piezoresistivity behavior of nanocomposites with nanoplatelet inclusions was investigated. Simulation results shown in Figure 4-18 for unstrained nanocomposites and three applied tensile strains ($\varepsilon=0.1\%$, 0.3% , 0.5%) demonstrate an increase in resistivity with applied strain.

In Figure 4-19 to Figure 4-22 the piezoresistivity behavior of nanoplatelet based conductive composites with four different filler volume fractions is presented. According to prediction data shown in Figure 4-19, nanocomposites exhibit somewhat erratic piezoresistivity behavior for low filler volume fractions, while the nanocomposite piezoresistivity behavior becomes smoother with increasing filler concentration.

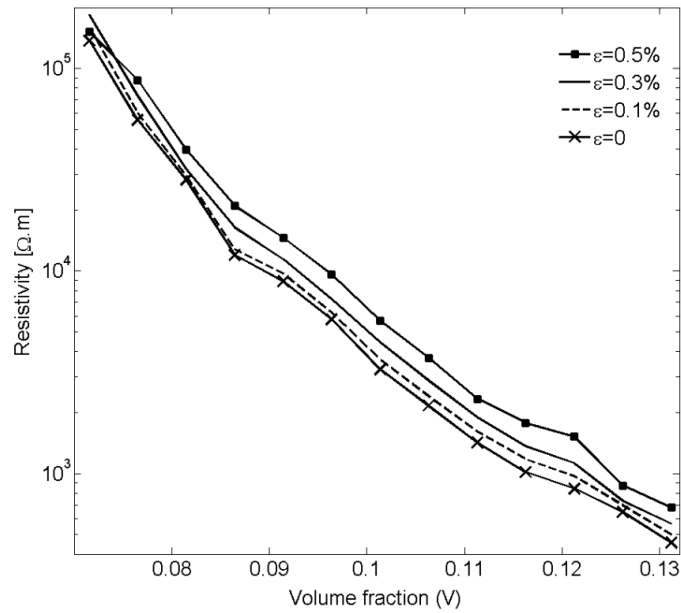


Figure 4-18: Resistivity vs. filler volume fraction demonstrating the response of an unconstrained nanoplatelet composite to applied tensile strain ε for a platelet diameter of $D=70$ nm.

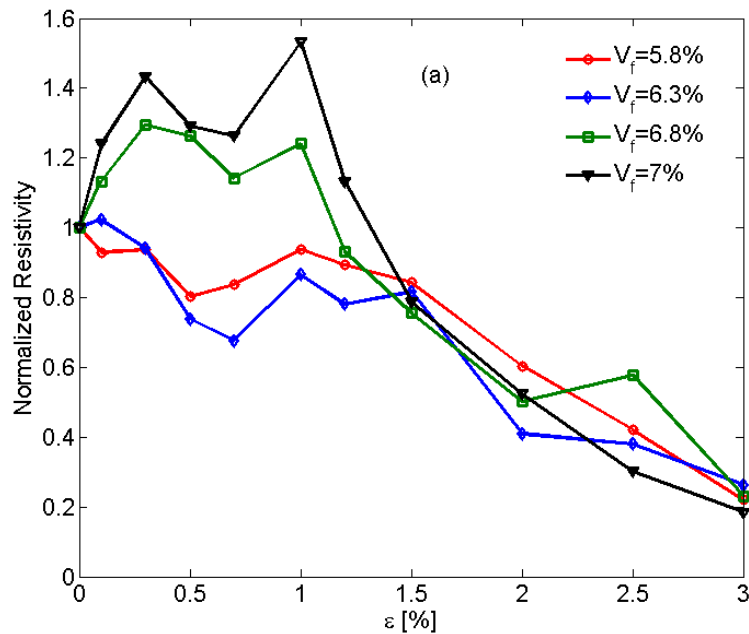


Figure 4-19: Erratic piezoresistivity behavior for low filler loadings

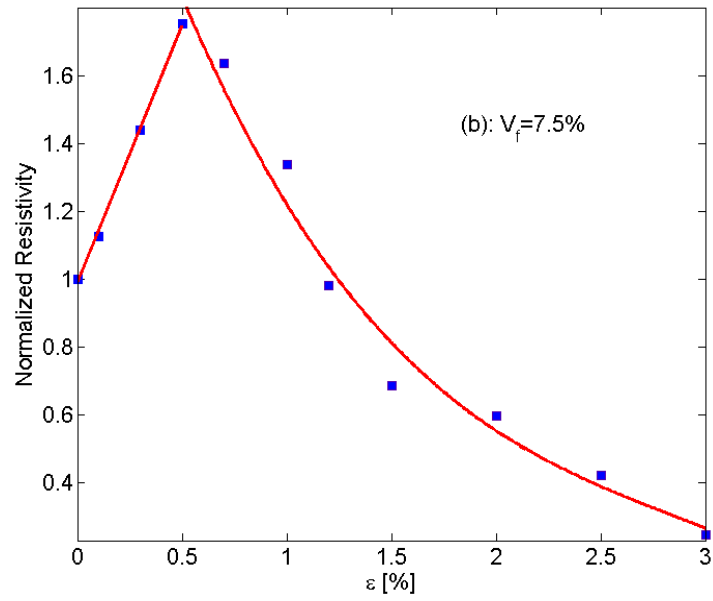


Figure 4-20: Piezoresistivity behavior for $V_f=7.5\%$;

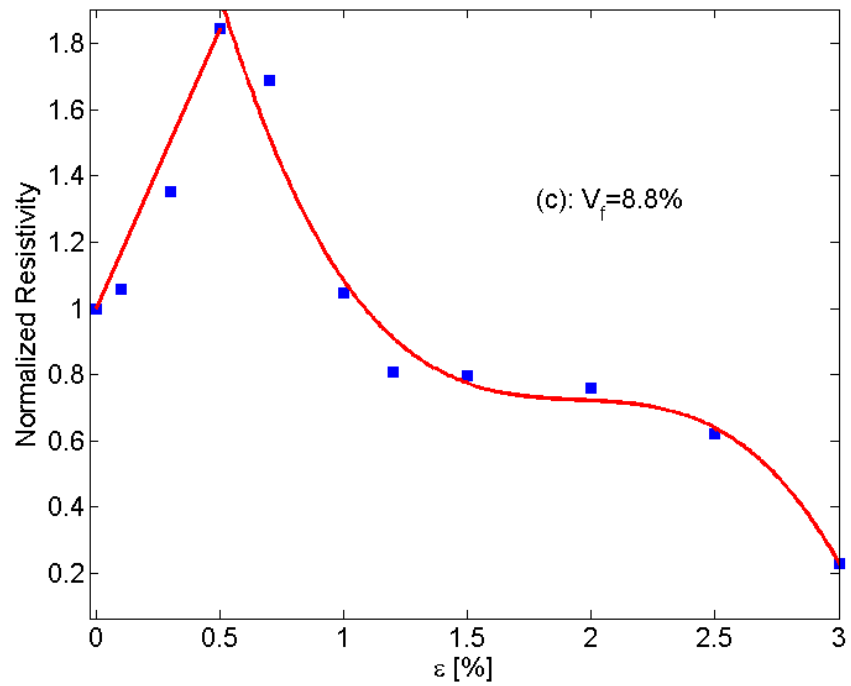


Figure 4-21: Piezoresistivity graph with plateau region for $V_f=8.8\%$

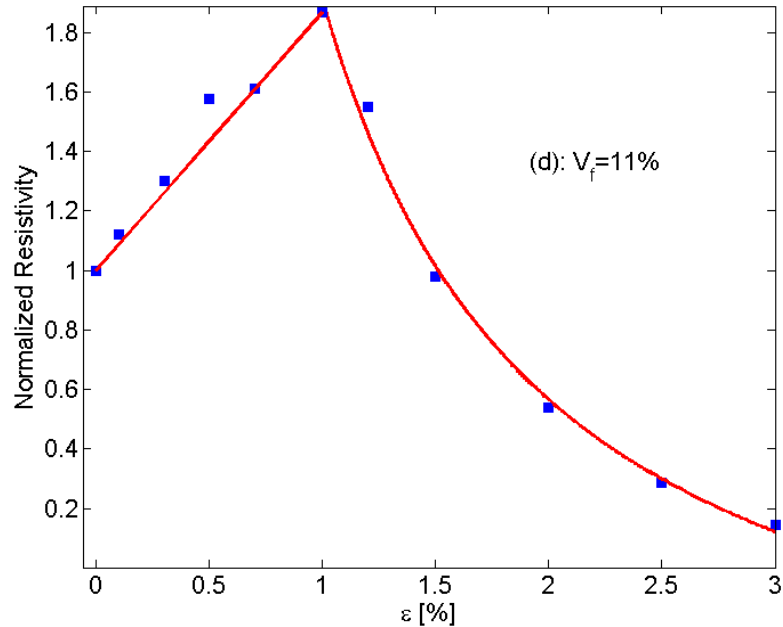


Figure 4-22: Piezoresistivity behavior for $V_f=11\%$.

As mentioned above, piezoresistivity in conductive composites arises from two major mechanisms, that is, changing particle proximity and orientation. Increasing the tensile strain increases the average interparticular distance, so an increase in resistivity of the conductive nanocomposite is expected. On the other hand, tensile strain raises the propensity for the formation of clusters, leading to a decrease in electrical resistivity. This conjecture is supported by the results shown in **Figure 4-20** and **Figure 4-22**. For small values of mechanical strain, piezoresistivity behavior is governed by changes in interparticular distance, causing resistivity to rise approximately linearly with strain. A critical strain can then be found at which the nanocomposite piezoresistivity behavior changes, that is, resistivity now decreases monotonically with increasing strain. Luheng et al. [215] reported similar behavior for silicone rubber composites filled with carbon black, i.e., a critical pressure was observed at which a change in the trend of the

piezoresistivity effect occurred. The existence of a critical pressure was also described by Lu et al. [150] for the piezoresistive behavior of polyethylene nanocomposites with exfoliated graphite. Li et al. [234] also reported a critical strain for carbon nanotube-graphene nanoplatelet hybrid composites. As illustrated by **Figure 4-23**, the electrical resistivity increased with mechanical strain up to a critical strain upon which resistivity begins to decrease with rising strain. The data presented in **Figure 4-20** to **Figure 4-22** further reveals an increase in critical strain for increasing filler volume fraction. Additional studies are warranted to further evaluate the effect of the governing parameters such as filler size and concentration on the critical strain.

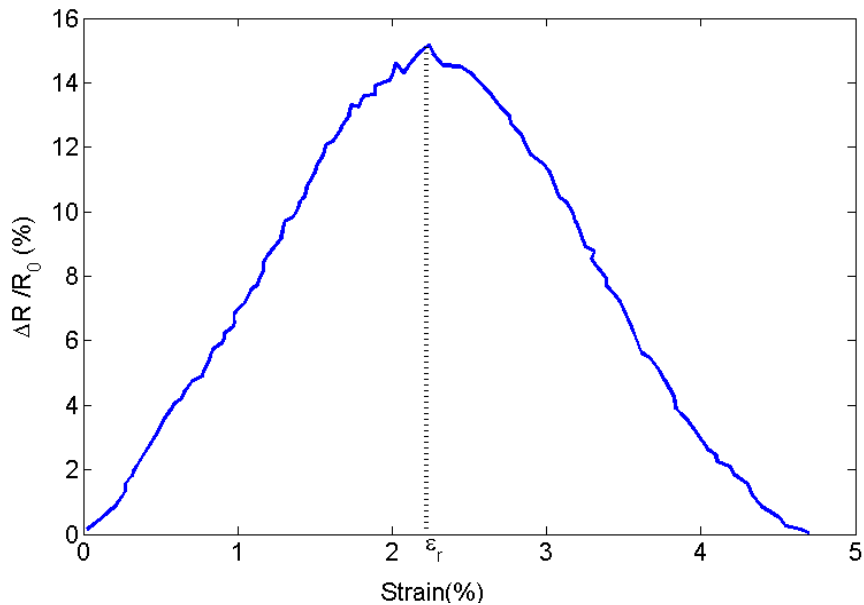


Figure 4-23: Piezoresistivity behavior and critical strain for a CNT-graphene nanoplatelet hybrid composite. (adapted from [234]).

The observed “switching behavior” and the existence of a critical strain have been reported in several other studies. Kalanadhabhatla [235] conducted a comprehensive discussion and literature review on the switching piezoresistivity behavior of conducting filler based nanocomposites. Two different kinds of piezoresistivity behavior and variations of resistivity trends have been reported in the technical literature. Some studies described negative gauge factors at the onset of tensile strain application, followed by an

increase in resistivity as strain is increasing. Some nanocomposites with fillers, such as carbon black [236], CNT [237, 238], and graphite nanosheets [239] were found to have a positive gauge factor for lower strains, while some studies reported a decreasing resistivity up to a critical strain with increasing tensile strain [240-243]. The various studies devoted to piezoresistivity of conducting filler/polymer composites indicate that geometrical properties such as filler aspect ratio and filler concentration play a critical role in the piezoresistivity behavior of conductive nanocomposites. The role of aspect ratio on piezoresistivity behavior can be comprehended by comparing the findings in [244-246]. In [246], graphite particles with diameters between 5 and 15 μm and thicknesses ranging from 1 to 2 μm dispersed in silicone rubber yielded a decrease in resistivity for compressive strains, while in [244], silicone/graphite nanosheet specimens with filler thicknesses of 30 to 80 nm and aspect ratios of 100 to 500 showed an increase in resistivity. As illustrated by **Figure 4-19** to **Figure 4-22**, the sensitivity of piezoresistive nanocomposites (slope of the curve for strains lower than critical strains) is governed by filler concentration. In another study, Kost *et al.* [247] showed that carbon black based conductive composites display higher sensing sensitivity for lower filler concentrations, which is in agreement with findings in the present study. Near the percolation region there are few percolation clusters, and the formation or destruction of percolation clusters caused by strain has thus a significant contribution toward the change in nanocomposite resistivity.

It is interesting to note that for some intermediate filler volume fractions, i.e., volume fractions between those shown in **Figure 4-20** and **Figure 4-22**, a diminished piezoresistivity effect can be observed for increasing strain as indicated by the plateau in the curve shown in **Figure 4-21**. This behavior can be explained considering aforementioned piezoresistivity mechanisms in conductive nanocomposites, that is, at strain levels within the plateau region none of the two-piezoresistivity mechanisms is dominant; thus their effects cancel each other, leading to diminutive piezoresistivity behavior.

4.5 Conclusions

Using a combined Monte Carlo and finite element modeling framework a theoretical study was carried out to investigate the electrical conductivity and piezoresistivity behavior of nanocomposites filled with conductive nanoplatelets such as graphene. The power law relationship describing the conductivity of such polymers for filler volume fractions greater than the percolation threshold was investigated and discussed. The critical exponent was approximately constant for all of the nanodisk sizes considered herein, which led to the conclusion that the exponent is controlled by filler geometry rather than size. In addition, the critical exponent in the power law description depends on the filler volume fraction. Near the percolation threshold, the exponent was found to match the often-cited value of 2, whereas the exponent deviates from this value for higher filler loadings. Modeling results further indicate a reduction in percolation threshold for decreasing nanodisks sizes and a strong effect of matrix electrical properties, i.e., the barrier height of the insulator. The investigation of the piezoresistivity behavior was performed through affine transformation. The filler volume fraction was found to play an important role in the piezoresistivity behavior. An erratic piezoresistivity behavior was observed for low filler volume fractions just exceeding the percolation threshold. For higher volume fractions an approximately linear correlation with strain was predicted up to a critical strain at which the resistivity behavior was found to change. For strains higher than the critical strain a monotonic decrease in electrical resistivity was observed. Overall, values of the critical strain were observed to rise with increasing filler volume fraction. Consequently, piezoresistivity behavior of nanoplatelet based conductive composites can be tailored by adjusting the conductive filler content.

4.6 Bibliography

- [46] N. Hu, Y. Karube, C. Yan, Z. Masuda, and H. Fukunaga, "Tunneling effect in a polymer/carbon nanotube nanocomposite strain sensor," *Acta Materialia*, vol. 56, pp. 2929-2936, Aug 2008.
- [57] J. Z. Kovacs, B. S. Velagala, K. Schulte, and W. Bauhofer, "Two percolation thresholds in carbon nanotube epoxy composites," *Composites Science and Technology*, vol. 67, pp. 922-928, Apr 2007.
- [75] Z. Ounaies, C. Park, K. E. Wise, E. J. Siochi, and J. S. Harrison, "Electrical properties of single wall carbon nanotube reinforced polyimide composites," *Composites Science and Technology*, vol. 63, pp. 1637-1646, Aug 2003.
- [90] C. Y. Li, E. T. Thostenson, and T. W. Chou, "Dominant role of tunneling resistance in the electrical conductivity of carbon nanotube-based composites," *Applied Physics Letters*, vol. 91, Nov 26 2007.

- [127] H. Pang, T. Chen, G. M. Zhang, B. Q. Zeng, and Z. M. Li, "An electrically conducting polymer/graphene composite with a very low percolation threshold," *Materials Letters*, vol. 64, pp. 2226-2229, Oct 31 2010.
- [150] J. R. Lu, X. F. Chen, W. Lu, and G. H. Chen, "The piezoresistive behaviors of polyethylene/foliated graphite nanocomposites," *European Polymer Journal*, vol. 42, pp. 1015-1021, May 2006.
- [187] J. Hicks, A. Behnam, and A. Ural, "A computational study of tunneling-percolation electrical transport in graphene-based nanocomposites," *Applied Physics Letters*, vol. 95, Nov 23 2009.
- [195] G. Ambrosetti, N. Johnner, C. Grimaldi, A. Danani, and P. Ryser, "Percolative properties of hard oblate ellipsoids of revolution with a soft shell," *Physical Review E*, vol. 78, Dec 2008.
- [197] M. Mathew, T. Schilling, and M. Oettel, "Connectivity percolation in suspensions of hard platelets," *Physical Review E*, vol. 85, Jun 20 2012.
- [208] H. A. Almohamad and S. Z. Selim, "An algorithm for computing the distance between two circular disks," *Applied Mathematical Modelling*, vol. 27, pp. 115-124, Feb 2003.
- [210] D. Stauffer and A. Aharony, *Introduction to percolation theory*: Taylor and Francis, 1994.
- [211] G. Gorrasi, E. Piperopoulos, M. Lanza, and C. Milone, "Effect of morphology of the filler on the electrical behaviour of poly(L-lactide) nanocomposites," *Journal of Physics and Chemistry of Solids*, vol. 74, pp. 1-6, Jan 2013.
- [212] A. Celzard, G. Furdin, J. F. Mareche, and E. McRae, "Non-linear current-voltage characteristics in anisotropic epoxy resin graphite flake composites," *Journal of Materials Science*, vol. 32, pp. 1849-1853, Apr 1 1997.
- [213] L. X. He and S. C. Tjong, "Zener tunneling in conductive graphite/epoxy composites: Dielectric breakdown aspects," *Express Polymer Letters*, vol. 7, pp. 375-382, Apr 2013.
- [214] J. G. Simmons, "Generalized Formula for the Electric Tunnel Effect between Similar Electrodes Separated by a Thin Insulating Film," *Journal of Applied Physics*, vol. 34, pp. 1793-1803, 1963.
- [215] W. Luheng, D. Tianhuai, and W. Peng, "Influence of carbon black concentration on piezoresistivity for carbon-black-filled silicone rubber composite," *Carbon*, vol. 47, pp. 3151-3157, Nov 2009.
- [216] G. T. Pham, *Characterization and modeling of piezo-resistive properties of carbon nanotube-based conductive polymer composites*: ProQuest, 2008.
- [217] C. Hu, Y. Gao, and Z. Sheng, "The piezoresistance coefficients of copper and copper-nickel alloys," *Journal of materials science*, vol. 35, pp. 381-386, 2000.
- [218] D. Grady and M. Ginsberg, "Piezoresistive effects in ytterbium stress transducers," *Journal of Applied Physics*, vol. 48, pp. 2179-2181, 1977.
- [219] Y. Huang, J. Wu, and K. C. Hwang, "Thickness of graphene and single-wall carbon nanotubes," *Physical Review B*, vol. 74, Dec 2006.
- [220] S. V. Morozov, K. S. Novoselov, M. I. Katsnelson, F. Schedin, D. C. Elias, J. A. Jaszczak, *et al.*, "Giant intrinsic carrier mobilities in graphene and its bilayer," *Physical Review Letters*, vol. 100, Jan 11 2008.
- [221] W. S. Bao, S. A. Meguid, Z. H. Zhu, and G. J. Weng, "Tunneling resistance and its effect on the electrical conductivity of carbon nanotube nanocomposites," *Journal of Applied Physics*, vol. 111, May 1 2012.
- [222] I. Balberg, D. Azulay, Y. Goldstein, J. Jedrzejewski, G. Ravid, and E. Savir, "The percolation staircase model and its manifestation in composite materials," *European Physical Journal B*, vol. 86, Oct 14 2013.
- [223] H. Zois, L. Apekis, and M. Omastova, "Electrical properties of carbon black-filled polymer composites," *Macromolecular Symposia*, vol. 170, pp. 249-256, Jun 2001.

- [224] J. Vilcakova, P. Saha, and O. Quadrat, "Electrical conductivity of carbon fibres/polyester resin composites in the percolation threshold region," *European Polymer Journal*, vol. 38, pp. 2343-2347, Dec 2002.
- [225] W. Bauhofer and J. Z. Kovacs, "A review and analysis of electrical percolation in carbon nanotube polymer composites," *Composites Science and Technology*, vol. 69, pp. 1486-1498, Aug 2009.
- [226] E. Tkalya, M. Ghislandi, A. Alekseev, C. Koning, and J. Loos, "Latex-based concept for the preparation of graphene-based polymer nanocomposites," *Journal of Materials Chemistry*, vol. 20, pp. 3035-3039, 2010.
- [227] V. Panwar, B. Kang, J. O. Park, S. Park, and R. M. Mehra, "Study of dielectric properties of styrene-acrylonitrile graphite sheets composites in low and high frequency region," *European Polymer Journal*, vol. 45, pp. 1777-1784, Jun 2009.
- [228] N. Johner, P. Ryser, C. Grimaldi, and I. Balberg, "Piezoresistivity and tunneling-percolation transport in apparently nonuniversal systems," *Physical Review B*, vol. 75, Mar 2007.
- [229] N. Johner, C. Grimaldi, I. Balberg, and P. Ryser, "Transport exponent in a three-dimensional continuum tunneling-percolation model," *Physical Review B*, vol. 77, May 2008.
- [230] S. B. Lee and S. Torquato, "Monte-Carlo Study of Correlated Continuum Percolation - Universality and Percolation Thresholds," *Physical Review A*, vol. 41, pp. 5338-5344, May 15 1990.
- [231] Y. Yu, S. Song, Z. Bu, X. Gu, G. Song, and L. Sun, "Influence of filler waviness and aspect ratio on the percolation threshold of carbon nanomaterials reinforced polymer nanocomposites," *Journal of Materials Science*, vol. 48, pp. 5727-5732, 2013.
- [232] S. Pfeifer, S. H. Park, and P. R. Bandaru, "Analysis of electrical percolation thresholds in carbon nanotube networks using the Weibull probability distribution," *Journal of Applied Physics*, vol. 108, Jul 15 2010.
- [233] C. Li, E. T. Thostenson, and T.-W. Chou, "Effect of nanotube waviness on the electrical conductivity of carbon nanotube-based composites," *Composites Science and Technology*, vol. 68, pp. 1445-1452, 2008.
- [234] W. K. Li, A. Dichiaro, and J. B. Bai, "Carbon nanotube-graphene nanoplatelet hybrids as high-performance multifunctional reinforcements in epoxy composites," *Composites Science and Technology*, vol. 74, pp. 221-227, Jan 24 2013.
- [235] S. K. Kalanadhabhatla, *Piezoresistivity Behavior of Polydimethylsiloxane Based Conducting Composites for Printing on Textiles*: North Carolina State University, 2012.
- [236] L. Flandin, A. Hiltner, and E. Baer, "Interrelationships between electrical and mechanical properties of a carbon black-filled ethylene-octene elastomer," *Polymer*, vol. 42, pp. 827-838, Jan 2001.
- [237] J. Lu, M. Lu, A. Bermak, and Y.-K. Lee, "Study of piezoresistance effect of carbon nanotube-PDMS composite materials for nanosensors," in *Nanotechnology, 2007. IEEE-NANO 2007. 7th IEEE Conference on*, 2007, pp. 1240-1243.
- [238] Z. M. Dang, M. J. Jiang, D. Xie, S. H. Yao, L. Q. Zhang, and J. B. Bai, "Supersensitive linear piezoresistive property in carbon nanotubes/silicone rubber nanocomposites," *Journal of Applied Physics*, vol. 104, Jul 15 2008.
- [239] R. Soltani and A. A. Katbab, "The role of interfacial compatibilizer in controlling the electrical conductivity and piezoresistive behavior of the nanocomposites based on RTV silicone rubber/graphite nanosheets," *Sensors and Actuators a-Physical*, vol. 163, pp. 213-219, Sep 2010.
- [240] M. K. Abyaneh and S. K. Kulkarni, "Giant piezoresistive response in zinc-polydimethylsiloxane composites under uniaxial pressure," *Journal of Physics D: Applied Physics*, vol. 41, p. 135405, 2008.
- [241] G. Ausanio, A. Barone, C. Campana, V. Iannotti, C. Luponio, G. Pepe, *et al.*, "Giant resistivity change induced by strain in a composite of conducting particles in an elastomer matrix," *Sensors and Actuators A: Physical*, vol. 127, pp. 56-62, 2006.
- [242] D. Beruto, M. Capurro, and G. Marro, "Piezoresistance behavior of silicone-graphite composites in the proximity of the electric percolation threshold," *Sensors and Actuators A: Physical*, vol. 117, pp. 301-308, 2005.

- [243] L. Chen, G. Chen, and L. Lu, "Piezoresistive Behavior Study on Finger-Sensing Silicone Rubber/Graphite Nanosheet Nanocomposites," *Advanced Functional Materials*, vol. 17, pp. 898-904, 2007.
- [244] L. Chen, G. H. Chen, and L. Lu, "Piezoresistive behavior study on finger-sensing silicone rubber/graphite nanosheet nanocomposites," *Advanced Functional Materials*, vol. 17, pp. 898-904, Apr 16 2007.
- [245] G. Ausanio, A. C. Barone, C. Campana, V. Iannotti, C. Luponio, G. P. Pepe, *et al.*, "Giant resistivity change induced by strain in a composite of conducting particles in an elastomer matrix," *Sensors and Actuators a-Physical*, vol. 127, pp. 56-62, Feb 28 2006.
- [246] D. T. Beruto, M. Capurro, and G. Marro, "Piezoresistance behavior of silicone-graphite composites in the proximity of the electric percolation threshold," *Sensors and Actuators a-Physical*, vol. 117, pp. 301-308, Jan 14 2005.
- [247] J. Kost, M. Narkis, and A. Foux, "Effects of Axial Stretching on the Resistivity of Carbon-Black Filled Silicone-Rubber," *Polymer Engineering and Science*, vol. 23, pp. 567-571, 1983.

CHAPTER 5

CURRENT-VOLTAGE CHARACTERISTICS OF NANOPATELET BASED CONDUCTIVE NANOCOMPOSITES¹

SYNOPSIS- In this chapter a numerical modeling approach was used to investigate the current-voltage behavior of conductive nanoplatelet based nanocomposites. A three-dimensional continuum Monte Carlo model was employed to randomly disperse the nanoplatelets in a cubic representative volume element. A nonlinear finite element based model was developed to evaluate the electrical behavior of the nanocomposite for different levels of the applied electric field. Also, the effect of filler loading on nonlinear conductivity behavior of nanocomposites was investigated. The validity of the developed model was verified through qualitative comparison of the simulation results with results obtained from experimental works.

5.1 Introduction

In recent years the nonlinear electrical conductivity behavior of nanoparticle modified polymers has received considerable attention by researchers, and several studies have been carried out to investigate the current-voltage characteristics of conductive nanocomposites. Even though several studies investigated the non-ohmic conductivity behavior of insulator polymers filled with conductive spherical and stick-like inclusions [75, 211, 248-250], to the best of the author's knowledge, all of the research in this field has been limited to experimental works. Experimental research devoted to the electric properties of nanoplatelet based nanocomposites investigated the electrical conductivity of polymers with exfoliated graphite sheets with sizes varying from a few microns to

¹ A version of this chapter published as: Oskouyi, A.B.; Sundararaj, U.; Mertiny, P. Current-voltage characteristics of nanoplatelet-based conductive nanocomposites. *Nanoscale Research Letters* 2014, 9, 369.

several hundred micron [213, 251-254], which allows for only limited prediction of the conductivity behavior of nanocomposites with submicron size inclusions.

These limitations motivated the present authors to conduct a numerical study to investigate the current-voltage behavior of polymers made electrically conductive through the uniform dispersion of conductive nanoplatelets. Specifically, the nonlinear electrical characteristics of conductive nanoplatelet based nanocomposites were investigated in the present study. Three-dimensional continuum Monte Carlo modeling was employed to simulate electrically conductive nanocomposites. To evaluate the electrical properties, the conductive nanoplatelets were assumed to create resistor networks inside a representative volume element (RVE), which was modeled using a three-dimensional nonlinear finite element approach. In this manner the effect of the voltage level on the nanocomposite electrical behavior such as electrical resistivity was investigated.

5.2 Methodology and Formulation

5.2.1 Monte Carlo Modeling

Theoretically, a nanocomposite is rendered electrically conductive by inclusions dispersed inside the polymer that form a conductive path through which an electrical current can pass such a path is usually termed a percolation network. **Figure 5-1** illustrates the conductivity mechanism of an insulator polymer made conductive through the formation of a percolation network. In this figure, elements in black, white and grey color indicate nanoplatelets that are individually dispersed, belong to an electrically connected cluster, or form a percolation network inside the RVE, respectively. Quantum tunneling of electrons through the insulator matrix is the dominant mechanism in the electric behavior of conductive nanocomposites. **Figure 5-2** illustrates the concept of a tunneling resistor for simulating electron tunneling through an insulator matrix and its role in the formation of a percolation network.

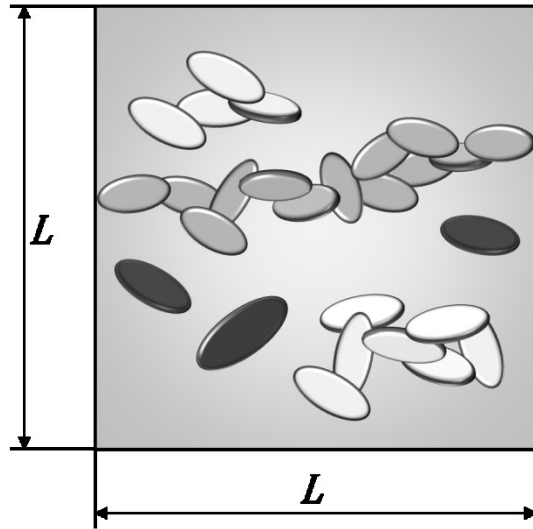


Figure 5-1: Schematic of a RVE containing individually dispersed nanoplatelets (black), platelets forming an electrically connected cluster (white), and particles creating a percolation network (grey).

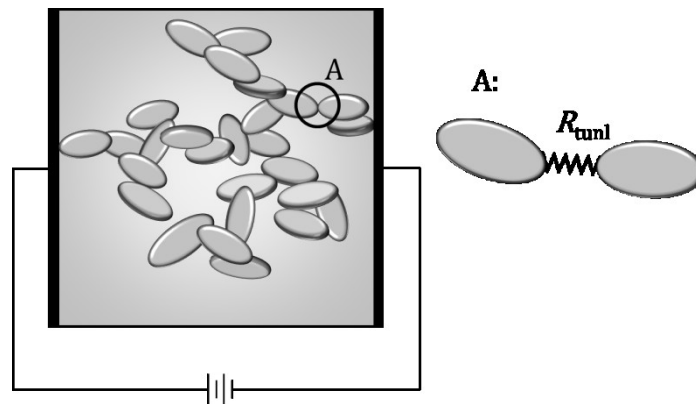


Figure 5-2: Illustration of tunneling resistors for simulating electron tunneling through the insulator matrix and the formation of a percolation network.

Electron tunneling through a potential barrier exhibits different behavior for different voltage levels, and thus, the percolation behavior of a polymer reinforced by conductive particles is governed by the level of the applied voltage. In a low voltage range ($eV \approx 0$) the tunneling resistivity is proportional to the insulator thickness, that is, the tunneling resistivity shows ohmic behavior [255]. For higher voltages, however, the tunneling

resistance is no longer constant for a given insulator thickness, and it has been shown to depend on the applied voltage level. It was derived by Simmons [255] that the electrical current density passing through an insulator is given by:

$$J = J_0 \left\{ \bar{\varphi} \exp\left(-A\bar{\varphi}^{\frac{1}{2}}\right) - (\bar{\varphi} + eV) \exp\left[-A\left(-A\bar{\varphi}^{\frac{1}{2}}\right)\right] \right\} \quad \text{Eq. 5-1}$$

where

$$J_0 = e/2\pi h(\beta\Delta s)^2$$

$$A = (4\pi\beta\Delta s/h)(2m)^{\frac{1}{2}}$$

Considering **Eq. 5-1**, even for comparatively low voltage levels the current density passing through the insulator matrix is nonlinearly dependent on the electric field. For vanishing voltages when $V \approx 0$, **Eq. 5-1** can be simplified as [255]:

$$J = \frac{e^2 \sqrt{2m\lambda}}{h^2} V \exp\left(-\frac{4\pi d}{h} \sqrt{2m\lambda}\right) \quad \text{Eq. 5-2}$$

The numerical evaluation of **Eq. 5-1** given in **Figure 5-4** indicates that a polymer only exhibits close to ohmic behavior when subjected to low electric fields, that is, the resistivity of the polymer is approximately constant in a small region near the ordinate axis (see insert in **Figure 5-4**), permitting the use of the linear approximation provided by **Eq. 5-2**.

In this study a rectangular potential barrier was assumed to model the electrical behavior of a tunneling resistor. Tunneling resistivity was numerically evaluated for $\lambda=0.5\text{eV}$ employing **Eq. 5-1** and illustrated in **Figure 5-5**. The tunneling resistance is drastically dependent on the insulator thickness, that is, tunneling resistance is sharply increasing as the insulator thickness is increasing. A cut-off distance can therefore be approximated at which tunneling resistors with length greater than this threshold do not appreciably contribute toward the overall conductivity of the nanocomposite. In [46] and [221] the cut-off distance was assumed to be 1.0 nm and 1.4 nm, respectively. It is expected that the resistivity of the insulator film is decreasing as the electrical field is

increasing, so, when dealing with higher voltage levels, tunneling resistors with length greater than these cut-off distances may play a role in the nanocomposite conductivity. Hence, it was conservatively assumed in this study that tunneling resistors with length less than 4 nm contribute toward the nanocomposite conductivity. The electrical conductivity of the polymeric matrix is governed by the electron tunneling phenomenon. In this context the "tunneling cut-off distance" is a qualitative criterion indicating that the tunneling resistors with length higher than this distance have no contribution toward the conductivity of the nanocomposite. In the technical literature, authors such as Bao [221] showed that tunneling paths longer than 1.4 nm play no appreciable role in the overall conductivity of CNT nanocomposites. But, according to **Figure 5-3** the tunneling conductivity strongly depends on the applied voltage level, and the conductivity of the polymer increases as the applied voltage is increasing. In other word, more tunneling resistors will contribute to the conductivity of the nanocomposite when a nanocomposite is subjected to a higher electrical field. To ensure that all tunneling paths for a given electrical field are taken into account the tunneling cut-off distance was set at a conservative value of 4 nm.

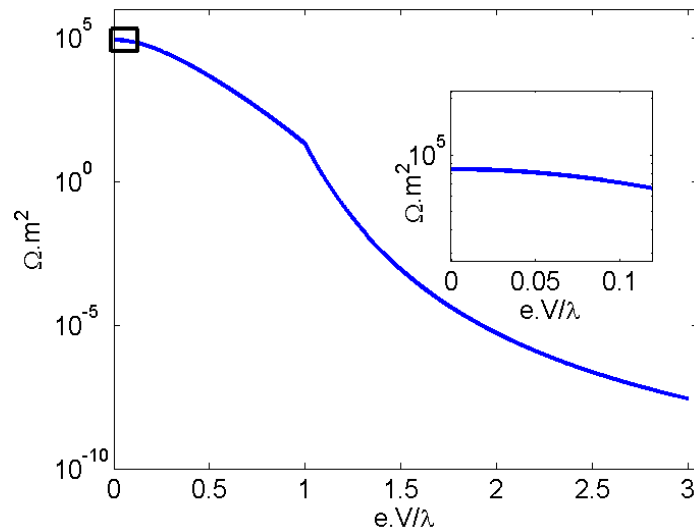


Figure 5-3: Resistivity per unit area of polymer with 4 nm thickness and a quantum tunneling barrier height λ of 1 eV, with respect to the normalized voltage eV/λ .

In a first step of this work, a three-dimensional continuum percolation model based on Monte Carlo simulation was used to study the percolation behavior of an insulator matrix reinforced with conductive nanoplatelet fillers. Additional details on this modeling approach can be found in an earlier publication [256] and in Chapter 3. In the simulation, circular nanoplatelets are randomly generated and added to the RVE. The shortest distance between adjacent particles is calculated, and particles with distance between them shorter than the cut-off distance are grouped into clusters. The formation of a cluster connecting two parallel faces of the RVE is considered the formation of a percolation network that allows electric current to pass through the RVE, rendering it conductive.

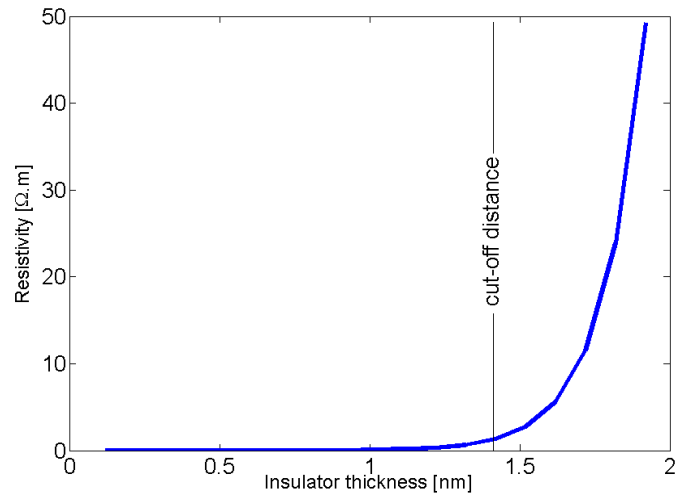


Figure 5-4: Tunneling resistivity versus insulator thickness

5.2.1 Finite Element Modeling

To study the electrical properties of nanocomposites, in particular their conductivity behavior, the employed modeling approach further involved the creation of a nonlinear three dimensional finite element resistor network. Considering the excellent conductivity of the considered nanoplatelets (e.g. $\sigma=10^8$ S/m for graphene), the electrical potential drop across the nanoplatelets was neglected. The tunneling resistors were modeled as non-ohmic, which resistivity is governed by **Eq. 5-1**. Employing appropriate finite element formulations the governing equation of an electrical resistor can be written as:

$$\begin{Bmatrix} I_{ij} \\ -I_{ij} \end{Bmatrix} = \begin{bmatrix} k_{ij} & -k_{ij} \\ -k_{ij} & k_{ij} \end{bmatrix} \begin{Bmatrix} V_i \\ V_j \end{Bmatrix} \quad \text{Eq. 5-3}$$

where I_{ij} is the electrical current passing between the i^{th} and j^{th} node; k_{ij} is the conductance of the resistor between nodes i and j ; V_i is the voltage of the i^{th} node measured with respect to a node connected to ground. The system of nonlinear equations governing the electrical behavior of the nanocomposite was obtained by assembling the governing equations for the individual elements. The resulting nonlinear system of equations was solved employing a Newton-Raphson method.

5.3 Results and Discussion

5.3.1 Effect of Electrical Field on the Nanocomposite Conductivity

The developed model was employed to investigate the electrical behavior of a polymer with $\lambda=0.5\text{eV}$ made conductive through the uniform dispersion of conductive circular nanoplatelets with a diameter of 100 nm. In the simulations the size of the RVE was chosen to be nine times the diameter of the nanodisks, which was ascertained to be large enough to minimize finite size effects. In Chapter 4, it was shown that the Monte Carlo simulation results are no longer appreciably RVE size dependent when the RVE size is about eight times the sum of $2R+d_t$, where R and d_t are the radius of the nanoplatelets and tunneling distance respectively.

The graph in **Figure 5-5** depicts the effect of filler loading on nanocomposite conductivity. As expected, a critical volume fraction indicated by a sharp increase in nanocomposite conductivity, i.e. the percolation threshold, can be inferred from the graph.

In the following, electric current densities passing through the nanocomposite RVE were computed for different electric field levels and filler volume fractions. As illustrated by **Figure 5-6**, the current density versus voltage curves were found to be nonlinear. The depicted electrical behavior of the conductive nanocomposite is thus clearly governed by the applied voltage in a non-ohmic manner, which, as mentioned above, matches the expectation for a conductive nanocomposite at higher electric field levels.

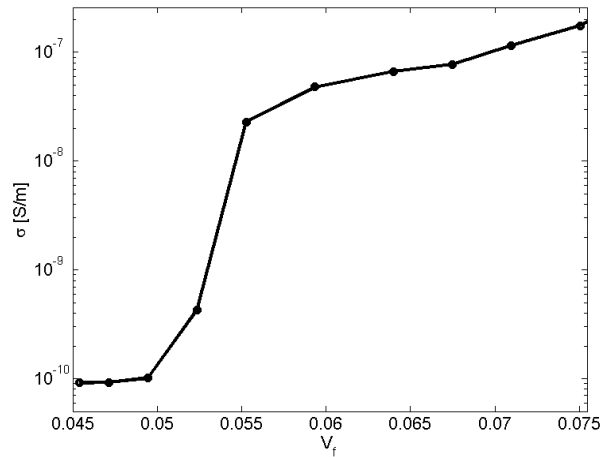


Figure 5-5: Conductivity of nanocomposite with respect to filler loading of conductive nanodisks

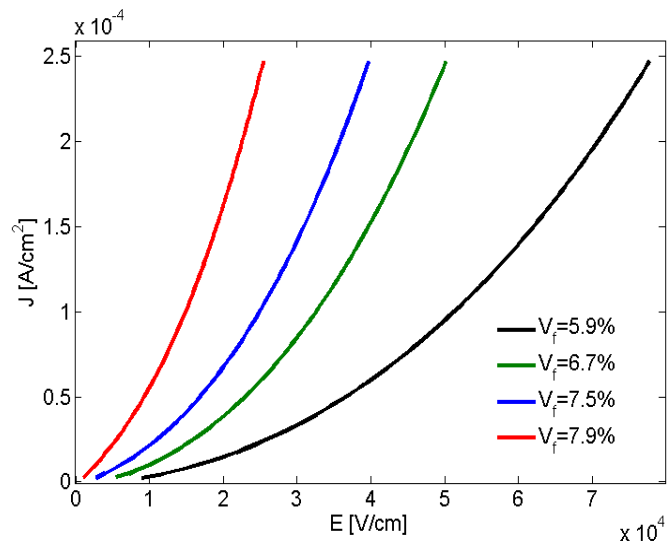


Figure 5-6: Electric current density of nanocomposites with 100 nm diameter nanoplatelets versus the applied electrical field.

Figure 5-7 shows the variation of resistivity as a function of the applied electric field E in order to compare the non-ohmic behavior for nanocomposites with different filler loadings. Note that resistivity values were normalized with respect to a reference resistivity measured at $E=0.8$ V/cm. The results as displayed in **Figure 5-7** indicate that

the magnitude of the applied electric field plays an important role in the conductivity of nanoplatelet based nanocomposites. The employed modeling approach predicts nanocomposite resistivity to be a nonlinear function of the applied voltage. Clearly, the nanocomposites exhibit non-ohmic behavior where the resistivity decreases with increasing voltage. Interestingly, the results in **Figure 5-8** also indicate a reduced drop in resistivity and decreased non-ohmic behavior for nanocomposites with higher filler volume fraction, that is, nanocomposites with higher filler loadings are less sensitivity to the applied electric field level.

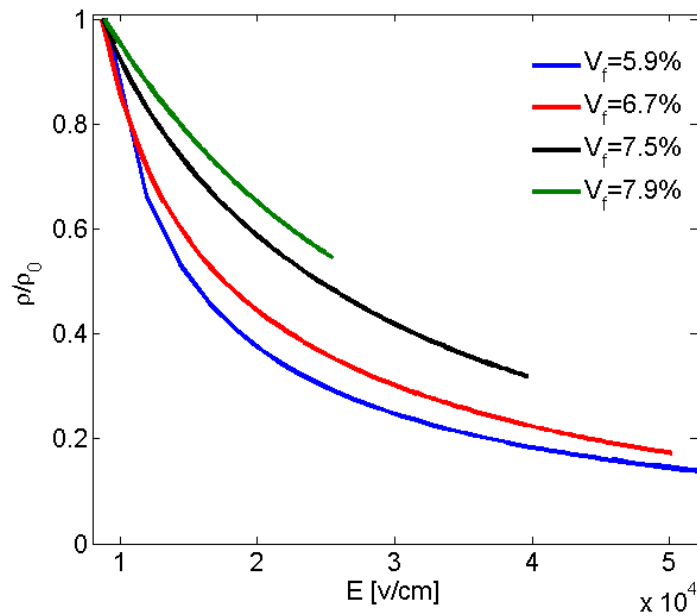


Figure 5-7: Normalized resistivity of nanocomposites with 100 nm nanodisks as a function of the applied electrical field

5.3.2 Comparison with Experimental Data

To corroborate the simulation results, conductive epoxy nanocomposite samples were produced by *in situ* polymerization and their electrical behavior assessed as illustrated by **Figure 5-8**. Bisphenol-A epoxy resin and non MDA polyamine curing agent (EPON 826 and EPIKURE 9551, by Hexion Specialty Chemicals, Columbus, Ohio, USA) were used for the fabrication of samples that were made electrically conductive by dispersing graphene nanoplatelets (xGnP-M-25, by XG Sciences, Lansing, Michigan, USA).

Graphene nanoplatelets were dispersed in acetone by sonication using a probe sonicator in an ice bath. In the following, epoxy was added to the mixture and sonication was repeated. The solvent was evaporated by heating the mixture on a magnetic stir plate and stirring with a Teflon coated magnet. Remaining acetone was removed by using a vacuum chamber. A stoichiometric amount of hardener (i.e. resin to hardener mass ratio: 2.77) was added to the mixture and mixed with a high-speed mechanical shear mixer. The mixture was again degassed using the vacuum chamber, and subsequently poured into a mold. A 2-hour cure cycle was then performed at 120°C. Resulting samples were machined into circular disks with 30 mm diameter and 3 mm thickness. The sample volume resistivities were measured at different applied voltages employing a Keithley 6517A electrometer connected to a Keithley test fixture (Keithley Instruments, Cleveland, Ohio, USA).

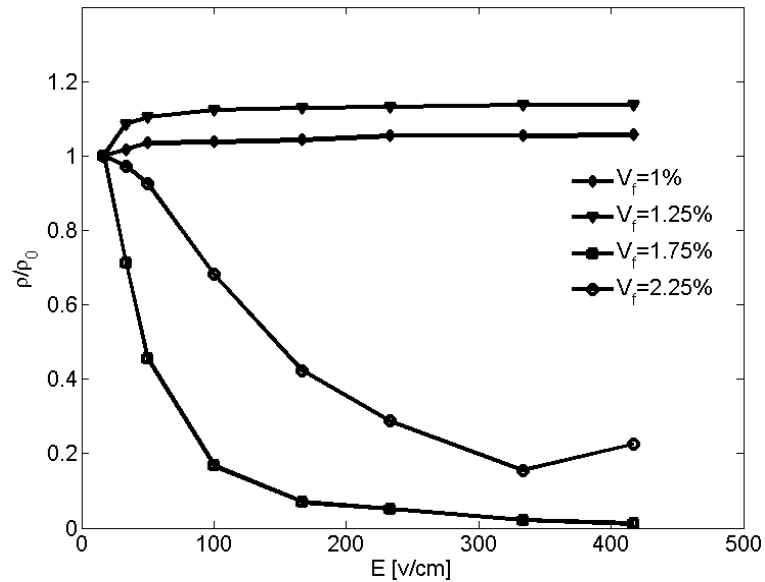


Figure 5-8: Normalized resistivity data versus applied electrical field from experiments with nanographene/epoxy samples

Data in **Figure 5-8** depicting the resistivity behavior of the epoxy nanocomposite samples was normalized with respect to the resistivity measured at an applied voltage of 10 V. Samples with 1% and 1.25% graphene volume fraction exhibited high resistivity levels indicating a filler loading below the percolation threshold. For higher graphene volume

fractions of 1.75% and 2.25%, measurements indicated that percolation was achieved, and resistivity was found to decrease with the increase of the applied electric field. As predicted by the preceding modeling work, sample resistivity was found to be less sensitive to the applied electrical field for higher filler loadings. Hence, modeling and simulation results are qualitatively in good agreement, indicating the validity of the assumptions undertaken for the numerical modeling. However, the data presented in **Figure 5-7** and **Figure 5-8** also signify that further studies are warranted to establish a quantitative agreement between numerical and experimental results. Monte Carlo modeling was conducted for a system of uniformly dispersed single size nanoparticle represented by circular disks, while in practice depending on the preparation procedure it may deviate from the undertaken assumptions.

5.3.3 Characterization of Resistivity Behavior

Gorrasi et al. [211] and Liu et al. [257] showed that the resistivity of carbon nanotube based nanocomposites as a function of the electric power $P=V \times I$ can be described by an exponential expression:

$$\rho = r P^\alpha \quad \text{Eq. 5-4}$$

where α is an index generally varying from -1 to 0. The value of α is indicative of the nonlinearity of the current-voltage relationship, i.e. $\alpha=0$ corresponds to ohmic behavior, and α decreases with increasing nonlinearity of the current-voltage curve; r is a parameter relating to the resistivity of the nanocomposite when the electrical power passing through the sample is 1 W [257].

Computed nanocomposite resistivities are displayed as a function of the electric power in the graph in **Figure 5-9**. Data obeying **Eq. 5-4** appear in the form of straight lines owing to the graph's logarithmic scale. As shown in **Figure 5-9**, the slope of the lines decreases as the nonlinearity is decreasing with increasing filler loading. The values of α as a function of filler volume fraction are provided in **Figure 5-10**. It is shown that α values are increasing with rising filler volume fraction. A discontinuity in α values can be observed in this graph for filler volume fractions of about 5%, which is associated with

the percolation volume fraction. The behavior of data simulated herein is qualitatively congruent with results reported in [211] for carbon nanotube nanocomposites.

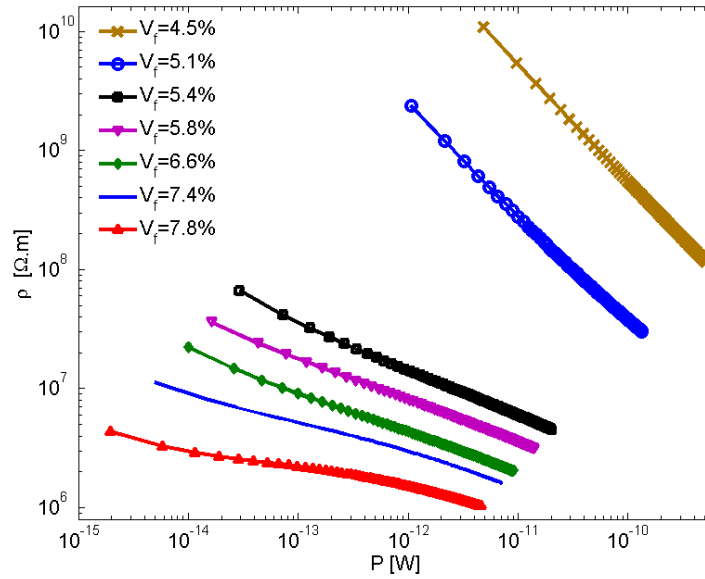


Figure 5-9: Resistivity of nanocomposites with 100 nm circular nanoplatelets as a function of electric power

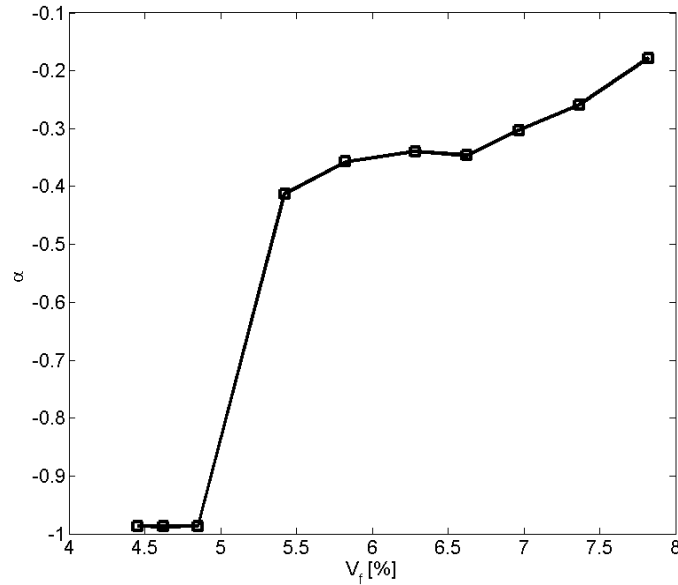


Figure 5-10: Value of α as a function of filler volume fraction for nanocomposites with 100 nm circular nanoplatelets

5.1 Conclusions

In this study the current-voltage behavior of conductive nanoplatelet based nanocomposites was investigated. To this end, a numerical modeling approach was developed. The simulations predicted the resistivity of nanoplatelet based nanocomposites to be strongly affected by the applied electric field. The nanocomposites exhibit non-ohmic behavior, that is, resistivity is a nonlinear function of the applied electric field. Further, nanocomposite resistivity was ascertained to decrease with increasing voltage, while the degree of nonlinear behavior was found to decline with rising filler volume fraction. A good qualitative agreement was observed between simulations and experimental data, the latter of which was obtained employing measurements on nanographene/epoxy nanocomposites. The qualitative agreement between numerical and experimental studies encourages conducting a more comprehensive study to establish a quantitative agreement. The analysis further revealed that nanocomposite resistivity as a function of electrical power can be described by an exponential relation, where the exponent is a measure of the deviation from non-ohmic behavior of the conductive nanocomposite.

5.2 Bibliography

- [46] N. Hu, Y. Karube, C. Yan, Z. Masuda, and H. Fukunaga, "Tunneling effect in a polymer/carbon nanotube nanocomposite strain sensor," *Acta Materialia*, vol. 56, pp. 2929-2936, Aug 2008.
- [75] Z. Ounaies, C. Park, K. E. Wise, E. J. Siochi, and J. S. Harrison, "Electrical properties of single wall carbon nanotube reinforced polyimide composites," *Composites Science and Technology*, vol. 63, pp. 1637-1646, Aug 2003.
- [211] G. Gorrasi, E. Piperopoulos, M. Lanza, and C. Milone, "Effect of morphology of the filler on the electrical behaviour of poly(L-lactide) nanocomposites," *Journal of Physics and Chemistry of Solids*, vol. 74, pp. 1-6, Jan 2013.
- [213] L. X. He and S. C. Tjong, "Zener tunneling in conductive graphite/epoxy composites: Dielectric breakdown aspects," *Express Polymer Letters*, vol. 7, pp. 375-382, Apr 2013.
- [221] W. S. Bao, S. A. Meguid, Z. H. Zhu, and G. J. Weng, "Tunneling resistance and its effect on the electrical conductivity of carbon nanotube nanocomposites," *Journal of Applied Physics*, vol. 111, May 1 2012.
- [248] S. V. Anand and D. R. Mahapatra, "Quasi-static and dynamic strain sensing using carbon nanotube/epoxy nanocomposite thin films," *Smart Materials and Structures*, vol. 18, Apr 2009.
- [249] M. H. G. Wichmann, S. T. Buschhorn, J. Gehrman, and K. Schulte, "Piezoresistive response of epoxy composites with carbon nanoparticles under tensile load," *Physical Review B*, vol. 80, Dec 2009.
- [250] C. Cattin and P. Hubert, "Network Formation and Electrical Conduction in Carbon Nanotube Modified Polydimethylsiloxane," in *MRS Proceedings*, 2012, pp. mrsf11-1410-dd05-07.

- [251] H. F. Lin, W. Lu, and G. H. Chen, "Nonlinear DC conduction behavior in epoxy resin/graphite nanosheets composites," *Physica B-Condensed Matter*, vol. 400, pp. 229-236, Nov 15 2007.
- [252] A. Celzard, G. Furdin, J. Mareche, and E. McRae, "Non-linear current-voltage characteristics in anisotropic epoxy resin-graphite flake composites," *Journal of materials science*, vol. 32, pp. 1849-1853, 1997.
- [253] Q. A. Zheng, Y. H. Song, G. Wu, and X. S. Yi, "Reversible nonlinear conduction behavior for high-density polyethylene/graphite powder composites near the percolation threshold," *Journal of Polymer Science Part B-Polymer Physics*, vol. 39, pp. 2833-2842, Nov 15 2001.
- [254] G. H. Chen, W. G. Weng, D. J. Wu, and C. L. Wu, "Nonlinear conduction in nylon-6/foiated graphite nanocomposites above the percolation threshold," *Journal of Polymer Science Part B-Polymer Physics*, vol. 42, pp. 155-167, Jan 1 2004.
- [255] J. G. Simmons, "Generalized formula for the electric tunnel effect between similar electrodes separated by a thin insulating film," *Journal of Applied Physics*, vol. 34, pp. 1793-1803, 2004.
- [256] A. B. Oskouyi and P. Mertiny, "Monte Carlo model for the study of percolation thresholds in composites filled with circular conductive nano-disks," *Procedia Engineering*, vol. 10, pp. 403-408, 2011.
- [257] C. H. Liu and S. S. Fan, "Nonlinear electrical conducting behavior of carbon nanotube networks in silicone elastomer," *Applied Physics Letters*, vol. 90, Jan 22 2007.

CHAPTER 6

EFFECT OF TEMPERATURE ON ELECTRICAL CONDUCTIVITY OF CNT AND GNP NANOCOMPOSITES¹

SYNOPSIS- The effect of the temperature on the electrical conductivity of polymer nanocomposites with carbon nanotube (CNT) and graphene nanoplatelet (GNP) fillers was investigated. A three-dimensional continuum Monte-Carlo model was developed to first form percolation networks. A three-dimensional resistor network was subsequently created to evaluate the nanocomposite electrical properties. The effect of temperature on the electrical conductivity of nanocomposites was thus investigated. Other aspects such as polymer tunneling and filler resistivities were considered as well. The presented comprehensive modeling approach is aimed at providing a better understanding of the electrical conductivity behavior of polymer nanocomposites in conjunction with experimental works.

6.1 Introduction

Temperature sensors are employed in wide range of applications. High sensitivity, linearity, stability, wide operating range and low cost are the main characteristics of an ideal temperature sensor [258]. Developing a sensor fulfilling all or most of these characteristics has been the topic of a great number of research works [258]. Thermocouples exhibit linear behavior but their high production cost restricts their applications. Transistor-based temperature sensors have linear behavior on a wide range of operation but they are associated with drawbacks such as low sensitivity [258]. Thermoresistive nanocomposite films can be employed for temperature sensing application. Low production cost, tailoring the shape can be listed as the main

¹ A version of this chapter has been published. AB. Oskouyi, U. Sundararaj and P. Mertiny. ASME 2013 International Mechanical Engineering Congress and Exposition. American Society of Mechanical Engineers, 2013.

advantageous of this group of the sensors. The electrical properties of polymers filled with carbon nano-tubes (CNT) and graphene nanoplatelets (GNP) have been the subject of extensive research in recent years [44, 90, 92, 183-185, 259-262]. Several experimental and numerical studies have been devoted to the investigation of the percolation threshold (i.e. the transition between electrical insulator and conductor), electrical conductivity properties and piezoresistivity effects. However, only a few studies have been conducted to investigate the effect of the temperature on the electrical characteristics of polymeric nanocomposites [75, 263-266]. Karimov et al. [258] investigated the effect of the temperature on the resistivity and Seebeck coefficient of the CNT-polymer nanocomposite. Yang et al. [267] studied the effect of the temperature on the resistivity of the aligned CNT-hydrogel nanocomposites. They showed that the resistance of the composite decreases linearly as the temperature is increasing. Neitzert et al. [268] showed that resistivity-temperature behavior of CNT-epoxy nanocomposites can be described by the exponential description developed by Sheng [269] for tunneling conduction in disordered materials. Matzeu et al. [270] developed a temperature sensor based on CNT/styrene composite. They reported a negative temperature coefficient for the developed sensor. Further, they showed that the sensitivity of the sensor increases as filler loading is decreasing. Sibinski et al. [271] conducted an study on the effect of the temperature on resistivity of CNT filled polymers. Their study indicates that resistivity-temperature curve of the nanocomposite exhibits quasi-linear characteristics. To the best of authors' knowledge, only scarce information on numerical or analytical studies devoted to the temperature-resistivity behavior of nanocomposites is available in the technical literature. Consequently, a need exists for suitable modeling approaches, especially since polymeric nanocomposites can potentially be employed in temperature sensing applications. These facts motivated the present authors to conduct an investigation of the temperature/resistivity characteristics of CNT and GNP filled polymers. A three-dimensional continuum Monte-Carlo (MC) model was developed, in which randomly dispersed fillers were included in a representative volume element (RVE). In subsequent modeling steps, finite element modeling was employed to evaluate the electrical characteristics and temperature effects of conductive nanocomposites.

6.2 Modeling Procedure

6.2.1 Initial Model Generation using MC Approach

MC simulation is a statistical technique that has widely been used to evaluate the electrical behavior of conductive composites, and several such models have been employed to predict the percolation threshold of polymers filled with conductive inclusions, see e.g. [44, 90, 92, 183-185]. The three-dimensional (3D) continuum MC model developed in the present work constitutes the basis for the successive evaluation of temperature effects in electrically conductive nanocomposites. The model provides for a random and uniform distribution of CNTs and GNPs inside a cubic RVE with edge length L .

Undertaking an approach similar to that provided in [46], a Monte Carlo model was developed to evaluate the percolation behavior of a system of CNT particles dispersed in three dimensional space. Three random numbers, (x_i, y_i, z_i) , were generated in the interval $(0, L)$, indicating the coordinate of one end of a rod-shaped CNT. The other end of the CNT was determined by choosing a random point on the surface of a sphere with radius l_f , where the center of the sphere is located at the initial end of the CNT and l_f is the length of the CNT. The algorithm presented in Marsaglia's work [272] was herein employed to choose a random point on the surface of the sphere, which guarantees the random orientation of the generated CNT. The Mersenne Twister [273] algorithm was employed in the present study for random number generation due to its long period and low computational cost. Rod-shaped CNT elements were thus randomly created and added to the RVE. In general, a large RVE size is desirable to guarantee the randomness of the MC simulation. However, the computational cost of the simulation also increases considerably with RVE size. Periodic boundary conditions decrease the computational cost by limiting the size of the RVE while preserving the randomness of the MC model. Any CNT with an end point located outside the RVE was cut, and the segment located outside the RVE was transferred to the opposite face of the RVE [274]. In this manner the obtained RVE can be employed for the formation of bigger RVE structures. The concept of the periodic boundary conditions is illustrated by **Figure 6-1**.

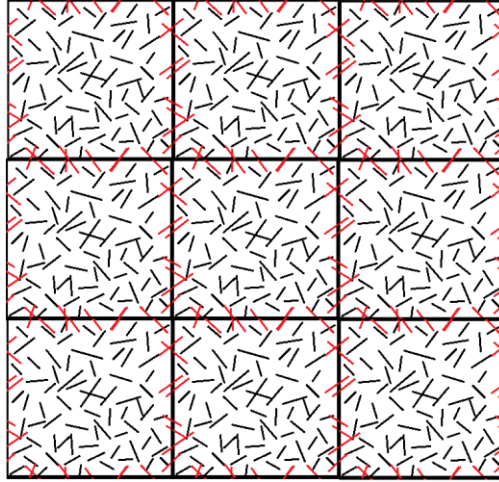


Figure 6-1: Schematic of periodic boundary conditions (elements in red color indicate CNTs crossing the RVE boundary).

A similar approach was undertaken to model disk-shape GNPs distributed in a 3D RVE. A random point was chosen inside the RVE indicating the center of the circular disk representing the GNP. A unit vector being perpendicular to the disk plane was generated employing the procedure described above in the context of CNT particles. Circular GNPs with a certain disk radius were added to the RVE only when geometrically feasible, that is, when disks did not intersect with each other. The procedure for avoiding intersecting disks was described in earlier works [275, 276], where additional details on the MC modeling approach for GNP nanocomposites are also given.

6.2.2 Modeling Electrical Connection Between Filler Particles

Considering quantum mechanical effects, the polymer occupying the space between the conductive filler particles was represented in this study by virtual tunneling resistors through which electrons can ‘pass’, making the nanocomposite conductive. The tunneling resistivity, ρ , for a quantum mechanical rectangular barrier and a low voltage level with respect to the thickness of the insulator, d , is described by **Eq. 6-1** [277].

$$\rho = \frac{h^2}{e^2 \sqrt{2m\lambda}} \exp\left(\frac{4\pi d}{h} \sqrt{2m\lambda}\right) \quad \text{Eq. 6-1}$$

where h , m and e are respectively the Planck constant, the mass of an electron and the quantum of electrical charge; λ is known as the barrier height in connection with quantum mechanical tunneling effects. Numerically evaluating **Eq. 6-1** for a set of appropriate parameters reveals that tunneling conductivity decreases sharply with increasing insulator thickness, see **Figure 6-2**. A cut-off distance was therefore assumed at which a tunneling resistor no longer contributes appreciably to the overall resistivity of the nanocomposite. In the present modeling approach the shortest mutual distance between filler particles was determined for all inclusions inside the RVE, and any pair of filler particles with a smallest mutual distance less than the electron tunneling cut-off distance was grouped as a cluster, indicating that electrical current can pass through the tunneling resistor formed between these adjacent particles. Hu et al. [46] set the electron tunneling cut-off distance to be 1 nm for CNT based polymeric composites. This distance corresponds to a conductivity of 10^2 Sm^{-1} , which is substantially greater than the CNT conductivity [16]. Bao et al. [221] considered an electron tunneling cut-off distance of 1.4 nm. At this value the transmission probability is less than 10^{-4} for most polymers with a quantum mechanical barrier height ranging from 1 to 5 eV. In this study an electron tunneling cut-off distance of 1.4 nm was assumed for CNT nanocomposites. For polymers filled with circular conductive nanoplatelets the present authors showed in a previous work [275] that tunneling resistors with length greater than 2 nm have no appreciable contribution toward the overall nanocomposite resistivity.

Increasing numbers of electrical connections between filler particles and their clusters ultimately leads to a transition of the nanocomposite from electrical insulator to conductor. The filler volume fraction at which this transition occurs is known as the percolation threshold. At this filler volume a percolation network is formed that allows electrical current to pass through the material. The schematic in **Figure 6-3** illustrates the mechanism which renders a polymer nanocomposite electrically conductive as the result of dispersed conductive inclusions.

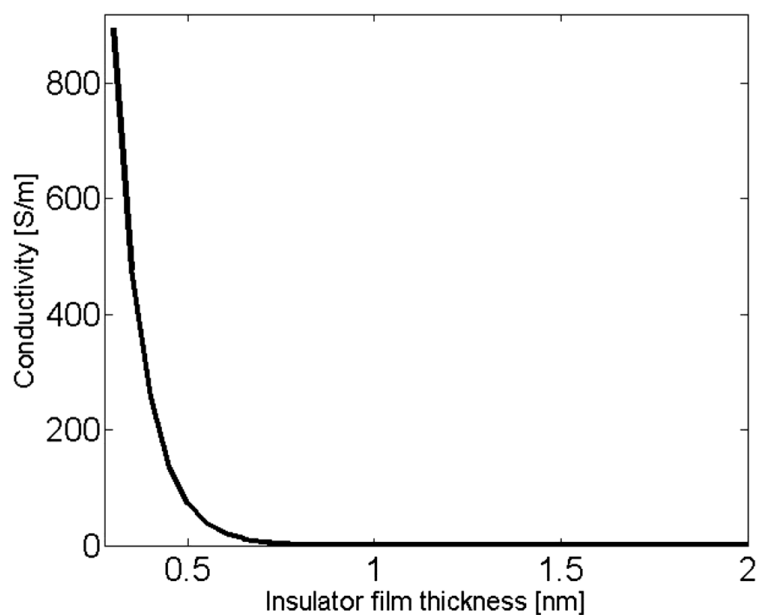


Figure 6-2: Tunneling conductivity versus insulator thickness for $\lambda = 1.5$.

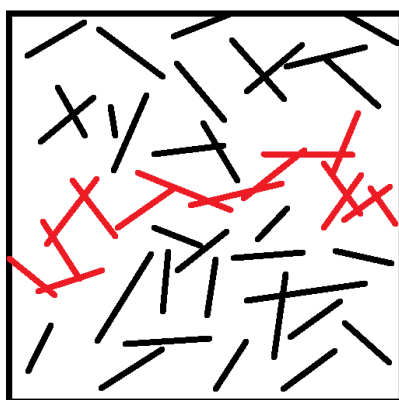


Figure 6-3: Schematic for the formation of a percolation network at the percolation threshold.

In order to determine the shortest mutual distance between two CNTs, the following technique was employed. A line segment in three-dimensional space was described as follows:

$$\frac{x - x_1^i}{x_2^i - x_1^i} = \frac{y - y_1^i}{y_2^i - y_1^i} = \frac{z - z_1^i}{z_2^i - z_1^i} = t_i \quad 0 \leq t_i \leq 1 \quad \text{Eq. 6-2}$$

In **Eq. 6-2**, (x_1^i, y_1^i, z_1^i) and (x_2^i, y_2^i, z_2^i) are the coordinates of the end points of the i^{th} CNT inside the RVE. The shortest distance d between the i^{th} and j^{th} CNT can be calculated by minimizing the following function:

$$d = \sqrt{(x_i - x_j)^2 + (y_i - y_j)^2 + (z_i - z_j)^2} \quad \text{Eq. 6-3}$$

where, considering **Eq. 6-2**, d is a function of t_i and t_j which are within the interval $[0,1]$. In order to determine the shortest distance between two circular nanodisks representing GNPs, the algorithm developed by Almohammad et al. [208] was employed. Details on this approach can be found in [276] and in CHAPTER 3.

As explained earlier, a nanocomposite is rendered conductive by an electrical current I passing through an insulator matrix due to quantum tunneling effects. Referring to [278] the effect of the temperature T on the tunneling current density J for intermediate voltages, where $eV \leq \lambda$, can be described by **Eq. 6-4**.

$$J(V, T) = J(V, T_0) \left\{ 1 + \left[3 \times 10^{-9} \times d^2 T^2 / (\lambda - V/2) \right] \right\} \quad \text{Eq. 6-4}$$

where d is expressed in Angstrom, T in degrees Kelvin and λ in Volts; T_0 represents absolute zero Kelvin (-273.15°C).

6.2.3 Model Completion using Finite Element Method

Using a finite element modeling approach, nanocomposite resistivity were evaluated forming three-dimensional resistor networks that consisted of rod-shaped CNT or disk-shape GNP elements, and tunneling resistors. Note that besides the tunneling resistivity also the intrinsic resistivity of CNTs was taken into account when predicting the electrical behavior of CNT nanocomposites. Using the procedures described above, the shortest mutual distance between filler particles and the points on them corresponding to the shortest distance were determined. Particles having a shortest mutual distance of less than the tunneling cut-off distance were connected by a tunneling resistor with a

resistivity given by **Eq. 6-1** and **Eq. 6-4**. If the shortest distance between two CNTs was less than a certain minimum value, a constant distance of d_{\min} was assumed for the resistivity calculation. According to Bao et al. [221] the minimum separation between CNTs should not be less than the van der Waals separation distance, d_{vdw} , which, for example, is 3.4 Å (0.34 nm) for graphene sheets. Considering the influence of polymer chains, Yu [91] showed that the minimum separation distance should be on the order of 1 nm for the case of good filler dispersion. Based on these considerations the distance between CNTs was determined as follows:

$$d_R = \begin{cases} d_{\min} & 0 \leq d \leq D + d_{\min} \\ d - D & D + d_{\min} \leq d \end{cases} \quad \text{Eq. 6-5}$$

where D , d , d_R are the CNT diameter, the shortest mutual distance between CNT axes, and the length of the tunneling resistor, respectively. The schematic in **Figure 6-4** and **Figure 6-5** illustrate the developed concept for the formation of a tunneling resistor and a resistor network.

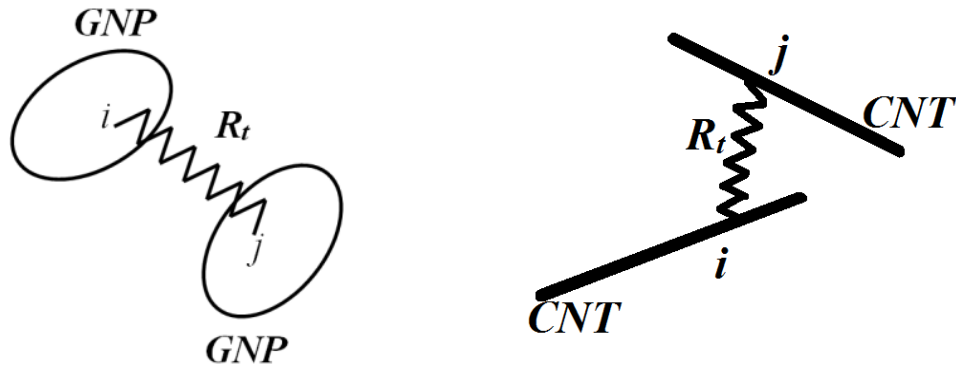


Figure 6-4: Schematic of the electron tunneling mechanism in CNT and GNP based conductive nanocomposites.

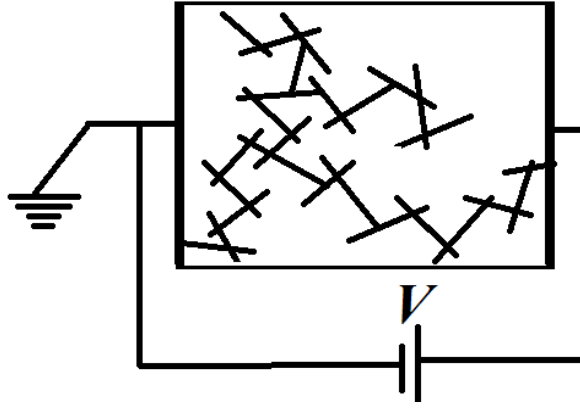


Figure 6-5: Schematic of the conductivity mechanism in conjunction with a percolation network.

In the finite element code developed to evaluate the resistivity of the resistor network, the governing equation for the k^{th} resistor with resistance R^k connecting the i^{th} and j^{th} nodes is given as follows:

$$\begin{bmatrix} I_i \\ I_j \end{bmatrix} = \begin{bmatrix} 1/R^k & -1/R^k \\ -1/R^k & 1/R^k \end{bmatrix} \begin{Bmatrix} V_i \\ V_j \end{Bmatrix} \quad \text{Eq. 6-6}$$

The conductivity matrix for the resistor network, $[K_{eq}]$, was formed by assembling the individual conductivity matrices from **Eq. 6-6**. It was assumed that an electrode is formed by the parallel faces of the RVE, and a given electrical direct current (DC) is passed through the nanocomposite. So, the boundary condition was set to be $-I_{inp}$ and I_{inp} at the electrode nodes. The voltage at the electrodes was obtained using **Eq. 6-7**.

$$[V] = inv[K_{eq}] \{I\} \quad \text{Eq. 6-7}$$

In order to avoid singularity effects for the conductivity matrix, the resistors without any contribution to the overall resistivity of the nanocomposite were not considered in composing the conductivity matrix. In other words, only the resistors that are involved in forming the percolation network were taken into account for computing the electrical properties. The finite element code developed to evaluate the conductivity of CNT resistor network is provided in A.2.

6.3 Results and Discussion

6.3.1 *Effect of Temperature on Conductivity of CNT Nanocomposites*

The developed MC model with dispersed CNTs comprises a cubic RVE with edge length of $L = 15 \mu\text{m}$. An average MWCNT length of $l_f = 5 \mu\text{m}$ and diameter of $D = 50 \text{ nm}$ were employed, corresponding to a CNT aspect ratio of 100. The given RVE dimension was chosen based on findings by Chen et al. [279], who evaluated the percolation threshold for a system of CNT fillers with length and diameter of 200nm and 2nm, respectively. The percolations thresholds predicted for RVEs with a side length of 600, 800 and 1000 nm yielded values of 0.551, 0.553, 0.548%, respectively (with a standard deviation of 0.0025). The repeatability of these results and the small value of the standard deviation indicate that when L/l_f is set to 3 or higher the simulation results show no appreciable sensitivity to the RVE size. Results obtained from the current MC simulation exhibited a filler volume fraction of 0.0061 for the formation of a percolation network, which is in good agreement with 0.6165 vol% reported in [46] as percolation threshold. In a second step the electrical behavior of the conductive nanocomposite was evaluated employing the developed finite element model. The electrical resistivity of nanocomposites was predicted for different electrical properties of the polymer matrix, i.e. $\lambda = 0.5, 1, 1.5 \text{ ev}$. Multi-wall CNTs were assumed as filler material with resistivities ranging from 10^{-4} to $10^{-7} \Omega\text{m}$ [280]. As an example, **Figure 6-6** illustrates the conductivity behavior of a nanocomposite evaluated at 300 K, for a matrix with $\lambda = 0.5 \text{ ev}$ filled with CNTs having a resistivity of $0.5\text{E-}6 \Omega\text{m}$.

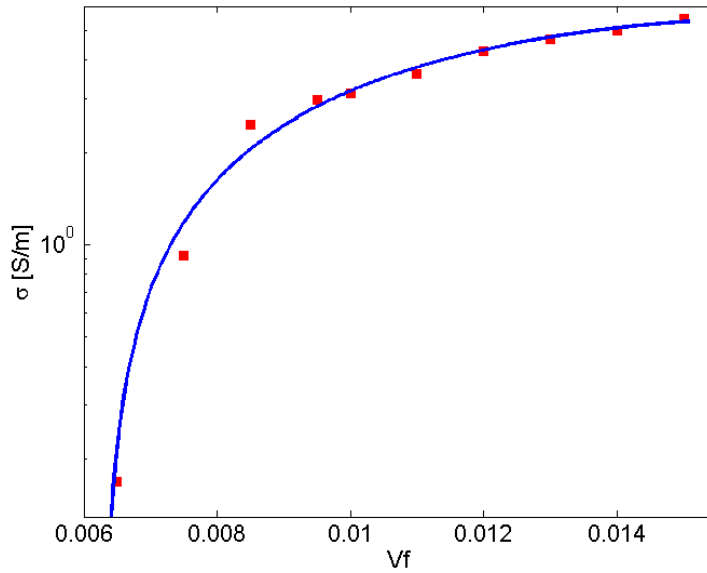


Figure 6-6: Electrical conductivity of a CNT nanocomposite with $\rho_{\text{CNT}} = 0.5\text{E-}6 \Omega\text{m}$, $\lambda = 0.5 \text{ eV}$.

The nanocomposite electrical behavior was evaluated at different temperatures ranging from 200 to 550 K. Considering the resistivity-temperature relationship of **Eq. 6-4**, a nonlinear behavior of the resistivity versus temperature curve is to be expected. In addition to the temperature, separation of the particles and the electrical field govern the nonlinearity behavior of the nanocomposite. The aforementioned governing parameters might work destructively exhibiting a quasi-linear behavior. The resistivity of the nanocomposite at a temperature of absolute zero, ρ_0 , was predicted through linear extrapolation; this value was subsequently employed to normalize nanocomposite resistivity data. The computed numerical results were compared with existing experimental works [264, 281] as shown in **Figure 6-7**. Simulation predictions presented in this figure are qualitatively in good agreement with experimental values. It should be noted that the reported experimental results were obtained for nanocomposites containing CNTs with an average diameter of 10 nm and a length varying from 0.1 to 10 μm . Comparing the experimental and numerical results indicates an insignificant difference in gradient G , where $G = (\Delta \rho/\rho_0)/T$. Evaluating the electrical resistivity for composites with different polymers reveals that the quantum mechanical barrier height of the polymer plays a major role for the resistivity-temperature characteristic of the

nanocomposite. As shown in **Figure 6-8**, the electrical resistivity is more sensitive to a change in temperature for polymers with lower barrier height.

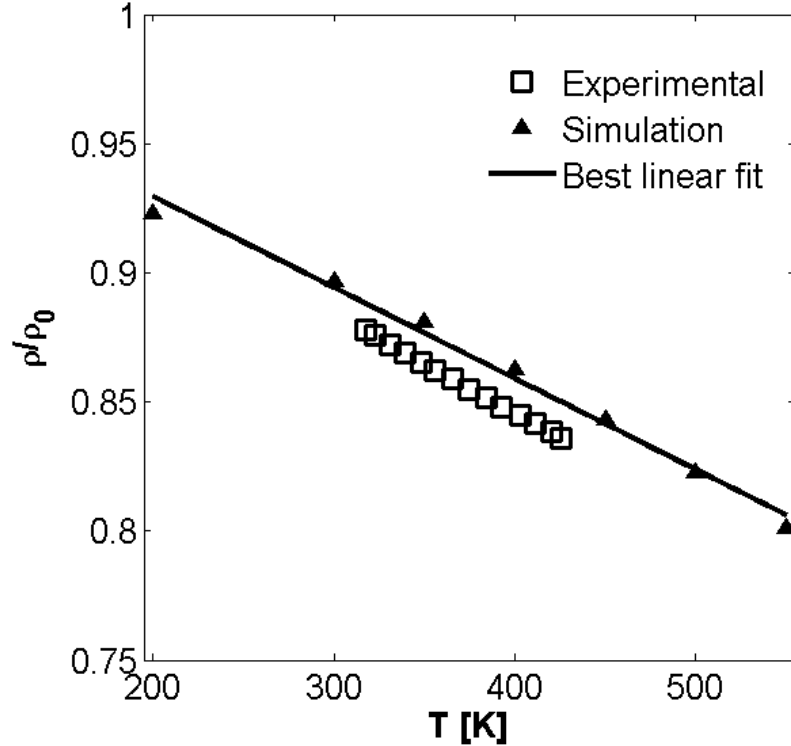


Figure 6-7: Qualitative comparison of experimental data [264, 281] with simulation results for a CNT nanocomposite with $\rho_{\text{CNT}} = 0.5\text{E-}6 \Omega\text{m}$, $\lambda = 0.5 \text{ eV}$, $V_f = 1\%$..

Next, the effect of filler resistivity on the temperature-resistivity behavior of the CNT nanocomposites was investigated. **Figure 6-9** shows the variation of electrical resistivity with respect to temperature for CNT nanocomposites for three different CNT resistivities and three different filler loadings (0.65%, 1%, 1.5%). It can be observed that the resistivity of nanocomposites with lower CNT resistivity is increasingly dependent on temperature. On the other hand, no significant effect of filler loading on the resistivity-temperature behavior of the nanocomposite can be ascertained. However, at the intermediate CNT resistivity the filler concentration affects the electrical resistivity by approximately 5%. At higher and lower resistivities, the effect of filler concentration appears diminished. Overall resistivity of the nanocomposite is composed of pristine resistivity of the CNTs and tunnelling. As it is given in **Eq. 6-4**, effect of the temperature

on the tunnelling conductivity is governed by the average particles separation and electrical potential difference, where they are ruled by the filler loading. Further studies should be planned to describe the contribution of the volume fraction and filler resistivity on resistivity of the composite.

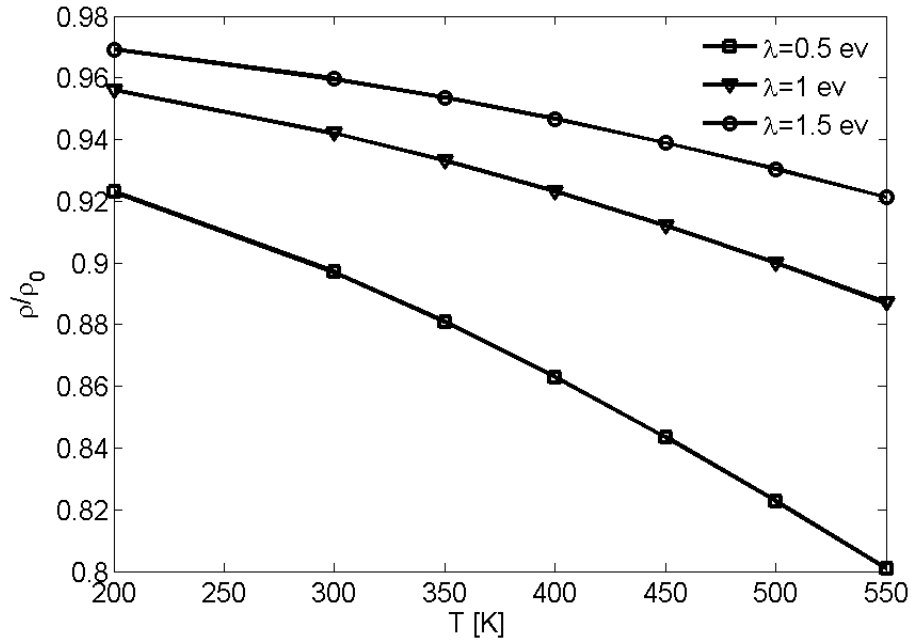


Figure 6-8: Effect of polymer electrical properties on the resistivity-temperature behavior for a CNT nanocomposite with $V_f = 1\%$ and $\rho_{CNT} = 0.5E-6 \Omega m$.

6.3.1 Effect of Temperature on Conductivity of GNP Nanocomposites

Modeling of GNP nanocomposites at different temperature levels was conducted for nanodisks with a diameter of 100 nm and thickness of 0.34 nm. Nanocomposite resistivity data was normalized with respect to a 300 K condition. Simulation results showing the effect of temperature on nanocomposite resistivity are depicted in **Figure 6-10**. As illustrated in this figure, the resistivity of GNP nanocomposites decreases monotonically with increasing temperature. Simulation results indicate that the sensitivity of the nanocomposite resistivity to temperature decreases as filler loading is increasing. Comparing the CNT nanocomposite resistivity-temperature behavior with that of GNP nanocomposites shows that the resistivity of GNP nanocomposite is affected to a greater

extent by temperature, suggesting a higher suitability of GNP nanocomposites for temperature sensing application.

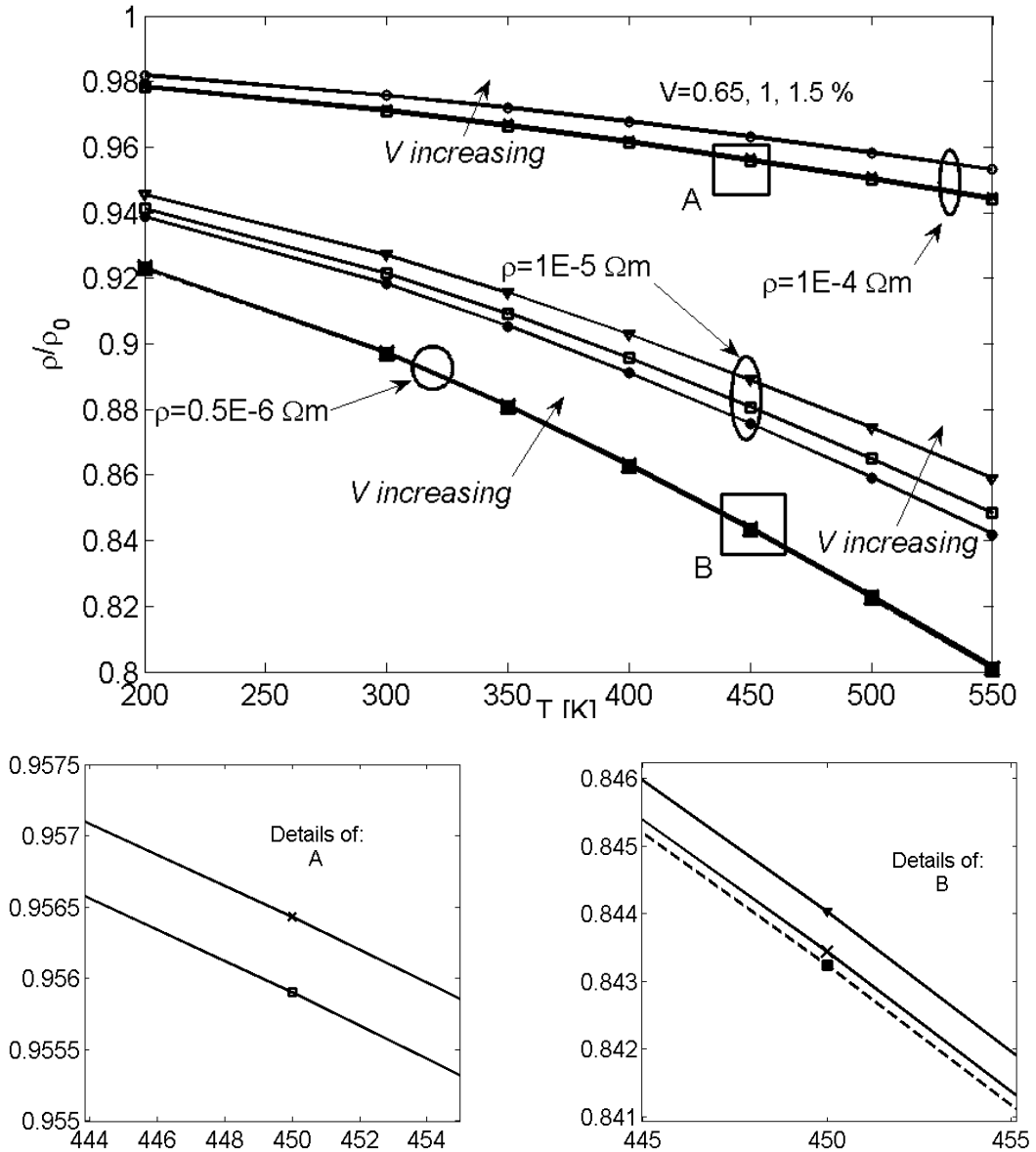


Figure 6-9: Effect of CNT resistivity on the resistivity-temperature behavior of CNT nanocomposites with $\lambda = 0.5$ eV.

As shown above, the resistivity of CNT and GNP nanocomposites decreases as temperature is increasing which is a characteristic behavior of semiconductors. Mott’s “variable range hopping” (VRH) model [266, 282] was employed to describe the observed nanocomposite behavior, i.e.

$$\rho = \rho_0 \exp\left[\left(\frac{T_0}{T}\right)^{1/D+1}\right] \quad \text{Eq. 6-8}$$

where ρ_0 and T_0 are constants and D is the dimensionality of the conduction process. The resistivities of GNP and CNT nanocomposites in terms of the absolute temperature are described using **Eq. 6-8** and the results are presented in **Figure 6-11** and **Figure 6-12**. The results indicate that Mott's VRH model is an effective tool to describe the resistivity-temperature behavior of GNP nanocomposites, whereas the VRH proposed model is less suitable for delineating the resistivity-temperature behavior of CNT nanocomposites.

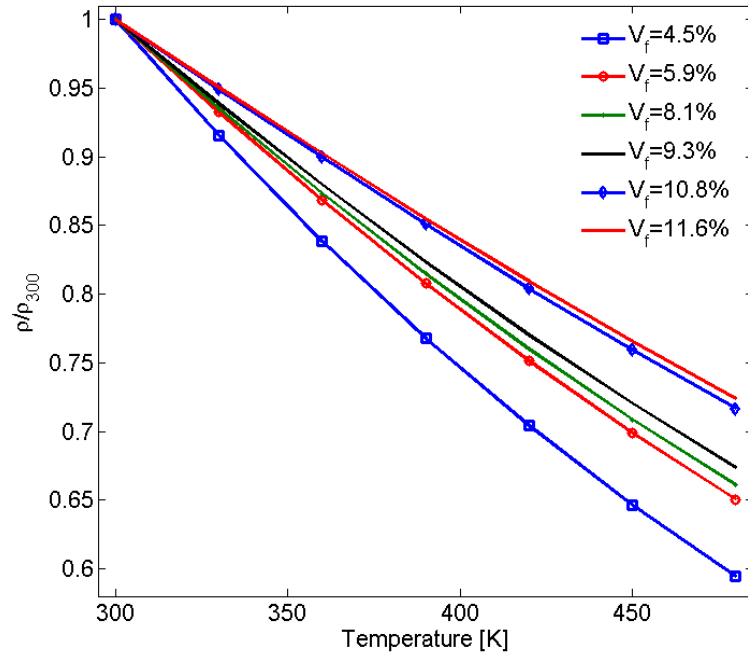


Figure 6-10: Normalized resistivity as a function of the temperature, from simulations with 100 nm nanodisks and $\lambda = 0.5$ eV.

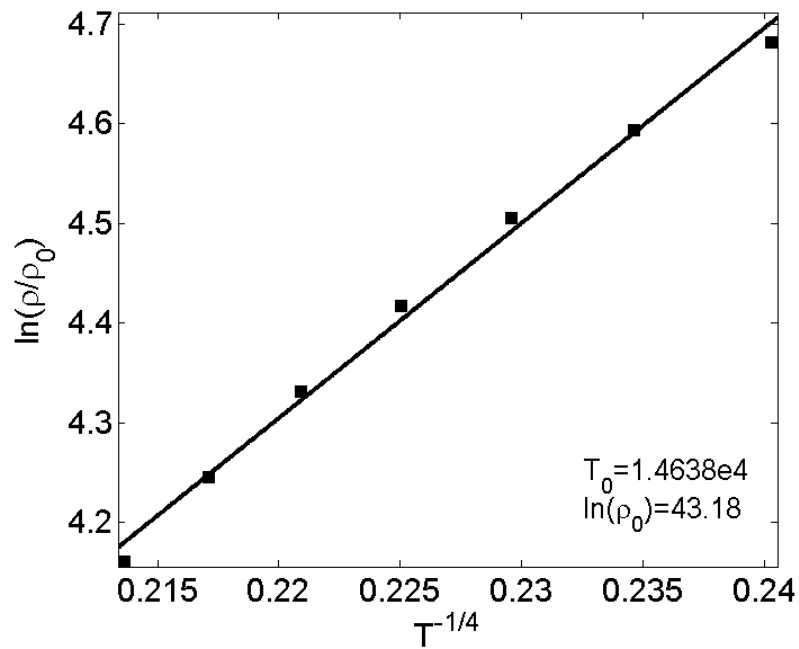


Figure 6-11: Fitting of GNP nanocomposite resistivity data according to the VRH model proposed by Mott [266, 282]

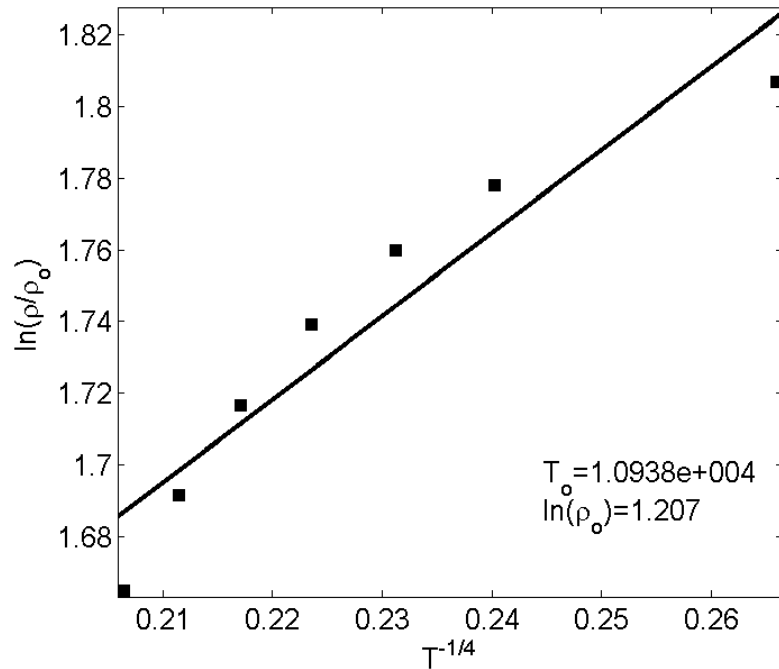


Figure 6-12: Fitting of CNT nanocomposite resistivity data according to the VRH model proposed by Mott [266, 282]. ($\lambda = 1$ eV, $V_f = 0.65\%$).

6.4 Conclusions

A comprehensive numerical study was conducted to evaluate the effect of temperature on the electrical behavior of CNT and GNP filled polymers. The study was carried out to investigate the temperature-resistivity behavior of nanocomposites involving a range of parameters, including filler electrical resistivity, quantum tunneling barrier height of the polymer matrix, and filler loading. Comparing the results obtained from the modeling work with existing experimental data confirmed good agreement. The simulations showed that a significant temperature effect can be realized for nanocomposites with favorable material properties. This dependence of electrical resistivity on temperature motivates future research to explore the feasibility of using CNT and GNP nanocomposites for temperature sensing applications.

6.5 Bibliography

- [44] H. M. Ma and X. L. Gao, "A three-dimensional Monte Carlo model for electrically conductive polymer matrix composites filled with curved fibers," *Polymer*, vol. 49, pp. 4230-4238, Sep 9 2008.
- [46] N. Hu, Y. Karube, C. Yan, Z. Masuda, and H. Fukunaga, "Tunneling effect in a polymer/carbon nanotube nanocomposite strain sensor," *Acta Materialia*, vol. 56, pp. 2929-2936, Aug 2008.
- [75] Z. Ounaies, C. Park, K. E. Wise, E. J. Siochi, and J. S. Harrison, "Electrical properties of single wall carbon nanotube reinforced polyimide composites," *Composites Science and Technology*, vol. 63, pp. 1637-1646, Aug 2003.
- [90] C. Y. Li, E. T. Thostenson, and T. W. Chou, "Dominant role of tunneling resistance in the electrical conductivity of carbon nanotube-based composites," *Applied Physics Letters*, vol. 91, Nov 26 2007.
- [91] Y. Yu, G. Song, and L. Sun, "Determinant role of tunneling resistance in electrical conductivity of polymer composites reinforced by well dispersed carbon nanotubes," *Journal of Applied Physics*, vol. 108, Oct 15 2010.
- [92] C. Li, E. T. Thostenson, and T. W. Chou, "Effect of nanotube waviness on the electrical conductivity of carbon nanotube-based composites," *Composites Science and Technology*, vol. 68, pp. 1445-1452, May 2008.
- [183] T. Natsuki, M. Endo, and T. Takahashi, "Percolation study of orientated short-fiber composites by a continuum model," *Physica a-Statistical Mechanics and Its Applications*, vol. 352, pp. 498-508, Jul 15 2005.
- [184] F. Dalmas, R. Dendievel, L. Chazeau, J. Y. Cavaille, and C. Gauthier, "Carbon nanotube-filled polymer of electrical conductivity in composites. Numerical simulation three-dimensional entangled fibrous networks," *Acta Materialia*, vol. 54, pp. 2923-2931, Jun 2006.
- [185] C. Y. Li and T. W. Chou, "Continuum percolation of nanocomposites with fillers of arbitrary shapes," *Applied Physics Letters*, vol. 90, Apr 23 2007.
- [208] H. A. Almohamad and S. Z. Selim, "An algorithm for computing the distance between two circular disks," *Applied Mathematical Modelling*, vol. 27, pp. 115-124, Feb 2003.
- [221] W. S. Bao, S. A. Meguid, Z. H. Zhu, and G. J. Weng, "Tunneling resistance and its effect on the electrical conductivity of carbon nanotube nanocomposites," *Journal of Applied Physics*, vol. 111, May 1 2012.

- [258] K. S. Karimov, M. Abid, M. Saleem, K. M. Akhmedov, M. M. Bashir, U. Shafique, *et al.*, "Temperature gradient sensor based on CNT composite," *Physica B: Condensed Matter*, vol. 446, pp. 39-42, 2014.
- [259] C. Heo and J. H. Chang, "Polyimide nanocomposites based on functionalized graphene sheets: Morphologies, thermal properties, and electrical and thermal conductivities," *Solid State Sciences*, vol. 24, pp. 6-14, Oct 2013.
- [260] J. S. Kim, J. H. Yun, I. Kim, and S. E. Shim, "Electrical properties of graphene/SBR nanocomposite prepared by latex heterocoagulation process at room temperature," *Journal of Industrial and Engineering Chemistry*, vol. 17, pp. 325-330, Mar 25 2011.
- [261] P. Manivel, S. Kanagaraj, A. Balamurugan, N. Ponpandian, D. Mangalaraj, and C. Viswanathan, "Rheological behavior and electrical properties of polypyrrole/thermally reduced graphene oxide nanocomposite," *Colloids and Surfaces a-Physicochemical and Engineering Aspects*, vol. 441, pp. 614-622, Jan 20 2014.
- [262] A. S. Patole, S. P. Patole, H. Kang, J. B. Yoo, T. H. Kim, and J. H. Ahn, "A facile approach to the fabrication of graphene/polystyrene nanocomposite by in situ microemulsion polymerization," *Journal of Colloid and Interface Science*, vol. 350, pp. 530-537, Oct 15 2010.
- [263] E. Logakis, C. Pandis, V. Peoglos, P. Pissis, J. Pionteck, P. Potschke, *et al.*, "Electrical/dielectric properties and conduction mechanism in melt processed polyamide/multi-walled carbon nanotubes composites," *Polymer*, vol. 50, pp. 5103-5111, Oct 9 2009.
- [264] H. C. Neitzert, L. Vertuccio, and A. Sorrentino, "Epoxy/MWCNT Composite as Temperature Sensor and Electrical Heating Element," *Ieee Transactions on Nanotechnology*, vol. 10, pp. 688-693, Jul 2011.
- [265] E. Bilotti, R. Zhang, H. Deng, M. Baxendale, and T. Peijs, "Fabrication and property prediction of conductive and strain sensing TPU/CNT nanocomposite fibres," *Journal of Materials Chemistry*, vol. 20, pp. 9449-9455, 2010.
- [266] A. Bahrami, Z. A. Talib, W. M. M. Yunus, K. Behzad, M. M. Abdi, and F. U. Din, "Low Temperature Hall Effect Investigation of Conducting Polymer-Carbon Nanotubes Composite Network," *International Journal of Molecular Sciences*, vol. 13, pp. 14917-14928, Nov 2012.
- [267] Z. Yang, Z. Cao, H. Sun, and Y. Li, "Composite Films Based on Aligned Carbon Nanotube Arrays and a Poly (N-Isopropyl Acrylamide) Hydrogel," *Advanced Materials*, vol. 20, pp. 2201-2205, 2008.
- [268] H. C. Neitzert, L. Vertuccio, and A. Sorrentino, "Epoxy/MWCNT composite as temperature sensor and electrical heating element," *Nanotechnology, IEEE Transactions on*, vol. 10, pp. 688-693, 2011.
- [269] P. Sheng, "Fluctuation-induced tunneling conduction in disordered materials," *Physical Review B*, vol. 21, p. 2180, 1980.
- [270] G. Matzeu, A. Pucci, S. Savi, M. Romanelli, and F. Di Francesco, "A temperature sensor based on a MWCNT/SEBS nanocomposite," *Sensors and Actuators A: Physical*, vol. 178, pp. 94-99, 2012.
- [271] M. Sibinski, M. Jakubowska, and M. Sloma, "Flexible temperature sensors on fibers," *Sensors*, vol. 10, pp. 7934-7946, 2010.
- [272] G. Marsaglia, "Choosing a Point from the Surface of a Sphere" *Ann. Math. Statist.*, vol. 43, pp. 373-700, 1972.
- [273] M. Matsumoto and T. Nishimura, "Mersenne twister: a 623-dimensionally equidistributed uniform pseudo-random number generator," *ACM Trans. Model. Comput. Simul.*, vol. 8, pp. 3-30, 1998.
- [274] Y. Yu, G. Song, and L. Sun, "Determinant role of tunneling resistance in electrical conductivity of polymer composites reinforced by well dispersed carbon nanotubes," *Journal of Applied Physics*, vol. 108, p. 084319, 2010.
- [275] A. Oskouyi, U. Sundararaj, and P. Mertiny, "Tunneling Conductivity and Piezoresistivity of Composites Containing Randomly Dispersed Conductive Nano-Platelets," *Materials*, vol. 7, pp. 2501-2521, 2014.

- [276] A. B. Oskouyi and P. Mertiny, "Monte Carlo model for the study of percolation thresholds in composites filled with circular conductive nano-disks," *Procedia Engineering*, vol. 10, pp. 403-408, // 2011.
- [277] J. G. Simmons, "Generalized Formula for the Electric Tunnel Effect between Similar Electrodes Separated by a Thin Insulating Film," *Journal of Applied Physics*, vol. 34, pp. 1793-1803, 1963.
- [278] J. G. Simmons, "Generalized Thermal J-V Characteristic for the Electric Tunnel Effect," *Journal of Applied Physics*, vol. 35, pp. 2655-2658, 1964.
- [279] Y. Chen, S. Wang, F. Pan, and J. Zhang, "A Numerical Study on Electrical Percolation of Polymer-Matrix Composites with Hybrid Fillers of Carbon Nanotubes and Carbon Black," *Journal of Nanomaterials*, vol. 2014, 2014.
- [280] T. Ebbesen, H. Lezec, H. Hiura, J. Bennett, H. Ghaemi, and T. Thio, "Electrical conductivity of individual carbon nanotubes," 1996.
- [281] H. C. Neitzert, A. Sorrentino, and L. Vertuccio, "Epoxy/MWCNT Composite Based Temperature Sensor with Linear Characteristics," in *Sensors and Microsystems*. vol. 54, P. Malcovati, A. Baschiroto, A. d'Amico, and C. Natale, Eds., ed: Springer Netherlands, 2010, pp. 241-245.
- [282] S. M. Shang, W. Zeng, and X. M. Tao, "High stretchable MWNTs/polyurethane conductive nanocomposites," *Journal of Materials Chemistry*, vol. 21, pp. 7274-7280, 2011.

CHAPTER 7

STRUCTURAL HEALTH MONITORING OF COMPOSITE PIPING USING ELECTRICAL IMPEDANCE TOMOGRAPHY

SYNOPSIS- Traditional nondestructive testing methods such as ultrasonic inspection and guided waves generally perform inadequately for the interrogation of polymer composite structures and polymer-metal assemblages. The development of alternative solutions for effective and reliable structural health monitoring in structures containing polymer constituents is therefore warranted. In the present study a novel method based on electrical impedance tomography was explored to detect damage and wear-induced material loss in polymeric piping structures. In order to utilize electrical impedance tomography for polymeric structures, the polymer phase is made conductive through dispersing graphene nanoplatelets. Finite element modeling was conducted with the aim of predicting the response of a degraded structure to an electrical input signal.

7.1 Introduction

Pressure vessels and piping are commonly used components in industrial facilities like refineries, petrochemical complexes and power plants. Hazards and potential risks associated with the thinning of pressure piping due to corrosion and erosion necessitate employing effective structural health monitoring (SHM) strategies to assure their safety and integrity [283]. Advantageous characteristics of polymers and fiber-reinforced polymer composites (FRPC), i.e. high specific strength and excellent corrosion resistance have encouraged engineers to employ such materials in an ever increasing range of industrial applications. The development and design of effective monitoring and fault detection solutions for polymer-based structures is critical for their broader implementation.

SHM schemes can be classified into passive or active methods [284]. Passive techniques, e.g. acoustic emission (AE) testing, typically require only sensors for signal acquisition, and measurements gained from the structure are compared with reference data [284]. Piezoelectric materials are most commonly used for sensors in passive sensing systems [284-286]. For example, Loutas and Kostopoulos [287] developed a damage assessment method for carbon reinforced composites using AE mechanisms. Oliveira and Marques [288] conducted a study on applying AE and artificial neural networks for SHM in glass fiber/polyester laminated structures.

In the case of active SHM techniques the structure is excited by an input signal, such as an ultrasonic wave. Active SHM methods have demonstrated good performance in estimating the severity and location of flaws [289]. In general, ultrasonic techniques are popular for detecting the severity and location of damage in structures [290-292], and methods employing guided-waves (GW) have frequently been employed in this context [289]. Raghavan and Cesnik [293] conducted a comprehensive literature review on using GW in SHM applications. The measurement principle is as follows: ultrasonic waves generated by the actuators propagate through the media with structural flaw such as crack. The damage is then detected through processing the signal received by the sensors. Piezoelectric sensors/actuators are mostly employed in generating and recording ultrasonic waves [289]. For example, Kim et al. [294] employed Lamb waves generated by surface mounted piezoceramics for damage assessment in layered composite structures. Castaings and Hoston [295] used ultrasonic guided waves for SHM of high-pressure composite vessels. A neural network method was employed in this context by Yuan et al. [296] for SHM of honey comb sandwich and carbon fiber composite structures. They developed a Lamb wave based method to detect delamination and impact damage.

Employing conventional SHM schemes for composite structures and polymer-metal assemblages is associated with several drawbacks. GW based SHM techniques have shown good reliability for detecting damage that is located even far from the transducers and sensors. However, their application for SHM of composite structures and polymer-

metal assemblages is associated with restrictions, i.e. poor transmission properties in structures with multiple interfaces [297].

In recent years, a great number of research works have been conducted to develop novel schemes to effectively evaluate complex material systems with polymeric constituents. Fiber Bragg grating sensing and embedded electrically conductive fibers can be listed as some of the recently developed methods for SHM of polymeric composites.

A considerable number of research works has been conducted related to SHM applications using optical fibers and fiber Bragg gratings (FGB) in composite structures. Generally, optical fibers consist of a silica core encompassed by a cladding material with lower index of refraction, making the optical fiber a waveguide [298]. FGB sensors are optical fibers that reflect a specific wavelength of light, called Bragg wavelength, travelling through the optical fiber. FGB sensors can be formed by creating a periodic variation of the refraction index along a segment of the optical fiber [298]. It has been shown that the Bragg wavelength depends on the state of the mechanical strain in the FGB sensors, making them good candidates for SHM applications. Majumder et al. [299] conducted a comprehensive literature review on FGB sensors in SHM applications. For example, Hao et al. [300] used FGB sensors for the non-destructive evaluation of FRP pressure vessels. Ramos et al. [301] developed a strain sensing patch using FGB sensors. Kister et al. [302] reported on the application of optical fibers in SHM of a glass-fiber composite bridge, where FGB sensors were used for real-time integrity monitoring.

The concept of applying electrically conductive fibers (e.g. long carbon fibers) in SHM of composite structures was introduced by Schulte et al. [303, 304]. They investigated the feasibility of employing resistivity measurements to achieve SHM capabilities. Later, M. Kupke et al. [305] developed a non-destructive testing method for fiber reinforced composites using direct-current and alternating-current electrical signals. Since measurements are based on changes in conductivity of the conductive fibers, this SHM concept is clearly restricted to composites containing suitable fibers. Moreover, damage features that do not appreciably alter the strain state and thus the resistivity of the conducting fibers, e.g. matrix damage with minor influence on fiber straining or damage

located too far from the fibers, cannot be monitored, which is a decisive limitation of this detection technique [306]. In general, the electrical response of composite structures with long conductive fibers yields adequate sensitivity to fiber breakage, whereas the sensitivity to flaws in the matrix is insignificant [3].

The development of nanoscale conductive inclusions and their low-cost fabrication methods have stimulated great interest within the research community in employing conductive particles to render insulator polymers conductive and develop novel conductive polymers. Suitably dispersing conductive particles within a polymer matrix is the basis for achieving electrically conductive polymers, and associated techniques have been the subject of intense research in recent decades [10, 11, 178-180, 304, 307]. The development of conductive nanocomposites with tailored properties, including piezoresistivity effects, provides the opportunity to employ such materials as an embedded sensing system for SHM in innovative composite structures. In this context, Loyola provided a comprehensive review of recently developed methods for SHM applications in polymeric composites [306].

Carbon black and carbon nanotubes (CNT) are the best known nanoparticles used in conductive polymers. Employing CNT particles in SHM applications has been the subject matter of a considerable number of research works. For example, Thostenson and Chou [307] studied electrical networks formed through dispersed CNT particles in a polymeric matrix to predict the delamination in composite structures. In a related work, they developed a CNT based SHM technique for mechanically fastened composite joints [308]. Several other research works have been devoted to CNT network based failure detection in polymeric composite structures [10, 11, 178, 309, 310].

Limited piezoresistivity of conductive polymers based on carbon black, and the high cost of CNTs make these two types of particles less attractive for many industrial applications. Polymers filled with conductive nanoplatelets like graphene platelets and exfoliated graphite, which are also economically priced, have shown significant conductivity and piezoresistivity behavior that make them an excellent choice for strain sensing and electrical applications. Graphene, which is a two-dimensional nanoparticle allotrope of

carbon, may be considered an alternative filler for making polymers conductive. Low cost and a high aspect ratio makes graphene sheets a promising candidate for a variety of novel material systems.

Using information gained in previous chapters on nanoplatelet modified polymers, e.g. electrical conductivity and piezoresistivity behavior, a finite element based study was carried out to evaluate the feasibility of employing graphene nanocomposites in SHM applications. In present work it is proposed to employ Electrical Impedance Tomography (EIT) to detect and localize damage and wear-induced material loss in polymeric piping structures which electrical conductivity has been enhanced by dispersing graphene nanoplatelets. The following two-phase approach was employed to meet the objectives of this original research:

1. An effectual model was implemented for the prediction of the electro-mechanical and piezoresistivity behavior of electrically conductive polymers that act as sensors.
2. A SHM and fault detection technology was developed that allows for monitoring material loss and other damage/defects utilizing measurements obtained from an innately non-discrete sensor.

7.2 Theoretical Approach

7.2.1 *Finite Element Modeling*

The existence of a defect such as a crack or localized material loss is assumed to alter the mechanical and electrical behavior of the structure. Further, it is assumed that conductive nanoparticles are dispersed in the polymer phase of the structure to provide the polymer with conductivity and piezoresistivity behavior. Given the proposed approach, the first part is dedicated to developing a model for predicting the response from the degraded structure to certain input signals. For this purpose, electrical current is injected from different contact points located on the conductive polymer material, and thus an electrical potential distribution for the structure is obtained.

For a low-frequency electrical current for which the effect of the magnetic field is negligible, the correlation between the conductivity distribution, electrical potential and electrical current can be simplified as [311]:

$$\sigma \nabla \phi = I \quad \text{Eq. 7-1}$$

and according to the Kirchoff's law, we have:

$$\nabla \cdot (\sigma \nabla \phi) = 0 \quad \text{Eq. 7-2}$$

where σ is the conductivity distribution, ϕ is the electrical potential field and I indicates the electrical current.

Considering an inhomogeneous conductivity throughout the polymer based phase it is difficult to find an analytical solution for **Eq. 7-1**. It is therefore proposed to construct a finite element model to investigate the electrical response of the degraded structure. An expression for **Eq. 7-1**. in terms of a finite element solution can be written as [312]:

$$\phi = \sum_{i=1}^n \alpha_i \phi_i \quad \text{Eq. 7-3}$$

where ϕ_i is the solution at i^{th} node, α_i is a basis function and n is the order of the element used to discretize the model.

Supposed the α_i is non-differentiable at the nodes, then, using a variational method, the weak form of the Laplace equation can be written as [312]:

$$\int V [\nabla \cdot (\sigma \nabla \phi)] dV = 0 \quad \text{Eq. 7-4}$$

Using **Eq. 7-1** and **Eq. 7-3** and employing a finite element formulation technique, it is found that

$$A\phi = I \quad \text{Eq. 7-5}$$

where A is a square matrix that is calculated through employing the conductivity distribution and basis function α_i . Boundary conditions at the electrode locations can be defined as [306, 313]:

$$\int_{s_l} \sigma \frac{\partial V}{\partial n} ds = I_l \quad \text{Eq. 7-6}$$

The system governing equation is obtained through assembling the individual element matrices. Solving this equation provides the response of the structure to the applied input signal.

7.2.1 *Electrical Impedance Tomography*

The objective herein is to detect possible defects employing the system response to electrical current stimuli. As it was explained earlier, electrical current is injected into the structure to obtain an electrical potential distribution. Now, the goal is to predict a possible conductivity distribution for the structure that is indicated by the given electrical potential mapping. It is proposed to use the EIT technique to obtain this conductivity distribution. In other words, EIT is the process of predicting the conductivity distribution through surface electrical potential measurements [311]. EIT is a technique known from medical imaging (i.e., gastric, brain, breast and lung imaging) [314-317]. **Figure 7-1** shows an EIT application example for lung imaging.

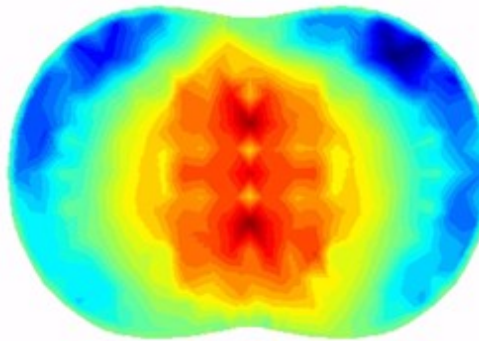


Figure 7-1: EIT application example for lung imaging. Lung image is reproduced with permission from [317].

EIT has also found applications in engineering (e.g. geophysics, industrial process imaging, damage detection) [180, 318-321]. Lazarovitch et al. employed this technique to identify a crack in carbon paper [318]. Seppanen et al. developed a nondestructive imaging method based on EIT to obtain information on voids and cracks inside concrete structures [322]. More examples of employing EIT in SHM applications can be found in

[323-325]. In addition to the listed works, a history of utilizing EIT for SHM applications can be found in the review article by Deng and Liu [326].

EIT problems are known to be severely ill-posed [321]. Consequently, it is not guaranteed that there is a unique solution for a reverse analysis. In order to overcome this challenge, electrical current is injected through different electrodes for a given EIT problem, and several surface electrical potential measurements are collected. An inverse analysis should then provide an electrical conductivity distribution prediction that satisfies all the taken measurements. In other words, the objective of the reverse analysis is proposing a conductivity distribution that minimizes the following cost function:

$$r = \sum_{i=1}^L \left(\phi|_{FEM} - \phi|_{Experimental} \right)^2 \quad \text{Eq. 7-7}$$

where r is the value of the cost function, $\phi|_{FEM}$ is the potential distribution obtained from the suggested conductivity distribution, and $\phi|_{Experimental}$ is the potential distribution obtained from measurements; L indicates the number of points where measurements were collected. The intention herein is to employ the EIT technique in conjunction with FEM for SHM, i.e. the detection of damage such as cracks or wear-induced localized material loss, in polymer composite pipes with a conductive polymer matrix.

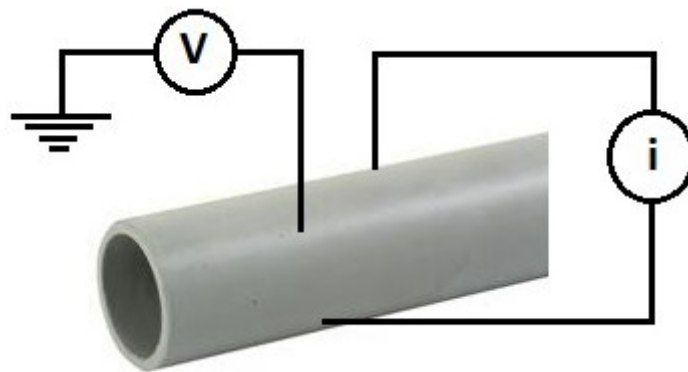


Figure 7-2: Schematic of the proposed technique for SHM in polymer composite piping.

As illustrated schematically in **Figure 7-2**, electrical current is injected into the pipe at different contact points, and the electrical potential distribution is obtained for each case yielding the defect location through conductivity mapping.

7.1 Simulation Results and Discussion

In order to employ experimental measurements to reconstruct the conductivity distribution using EIT, a predictive model needs to be developed. Finite element modeling was herein conducted using COMSOL MultiPhysics 4.3 (COMSOL Inc., Burlington, MA, USA). As illustrated in **Figure 7-3** and **Figure 7-4** a sufficiently long pipe segment was modeled to minimize boundary effects due to finite length. The model was discretized by using over 8500 tetrahedral 3D elements and the results were obtained by using stationary solver. A sensing array consisting of 32 electrodes arranged in a square pattern was used for EIT measurements. For each set of measurements, one of the electrodes was grounded, and electrical current was injected from a different electrode. A defect was represented by an ellipsoid, which semi-axes represent the length, width and depth of the defect region. For example, an electrode arrangement on the outer pipe surface and an internal defect are illustrated in **Figure 7-3** and **Figure 7-4**, respectively.

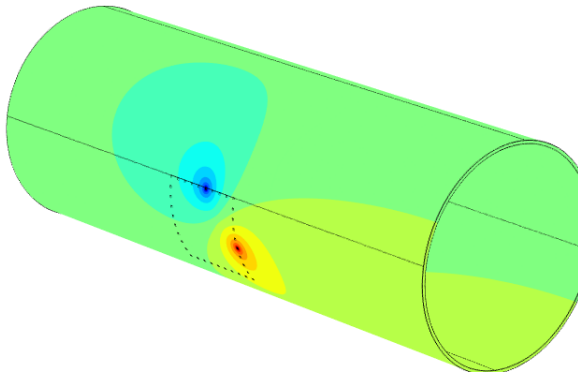


Figure 7-3: Modeling of the sensing electrodes on the outer surface of the pipeline segment.

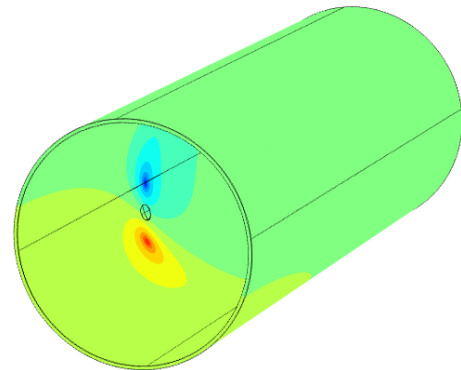


Figure 7-4: Corrosion in pipe represented by ellipsoid.

In preceding chapters and in [275], the electrical behavior of polymer material made conductive through the dispersion of graphene nanoplatelets (GNP) was explored, which included the study of non-ohmic electrical behavior that is governed by the level of the

applied electrical field. Shown in **Figure 7-5** is the dependency of nanocomposite electrical conductivity on the intensity of the applied electrical field.

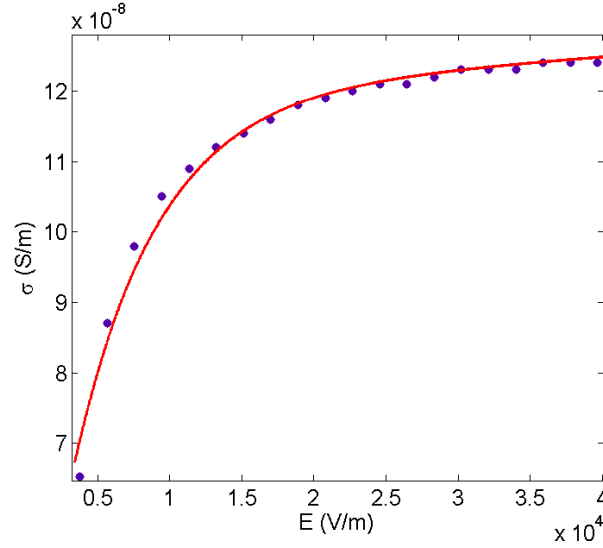


Figure 7-5: Conductivity of the conductive nanocomposite as a function of the electrical field.

As mentioned earlier, EIT problems are ill-posed, and reconstruction of the conductivity map using experimental measurements may not lead to a unique solution. Different terminal-ground configurations (TGC) are employed here as an effective means for resolving this problem. The current injection pattern given in **Figure 7-6** was proposed for conducting the EIT measurements. The terminal where the electrical current is injected is connected to the corresponding ground electrode by the imaginary lines. The TGC are labeled using the description given in **Eq. 7-8**, where i is the configuration index. For example, given the expressions in **Eq. 7-8**, for the 14th TGC, electrode number 11 is grounded and the electrical current is injected through electrode number 6.

$$\begin{cases} 1 \leq i \leq 8 & 33 - i \text{ and } 8 + i \\ 9 \leq i \leq 16 & i - 8 \text{ and } 25 - i \\ 17 \leq i \leq 24 & i - 33 \text{ and } 8 + i \\ 25 \leq i \leq 40 & i - 24 \text{ and } 57 - i \end{cases} \quad \text{Eq. 7-8}$$

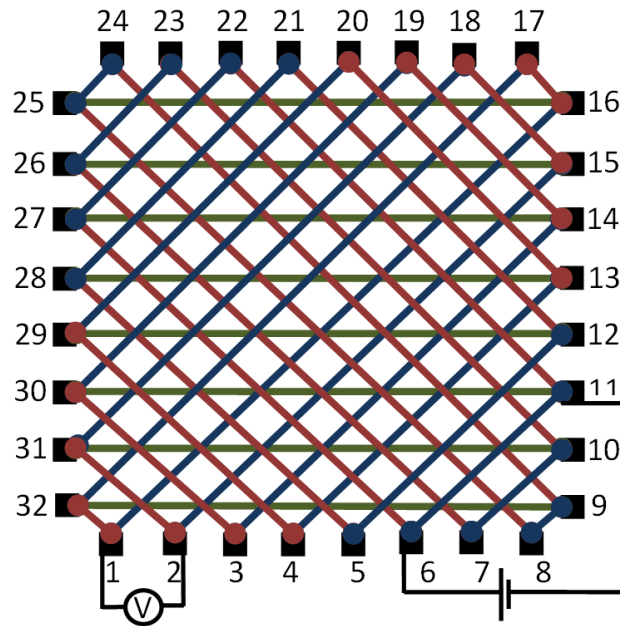


Figure 7-6: Electrode configuration schematic for the sensing array and current injection patterns. Based on the concept developed in [180].

Several sets of measurements were conducted for a pipe with and without defect. The pipe was modeled as a hollow cylinder with inner diameter of 700 mm and thickness of 10 mm. The ellipsoid representing a defect had a thickness, length and width of 6.5 mm, 3.5 mm, 8 mm, respectively. The length of the sensing array was 300 mm. The Cartesian coordinates identifying the defect center were 70 mm and 120 mm for the origin of the coordinate system being located at the center of the measurement array. The injected electrical current was set to $0.01 \mu A$.

Boundary measurements are required to reconstruct the conductivity distribution. Clearly, boundary measurements with high sensitivity to the defect are most desirable for EIT applications. Results for the EIT measurements conducted for several TGC are illustrated by **Figure 7-7**. In each measurement set, the boundary electrical potential is measured with respect to the ground electrode. **Figure 7-7** provides the measurements for four TGC. The corresponding electrode numbers can be obtained employing **Eq. 7-8**. In an effort to find a measurement scheme with defect high sensitivity, another measuring scheme was proposed, that is, for each TGC the electrical potential difference between

two adjacent electrodes was collected. Data thus collected is displayed in **Figure 7-8**. The abscissa indicates the index of an electrode pair used for the electrical potential difference measurement. For example, $x=i$ is corresponding to the electrical potential measurement between the i^{th} and $(i+1)^{th}$ electrodes. In the following, in order to evaluate the sensitivity of the two proposed EIT measurement schemes, measurements were repeated for the defect-free pipe model. These measurements were compared with data from the pipe with defect. The differences between data from the first and second measurement scheme are given in **Figure 7-9** and **Figure 7-10**, respectively.

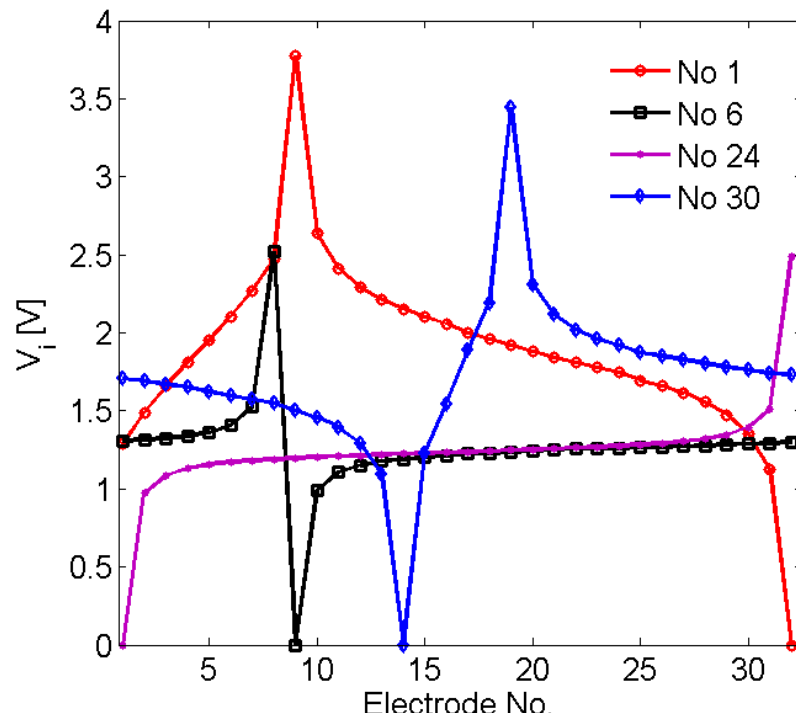


Figure 7-7: EIT measurements based on scheme one.

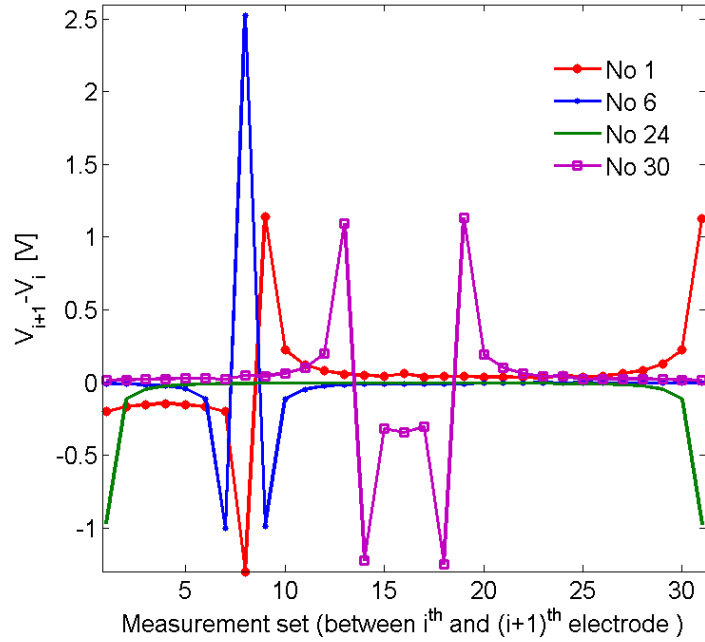


Figure 7-8: EIT measurements based of scheme.

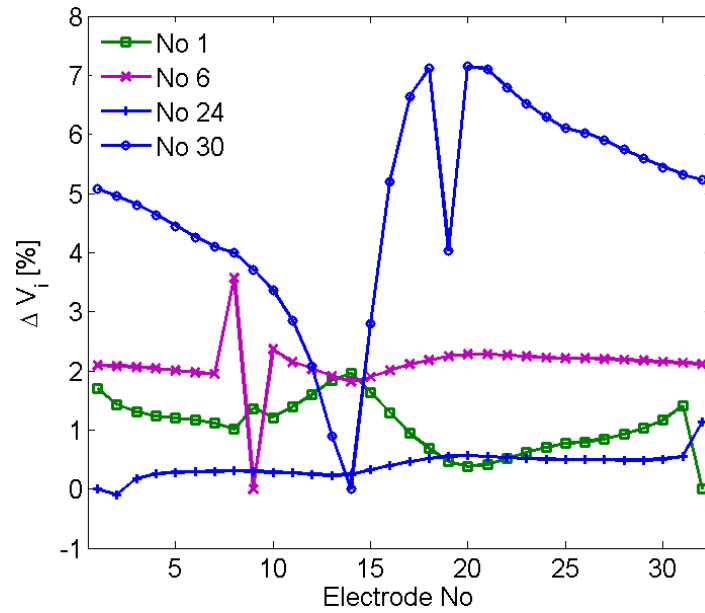


Figure 7-9: Comparison of the EIT measurements for the damaged and undamaged pipe based on scheme one.

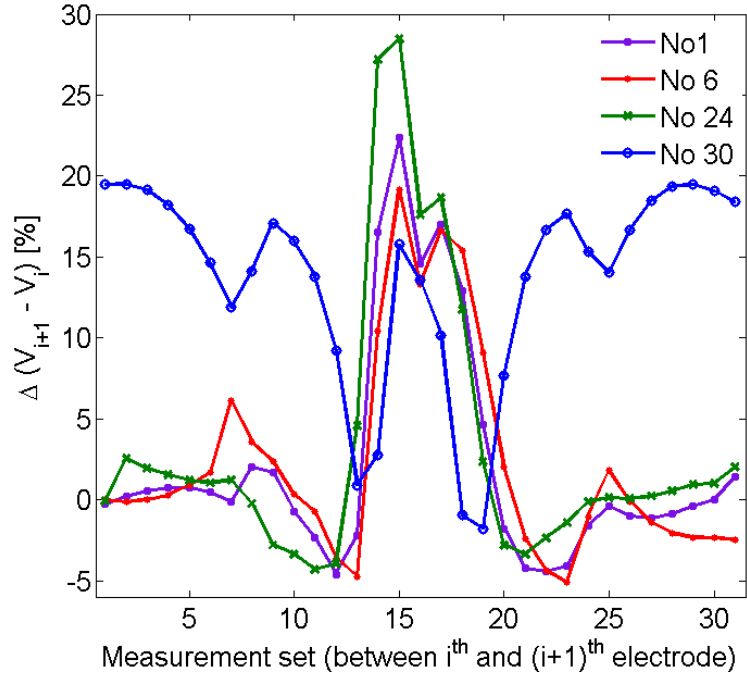


Figure 7-10: Comparison of the EIT measurements for the damaged and undamaged pipe based on scheme 2.

Comparison of the results shown in **Figure 7-9** and **Figure 7-10** indicates that for identical TGC the difference between the EIT measurements obtained for the damaged and undamaged pipe is much more significant when employing the second measuring scheme. Since measurement schemes with high defect sensitivity are most desirable in solving the given problem, the second scheme is more effective in predicting the defect using surface measurements. The high sensitivity of the proposed EIT approach confirms the feasibility and capability of the developed method for SHM in polymeric piping containing an electrically conductive polymer phase. Based on this finding, further research is warranted to develop an efficient algorithm for predicting the characteristics and severity of defects (inverse problem).

7.2 Conclusion

A study was conducted to evaluate the feasibility of employing conductive nanocomposites for structural health monitoring applications. The electrical characteristics of graphene nanoplatelet based conductive nanocomposites obtained from

methods described in preceding chapters were employed in this study. A structural health monitoring paradigm was developed based on electrical impedance tomography to detect to defects in polymeric piping. The observed high defect sensitivity of the proposed electrical impedance tomography technique indicates its feasibility and efficacy for structural health monitoring applications in polymer-based piping structures.

7.3 Bibliography

- [3] L. M. Gao, E. T. Thostenson, Z. G. Zhang, and T. W. Chou, "Coupled carbon nanotube network and acoustic emission monitoring for sensing of damage development in composites," *Carbon*, vol. 47, pp. 1381-1388, Apr 2009.
- [10] N. D. Alexopoulos, C. Bartholome, P. Poulin, and Z. Marioli-Riga, "Structural health monitoring of glass fiber reinforced composites using embedded carbon nanotube (CNT) fibers," *Composites Science and Technology*, vol. 70, pp. 260-271, Feb 2010.
- [11] L. Boeger, M. H. G. Wichmann, L. O. Meyer, and K. Schulte, "Load and health monitoring in glass fibre reinforced composites with an electrically conductive nanocomposite epoxy matrix," *Composites Science and Technology*, vol. 68, pp. 1886-1894, Jun 2008.
- [178] E. T. Thostenson and T. W. Chou, "Real-time in situ sensing of damage evolution in advanced fiber composites using carbon nanotube networks," *Nanotechnology*, vol. 19, May 28 2008.
- [179] K. J. Loh, J. P. Lynch, and N. A. Kotov, "Passive wireless sensing using SWNT-based multifunctional thin film patches," *International Journal of Applied Electromagnetics and Mechanics*, vol. 28, pp. 87-94, 2008.
- [180] K. J. Loh, T. C. Hou, J. P. Lynch, and N. A. Kotov, "Carbon Nanotube Sensing Skins for Spatial Strain and Impact Damage Identification," *Journal of Nondestructive Evaluation*, vol. 28, pp. 9-25, Mar 2009.
- [275] A. Oskouyi, U. Sundararaj, and P. Mertiny, "Tunneling Conductivity and Piezoresistivity of Composites Containing Randomly Dispersed Conductive Nano-Platelets," *Materials*, vol. 7, pp. 2501-2521, 2014.
- [283] J.-H. Lee and S.-J. Lee, "Application of laser-generated guided wave for evaluation of corrosion in carbon steel pipe," *NDT & E International*, vol. 42, pp. 222-227, 4// 2009.
- [284] S. Hurlebaus and L. Gaul, "Smart structure dynamics," *Mechanical Systems and Signal Processing*, vol. 20, pp. 255-281, Feb 2006.
- [285] K. Y. Choi and F. K. Chang, "Identification of impact force and location using distributed sensors," *Aiaa Journal*, vol. 34, pp. 136-142, Jan 1996.
- [286] K. Kishimoto, H. Inoue, M. Hamada, and T. Shibuya, "Time frequency analysis of dispersive waves by means of wavelet transform," *Journal of Applied Mechanics-Transactions of the Asme*, vol. 62, pp. 841-846, Dec 1995.
- [287] T. H. Loutas and V. Kostopoulos, "Health monitoring of carbon/carbon, woven reinforced composites: Damage assessment by using advanced signal processing techniques. Part II: Acousto-ultrasonics monitoring of damage development," *Composites Science and Technology*, vol. 69, pp. 273-283, Feb 2009.
- [288] R. de Oliveira and A. T. Marques, "Health monitoring of FRP using acoustic emission and artificial neural networks," *Computers & Structures*, vol. 86, pp. 367-373, Feb 2008.
- [289] C. E. S. C. Ajay Raghavan, "Review of Guided-wave Structural Health Monitoring," *The Shock and Vibration Digest*, vol. 39, pp. 92-114, 2007.

- [290] C. Ramadas, J. Padiyar, K. Balasubramaniam, M. Joshi, and C. V. Krishnamurthy, "Lamb wave based ultrasonic imaging of interface delamination in a composite T-joint," *Ndt & E International*, vol. 44, pp. 523-530, Oct 2011.
- [291] V. Giurgiutiu, A. Zagrai, and J. J. Bao, "Damage identification in aging aircraft structures with piezoelectric wafer active sensors," *Journal of Intelligent Material Systems and Structures*, vol. 15, pp. 673-687, Sep-Oct 2004.
- [292] M. Castaings and B. Hosten, "Lamb and SH waves generated and detected by air-coupled ultrasonic transducers in composite material plates," *Ndt & E International*, vol. 34, pp. 249-258, Jun 2001.
- [293] A. Raghavan and C. E. Cesnik, "Review of guided-wave structural health monitoring," *Shock and Vibration Digest*, vol. 39, pp. 91-116, 2007.
- [294] Y. H. Kim, D. H. Kim, J. H. Han, and C. G. Kim, "Damage assessment in layered composites using spectral analysis and Lamb wave," *Composites Part B-Engineering*, vol. 38, pp. 800-809, 2007.
- [295] M. Castaings and B. Hosten, "Ultrasonic guided waves for health monitoring of high-pressure composite tanks," *Ndt & E International*, vol. 41, pp. 648-655, Dec 2008.
- [296] S. Yuan, L. Wang, and G. Peng, "Neural network method based on a new damage signature for structural health monitoring," *Thin-Walled Structures*, vol. 43, pp. 553-563, 2005.
- [297] B. R. Loyola, V. La Saponara, K. J. Loh, T. M. Briggs, G. O'Bryan, and J. L. Skinner, "Spatial Sensing Using Electrical Impedance Tomography," *Ieee Sensors Journal*, vol. 13, pp. 2357-2367, Jun 2013.
- [298] R. de Oliveira, C. A. Ramos, and A. T. Marques, "Health monitoring of composite structures by embedded FBG and interferometric Fabry-Perot sensors," *Computers & Structures*, vol. 86, pp. 340-346, Feb 2008.
- [299] M. Majumder, T. K. Gangopadhyay, A. K. Chakraborty, K. Dasgupta, and D. K. Bhattacharya, "Fibre Bragg gratings in structural health monitoring - Present status and applications," *Sensors and Actuators a-Physical*, vol. 147, pp. 150-164, Sep 15 2008.
- [300] J. C. Hao, A. S. Leng, and Z. Wei, "Non-destructive evaluation of composite pressure vessel by using FBG sensors," *Chinese Journal of Aeronautics*, vol. 20, pp. 120-123, Apr 2007.
- [301] C. A. Ramos, R. de Oliveira, and A. T. Marques, "Design of an optical fibre sensor patch for longitudinal strain measurement in structures," *Materials & Design*, vol. 30, pp. 2323-2331, Aug 2009.
- [302] G. Kister, R. A. Badcock, Y. M. Gebremichael, W. J. O. Boyle, K. T. V. Grattan, G. F. Fernando, *et al.*, "Monitoring of an all-composite bridge using Bragg grating sensors," *Construction and Building Materials*, vol. 21, pp. 1599-1604, Jul 2007.
- [303] K. Schulte and C. Baron, "Load and Failure Analyses of Cfrp Laminates by Means of Electrical-Resistivity Measurements," *Composites Science and Technology*, vol. 36, pp. 63-76, 1989.
- [304] C. Y. Li and T. W. Chou, "Modeling of damage sensing in fiber composites using carbon nanotube networks," *Composites Science and Technology*, vol. 68, pp. 3373-3379, Dec 2008.
- [305] M. Kupke, K. Schulte, and R. Schuler, "Non-destructive testing of FRP by d.c. and a.c. electrical methods," *Composites Science and Technology*, vol. 61, pp. 837-847, 2001.
- [306] B. R. Loyola, "Distributed In Situ Health Monitoring of Conductive Self-Sensing Fiber-Reinforced Polymers Using Electrical Impedance Tomography," DOCTOR OF PHILOSOPHY, UNIVERSITY OF CALIFORNIA DAVIS Davis, CA, USA, 2012.
- [307] E. T. Thostenson and T. W. Chou, "Carbon nanotube networks: Sensing of distributed strain and damage for life prediction and self healing," *Advanced Materials*, vol. 18, pp. 2837-+, Nov 3 2006.
- [308] E. T. Thostenson and T. W. Chou, "Carbon nanotube-based health monitoring of mechanically fastened composite joints," *Composites Science and Technology*, vol. 68, pp. 2557-2561, Sep 2008.
- [309] W. Zhang, V. Sakalkar, and N. Koratkar, "In situ health monitoring and repair in composites using carbon nanotube additives," *Applied Physics Letters*, vol. 91, Sep 24 2007.

- [310] M. Nofar, S. V. Hoa, and M. D. Pugh, "Failure detection and monitoring in polymer matrix composites subjected to static and dynamic loads using carbon nanotube networks," *Composites Science and Technology*, vol. 69, pp. 1599-1606, Aug 2009.
- [311] D. S. Holder, *Electrical Impedance Tomography: Methods, History and Applications*: IOP Publishing 2005.
- [312] K. J.-H. Loh, "Development of Multifunctional Carbon Nanotube Nanocomposite Sensors for Structural Health Monitoring," PhD, University of Michigan, Ann Arbor, MI, USA, 2008.
- [313] K. Paulson, W. Breckon, and M. Pidcock, "Electrode Modeling in Electrical-Impedance Tomography," *Siam Journal on Applied Mathematics*, vol. 52, pp. 1012-1022, Aug 1992.
- [314] J. Riera, P. J. Riu, P. Casan, and J. R. Masclans, "Electrical impedance tomography in acute lung injury," *Medicina Intensiva*, vol. 35, pp. 509-517, Nov 2011.
- [315] O. Gilad, A. Ghosh, D. I. Oh, and D. S. Holder, "A method for recording resistance changes non-invasively during neuronal depolarization with a view to imaging brain activity with electrical impedance tomography," *Journal of Neuroscience Methods*, vol. 180, pp. 87-96, May 30 2009.
- [316] C. S. Chaw, E. Yazaki, and D. F. Evans, "The effect of pH change on the gastric emptying of liquids measured by electrical impedance tomography and pH-sensitive radiotelemetry capsule," *International Journal of Pharmaceutics*, vol. 227, pp. 167-175, Oct 4 2001.
- [317] N. Kerrouche, C. McLeod, and W. Lionheart, "Time series of EIT chest images using singular value decomposition and Fourier transform," *Physiological Measurement*, vol. 22, p. 147, 2001.
- [318] R. Lazarovitch, D. Rittel, and I. Bucher, "Experimental crack identification using electrical impedance tomography," *Ndt & E International*, vol. 35, pp. 301-316, Jul 2002.
- [319] K. Bryan and M. Vogelius, "A Computational Algorithm to Determine Crack Locations from Electrostatic Boundary Measurements - the Case of Multiple Cracks," *International Journal of Engineering Science*, vol. 32, pp. 579-603, Apr 1994.
- [320] P. G. Kaup, F. Santosa, and M. Vogelius, "Method for imaging corrosion damage in thin plates from electrostatic data," *Inverse Problems*, vol. 12, pp. 279-293, Jun 1996.
- [321] T. C. Hou, K. J. Loh, and J. P. Lynch, "Spatial conductivity mapping of carbon nanotube composite thin films by electrical impedance tomography for sensing applications," *Nanotechnology*, vol. 18, Aug 8 2007.
- [322] A. Seppanen, K. Karhunen, A. Lehtikainen, J. P. Kaipio, and P. J. M. Monteiro, "Electrical resistance tomography imaging of concrete," *Concrete Repair, Rehabilitation and Retrofitting II*, pp. 231-232, 2009.
- [323] K. Karhunen, A. Seppanen, A. Lehtikainen, P. J. M. Monteiro, and J. P. Kaipio, "Electrical Resistance Tomography imaging of concrete," *Cement and Concrete Research*, vol. 40, pp. 137-145, Jan 2010.
- [324] T. C. Hou and J. P. Lynch, "Electrical Impedance Tomographic Methods for Sensing Strain Fields and Crack Damage in Cementitious Structures," *Journal of Intelligent Material Systems and Structures*, vol. 20, pp. 1363-1379, Jul 2009.
- [325] X. Y. Zhang, Z. Q. Li, and S. R. Zhu, "A Novel Electrical Resistance Tomography System of Carbon Fiber Smart Layer for Structural Health Monitoring," *2009 Ieee International Conference on Intelligent Computing and Intelligent Systems, Proceedings, Vol 4*, pp. 132-135, 2009.
- [326] Y. M. Deng and X. Liu, "Electromagnetic Imaging Methods for Nondestructive Evaluation Applications," *Sensors*, vol. 11, pp. 11774-11808, Dec 2011.

CHAPTER 8

CONCLUSIONS AND RECOMMENDATIONS

8.1 Findings and Contributions

A comprehensive numerical modeling scheme was developed throughout the course of this thesis project to explore the conductivity characteristics of conductive filler modified insulating polymers. The thorough literature review in CHAPTER 2 on conductivity properties of carbon allotropes modified polymers showed that research conducted on conductive nanocomposites is limited with regards to evaluating electrical properties of polymers rendered conductive through the dispersion of single layer circular nanodisks. Moreover, some reported findings on the conductivity behavior of nanocomposites are inconsistent, for example, with respect to the critical volume fraction and the critical exponent describing post-percolation behavior. Hence, the current in-depth investigation using numerical methods is warranted and makes valuable contributions for a better fundamental understanding of conductivity mechanisms in conductive nanocomposites.

CHAPTER 3 was devoted to developing a three-dimensional continuum Monte Carlo model to evaluate the percolation behavior of a system of monodisperse and polydisperse circular nanoplatelets. The effect of governing parameters such as particle size and tunneling resistivity on the percolation threshold was investigated and an equation was proposed to correlate the percolation threshold and dimensionless variables obtained through dimensional analysis.

In CHAPTER 4 the electrical conductivity and piezoresistivity behavior of nanocomposites were examined. Based on the Monte Carlo modeling approach a finite element based three-dimensional resistor network was developed and employed to explore the electrical conductivity of nanoplatelet based nanocomposites. Parameters that

play a dominant role in the conductivity behavior of nanocomposites, including the electrical potential barrier height of the polymer, filler loading and filler size were explored. The results indicated good agreement between the critical exponent for post-percolation behavior obtained in this study and the value predicted in conjunction with three-dimensional percolation problems. It was further ascertained that the investigated nanoplatelet based composites exhibit promising piezoresistive behavior for potential strain sensing application.

In CHAPTER 5 the current-voltage behavior of conductive nanoplatelet based nanocomposites was investigated. The simulations predicted the resistivity of nanoplatelet based nanocomposites to be strongly affected by the applied electric field. Further, nanocomposite resistivity was ascertained to decrease with increasing voltage, while the degree of nonlinear behavior was found to decline with rising filler content.

CHAPTER 6 was devoted to the effect of the temperature on the electrical conductivity of polymer nanocomposites with carbon nanotube and graphene nanoplatelet fillers. Using again a modeling approach with a three-dimensional resistor network, simulations were conducted that indicated a significant temperature effect of nanocomposites. This dependence of electrical resistivity on temperature for nanocomposites with favorable material composition motivates future research to explore the feasibility of using carbon nanotube and graphene nanoplatelet nanocomposites for temperature sensing applications. The results show that Mott's variable range hopping (VRH) model is an effective tool for describing the conductivity-temperature behavior of graphene nanoplatelet nanocomposites, whereas the VRH proposed model is less suitable for delineating the conductivity-temperature behavior of carbon nanotube nanocomposites.

The study described in CHAPTER 7 was conducted to evaluate the feasibility of employing conductive nanocomposites for structural health (SHM) monitoring applications. A SHM paradigm was developed based on electrical impedance tomography to detect damage such as cracking and material loss (e.g. due to wear or corrosive attack) in polymer based piping systems (e.g. polymer liners) that are modified with graphene nanoplatelets. The proposed electrical impedance tomography technique

yielded high sensitivity to defects which indicates its feasibility and makes it a promising method for structural health monitoring applications.

8.2 Future Research Work

The modeling work conducted in the research project yielded valuable contributions to the field of nanocomposite materials. At the same time the work identifies opportunities for future studies. Suggested areas of future work are as follows.

- Experimental studies

As described in the literature review, a large number of experimental studies has been conducted on the conductivity behavior of nanocomposites. Experimental examinations have mostly focused on the percolation threshold, electrical conductivity and critical power-law description exponent, but these studies are largely moot regarding the characteristics and associated effects of the filler inside the host matrix, such as particle size and morphology, size distribution and particle agglomerations. Scanning and tunneling electron microscopy has been employed for qualitative comparisons. However, in order to find agreement between numerical and experimental studies a comprehensive characterization and statistical study needs to be undertaken to define suitable and equivalent filler entities that can be implemented in numerical simulation.

- Hybrid conductive nanocomposites

In this thesis research a numerical approach was undertaken to model the percolation conductivity of carbon nanotube and graphene nanoplatelet based nanocomposites. Developing the current numerical modeling to evaluate the conductivity behavior of hybrid nanocomposites consisting of two different conductive filler constituents is recommended as an interesting extension to the present work. Exploring the effect of governing parameters such as volume fraction of constituents on the conductivity and piezoresistivity of nanocomposite is seen as an attractive topic for future studies.

BIBLIOGRAPHY

- [1] J. S. Hwang, "Carbon black filled electrospun fiberweb: Electrical and mechanical properties," PhD, North Carolina State University Raleigh, NC, 2006.
- [2] J. H. Lee and S. J. Lee, "Application of laser-generated guided wave for evaluation of corrosion in carbon steel pipe," *Ndt & E International*, vol. 42, pp. 222-227, Apr 2009.
- [3] L. M. Gao, E. T. Thostenson, Z. G. Zhang, and T. W. Chou, "Coupled carbon nanotube network and acoustic emission monitoring for sensing of damage development in composites," *Carbon*, vol. 47, pp. 1381-1388, Apr 2009.
- [4] S. G. Miller, J. L. Bauer, M. J. Maryanski, P. J. Heimann, J. P. Barlow, J. M. Gosau, *et al.*, "Characterization of epoxy functionalized graphite nanoparticles and the physical properties of epoxy matrix nanocomposites," *Composites Science and Technology*, vol. 70, pp. 1120-1125, Jul 2010.
- [5] W. Thongruang, R. J. Spontak, and C. M. Balik, "Correlated electrical conductivity and mechanical property analysis of high-density polyethylene filled with graphite and carbon fiber," *Polymer*, vol. 43, pp. 2279-2286, Apr 2002.
- [6] H. Koerner, W. D. Liu, M. Alexander, P. Mirau, H. Dowty, and R. A. Vaia, "Deformation-morphology correlations in electrically conductive carbon nanotube thermoplastic polyurethane nanocomposites," *Polymer*, vol. 46, pp. 4405-4420, May 26 2005.
- [7] M. H. Al-Saleh and U. Sundararaj, "Electromagnetic interference (EMI) shielding effectiveness of PP/PS polymer blends containing high structure carbon black (vol 298, pg 621, 2008)," *Macromolecular Materials and Engineering*, vol. 293, pp. 789-789, Sep 12 2008.
- [8] P. Saini, V. Choudhary, B. P. Singh, R. B. Mathur, and S. K. Dhawan, "Polyaniline-MWCNT nanocomposites for microwave absorption and EMI shielding," *Materials Chemistry and Physics*, vol. 113, pp. 919-926, Feb 15 2009.
- [9] X. S. Yi, G. Z. Wu, and Y. Pan, "Properties and applications of filled conductive polymer composites," *Polymer International*, vol. 44, pp. 117-124, Oct 1997.
- [10] N. D. Alexopoulos, C. Bartholome, P. Poulin, and Z. Marioli-Riga, "Structural health monitoring of glass fiber reinforced composites using embedded carbon nanotube (CNT) fibers," *Composites Science and Technology*, vol. 70, pp. 260-271, Feb 2010.
- [11] L. Boeger, M. H. G. Wichmann, L. O. Meyer, and K. Schulte, "Load and health monitoring in glass fibre reinforced composites with an electrically conductive nanocomposite epoxy matrix," *Composites Science and Technology*, vol. 68, pp. 1886-1894, Jun 2008.
- [12] V. Eswaraiah, K. Balasubramaniam, and S. Ramaprabhu, "Functionalized graphene reinforced thermoplastic nanocomposites as strain sensors in structural health monitoring," *Journal of Materials Chemistry*, vol. 21, pp. 12626-12628, 2011.
- [13] K. R. Paton, E. Varrla, C. Backes, R. J. Smith, U. Khan, A. O'Neill, *et al.*, "Scalable production of large quantities of defect-free few-layer graphene by shear exfoliation in liquids," *Nature materials*, vol. 13, pp. 624-630, 2014.
- [14] L. L. Wu, X. Lv, and C. C. Zhang, "Effect of modified graphene addition on the electrical properties of epoxy resin composite," *Advanced Materials, Pts 1-4*, vol. 239-242, pp. 55-58, 2011.
- [15] M. Al-Saleh, "Nanostructured Conductive Polymeric Materials," PhD, Chemical and Materials Engineering, University of Alberta, Edmonton, Alberta, Canada, 2009.
- [16] W. Henry and E. George, "Electrically conducting cements containing epoxy resins and silver," ed: Google Patents, 1956.
- [17] J. P. Franey, T. E. Graedel, G. J. Gualtieri, G. W. Kammlot, J. Kelber, D. L. Malm, *et al.*, "The morphology and corrosion resistance of a conductive silver-epoxy paste," *Journal of Materials Science*, vol. 16, pp. 2360-2368, 1981/09/01 1981.
- [18] H. Jiang, K.-s. Moon, Y. Li, and C. Wong, "Surface functionalized silver nanoparticles for ultrahigh conductive polymer composites," *Chemistry of Materials*, vol. 18, pp. 2969-2973, 2006.
- [19] A. J. Lovinger, "Development of electrical conduction in silver-filled epoxy adhesives," 1979.
- [20] D. W. Marshall and J. C. Agarwal, "Copper filled conductive epoxy," ed: Google Patents, 1976.

- [21] B. Lin, G. A. Gelves, J. A. Haber, and U. Sundararaj, "Electrical, rheological, and mechanical properties of polystyrene/copper nanowire nanocomposites," *Industrial & engineering chemistry research*, vol. 46, pp. 2481-2487, 2007.
- [22] M. H. Al-Saleh, G. A. Gelves, and U. Sundararaj, "Copper nanowire/polystyrene nanocomposites: lower percolation threshold and higher EMI shielding," *Composites Part A: Applied Science and Manufacturing*, vol. 42, pp. 92-97, 2011.
- [23] M. Arjmand, M. Mahmoodi, G. A. Gelves, S. Park, and U. Sundararaj, "Electrical and electromagnetic interference shielding properties of flow-induced oriented carbon nanotubes in polycarbonate," *Carbon*, vol. 49, pp. 3430-3440, 2011.
- [24] S. Iijima, "Helical Microtubules of Graphitic Carbon," *Nature*, vol. 354, pp. 56-58, Nov 7 1991.
- [25] O. Lourie and H. D. Wagner, "Evaluation of Young's modulus of carbon nanotubes by micro-Raman spectroscopy," *Journal of Materials Research*, vol. 13, pp. 2418-2422, Sep 1998.
- [26] M. B. Nardelli, B. I. Yakobson, and J. Bernholc, "Brittle and ductile behavior in carbon nanotubes," *Physical Review Letters*, vol. 81, pp. 4656-4659, Nov 23 1998.
- [27] D. A. Walters, L. M. Ericson, M. J. Casavant, J. Liu, D. T. Colbert, K. A. Smith, *et al.*, "Elastic strain of freely suspended single-wall carbon nanotube ropes," *Applied Physics Letters*, vol. 74, pp. 3803-3805, Jun 21 1999.
- [28] G. J. W. D. Qian, W.K. Liu, M.F. Yu, R. S. Ruoff, G. J. Wagner, W. K. Liu, "Mechanics of carbon nanotubes," *Appl. Mech. Rev.*, vol. 55, pp. 495-533, 2005
- [29] P. C. Ma, N. A. Siddiqui, G. Marom, and J. K. Kim, "Dispersion and functionalization of carbon nanotubes for polymer-based nanocomposites: A review," *Composites Part a-Applied Science and Manufacturing*, vol. 41, pp. 1345-1367, Oct 2010.
- [30] M. Scarselli, P. Castrucci, and M. De Crescenzi, "Electronic and optoelectronic nano-devices based on carbon nanotubes," *Journal of Physics: Condensed Matter*, vol. 24, p. 313202, 2012.
- [31] J. Prasek, J. Drbohlavova, J. Chomoucka, J. Hubalek, O. Jasek, V. Adam, *et al.*, "Methods for carbon nanotubes synthesis-review," *Journal of Materials Chemistry*, vol. 21, pp. 15872-15884, 2011.
- [32] J. Liu, S. S. Fan, and H. J. Dai, "Recent advances in methods of forming carbon nanotubes," *Mrs Bulletin*, vol. 29, pp. 244-250, Apr 2004.
- [33] X. L. Zhao, M. Wang, M. Ohkohchi, and Y. Ando, "Morphology of carbon nanotubes prepared by carbon arc," *Japanese Journal of Applied Physics Part 1-Regular Papers Short Notes & Review Papers*, vol. 35, pp. 4451-4456, Aug 1996.
- [34] X. Zhao, M. Ohkohchi, M. Wang, S. Iijima, T. Ichihashi, and Y. Ando, "Preparation of high-grade carbon nanotubes by hydrogen arc discharge," *Carbon*, vol. 35, pp. 775-781, 1997.
- [35] N. Parkansky, R. L. Boxman, B. Alterkop, I. Zontag, Y. Lereah, and Z. Barkay, "Single-pulse arc production of carbon nanotubes in ambient air," *Journal of Physics D-Applied Physics*, vol. 37, pp. 2715-2719, Oct 7 2004.
- [36] Y. Y. Tsai, J. S. Su, C. Y. Su, and W. H. He, "Production of carbon nanotubes by single-pulse discharge in air," *Journal of Materials Processing Technology*, vol. 209, pp. 4413-4416, May 1 2009.
- [37] Y. Saito, M. Okuda, and T. Koyama, "Carbon nanocapsules and single-wall nanotubes formed by arc evaporation," *Surface Review and Letters*, vol. 3, pp. 863-867, Feb 1996.
- [38] H. W. Kroto, J. R. Heath, S. C. O'Brien, R. F. Curl, and R. E. Smalley, "C-60 - Buckminsterfullerene," *Nature*, vol. 318, pp. 162-163, 1985.
- [39] T. Guo, P. Nikolaev, A. G. Rinzler, D. Tomanek, D. T. Colbert, and R. E. Smalley, "Self-Assembly of Tubular Fullerenes," *Journal of Physical Chemistry*, vol. 99, pp. 10694-10697, Jul 6 1995.
- [40] M. Kusaba and Y. Tsunawaki, "Production of single-wall carbon nanotubes by a XeCl excimer laser ablation," *Thin Solid Films*, vol. 506, pp. 255-258, May 26 2006.
- [41] M. Joseyacaman, M. Mikiyoshida, L. Rendon, and J. G. Santiesteban, "Catalytic Growth of Carbon Microtubules with Fullerene Structure," *Applied Physics Letters*, vol. 62, pp. 202-204, Jan 11 1993.
- [42] O. Lee, J. Jung, S. Doo, S. S. Kim, T. H. Noh, K. I. Kim, *et al.*, "Effects of temperature and catalysts on the synthesis of carbon nanotubes by chemical vapor deposition," *Metals and Materials International*, vol. 16, pp. 663-667, Aug 2010.

- [43] N. Inami, M. A. Mohamed, E. Shikoh, and A. Fujiwara, "Synthesis-condition dependence of carbon nanotube growth by alcohol catalytic chemical vapor deposition method," *Science and Technology of Advanced Materials*, vol. 8, pp. 292-295, May 2007.
- [44] H. M. Ma and X. L. Gao, "A three-dimensional Monte Carlo model for electrically conductive polymer matrix composites filled with curved fibers," *Polymer*, vol. 49, pp. 4230-4238, Sep 9 2008.
- [45] W. S. Bao, S. A. Meguid, Z. H. Zhu, and M. J. Meguid, "Modeling electrical conductivities of nanocomposites with aligned carbon nanotubes," *Nanotechnology*, vol. 22, Dec 2 2011.
- [46] N. Hu, Y. Karube, C. Yan, Z. Masuda, and H. Fukunaga, "Tunneling effect in a polymer/carbon nanotube nanocomposite strain sensor," *Acta Materialia*, vol. 56, pp. 2929-2936, Aug 2008.
- [47] L. Berhan and A. M. Sastry, "Modeling percolation in high-aspect-ratio fiber systems. II. The effect of waviness on the percolation onset," *Physical Review E*, vol. 75, Apr 2007.
- [48] N. Hu, Y. Karube, M. Arai, T. Watanabe, C. Yan, Y. Li, *et al.*, "Investigation on sensitivity of a polymer/carbon nanotube composite strain sensor," *Carbon*, vol. 48, pp. 680-687, Mar 2010.
- [49] A. Oskouyi, U. Sundararaj, and P. Mertiny, "A numerical model to study the effect of temperature on electrical conductivity of polymer-CNT nanocomposite," in *ASME International Mechanical Engineering Congress & Exposition, IMECE2013*, 2013.
- [50] M. S. Han, Y. K. Lee, C. H. Yun, H. S. Lee, C. J. Lee, and W. N. Kim, "Bent-shape effects of multi-walled carbon nanotube on the electrical conductivity and rheological properties of polycarbonate/multi-walled carbon nanotube nanocomposites," *Synthetic Metals*, vol. 161, pp. 1629-1634, Aug 2011.
- [51] L. X. He and S. C. Tjong, "Carbon nanotube/epoxy resin composite: Correlation between state of nanotube dispersion and Zener tunneling parameters," *Synthetic Metals*, vol. 162, pp. 2277-2281, Dec 31 2012.
- [52] R. Bhatia, V. Prasad, and R. Menon, "Characterization, electrical percolation and magnetization studies of polystyrene/multiwall carbon nanotube composite films," *Materials Science and Engineering B-Advanced Functional Solid-State Materials*, vol. 175, pp. 189-194, Dec 15 2010.
- [53] O. Osazuwa, K. Petrie, M. Kontopoulou, P. Xiang, Z. B. Ye, and A. Docoslis, "Characterization of non-covalently, non-specifically functionalized multi-wall carbon nanotubes and their melt compounded composites with an ethylene-octene copolymer," *Composites Science and Technology*, vol. 73, pp. 27-33, Nov 23 2012.
- [54] B. Krause, M. Ritschel, C. Taschner, S. Oswald, W. Gruner, A. Leonhardt, *et al.*, "Comparison of nanotubes produced by fixed bed and aerosol-CVD methods and their electrical percolation behaviour in melt mixed polyamide 6.6 composites," *Composites Science and Technology*, vol. 70, pp. 151-160, Jan 2010.
- [55] Z. M. Dang, K. Shehzad, J. W. Zha, A. Mujahid, T. Hussain, J. Nie, *et al.*, "Complementary percolation characteristics of carbon fillers based electrically percolative thermoplastic elastomer composites," *Composites Science and Technology*, vol. 72, pp. 28-35, Dec 6 2011.
- [56] J. K. W. Sandler, J. E. Kirk, I. A. Kinloch, M. S. P. Shaffer, and A. H. Windle, "Ultra-low electrical percolation threshold in carbon-nanotube-epoxy composites," *Polymer*, vol. 44, pp. 5893-5899, Sep 2003.
- [57] J. Z. Kovacs, B. S. Velagala, K. Schulte, and W. Bauhofer, "Two percolation thresholds in carbon nanotube epoxy composites," *Composites Science and Technology*, vol. 67, pp. 922-928, Apr 2007.
- [58] E. Logakis, E. Pollatos, C. Pandis, V. Peoglos, I. Zuburtikudis, C. G. Delides, *et al.*, "Structure-property relationships in isotactic polypropylene/multi-walled carbon nanotubes nanocomposites," *Composites Science and Technology*, vol. 70, pp. 328-335, Feb 2010.
- [59] A. W. Musumeci, G. G. Silva, J. W. Liu, W. N. Martens, and E. R. Waclawik, "Structure and conductivity of multi-walled carbon nanotube/poly(3-hexylthiophene) composite films," *Polymer*, vol. 48, pp. 1667-1678, Mar 8 2007.
- [60] I. A. E. Kymakis, G.A.J. Amaratunga, "Single-walled carbon nanotube-polymer composites: electrical, optical and structural investigation," *Synth. Met.*, vol. 127, pp. 59-62, 2002.
- [61] E. T. Thostenson, S. Ziaee, and T. W. Chou, "Processing and electrical properties of carbon nanotube/vinyl ester nanocomposites," *Composites Science and Technology*, vol. 69, pp. 801-804, May 2009.
- [62] J. H. Yang, T. Xu, A. Lu, Q. Zhang, H. Tan, and Q. Fu, "Preparation and properties of poly (p-phenylene sulfide)/multiwall carbon nanotube composites obtained by melt compounding," *Composites Science and Technology*, vol. 69, pp. 147-153, Feb 2009.

- [63] A. Battisti, A. A. Skordos, and I. K. Partridge, "Percolation threshold of carbon nanotubes filled unsaturated polyesters," *Composites Science and Technology*, vol. 70, pp. 633-637, Apr 2010.
- [64] Y. Z. Pan and L. Li, "Percolation and gel-like behavior of multiwalled carbon nanotube/polypropylene composites influenced by nanotube aspect ratio," *Polymer*, vol. 54, pp. 1218-1226, Feb 5 2013.
- [65] Z. F. Li, G. H. Luo, F. Wei, and Y. Huang, "Microstructure of carbon nanotubes/PET conductive composites fibers and their properties," *Composites Science and Technology*, vol. 66, pp. 1022-1029, Jun 2006.
- [66] G. D. Liang, S. P. Bao, and S. C. Tjong, "Microstructure and properties of polypropylene composites filled with silver and carbon nanotube nanoparticles prepared by melt-compounding," *Materials Science and Engineering B-Solid State Materials for Advanced Technology*, vol. 142, pp. 55-61, Sep 25 2007.
- [67] O. Meincke, D. Kaempfer, H. Weickmann, C. Friedrich, M. Vathauer, and H. Warth, "Mechanical properties and electrical conductivity of carbon-nanotube filled polyamide-6 and its blends with acrylonitrile/butadiene/styrene," *Polymer*, vol. 45, pp. 739-748, Feb 1 2004.
- [68] G. J. Hu, C. G. Zhao, S. M. Zhang, M. S. Yang, and Z. G. Wang, "Low percolation thresholds of electrical conductivity and rheology in poly(ethylene terephthalate) through the networks of multi-walled carbon nanotubes," *Polymer*, vol. 47, pp. 480-488, Jan 2006.
- [69] H. E. Miltner, N. Grossiord, K. B. Lu, J. Loos, C. E. Koning, and B. Van Mele, "Isotactic polypropylene/carbon nanotube composites prepared by latex technology. Thermal analysis of carbon nanotube-induced nucleation," *Macromolecules*, vol. 41, pp. 5753-5762, Aug 12 2008.
- [70] M. Felisberto, A. Arias-Duran, J. A. Ramos, I. Mondragon, R. Candal, S. Goyanes, *et al.*, "Influence of filler alignment in the mechanical and electrical properties of carbon nanotubes/epoxy nanocomposites," *Physica B-Condensed Matter*, vol. 407, pp. 3181-3183, Aug 15 2012.
- [71] S. Chakraborty, J. Pionteck, B. Krause, S. Banerjee, and B. Voit, "Influence of different carbon nanotubes on the electrical and mechanical properties of melt mixed poly(ether sulfone)-multi walled carbon nanotube composites," *Composites Science and Technology*, vol. 72, pp. 1933-1940, 10/12/ 2012.
- [72] M. S. de Luna, L. Pellegrino, M. Daghetta, C. V. Mazzocchia, D. Acierno, and G. Filippone, "Importance of the morphology and structure of the primary aggregates for the dispersibility of carbon nanotubes in polymer melts," *Composites Science and Technology*, vol. 85, pp. 17-22, Aug 21 2013.
- [73] K. Tsuchiya, A. Sakai, T. Nagaoka, K. Uchida, T. Furukawa, and H. Yajima, "High electrical performance of carbon nanotubes/rubber composites with low percolation threshold prepared with a rotation-revolution mixing technique," *Composites Science and Technology*, vol. 71, pp. 1098-1104, May 31 2011.
- [74] K. Wongtimnoi, B. Guiffard, A. Bogner-Van de Moortele, L. Seveyrat, and J. Y. Cavaille, "Electrostrictive thermoplastic polyurethane-based nanocomposites filled with carboxyl-functionalized multi-walled carbon nanotubes (MWCNT-COOH): Properties and improvement of electromechanical activity," *Composites Science and Technology*, vol. 85, pp. 23-28, Aug 21 2013.
- [75] Z. Ounaies, C. Park, K. E. Wise, E. J. Siochi, and J. S. Harrison, "Electrical properties of single wall carbon nanotube reinforced polyimide composites," *Composites Science and Technology*, vol. 63, pp. 1637-1646, Aug 2003.
- [76] Q. M. Liu, J. C. Tu, X. Wang, W. X. Yu, W. T. Zheng, and Z. D. Zhao, "Electrical conductivity of carbon nanotube/poly(vinylidene fluoride) composites prepared by high-speed mechanical mixing," *Carbon*, vol. 50, pp. 339-341, Jan 2012.
- [77] S. C. Tjong, G. D. Liang, and S. P. Bao, "Electrical behavior of polypropylene/multiwalled carbon nanotube nanocomposites with low percolation threshold," *Scripta Materialia*, vol. 57, pp. 461-464, Sep 2007.
- [78] Y. P. Mamunya, V. V. Levchenko, A. Rybak, G. Boiteux, E. V. Lebedev, J. Ulanski, *et al.*, "Electrical and thermomechanical properties of segregated nanocomposites based on PVC and multiwalled carbon nanotubes," *Journal of Non-Crystalline Solids*, vol. 356, pp. 635-641, Apr 1 2010.
- [79] C. C. Chu, K. L. White, P. Liu, X. Zhang, and H. J. Sue, "Electrical conductivity and thermal stability of polypropylene containing well-dispersed multi-walled carbon nanotubes disentangled with exfoliated nanoplatelets," *Carbon*, vol. 50, pp. 4711-4721, Oct 2012.
- [80] H. Aarab, M. Baitoul, J. Wery, R. Almairac, S. Lefrant, E. Faulques, *et al.*, "Electrical and optical properties of PPV and single-walled carbon nanotubes composite films," *Synthetic Metals*, vol. 155, pp. 63-67, Oct 15 2005.

- [81] S. Kara, E. Arda, F. Dolastir, and O. Pekcan, "Electrical and optical percolations of polystyrene latex-multiwalled carbon nanotube composites," *Journal of Colloid and Interface Science*, vol. 344, pp. 395-401, Apr 15 2010.
- [82] X. W. Jiang, Y. Z. Bin, and M. Matsuo, "Electrical and mechanical properties of polyimide-carbon nanotubes composites fabricated by in situ polymerization," *Polymer*, vol. 46, pp. 7418-7424, Aug 23 2005.
- [83] O. Chauvet, J. M. Benoit, and B. Corraze, "Electrical, magneto-transport and localization of charge carriers in nanocomposites based on carbon nanotubes," *Carbon*, vol. 42, pp. 949-952, 2004.
- [84] S. U. Khan, J. R. Pothnis, and J.-K. Kim, "Effects of carbon nanotube alignment on electrical and mechanical properties of epoxy nanocomposites," *Composites Part A: Applied Science and Manufacturing*, vol. 49, pp. 26-34, 6// 2013.
- [85] A. Moisala, Q. Li, I. A. Kinloch, and A. H. Windle, "Thermal and electrical conductivity of single- and multi-walled carbon nanotube-epoxy composites," *Composites Science and Technology*, vol. 66, pp. 1285-1288, Aug 2006.
- [86] S. Barrau, P. Demont, A. Peigney, C. Laurent, and C. Lacabanne, "DC and AC conductivity of carbon nanotubes-polyepoxy composites," *Macromolecules*, vol. 36, pp. 5187-5194, Jul 15 2003.
- [87] O. Regev, P. N. B. ElKati, J. Loos, and C. E. Koning, "Preparation of conductive nanotube-polymer composites using latex technology," *Advanced Materials*, vol. 16, pp. 248+, Feb 3 2004.
- [88] O. Gryshchuk, J. Karger-Kocsis, R. Thomann, Z. Konya, and I. Kiricsi, "Multiwall carbon nanotube modified vinylester and vinylester - based hybrid resins," *Composites Part a-Applied Science and Manufacturing*, vol. 37, pp. 1252-1259, 2006.
- [89] Q. Lin, L. Qu, B. Luo, C. Fang, and K. Luo, "Preparation and properties of multiwall carbon nanotubes/carbon foam composites," *Journal of Analytical and Applied Pyrolysis*, vol. 105, pp. 177-182, 1// 2014.
- [90] C. Y. Li, E. T. Thostenson, and T. W. Chou, "Dominant role of tunneling resistance in the electrical conductivity of carbon nanotube-based composites," *Applied Physics Letters*, vol. 91, Nov 26 2007.
- [91] Y. Yu, G. Song, and L. Sun, "Determinant role of tunneling resistance in electrical conductivity of polymer composites reinforced by well dispersed carbon nanotubes," *Journal of Applied Physics*, vol. 108, Oct 15 2010.
- [92] C. Li, E. T. Thostenson, and T. W. Chou, "Effect of nanotube waviness on the electrical conductivity of carbon nanotube-based composites," *Composites Science and Technology*, vol. 68, pp. 1445-1452, May 2008.
- [93] F. Dalmas, R. Dendievel, L. Chazeau, J.-Y. Cavallé, and C. Gauthier, "Carbon nanotube-filled polymer composites. Numerical simulation of electrical conductivity in three-dimensional entangled fibrous networks," *Acta Materialia*, vol. 54, pp. 2923-2931, 6// 2006.
- [94] B. E. Kilbride, J. N. Coleman, J. Fraysse, P. Fournet, M. Cadek, A. Drury, *et al.*, "Experimental observation of scaling laws for alternating current and direct current conductivity in polymer-carbon nanotube composite thin films," *Journal of Applied Physics*, vol. 92, pp. 4024-4030, Oct 1 2002.
- [95] M. Foygel, R. D. Morris, D. Anez, S. French, and V. L. Sobolev, "Theoretical and computational studies of carbon nanotube composites and suspensions: Electrical and thermal conductivity," *Physical Review B*, vol. 71, Mar 2005.
- [96] M. J. Allen, V. C. Tung, and R. B. Kaner, "Honeycomb Carbon: A Review of Graphene," *Chemical Reviews*, vol. 110, pp. 132-145, Jan 2010.
- [97] J. H. Chen, C. Jang, S. D. Xiao, M. Ishigami, and M. S. Fuhrer, "Intrinsic and extrinsic performance limits of graphene devices on SiO₂," *Nature Nanotechnology*, vol. 3, pp. 206-209, Apr 2008.
- [98] Y. W. Zhu, S. Murali, W. W. Cai, X. S. Li, J. W. Suk, J. R. Potts, *et al.*, "Graphene and Graphene Oxide: Synthesis, Properties, and Applications (vol 22, pg 3906, 2010)," *Advanced Materials*, vol. 22, pp. 5226-5226, Dec 7 2010.
- [99] C. Lee, X. D. Wei, J. W. Kysar, and J. Hone, "Measurement of the elastic properties and intrinsic strength of monolayer graphene," *Science*, vol. 321, pp. 385-388, Jul 18 2008.
- [100] A. K. Geim and K. S. Novoselov, "The rise of graphene," *Nature Materials*, vol. 6, pp. 183-191, Mar 2007.
- [101] G. Chen, D. Wu, W. Weng, and C. Wu, "Exfoliation of graphite flake and its nanocomposites," *Carbon*, vol. 41, pp. 619-621, // 2003.
- [102] W. S. Hummers and R. E. Offeman, "Preparation of Graphitic Oxide," *Journal of the American Chemical Society*, vol. 80, pp. 1339-1339, 1958.

- [103] D. R. Dreyer, S. Park, C. W. Bielawski, and R. S. Ruoff, "The chemistry of graphene oxide," *Chem Soc Rev*, vol. 39, pp. 228-40, Jan 2010.
- [104] Y. Xu, H. Bai, G. Lu, C. Li, and G. Shi, "Flexible graphene films via the filtration of water-soluble noncovalent functionalized graphene sheets," *J Am Chem Soc*, vol. 130, pp. 5856-7, May 7 2008.
- [105] S. Stankovich, D. A. Dikin, R. D. Piner, K. A. Kohlhaas, A. Kleinhammes, Y. Jia, *et al.*, "Synthesis of graphene-based nanosheets via chemical reduction of exfoliated graphite oxide," *Carbon*, vol. 45, pp. 1558-1565, Jun 2007.
- [106] S. Park and R. S. Ruoff, "Chemical methods for the production of graphenes (vol 4, pg 217, 2009)," *Nature Nanotechnology*, vol. 5, pp. 309-309, Apr 2010.
- [107] J. R. Lomeda, C. D. Doyle, D. V. Kosynkin, W. F. Hwang, and J. M. Tour, "Diazonium Functionalization of Surfactant-Wrapped Chemically Converted Graphene Sheets," *Journal of the American Chemical Society*, vol. 130, pp. 16201-16206, Dec 3 2008.
- [108] V. C. Tung, M. J. Allen, Y. Yang, and R. B. Kaner, "High-throughput solution processing of large-scale graphene," *Nature Nanotechnology*, vol. 4, pp. 25-29, Jan 2009.
- [109] G. X. Wang, J. Yang, J. Park, X. L. Gou, B. Wang, H. Liu, *et al.*, "Facile synthesis and characterization of graphene nanosheets," *Journal of Physical Chemistry C*, vol. 112, pp. 8192-8195, Jun 5 2008.
- [110] V. Eswaraiyah, S. S. J. Aravind, and S. Ramaprabhu, "Top down method for synthesis of highly conducting graphene by exfoliation of graphite oxide using focused solar radiation," *Journal of Materials Chemistry*, vol. 21, pp. 6800-6803, 2011.
- [111] K. S. Kim, Y. Zhao, H. Jang, S. Y. Lee, J. M. Kim, K. S. Kim, *et al.*, "Large-scale pattern growth of graphene films for stretchable transparent electrodes," *Nature*, vol. 457, pp. 706-710, Feb 5 2009.
- [112] L. Brown, R. Hovden, P. Huang, M. Wojcik, D. A. Muller, and J. Park, "Twinning and Twisting of Tri- and Bilayer Graphene," *Nano Letters*, vol. 12, pp. 1609-1615, Mar 2012.
- [113] G. Nandamuri, S. Roumimov, and R. Solanki, "Chemical vapor deposition of graphene films," *Nanotechnology*, vol. 21, Apr 9 2010.
- [114] A. Malesevic, R. Vitchev, K. Schouteden, A. Volodin, L. Zhang, G. Van Tendeloo, *et al.*, "Synthesis of few-layer graphene via microwave plasma-enhanced chemical vapour deposition," *Nanotechnology*, vol. 19, Jul 30 2008.
- [115] E. Dervishi, Z. R. Li, F. Watanabe, A. Biswas, Y. Xu, A. R. Biris, *et al.*, "Large-scale graphene production by RF-cCVD method," *Chemical Communications*, pp. 4061-4063, 2009.
- [116] A. Reina, X. T. Jia, J. Ho, D. Nezich, H. B. Son, V. Bulovic, *et al.*, "Large Area, Few-Layer Graphene Films on Arbitrary Substrates by Chemical Vapor Deposition," *Nano Letters*, vol. 9, pp. 30-35, Jan 2009.
- [117] S. Shivaraman, R. A. Barton, X. Yu, J. Alden, L. Herman, M. V. S. Chandrashekar, *et al.*, "Free-Standing Epitaxial Graphene," *Nano Letters*, vol. 9, pp. 3100-3105, Sep 2009.
- [118] M. Zhou, J. Tang, Q. Cheng, G. Xu, P. Cui, and L.-C. Qin, "Few-layer graphene obtained by electrochemical exfoliation of graphite cathode," *Chemical Physics Letters*, vol. 572, pp. 61-65, 2013.
- [119] C.-Y. Su, A.-Y. Lu, Y. Xu, F.-R. Chen, A. N. Khlobystov, and L.-J. Li, "High-quality thin graphene films from fast electrochemical exfoliation," *Acs Nano*, vol. 5, pp. 2332-2339, 2011.
- [120] G. Wang, B. Wang, J. Park, Y. Wang, B. Sun, and J. Yao, "Highly efficient and large-scale synthesis of graphene by electrolytic exfoliation," *Carbon*, vol. 47, pp. 3242-3246, 2009.
- [121] X. Zhang, D. Zhang, Y. Chen, X. Sun, and Y. Ma, "Electrochemical reduction of graphene oxide films: Preparation, characterization and their electrochemical properties," *Chinese Science Bulletin*, vol. 57, pp. 3045-3050, 2012.
- [122] Z. S. Wu, W. C. Ren, L. B. Gao, J. P. Zhao, Z. P. Chen, B. L. Liu, *et al.*, "Synthesis of Graphene Sheets with High Electrical Conductivity and Good Thermal Stability by Hydrogen Arc Discharge Exfoliation," *Acs Nano*, vol. 3, pp. 411-417, Feb 2009.
- [123] A. Hirsch, "Unzipping Carbon Nanotubes: A Peeling Method for the Formation of Graphene Nanoribbons," *Angewandte Chemie-International Edition*, vol. 48, pp. 6594-6596, 2009.
- [124] Y. Hernandez, V. Nicolosi, M. Lotya, F. M. Blighe, Z. Y. Sun, S. De, *et al.*, "High-yield production of graphene by liquid-phase exfoliation of graphite," *Nature Nanotechnology*, vol. 3, pp. 563-568, Sep 2008.

- [125] H. B. Zhang, W. G. Zheng, Q. Yan, Y. Yang, J. W. Wang, Z. H. Lu, *et al.*, "Electrically conductive polyethylene terephthalate/graphene nanocomposites prepared by melt compounding," *Polymer*, vol. 51, pp. 1191-1196, Mar 2 2010.
- [126] S. Stankovich, D. A. Dikin, G. H. B. Dommett, K. M. Kohlhaas, E. J. Zimney, E. A. Stach, *et al.*, "Graphene-based composite materials," *Nature*, vol. 442, pp. 282-286, Jul 20 2006.
- [127] H. Pang, T. Chen, G. M. Zhang, B. Q. Zeng, and Z. M. Li, "An electrically conducting polymer/graphene composite with a very low percolation threshold," *Materials Letters*, vol. 64, pp. 2226-2229, Oct 31 2010.
- [128] S. Araby, L. Q. Zhang, H. C. Kuan, J. B. Dai, P. Majewski, and J. Ma, "A novel approach to electrically and thermally conductive elastomers using graphene," *Polymer*, vol. 54, pp. 3663-3670, Jun 2013.
- [129] J. H. Du, L. Zhao, Y. Zeng, L. L. Zhang, F. Li, P. F. Liu, *et al.*, "Comparison of electrical properties between multi-walled carbon nanotube and graphene nanosheet/high density polyethylene composites with a segregated network structure," *Carbon*, vol. 49, pp. 1094-1100, Apr 2011.
- [130] M. Kujawski, J. D. Pearse, and E. Smela, "Elastomers filled with exfoliated graphite as compliant electrodes," *Carbon*, vol. 48, pp. 2409-2417, Aug 2010.
- [131] E. H. L. Falcao, R. G. Blair, J. J. Mack, L. M. Viculis, C. W. Kwon, M. Bendikov, *et al.*, "Microwave exfoliation of a graphite intercalation compound," *Carbon*, vol. 45, pp. 1367-1369, May 2007.
- [132] T. Wei, Z. J. Fan, G. L. Luo, C. Zheng, and D. S. Xie, "A rapid and efficient method to prepare exfoliated graphite by microwave irradiation," *Carbon*, vol. 47, pp. 337-339, Jan 2009.
- [133] J. W. Shang, Y. H. Zhang, L. Yu, B. Shen, F. Z. Lv, and P. K. Chu, "Fabrication and dielectric properties of oriented polyvinylidene fluoride nanocomposites incorporated with graphene nanosheets," *Materials Chemistry and Physics*, vol. 134, pp. 867-874, Jun 15 2012.
- [134] S. Vadukumpully, J. Paul, N. Mahanta, and S. Valiyaveetil, "Flexible conductive graphene/poly(vinyl chloride) composite thin films with high mechanical strength and thermal stability," *Carbon*, vol. 49, pp. 198-205, 1// 2011.
- [135] W. E. Mahmoud, "Morphology and physical properties of poly(ethylene oxide) loaded graphene nanocomposites prepared by two different techniques," *European Polymer Journal*, vol. 47, pp. 1534-1540, Aug 2011.
- [136] H. L. Hu, G. Zhang, L. G. Xiao, H. J. Wang, Q. S. Zhang, and Z. D. Zhao, "Preparation and electrical conductivity of graphene/ultrahigh molecular weight polyethylene composites with a segregated structure," *Carbon*, vol. 50, pp. 4596-4599, Oct 2012.
- [137] N. Yousefi, X. Y. Lin, Q. B. Zheng, X. Shen, J. R. Pothnis, J. J. Jia, *et al.*, "Simultaneous in situ reduction, self-alignment and covalent bonding in graphene oxide/epoxy composites," *Carbon*, vol. 59, pp. 406-417, Aug 2013.
- [138] Q. Zheng, W. H. Ip, X. Lin, N. Yousefi, K. K. Yeung, Z. Li, *et al.*, "Transparent conductive films consisting of ultralarge graphene sheets produced by Langmuir-Blodgett assembly," *ACS Nano*, vol. 5, pp. 6039-51, Jul 26 2011.
- [139] Y. Geng, S. J. Wang, and J. K. Kim, "Preparation of graphite nanoplatelets and graphene sheets," *J Colloid Interface Sci*, vol. 336, pp. 592-8, Aug 15 2009.
- [140] W. J. Li, X. Z. Tang, H. B. Zhang, Z. G. Jiang, Z. Z. Yu, X. S. Du, *et al.*, "Simultaneous surface functionalization and reduction of graphene oxide with octadecylamine for electrically conductive polystyrene composites," *Carbon*, vol. 49, pp. 4724-4730, Nov 2011.
- [141] F. Yavari, M. A. Rafiee, J. Rafiee, Z. Z. Yu, and N. Koratkar, "Dramatic Increase in Fatigue Life in Hierarchical Graphene Composites," *Acs Applied Materials & Interfaces*, vol. 2, pp. 2738-2743, Oct 2010.
- [142] H. B. Zhang, W. G. Zheng, Q. Yan, Z. G. Jiang, and Z. Z. Yu, "The effect of surface chemistry of graphene on rheological and electrical properties of polymethylmethacrylate composites," *Carbon*, vol. 50, pp. 5117-5125, Nov 2012.
- [143] S. T. Hsiao, C. C. M. Ma, H. W. Tien, W. H. Liao, Y. S. Wang, S. M. Li, *et al.*, "Using a non-covalent modification to prepare a high electromagnetic interference shielding performance graphene nanosheet/water-borne polyurethane composite," *Carbon*, vol. 60, pp. 57-66, Aug 2013.
- [144] R. K. Layek, S. Samanta, D. P. Chatterjee, and A. K. Nandi, "Physical and mechanical properties of poly(methyl methacrylate) -functionalized graphene/poly(vinylidene fluoride) nanocomposites Piezoelectric beta polymorph formation," *Polymer*, vol. 51, pp. 5846-5856, Nov 12 2010.
- [145] K.-H. Liao, Y. Qian, and C. W. Macosko, "Ultralow percolation graphene/polyurethane acrylate nanocomposites," *Polymer*, vol. 53, pp. 3756-3761, 2012.

- [146] A. Oskouyi, U. Sundararaj, and P. Mertiny, "Tunneling conductivity and piezo-resistivity of composites containing randomly dispersed conductive nano-platelets," *Journal of materials*, vol. Article in press, 2014.
- [147] F. R. Al-Solamy, A. A. Al-Ghamdi, and W. E. Mahmoud, "Piezoresistive behavior of graphite nanoplatelets based rubber nanocomposites," *Polymers for Advanced Technologies*, vol. 23, pp. 478-482, Mar 2012.
- [148] S. Y. Qu and S. C. Wong, "Piezoresistive behavior of polymer reinforced by expanded graphite," *Composites Science and Technology*, vol. 67, pp. 231-237, Feb 2007.
- [149] Y. Hou, D. R. Wang, X. M. Zhang, H. Zhao, J. W. Zha, and Z. M. Dang, "Positive piezoresistive behavior of electrically conductive alkyl-functionalized graphene/polydimethylsilicone nanocomposites," *Journal of Materials Chemistry C*, vol. 1, pp. 515-521, 2013.
- [150] J. R. Lu, X. F. Chen, W. Lu, and G. H. Chen, "The piezoresistive behaviors of polyethylene/foliated graphite nanocomposites," *European Polymer Journal*, vol. 42, pp. 1015-1021, May 2006.
- [151] L. M. Chiacchiarelli, M. Rallini, M. Monti, D. Puglia, J. M. Kenny, and L. Torre, "The role of irreversible and reversible phenomena in the piezoresistive behavior of graphene epoxy nanocomposites applied to structural health monitoring," *Composites Science and Technology*, vol. 80, pp. 73-79, May 17 2013.
- [152] M. Y. Han, B. Ozyilmaz, Y. B. Zhang, and P. Kim, "Energy band-gap engineering of graphene nanoribbons," *Physical Review Letters*, vol. 98, May 18 2007.
- [153] D. V. Kosynkin, A. L. Higginbotham, A. Sinitskii, J. R. Lomeda, A. Dimiev, B. K. Price, *et al.*, "Longitudinal unzipping of carbon nanotubes to form graphene nanoribbons," *Nature*, vol. 458, pp. 872-U5, Apr 16 2009.
- [154] J. Campos-Delgado, J. M. Romo-Herrera, X. T. Jia, D. A. Cullen, H. Muramatsu, Y. A. Kim, *et al.*, "Bulk production of a new form of sp(2) carbon: Crystalline graphene nanoribbons," *Nano Letters*, vol. 8, pp. 2773-2778, Sep 2008.
- [155] A. Oskouyi, U. Sundararaj, and P. Mertiny, "Electrical conductivity of polymers with variable-sized conductive nanoplatelets," presented at the 6th ECCOMAS Conference on Smart Structures and Materials, SMART2013, Politecnico di Torino, 2013.
- [156] A. Oskouyi, U. Sundararaj, and P. Mertiny, "Current-voltage characteristics of nanoplatelet based conductive nano-composites," presented at the The 19th international conference on composite materials, Montreal, Canada.
- [157] A. B. Oskouyi and P. Mertiny, "Monte Carlo model for the study of percolation thresholds in composites filled with circular conductive nano-disks," *11th International Conference on the Mechanical Behavior of Materials (Icm11)*, vol. 10, 2011.
- [158] K. U. Lee, K. J. Park, O. J. Kwon, and J. J. Kim, "Carbon sphere as a black pigment for an electronic paper," *Current Applied Physics*, vol. 13, pp. 419-424, Mar 2013.
- [159] A. I. Medalia and L. W. Richards, "Tinting Strength of Carbon-Black," *Journal of Colloid and Interface Science*, vol. 40, pp. 233-&, 1972.
- [160] W. Zhang, R. S. Blackburn, and A. A. Dehghani-Sanij, "Effect of carbon black concentration on electrical conductivity of epoxy resin-carbon black-silica nanocomposites," *Journal of Materials Science*, vol. 42, pp. 7861-7865, Sep 2007.
- [161] S. Praveen, P. K. Chattopadhyay, P. Albert, V. G. Dalvi, B. C. Chakraborty, and S. Chattopadhyay, "Synergistic effect of carbon black and nanoclay fillers in styrene butadiene rubber matrix: Development of dual structure," *Composites Part a-Applied Science and Manufacturing*, vol. 40, pp. 309-316, Mar 2009.
- [162] M. Mohsen, M. H. Abd-El Salam, A. Ashry, A. Ismail, and H. Ismail, "Positron annihilation spectroscopy in carbon black-silica-styrene butadiene rubber (SBR) composites under deformation," *Polymer Degradation and Stability*, vol. 87, pp. 381-388, Mar 2005.
- [163] S. R. Mahapatra, V. Sridhar, and D. K. Tripathy, "Impedance analysis and electromagnetic interference shielding effectiveness of conductive carbon black reinforced microcellular EPDM rubber vulcanizates," *Polymer Composites*, vol. 29, pp. 465-472, May 2008.
- [164] N. C. Das, T. K. Chaki, D. Khastgir, and A. Chakraborty, "Electromagnetic interference shielding effectiveness of conductive carbon black and carbon fiber-filled composites based on rubber and rubber blends," *Advances in Polymer Technology*, vol. 20, pp. 226-236, Fal 2001.

- [165] R. Q. Ou, R. A. Gerhardt, C. Marrett, A. Moulart, and J. S. Colton, "Assessment of percolation and homogeneity in ABS/carbon black composites by electrical measurements," *Composites Part B-Engineering*, vol. 34, pp. 607-614, 2003.
- [166] J. R. Li, J. R. Xu, M. Q. Zhang, and M. Z. Rong, "Carbon black/polystyrene composites as candidates for gas sensing materials," *Carbon*, vol. 41, pp. 2353-2360, 2003.
- [167] A. Katada, Y. Konishi, T. Isogai, Y. Tominaga, S. Asai, and M. Sumita, "Dynamic percolation phenomenon of poly(methyl methacrylate)/surface fluorinated carbon black composite," *Journal of Applied Polymer Science*, vol. 89, pp. 1151-1155, Jul 25 2003.
- [168] O. Koysuren, S. Yesil, and G. Bayram, "Effect of composite preparation techniques on electrical and mechanical properties and morphology of nylon 6 based conductive polymer composites," *Journal of applied polymer science*, vol. 102, pp. 2520-2526, 2006.
- [169] J. Hwang, J. Muth, and T. Ghosh, "Electrical and mechanical properties of carbon-black-filled, electrospun nanocomposite fiber webs," *Journal of Applied Polymer Science*, vol. 104, pp. 2410-2417, May 15 2007.
- [170] C. G. Ma, D. Y. Xi, and M. Liu, "Epoxy resin/polyetherimide/carbon black conductive polymer composites with a double percolation structure by reaction-induced phase separation," *Journal of Composite Materials*, vol. 47, pp. 1153-1160, Apr 2013.
- [171] X. Y. Ji, H. Li, D. Hui, K. T. Hsiao, J. P. Ou, and A. K. T. Lau, "I-V characteristics and electro-mechanical response of different carbon black/epoxy composites," *Composites Part B-Engineering*, vol. 41, pp. 25-32, Jan 2010.
- [172] X. Q. Liu, H. Q. Xing, L. L. Zhao, and X. S. Chen, "Study on NTC Electrical Behavior of Carbon Black/PVC Composite," *Proceedings of the 2nd International Conference on Electronic & Mechanical Engineering and Information Technology (Emeit-2012)*, vol. 23, 2012.
- [173] M. N. J. YACUBOWICZ, L. BENGUIGUI, "Electrical and Dielectric Properties of Segregated Carbon Black-Polyethylene Systems," *POLYMER ENGINEERING AND SCIENCE*, vol. 30, pp. 459-468, 1990.
- [174] L. A. H. Zois, M. Omastova, "Electrical Properties and Percolation Phenomena in Carbon Black Filled Polymer Composites," presented at the 10th International Symposium on Electrets, 1999.
- [175] A. L. Juris Zavickis, Maris Knite, "The downshift of the electrical percolation threshold in polyisoprene-nanostructured carbon composites," *ENERGETIKA*, vol. 57, pp. 44-49, 2011.
- [176] W. G. Zheng, S. C. Wong, and H. J. Sue, "Transport behavior of PMMA/expanded graphite nanocomposites," *Polymer*, vol. 43, pp. 6767-6773, Dec 2002.
- [177] W. Lu, J. X. Weng, D. J. Wu, C. L. Wu, and G. H. Chen, "Epoxy resin/graphite electrically conductive nanosheet nanocomposite," *Materials and Manufacturing Processes*, vol. 21, pp. 167-171, 2006.
- [178] E. T. Thostenson and T. W. Chou, "Real-time in situ sensing of damage evolution in advanced fiber composites using carbon nanotube networks," *Nanotechnology*, vol. 19, May 28 2008.
- [179] K. J. Loh, J. P. Lynch, and N. A. Kotov, "Passive wireless sensing using SWNT-based multifunctional thin film patches," *International Journal of Applied Electromagnetics and Mechanics*, vol. 28, pp. 87-94, 2008.
- [180] K. J. Loh, T. C. Hou, J. P. Lynch, and N. A. Kotov, "Carbon Nanotube Sensing Skins for Spatial Strain and Impact Damage Identification," *Journal of Nondestructive Evaluation*, vol. 28, pp. 9-25, Mar 2009.
- [181] G. E. Pike and C. H. Seager, "Percolation and Conductivity - Computer Study .1.," *Physical Review B*, vol. 10, pp. 1421-1434, 1974.
- [182] I. Balberg and N. Binenbaum, "Cluster structure and conductivity of three-dimensional continuum systems," *Physical Review A*, vol. 31, p. 1222, 1985.
- [183] T. Natsuki, M. Endo, and T. Takahashi, "Percolation study of orientated short-fiber composites by a continuum model," *Physica a-Statistical Mechanics and Its Applications*, vol. 352, pp. 498-508, Jul 15 2005.
- [184] F. Dalmas, R. Dendievel, L. Chazeau, J. Y. Cavaille, and C. Gauthier, "Carbon nanotube-filled polymer of electrical conductivity in composites. Numerical simulation three-dimensional entangled fibrous networks," *Acta Materialia*, vol. 54, pp. 2923-2931, Jun 2006.
- [185] C. Y. Li and T. W. Chou, "Continuum percolation of nanocomposites with fillers of arbitrary shapes," *Applied Physics Letters*, vol. 90, Apr 23 2007.

- [186] S. F. Wang and A. A. Ogale, "Continuum Space Simulation and Experimental Characterization of Electrical Percolation Behavior of Particulate Composites," *Composites Science and Technology*, vol. 46, pp. 93-103, 1993.
- [187] J. Hicks, A. Behnam, and A. Ural, "A computational study of tunneling-percolation electrical transport in graphene-based nanocomposites," *Applied Physics Letters*, vol. 95, Nov 23 2009.
- [188] L. Li and J. E. Morris, "Electrical conduction models for isotropically conductive adhesive joints," *Ieee Transactions on Components Packaging and Manufacturing Technology Part A*, vol. 20, pp. 3-8, Mar 1997.
- [189] Y. B. Yi and E. Tawerghi, "Geometric percolation thresholds of interpenetrating plates in three-dimensional space," *Physical Review E*, vol. 79, Apr 2009.
- [190] J. A. Quintanilla and R. M. Ziff, "Asymmetry in the percolation thresholds of fully penetrable disks with two different radii," *Physical Review E*, vol. 76, Nov 2007.
- [191] J. Quintanilla, "Measurement of the percolation threshold for fully penetrable disks of different radii," *Physical Review E*, vol. 63, pp. art. no.-061108, Jun 2001.
- [192] J. Quintanilla, S. Torquato, and R. M. Ziff, "Efficient measurement of the percolation threshold for fully penetrable discs," *Journal of Physics a-Mathematical and General*, vol. 33, pp. L399-L407, Oct 27 2000.
- [193] L. Vovchenko and V. Vovchenko, "Simulation of percolation threshold in composites filled with conducting particles of various morphologies," *Materialwissenschaft Und Werkstofftechnik*, vol. 42, pp. 70-74, Jan 2011.
- [194] R. H. J. Otten and P. van der Schoot, "Connectivity percolation of polydisperse anisotropic nanofillers," *Journal of Chemical Physics*, vol. 134, Mar 7 2011.
- [195] G. Ambrosetti, N. Johner, C. Grimaldi, A. Danani, and P. Ryser, "Percolative properties of hard oblate ellipsoids of revolution with a soft shell," *Physical Review E*, vol. 78, Dec 2008.
- [196] G. Ambrosetti, C. Grimaldi, I. Balberg, T. Maeder, A. Danani, and P. Ryser, "Solution of the tunneling-percolation problem in the nanocomposite regime," *Physical Review B*, vol. 81, Apr 15 2010.
- [197] M. Mathew, T. Schilling, and M. Oettel, "Connectivity percolation in suspensions of hard platelets," *Physical Review E*, vol. 85, Jun 20 2012.
- [198] W. Xia and M. F. Thorpe, "Percolation Properties of Random Ellipses," *Physical Review A*, vol. 38, pp. 2650-2656, Sep 1 1988.
- [199] J. Li and J. K. Kim, "Percolation threshold of conducting polymer composites containing 3D randomly distributed graphite nanoplatelets," *Composites Science and Technology*, vol. 67, pp. 2114-2120, Aug 2007.
- [200] G. R. Grimmett, "Percolation (Grundlehren der mathematischen Wissenschaften)," ed: Springer: Berlin, Germany, 2010.
- [201] M. Sahini and M. Sahimi, *Applications of percolation theory*: CRC Press, 1994.
- [202] T. Cazenave, "Nested Monte-Carlo Expression Discovery," in *ECAI*, 2010, pp. 1057-1058.
- [203] M. Matsumoto and T. Nishimura, "Mersenne twister: a 623-dimensionally equidistributed uniform pseudo-random number generator," *ACM Transactions on Modeling and Computer Simulation (TOMACS)*, vol. 8, pp. 3-30, 1998.
- [204] N. C. Diaz, A. V. Gil, and M. J. Vargas, "Assessment of the suitability of different random number generators for Monte Carlo simulations in gamma-ray spectrometry," *Applied Radiation and Isotopes*, vol. 68, pp. 469-473, Mar 2010.
- [205] J. Cook, "Rational formulae for the production of a spherically symmetric probability distribution," *Mathematics of Computation*, vol. 11, pp. 81-82, 1957.
- [206] A. A. Ogale and S. F. Wang, "Simulation of the Percolation Behavior of Quasi and Transversely Isotropic Short-Fiber Composites with a Continuum Model," *Composites Science and Technology*, vol. 46, pp. 379-388, 1993.
- [207] Z. Neda, R. Florian, and Y. Brechet, "Reconsideration of continuum percolation of isotropically oriented sticks in three dimensions," *Physical Review E*, vol. 59, pp. 3717-3719, Mar 1999.
- [208] H. A. Almohamad and S. Z. Selim, "An algorithm for computing the distance between two circular disks," *Applied Mathematical Modelling*, vol. 27, pp. 115-124, Feb 2003.
- [209] K. I. Bolotin, K. Sikes, Z. Jiang, M. Klima, G. Fudenberg, J. Hone, *et al.*, "Ultrahigh electron mobility in suspended graphene," *Solid State Communications*, vol. 146, pp. 351-355, 2008.
- [210] D. Stauffer and A. Aharony, *Introduction to percolation theory*: Taylor and Francis, 1994.

- [211] G. Gorrasi, E. Piperopoulos, M. Lanza, and C. Milone, "Effect of morphology of the filler on the electrical behaviour of poly(L-lactide) nanocomposites," *Journal of Physics and Chemistry of Solids*, vol. 74, pp. 1-6, Jan 2013.
- [212] A. Celzard, G. Furdin, J. F. Mareche, and E. McRae, "Non-linear current-voltage characteristics in anisotropic epoxy resin graphite flake composites," *Journal of Materials Science*, vol. 32, pp. 1849-1853, Apr 1 1997.
- [213] L. X. He and S. C. Tjong, "Zener tunneling in conductive graphite/epoxy composites: Dielectric breakdown aspects," *Express Polymer Letters*, vol. 7, pp. 375-382, Apr 2013.
- [214] J. G. Simmons, "Generalized Formula for the Electric Tunnel Effect between Similar Electrodes Separated by a Thin Insulating Film," *Journal of Applied Physics*, vol. 34, pp. 1793-1803, 1963.
- [215] W. Luheng, D. Tianhuai, and W. Peng, "Influence of carbon black concentration on piezoresistivity for carbon-black-filled silicone rubber composite," *Carbon*, vol. 47, pp. 3151-3157, Nov 2009.
- [216] G. T. Pham, *Characterization and modeling of piezo-resistive properties of carbon nanotube-based conductive polymer composites*: ProQuest, 2008.
- [217] C. Hu, Y. Gao, and Z. Sheng, "The piezoresistance coefficients of copper and copper-nickel alloys," *Journal of materials science*, vol. 35, pp. 381-386, 2000.
- [218] D. Grady and M. Ginsberg, "Piezoresistive effects in ytterbium stress transducers," *Journal of Applied Physics*, vol. 48, pp. 2179-2181, 1977.
- [219] Y. Huang, J. Wu, and K. C. Hwang, "Thickness of graphene and single-wall carbon nanotubes," *Physical Review B*, vol. 74, Dec 2006.
- [220] S. V. Morozov, K. S. Novoselov, M. I. Katsnelson, F. Schedin, D. C. Elias, J. A. Jaszczak, *et al.*, "Giant intrinsic carrier mobilities in graphene and its bilayer," *Physical Review Letters*, vol. 100, Jan 11 2008.
- [221] W. S. Bao, S. A. Meguid, Z. H. Zhu, and G. J. Weng, "Tunneling resistance and its effect on the electrical conductivity of carbon nanotube nanocomposites," *Journal of Applied Physics*, vol. 111, May 1 2012.
- [222] I. Balberg, D. Azulay, Y. Goldstein, J. Jedrzejewski, G. Ravid, and E. Savir, "The percolation staircase model and its manifestation in composite materials," *European Physical Journal B*, vol. 86, Oct 14 2013.
- [223] H. Zois, L. Apekis, and M. Omastova, "Electrical properties of carbon black-filled polymer composites," *Macromolecular Symposia*, vol. 170, pp. 249-256, Jun 2001.
- [224] J. Vilcakova, P. Saha, and O. Quadrat, "Electrical conductivity of carbon fibres/polyester resin composites in the percolation threshold region," *European Polymer Journal*, vol. 38, pp. 2343-2347, Dec 2002.
- [225] W. Bauhofer and J. Z. Kovacs, "A review and analysis of electrical percolation in carbon nanotube polymer composites," *Composites Science and Technology*, vol. 69, pp. 1486-1498, Aug 2009.
- [226] E. Tkalya, M. Ghislandi, A. Alekseev, C. Koning, and J. Loos, "Latex-based concept for the preparation of graphene-based polymer nanocomposites," *Journal of Materials Chemistry*, vol. 20, pp. 3035-3039, 2010.
- [227] V. Panwar, B. Kang, J. O. Park, S. Park, and R. M. Mehra, "Study of dielectric properties of styrene-acrylonitrile graphite sheets composites in low and high frequency region," *European Polymer Journal*, vol. 45, pp. 1777-1784, Jun 2009.
- [228] N. Johner, P. Ryser, C. Grimaldi, and I. Balberg, "Piezoresistivity and tunneling-percolation transport in apparently nonuniversal systems," *Physical Review B*, vol. 75, Mar 2007.
- [229] N. Johner, C. Grimaldi, I. Balberg, and P. Ryser, "Transport exponent in a three-dimensional continuum tunneling-percolation model," *Physical Review B*, vol. 77, May 2008.
- [230] S. B. Lee and S. Torquato, "Monte-Carlo Study of Correlated Continuum Percolation - Universality and Percolation Thresholds," *Physical Review A*, vol. 41, pp. 5338-5344, May 15 1990.
- [231] Y. Yu, S. Song, Z. Bu, X. Gu, G. Song, and L. Sun, "Influence of filler waviness and aspect ratio on the percolation threshold of carbon nanomaterials reinforced polymer nanocomposites," *Journal of Materials Science*, vol. 48, pp. 5727-5732, 2013.
- [232] S. Pfeifer, S. H. Park, and P. R. Bandaru, "Analysis of electrical percolation thresholds in carbon nanotube networks using the Weibull probability distribution," *Journal of Applied Physics*, vol. 108, Jul 15 2010.
- [233] C. Li, E. T. Thostenson, and T.-W. Chou, "Effect of nanotube waviness on the electrical conductivity of carbon nanotube-based composites," *Composites Science and Technology*, vol. 68, pp. 1445-1452, 2008.

- [234] W. K. Li, A. Dichiara, and J. B. Bai, "Carbon nanotube-graphene nanoplatelet hybrids as high-performance multifunctional reinforcements in epoxy composites," *Composites Science and Technology*, vol. 74, pp. 221-227, Jan 24 2013.
- [235] S. K. Kalanadhabhatla, *Piezoresistivity Behavior of Polydimethylsiloxane Based Conducting Composites for Printing on Textiles*: North Carolina State University, 2012.
- [236] L. Flandin, A. Hiltner, and E. Baer, "Interrelationships between electrical and mechanical properties of a carbon black-filled ethylene-octene elastomer," *Polymer*, vol. 42, pp. 827-838, Jan 2001.
- [237] J. Lu, M. Lu, A. Bermak, and Y.-K. Lee, "Study of piezoresistance effect of carbon nanotube-PDMS composite materials for nanosensors," in *Nanotechnology, 2007. IEEE-NANO 2007. 7th IEEE Conference on*, 2007, pp. 1240-1243.
- [238] Z. M. Dang, M. J. Jiang, D. Xie, S. H. Yao, L. Q. Zhang, and J. B. Bai, "Supersensitive linear piezoresistive property in carbon nanotubes/silicone rubber nanocomposites," *Journal of Applied Physics*, vol. 104, Jul 15 2008.
- [239] R. Soltani and A. A. Katbab, "The role of interfacial compatibilizer in controlling the electrical conductivity and piezoresistive behavior of the nanocomposites based on RTV silicone rubber/graphite nanosheets," *Sensors and Actuators a-Physical*, vol. 163, pp. 213-219, Sep 2010.
- [240] M. K. Abyaneh and S. K. Kulkarni, "Giant piezoresistive response in zinc-polydimethylsiloxane composites under uniaxial pressure," *Journal of Physics D: Applied Physics*, vol. 41, p. 135405, 2008.
- [241] G. Ausanio, A. Barone, C. Campana, V. Iannotti, C. Luponio, G. Pepe, *et al.*, "Giant resistivity change induced by strain in a composite of conducting particles in an elastomer matrix," *Sensors and Actuators A: Physical*, vol. 127, pp. 56-62, 2006.
- [242] D. Beruto, M. Capurro, and G. Marro, "Piezoresistance behavior of silicone-graphite composites in the proximity of the electric percolation threshold," *Sensors and Actuators A: Physical*, vol. 117, pp. 301-308, 2005.
- [243] L. Chen, G. Chen, and L. Lu, "Piezoresistive Behavior Study on Finger-Sensing Silicone Rubber/Graphite Nanosheet Nanocomposites," *Advanced Functional Materials*, vol. 17, pp. 898-904, 2007.
- [244] L. Chen, G. H. Chen, and L. Lu, "Piezoresistive behavior study on finger-sensing silicone rubber/graphite nanosheet nanocomposites," *Advanced Functional Materials*, vol. 17, pp. 898-904, Apr 16 2007.
- [245] G. Ausanio, A. C. Barone, C. Campana, V. Iannotti, C. Luponio, G. P. Pepe, *et al.*, "Giant resistivity change induced by strain in a composite of conducting particles in an elastomer matrix," *Sensors and Actuators a-Physical*, vol. 127, pp. 56-62, Feb 28 2006.
- [246] D. T. Beruto, M. Capurro, and G. Marro, "Piezoresistance behavior of silicone-graphite composites in the proximity of the electric percolation threshold," *Sensors and Actuators a-Physical*, vol. 117, pp. 301-308, Jan 14 2005.
- [247] J. Kost, M. Narkis, and A. Foux, "Effects of Axial Stretching on the Resistivity of Carbon-Black Filled Silicone-Rubber," *Polymer Engineering and Science*, vol. 23, pp. 567-571, 1983.
- [248] S. V. Anand and D. R. Mahapatra, "Quasi-static and dynamic strain sensing using carbon nanotube/epoxy nanocomposite thin films," *Smart Materials and Structures*, vol. 18, Apr 2009.
- [249] M. H. G. Wichmann, S. T. Buschhorn, J. Gehrmann, and K. Schulte, "Piezoresistive response of epoxy composites with carbon nanoparticles under tensile load," *Physical Review B*, vol. 80, Dec 2009.
- [250] C. Cattin and P. Hubert, "Network Formation and Electrical Conduction in Carbon Nanotube Modified Polydimethylsiloxane," in *MRS Proceedings*, 2012, pp. mrsf11-1410-dd05-07.
- [251] H. F. Lin, W. Lu, and G. H. Chen, "Nonlinear DC conduction behavior in epoxy resin/graphite nanosheets composites," *Physica B-Condensed Matter*, vol. 400, pp. 229-236, Nov 15 2007.
- [252] A. Celzard, G. Furdin, J. Mareche, and E. McRae, "Non-linear current-voltage characteristics in anisotropic epoxy resin-graphite flake composites," *Journal of materials science*, vol. 32, pp. 1849-1853, 1997.
- [253] Q. A. Zheng, Y. H. Song, G. Wu, and X. S. Yi, "Reversible nonlinear conduction behavior for high-density polyethylene/graphite powder composites near the percolation threshold," *Journal of Polymer Science Part B-Polymer Physics*, vol. 39, pp. 2833-2842, Nov 15 2001.
- [254] G. H. Chen, W. G. Weng, D. J. Wu, and C. L. Wu, "Nonlinear conduction in nylon-6/foiled graphite nanocomposites above the percolation threshold," *Journal of Polymer Science Part B-Polymer Physics*, vol. 42, pp. 155-167, Jan 1 2004.

- [255] J. G. Simmons, "Generalized formula for the electric tunnel effect between similar electrodes separated by a thin insulating film," *Journal of Applied Physics*, vol. 34, pp. 1793-1803, 2004.
- [256] A. B. Oskouyi and P. Mertiny, "Monte Carlo model for the study of percolation thresholds in composites filled with circular conductive nano-disks," *Procedia Engineering*, vol. 10, pp. 403-408, 2011.
- [257] C. H. Liu and S. S. Fan, "Nonlinear electrical conducting behavior of carbon nanotube networks in silicone elastomer," *Applied Physics Letters*, vol. 90, Jan 22 2007.
- [258] K. S. Karimov, M. Abid, M. Saleem, K. M. Akhmedov, M. M. Bashir, U. Shafique, *et al.*, "Temperature gradient sensor based on CNT composite," *Physica B: Condensed Matter*, vol. 446, pp. 39-42, 2014.
- [259] C. Heo and J. H. Chang, "Polyimide nanocomposites based on functionalized graphene sheets: Morphologies, thermal properties, and electrical and thermal conductivities," *Solid State Sciences*, vol. 24, pp. 6-14, Oct 2013.
- [260] J. S. Kim, J. H. Yun, I. Kim, and S. E. Shim, "Electrical properties of graphene/SBR nanocomposite prepared by latex heterocoagulation process at room temperature," *Journal of Industrial and Engineering Chemistry*, vol. 17, pp. 325-330, Mar 25 2011.
- [261] P. Manivel, S. Kanagaraj, A. Balamurugan, N. Ponpandian, D. Mangalaraj, and C. Viswanathan, "Rheological behavior and electrical properties of polypyrrole/thermally reduced graphene oxide nanocomposite," *Colloids and Surfaces a-Physicochemical and Engineering Aspects*, vol. 441, pp. 614-622, Jan 20 2014.
- [262] A. S. Patole, S. P. Patole, H. Kang, J. B. Yoo, T. H. Kim, and J. H. Ahn, "A facile approach to the fabrication of graphene/polystyrene nanocomposite by in situ microemulsion polymerization," *Journal of Colloid and Interface Science*, vol. 350, pp. 530-537, Oct 15 2010.
- [263] E. Logakis, C. Pandis, V. Peoglos, P. Pissis, J. Pionteck, P. Potschke, *et al.*, "Electrical/dielectric properties and conduction mechanism in melt processed polyamide/multi-walled carbon nanotubes composites," *Polymer*, vol. 50, pp. 5103-5111, Oct 9 2009.
- [264] H. C. Neitzert, L. Vertuccio, and A. Sorrentino, "Epoxy/MWCNT Composite as Temperature Sensor and Electrical Heating Element," *Ieee Transactions on Nanotechnology*, vol. 10, pp. 688-693, Jul 2011.
- [265] E. Bilotti, R. Zhang, H. Deng, M. Baxendale, and T. Peijs, "Fabrication and property prediction of conductive and strain sensing TPU/CNT nanocomposite fibres," *Journal of Materials Chemistry*, vol. 20, pp. 9449-9455, 2010.
- [266] A. Bahrami, Z. A. Talib, W. M. M. Yunus, K. Behzad, M. M. Abdi, and F. U. Din, "Low Temperature Hall Effect Investigation of Conducting Polymer-Carbon Nanotubes Composite Network," *International Journal of Molecular Sciences*, vol. 13, pp. 14917-14928, Nov 2012.
- [267] Z. Yang, Z. Cao, H. Sun, and Y. Li, "Composite Films Based on Aligned Carbon Nanotube Arrays and a Poly (N-Isopropyl Acrylamide) Hydrogel," *Advanced Materials*, vol. 20, pp. 2201-2205, 2008.
- [268] H. C. Neitzert, L. Vertuccio, and A. Sorrentino, "Epoxy/MWCNT composite as temperature sensor and electrical heating element," *Nanotechnology, IEEE Transactions on*, vol. 10, pp. 688-693, 2011.
- [269] P. Sheng, "Fluctuation-induced tunneling conduction in disordered materials," *Physical Review B*, vol. 21, p. 2180, 1980.
- [270] G. Matzeu, A. Pucci, S. Savi, M. Romanelli, and F. Di Francesco, "A temperature sensor based on a MWCNT/SEBS nanocomposite," *Sensors and Actuators A: Physical*, vol. 178, pp. 94-99, 2012.
- [271] M. Sibinski, M. Jakubowska, and M. Sloma, "Flexible temperature sensors on fibers," *Sensors*, vol. 10, pp. 7934-7946, 2010.
- [272] G. Marsaglia, "Choosing a Point from the Surface of a Sphere" *Ann. Math. Statist.*, vol. 43, pp. 373-700, 1972.
- [273] M. Matsumoto and T. Nishimura, "Mersenne twister: a 623-dimensionally equidistributed uniform pseudo-random number generator," *ACM Trans. Model. Comput. Simul.*, vol. 8, pp. 3-30, 1998.
- [274] Y. Yu, G. Song, and L. Sun, "Determinant role of tunneling resistance in electrical conductivity of polymer composites reinforced by well dispersed carbon nanotubes," *Journal of Applied Physics*, vol. 108, p. 084319, 2010.
- [275] A. Oskouyi, U. Sundararaj, and P. Mertiny, "Tunneling Conductivity and Piezoresistivity of Composites Containing Randomly Dispersed Conductive Nano-Platelets," *Materials*, vol. 7, pp. 2501-2521, 2014.
- [276] A. B. Oskouyi and P. Mertiny, "Monte Carlo model for the study of percolation thresholds in composites filled with circular conductive nano-disks," *Procedia Engineering*, vol. 10, pp. 403-408, // 2011.

- [277] J. G. Simmons, "Generalized Formula for the Electric Tunnel Effect between Similar Electrodes Separated by a Thin Insulating Film," *Journal of Applied Physics*, vol. 34, pp. 1793-1803, 1963.
- [278] J. G. Simmons, "Generalized Thermal J-V Characteristic for the Electric Tunnel Effect," *Journal of Applied Physics*, vol. 35, pp. 2655-2658, 1964.
- [279] Y. Chen, S. Wang, F. Pan, and J. Zhang, "A Numerical Study on Electrical Percolation of Polymer-Matrix Composites with Hybrid Fillers of Carbon Nanotubes and Carbon Black," *Journal of Nanomaterials*, vol. 2014, 2014.
- [280] T. Ebbesen, H. Lezec, H. Hiura, J. Bennett, H. Ghaemi, and T. Thio, "Electrical conductivity of individual carbon nanotubes," 1996.
- [281] H. C. Neitzert, A. Sorrentino, and L. Vertuccio, "Epoxy/MWCNT Composite Based Temperature Sensor with Linear Characteristics," in *Sensors and Microsystems*. vol. 54, P. Malcovati, A. Baschiroto, A. d'Amico, and C. Natale, Eds., ed: Springer Netherlands, 2010, pp. 241-245.
- [282] S. M. Shang, W. Zeng, and X. M. Tao, "High stretchable MWNTs/polyurethane conductive nanocomposites," *Journal of Materials Chemistry*, vol. 21, pp. 7274-7280, 2011.
- [283] J.-H. Lee and S.-J. Lee, "Application of laser-generated guided wave for evaluation of corrosion in carbon steel pipe," *NDT & E International*, vol. 42, pp. 222-227, 4// 2009.
- [284] S. Hurlbaeus and L. Gaul, "Smart structure dynamics," *Mechanical Systems and Signal Processing*, vol. 20, pp. 255-281, Feb 2006.
- [285] K. Y. Choi and F. K. Chang, "Identification of impact force and location using distributed sensors," *Aiaa Journal*, vol. 34, pp. 136-142, Jan 1996.
- [286] K. Kishimoto, H. Inoue, M. Hamada, and T. Shibuya, "Time frequency analysis of dispersive waves by means of wavelet transform," *Journal of Applied Mechanics-Transactions of the Asme*, vol. 62, pp. 841-846, Dec 1995.
- [287] T. H. Loutas and V. Kostopoulos, "Health monitoring of carbon/carbon, woven reinforced composites: Damage assessment by using advanced signal processing techniques. Part II: Acousto-ultrasonics monitoring of damage development," *Composites Science and Technology*, vol. 69, pp. 273-283, Feb 2009.
- [288] R. de Oliveira and A. T. Marques, "Health monitoring of FRP using acoustic emission and artificial neural networks," *Computers & Structures*, vol. 86, pp. 367-373, Feb 2008.
- [289] C. E. S. C. Ajay Raghavan, "Review of Guided-wave Structural Health Monitoring," *The Shock and Vibration Digest*, vol. 39, pp. 92-114, 2007.
- [290] C. Ramadas, J. Padiyar, K. Balasubramaniam, M. Joshi, and C. V. Krishnamurthy, "Lamb wave based ultrasonic imaging of interface delamination in a composite T-joint," *Ndt & E International*, vol. 44, pp. 523-530, Oct 2011.
- [291] V. Giurgiutiu, A. Zagrai, and J. J. Bao, "Damage identification in aging aircraft structures with piezoelectric wafer active sensors," *Journal of Intelligent Material Systems and Structures*, vol. 15, pp. 673-687, Sep-Oct 2004.
- [292] M. Castaings and B. Hosten, "Lamb and SH waves generated and detected by air-coupled ultrasonic transducers in composite material plates," *Ndt & E International*, vol. 34, pp. 249-258, Jun 2001.
- [293] A. Raghavan and C. E. Cesnik, "Review of guided-wave structural health monitoring," *Shock and Vibration Digest*, vol. 39, pp. 91-116, 2007.
- [294] Y. H. Kim, D. H. Kim, J. H. Han, and C. G. Kim, "Damage assessment in layered composites using spectral analysis and Lamb wave," *Composites Part B-Engineering*, vol. 38, pp. 800-809, 2007.
- [295] M. Castaings and B. Hosten, "Ultrasonic guided waves for health monitoring of high-pressure composite tanks," *Ndt & E International*, vol. 41, pp. 648-655, Dec 2008.
- [296] S. Yuan, L. Wang, and G. Peng, "Neural network method based on a new damage signature for structural health monitoring," *Thin-Walled Structures*, vol. 43, pp. 553-563, 2005.
- [297] B. R. Loyola, V. La Saponara, K. J. Loh, T. M. Briggs, G. O'Bryan, and J. L. Skinner, "Spatial Sensing Using Electrical Impedance Tomography," *Ieee Sensors Journal*, vol. 13, pp. 2357-2367, Jun 2013.
- [298] R. de Oliveira, C. A. Ramos, and A. T. Marques, "Health monitoring of composite structures by embedded FBG and interferometric Fabry-Perot sensors," *Computers & Structures*, vol. 86, pp. 340-346, Feb 2008.

- [299] M. Majumder, T. K. Gangopadhyay, A. K. Chakraborty, K. Dasgupta, and D. K. Bhattacharya, "Fibre Bragg gratings in structural health monitoring - Present status and applications," *Sensors and Actuators a-Physical*, vol. 147, pp. 150-164, Sep 15 2008.
- [300] J. C. Hao, A. S. Leng, and Z. Wei, "Non-destructive evaluation of composite pressure vessel by using FBG sensors," *Chinese Journal of Aeronautics*, vol. 20, pp. 120-123, Apr 2007.
- [301] C. A. Ramos, R. de Oliveira, and A. T. Marques, "Design of an optical fibre sensor patch for longitudinal strain measurement in structures," *Materials & Design*, vol. 30, pp. 2323-2331, Aug 2009.
- [302] G. Kister, R. A. Badcock, Y. M. Gebremichael, W. J. O. Boyle, K. T. V. Grattan, G. F. Fernando, *et al.*, "Monitoring of an all-composite bridge using Bragg grating sensors," *Construction and Building Materials*, vol. 21, pp. 1599-1604, Jul 2007.
- [303] K. Schulte and C. Baron, "Load and Failure Analyses of Cfrp Laminates by Means of Electrical-Resistivity Measurements," *Composites Science and Technology*, vol. 36, pp. 63-76, 1989.
- [304] C. Y. Li and T. W. Chou, "Modeling of damage sensing in fiber composites using carbon nanotube networks," *Composites Science and Technology*, vol. 68, pp. 3373-3379, Dec 2008.
- [305] M. Kupke, K. Schulte, and R. Schuler, "Non-destructive testing of FRP by d.c. and a.c. electrical methods," *Composites Science and Technology*, vol. 61, pp. 837-847, 2001.
- [306] B. R. Loyola, "Distributed In Situ Health Monitoring of Conductive Self-Sensing Fiber-Reinforced Polymers Using Electrical Impedance Tomography," DOCTOR OF PHILOSOPHY, UNIVERSITY OF CALIFORNIA DAVIS Davis, CA, USA, 2012.
- [307] E. T. Thostenson and T. W. Chou, "Carbon nanotube networks: Sensing of distributed strain and damage for life prediction and self healing," *Advanced Materials*, vol. 18, pp. 2837-+, Nov 3 2006.
- [308] E. T. Thostenson and T. W. Chou, "Carbon nanotube-based health monitoring of mechanically fastened composite joints," *Composites Science and Technology*, vol. 68, pp. 2557-2561, Sep 2008.
- [309] W. Zhang, V. Sakalkar, and N. Koratkar, "In situ health monitoring and repair in composites using carbon nanotube additives," *Applied Physics Letters*, vol. 91, Sep 24 2007.
- [310] M. Nofar, S. V. Hoa, and M. D. Pugh, "Failure detection and monitoring in polymer matrix composites subjected to static and dynamic loads using carbon nanotube networks," *Composites Science and Technology*, vol. 69, pp. 1599-1606, Aug 2009.
- [311] D. S. Holder, *Electrical Impedance Tomography: Methods, History and Applications*: IOP Publishing 2005.
- [312] K. J.-H. Loh, "Development of Multifunctional Carbon Nanotube Nanocomposite Sensors for Structural Health Monitoring," PhD, University of Michigan, Ann Arbor, MI, USA, 2008.
- [313] K. Paulson, W. Breckon, and M. Pidcock, "Electrode Modeling in Electrical-Impedance Tomography," *Siam Journal on Applied Mathematics*, vol. 52, pp. 1012-1022, Aug 1992.
- [314] J. Riera, P. J. Riu, P. Casan, and J. R. Masclans, "Electrical impedance tomography in acute lung injury," *Medicina Intensiva*, vol. 35, pp. 509-517, Nov 2011.
- [315] O. Gilad, A. Ghosh, D. I. Oh, and D. S. Holder, "A method for recording resistance changes non-invasively during neuronal depolarization with a view to imaging brain activity with electrical impedance tomography," *Journal of Neuroscience Methods*, vol. 180, pp. 87-96, May 30 2009.
- [316] C. S. Chaw, E. Yazaki, and D. F. Evans, "The effect of pH change on the gastric emptying of liquids measured by electrical impedance tomography and pH-sensitive radiotelemetry capsule," *International Journal of Pharmaceutics*, vol. 227, pp. 167-175, Oct 4 2001.
- [317] N. Kerrouche, C. McLeod, and W. Lionheart, "Time series of EIT chest images using singular value decomposition and Fourier transform," *Physiological Measurement*, vol. 22, p. 147, 2001.
- [318] R. Lazarovitch, D. Rittel, and I. Bucher, "Experimental crack identification using electrical impedance tomography," *Ndt & E International*, vol. 35, pp. 301-316, Jul 2002.
- [319] K. Bryan and M. Vogelius, "A Computational Algorithm to Determine Crack Locations from Electrostatic Boundary Measurements - the Case of Multiple Cracks," *International Journal of Engineering Science*, vol. 32, pp. 579-603, Apr 1994.

- [320] P. G. Kaup, F. Santosa, and M. Vogelius, "Method for imaging corrosion damage in thin plates from electrostatic data," *Inverse Problems*, vol. 12, pp. 279-293, Jun 1996.
- [321] T. C. Hou, K. J. Loh, and J. P. Lynch, "Spatial conductivity mapping of carbon nanotube composite thin films by electrical impedance tomography for sensing applications," *Nanotechnology*, vol. 18, Aug 8 2007.
- [322] A. Seppanen, K. Karhunen, A. Lehtikoinen, J. P. Kaipio, and P. J. M. Monteiro, "Electrical resistance tomography imaging of concrete," *Concrete Repair, Rehabilitation and Retrofitting II*, pp. 231-232, 2009.
- [323] K. Karhunen, A. Seppanen, A. Lehtikoinen, P. J. M. Monteiro, and J. P. Kaipio, "Electrical Resistance Tomography imaging of concrete," *Cement and Concrete Research*, vol. 40, pp. 137-145, Jan 2010.
- [324] T. C. Hou and J. P. Lynch, "Electrical Impedance Tomographic Methods for Sensing Strain Fields and Crack Damage in Cementitious Structures," *Journal of Intelligent Material Systems and Structures*, vol. 20, pp. 1363-1379, Jul 2009.
- [325] X. Y. Zhang, Z. Q. Li, and S. R. Zhu, "A Novel Electrical Resistance Tomography System of Carbon Fiber Smart Layer for Structural Health Monitoring," *2009 Ieee International Conference on Intelligent Computing and Intelligent Systems, Proceedings, Vol 4*, pp. 132-135, 2009.
- [326] Y. M. Deng and X. Liu, "Electromagnetic Imaging Methods for Nondestructive Evaluation Applications," *Sensors*, vol. 11, pp. 11774-11808, Dec 2011.

APPENDIX A SAMPLE DEVELOPED COMPUTER ROUTINES

A.1 Routine to Generate 3D Circular Nanodisk and Form MC Model

The following codes and routines are developed based form a 3D network of circular disks distributed in a cubic representative volume element based on Monte Carlo method. The main subroutines developed and employed in present study are provided.

```
program MONTECARLO

    implicit none
    double precision celllength
    character(20) :: string
    integer myrank , KK ,iin ,counter , cr , ONP
    INTEGER ij,x6,NP, NB, NC, SUM, CONP, RX, RY, RZ, Nf, I, J, K, NMAX, DNMAX ,
    PAR, PARAMET, DD, MTSEED, Q , PC
    REAL TUNL , R , L , tk , NEWPARTICLE(1,6),x1,x2,x3
    INTEGER, ALLOCATABLE :: POSITION(:, :, :, :), DPOSITION(:, :, :, :)
    INTEGER, ALLOCATABLE :: XX(:, ), NPC(:, ), NXX(:, )
    REAL, ALLOCATABLE :: PARTICLE(:, ) , DPARTICLE(:, ) , OPARTICLE ( :, )
    COMMON TUNL , R , L , tk , NMAX , NP, NB , MTSEED
    cr=0
    ONP=0
    open (12 , FILE='montecarlo.dat', STATUS='unknown')
    Do while (cr.eq.0)
    read(12 , * , end=1980) x1,x2,x3
    ONP=ONP+1
    end do
    1980 close(unit=12)
    if (INT(real(ONP/2)).NE.real(ONP/2)) then
        ONP=ONP-1
```

```

end if
ONP=ONP/2
if (ONP.NE.0) then
    allocate(OPARTICLE(ONP,6))
    open (12 , FILE='montecarlo.dat', STATUS='OLD')
    REWIND (12)
    Do i=1,ONP
        read(12 , * ) OPARTICLE(i,1),OPARTICLE(i,2),OPARTICLE(i,3)
        read(12 , * ) OPARTICLE(i,4),OPARTICLE(i,5),OPARTICLE(i,6)
    end do
    close (unit=12)
end if
open (15 , FILE='input.dat', STATUS='OLD')
read (15 , * ) TUNL , R , L , tk , MTSEED
close (unit=15)
NB=INT(L/(1.2*TUNL+2*R))-1
NB=min(NB,300)
MTSEED=MTSEED+2*ONP
!*****
!*****
!***      Initial Setting      **
!*****
!*****
allocate (DPOSITION(1,1,1,1))
DPOSITION(:, :, :, :)=0
allocate(PARTICLE(1,6))
PARTICLE(:, :)=0
allocate(POSITION(NB,NB,NB,2))
POSITION(:, :, :, :)=0
allocate (DPARTICLE(1,6))
DPARTICLE(:, :)=0
NP=0
NMAX=0
celllength=dbl(L)/dbl(NB)
OPEN (12, FILE = 'montecarlo.dat',ACTION='write', ACCESS = 'APPEND', STATUS
= 'unknown')
100 if (NP.LT.ONP) then
    NEWPARTICLE(1,1:6)=OPARTICLE(NP+1,1:6)
    RX=1+INT((NEWPARTICLE(1,1))/celllength)
    IF (RX.GT.NB) THEN; RX=NB; ENDIF

```

```

RY=1+INT((NEWPARTICLE(1,2))/celllength)
IF (RY.GT.NB) THEN; RY=NB; ENDIF
RZ=1+INT((NEWPARTICLE(1,3))/celllength)
IF (RZ.GT.NB) THEN; RZ=NB; ENDIF
else
    CALL PARTICLEADD(NEWPARTICLE,RX,RY,RZ,PARTICLE,POSITION)
end if
NP=NP+1
DNMAX=MAX(NMAX,1+POSITION(RX,RY,RZ,1))
if (DNMAX.NE.NMAX) then
    DEALLOCATE (DPOSITION)
    ALLOCATE (DPOSITION(NB,NB,NB,NMAX+1))
    DPOSITION(:, :, :, :)=0
    DPOSITION(:, :, :, :)=POSITION(:, :, :, :)
    DEALLOCATE (POSITION)
    ALLOCATE (POSITION(NB,NB,NB, DNMAX+1))
    POSITION(:, :, :, :)=0
    POSITION(:, :, :, 1:NMAX+1)=DPOSITION(:, :, :, 1:NMAX+1)
end if
POSITION(RX,RY,RZ,1)=POSITION(RX,RY,RZ,1)+1
POSITION(RX,RY,RZ,POSITION(RX,RY,RZ,1)+1)=NP
DEALLOCATE (DPARTICLE)
ALLOCATE (DPARTICLE(NP-1,6))
DPARTICLE(:, :)=0
DPARTICLE(:, :)=PARTICLE(:, :)
DEALLOCATE (PARTICLE)
ALLOCATE (PARTICLE(NP,6))
PARTICLE(:, :)=0
PARTICLE(1:NP-1,1:6)=DPARTICLE(1:NP-1,1:6)
PARTICLE(NP,1:6)=NEWPARTICLE(1,1:6)
NMAX=DNMAX
if (NP.GT.ONP) then
!OPEN(12,FILE='montecarlo.dat',ACTION='write',ACCESS='APPEND',STATUS='unknown')
    write (unit=12,fmt=*) NEWPARTICLE(1,1) , NEWPARTICLE(1,2) , NEWPARTICLE(1,3)
    write (unit=12,fmt=*) NEWPARTICLE(1,4) , NEWPARTICLE(1,5) , NEWPARTICLE(1,6)
call flush(12)
end if
GO TO 100
end program MONTECARLO
!*****

```



```

IF (RY.GT.NB1) THEN; RY=NB1; ENDIF
RZ=1+INT((NEWPARTICLE(1,3))/celllength)
IF (RZ.GT.NB1) THEN; RZ=NB1; ENDIF
PARAMET=1
DO KK=1,27
I=RX+looki(KK)
J=RY+lookj(KK)
K=RZ+lookk(KK)
IF ((I.GT.0) .AND. (I.LE.NB1) .AND. (J.GT.0) .AND. (J.LE.NB1) .AND. (K.GT.0)
.AND. (K.LE.NB1)) THEN
! NUMBER=POSITION (I,J,K,1) !Number of the patrticles in position I,J,K
IF (POSITION (I,J,K,1).GT.0) THEN
DO Q=1,POSITION (I,J,K,1) ! Q is a dummy counter.
PSPEC(1,1:6)=PARTICLE(POSITION(I,J,K,Q+1) , 1:6)
CALL DISKINT(PARAMET,PSPEC,NEWPARTICLE)
IF (PARAMET.EQ.0) THEN
GO TO 7000
END IF
END DO
END IF
END IF
END DO
end subroutine PARTICLEADD
!*****
!***          End of the subroutine "PARTICLEADD"          ****
!*****

```

```

!*          *Index of common variables: 2
SUBROUTINE SPHERPOINT(ns1,ns2,ns3)
implicit none
integer PARAMET, NMAX2 , NP2, NB2 , MTSEED2
real TUNL2, R2, L2, tk2, distance, V1 , V2 , V3 , V4,ns1,ns2,ns3, grnd
COMMON TUNL2 , R2 , L2 , tk2 , NMAX2 , NP2, NB2 , MTSEED2
2000          V1=(2*grnd())-1
              V2=(2*grnd())-1
              V3=(2*grnd())-1
              V4=(2*grnd())-1
if ((V1**2 + V2**2 + V3**2 + V4**2 ).GE.1) then
Go to 2000

```

```

endif
ns1=2*(V2*V4+V1*V3)/(V1**2+V2**2+V3**2+V4**2)
ns2=2*(V3*V4-V1*V2)/(V1**2+V2**2+V3**2+V4**2)
ns3=(V1**2+V4**2-V2**2-V3**2)/(V1**2+V2**2+V3**2+V4**2)
end subroutine SPHERPOINT
!*****
!***          End of the subroutine " SPHERPOINT"          ****
!*****

!*          *Index of common variables: 3
subroutine diskdist( distance , NEWPARTICLE , PARTICLE1 )
implicit none
real distance,NEWPARTICLE(1,6),PARTICLE1(1,6), TUNL3 , R3 ,
L3,tk3,d1,d2,CL(1,3),e1,e2,dmin,doo,dpo,dp
integer NMAX3 , NP3, NB3 , MTSEED3
COMMON TUNL3 , R3 , L3 , tk3 , NMAX3 , NP3 , NB3 , MTSEED3
d1=- ( NEWPARTICLE(1,1)*NEWPARTICLE(1,4) + NEWPARTICLE(1,2)*NEWPARTICLE(1,5) +
NEWPARTICLE(1,3)*NEWPARTICLE(1,6) )
d2=- ( PARTICLE1(1,1)*PARTICLE1(1,4) + PARTICLE1(1,2)*PARTICLE1(1,5) +
PARTICLE1(1,3)*PARTICLE1(1,6) )
CL(1,1)=( NEWPARTICLE(1,5)*PARTICLE1(1,6) - NEWPARTICLE(1,6)*PARTICLE1(1,5) )
CL(1,2)=( NEWPARTICLE(1,6)*PARTICLE1(1,4) - NEWPARTICLE(1,4)*PARTICLE1(1,6) )
CL(1,3)=( NEWPARTICLE(1,4)*PARTICLE1(1,5) - NEWPARTICLE(1,5)*PARTICLE1(1,4) )
if ( CL(1,1).EQ.0 .AND. CL(1,2).EQ.0 .AND. CL(1,3).EQ.0 ) then
dp=abs(d1-d2)
doo=SQRT( (NEWPARTICLE(1,1)-PARTICLE1(1,1))**2 + (NEWPARTICLE(1,2)-
PARTICLE1(1,2))**2 + (NEWPARTICLE(1,3)-PARTICLE1(1,3))**2 )
dpo=SQRT( doo**2 - dp**2 )
if (dpo.GT.2*R3) then
e1=dpo-(R3+R3)
e2=dp
distance=SQRT ( (e1)**2 + (e2)**2 )
else
distance=dp
end if
else
call dist(dmin , NEWPARTICLE , PARTICLE1)
distance=dmin
end if

```

```

end subroutine diskdist
!*****
!***          End of the subroutine "diskdist"          ****
!*****

-----

!**          (index=4)          **
subroutine DISKINT(CONP,PSPEC,NEWPARTICLE)
  implicit none
  integer CONP ,c, NMAX4 , NP4 , NB4 , MTSEED4
  real PSPEC(1,6),NEWPARTICLE(1,6),norm,doo,cp(2,2),p(3),CL(3),TUNL4 , R4 , L4
, tk4 , tmin1,tmin2,t1(3),t2(3),dop,ot1,ot2,tt,tt1,tt2,det,d1,d2
  COMMON TUNL4 , R4 , L4 , tk4 , NMAX4 , NP4 , NB4 , MTSEED4
  d1=- ( NEWPARTICLE(1,1)*NEWPARTICLE(1,4) + NEWPARTICLE(1,2)*NEWPARTICLE(1,5) +
NEWPARTICLE(1,3)*NEWPARTICLE(1,6) )
  d2=- ( PSPEC(1,1)*PSPEC(1,4) + PSPEC(1,2)*PSPEC(1,5) + PSPEC(1,3)*PSPEC(1,6) )
  CL(1)= ( NEWPARTICLE(1,5)*PSPEC(1,6) - NEWPARTICLE(1,6)*PSPEC(1,5) )
  CL(2)= ( NEWPARTICLE(1,6)*PSPEC(1,4) - NEWPARTICLE(1,4)*PSPEC(1,6) )
  CL(3)= ( NEWPARTICLE(1,4)*PSPEC(1,5) - NEWPARTICLE(1,5)*PSPEC(1,4) )
  norm =SQRT( (CL(1))**2 + (CL(2))**2 + (CL(3))**2 )
  c=1
  if (norm.GT.0) then
    CL(1:3)=CL(1:3)/norm
  end if
  doo=SQRT( (NEWPARTICLE(1,1)-PSPEC(1,1))**2 + (NEWPARTICLE(1,2)-PSPEC(1,2))**2
+ (NEWPARTICLE(1,3)-PSPEC(1,3))**2 )
  dop=SQRT(doo**2-(d1-d2)**2)
  if ((norm.EQ.0)) then
    if ((abs(d1-d2)).LT.tk4.AND. dop.LT.(R4+R4)) then
      CONP=0
    else
      CONP=1
    end if
  c=0
  end if
  if ( ( NEWPARTICLE(1,4)*PSPEC(1,5) - NEWPARTICLE(1,5)*PSPEC(1,4) ) .NE. 0
.AND. c.EQ.1) then
    det=( NEWPARTICLE(1,4)*PSPEC(1,5) - NEWPARTICLE(1,5)*PSPEC(1,4) )
    cp(1,1)=(PSPEC(1,5))/det
    cp(1,2)=(-NEWPARTICLE(1,5))/det
    cp(2,1)=(-PSPEC(1,4))/det

```

```

cp(2,2)=(NEWPARTICLE(1,4))/det
p(1)=cp(1,1)*(-d1) + cp(1,2)*(-d2)
p(2)=cp(2,1)*(-d1) + cp(2,2)*(-d2)
p(3)=0

c=0
end if
if (( NEWPARTICLE(1,5)*PSPEC(1,6) - NEWPARTICLE(1,6)*PSPEC(1,5) ).NE. 0
.AND. c.EQ.1) then
det=( NEWPARTICLE(1,5)*PSPEC(1,6) - NEWPARTICLE(1,6)*PSPEC(1,5) )
cp(1,1)=(PSPEC(1,6))/det
cp(1,2)=(-NEWPARTICLE(1,6))/det
cp(2,1)=(-PSPEC(1,5))/det
cp(2,2)=(NEWPARTICLE(1,5))/det
p(1)=0
p(2)=cp(1,1)*(-d1) + cp(1,2)*(-d2)
p(3)=cp(2,1)*(-d1) + cp(2,2)*(-d2)
c=0
end if
if (( NEWPARTICLE(1,4)*PSPEC(1,6) - NEWPARTICLE(1,6)*PSPEC(1,4) ).NE. 0
.AND. c.EQ.1) then
det=( NEWPARTICLE(1,4)*PSPEC(1,6) - NEWPARTICLE(1,6)*PSPEC(1,4) )
cp(1,1)=(PSPEC(1,6))/det
cp(1,2)=(-NEWPARTICLE(1,6))/det
cp(2,1)=(-PSPEC(1,4))/det
cp(2,2)=(NEWPARTICLE(1,4))/det
p(1)=cp(1,1)*(-d1) + cp(1,2)*(-d2)
p(2)=0
p(3)=cp(2,1)*(-d1) + cp(2,2)*(-d2)
c=0
end if
if (( NEWPARTICLE(1,4)*PSPEC(1,5) - NEWPARTICLE(1,5)*PSPEC(1,4) ).NE. 0
.AND. c.EQ.1) then
det=( NEWPARTICLE(1,4)*PSPEC(1,5) - NEWPARTICLE(1,5)*PSPEC(1,4) )
cp(1,1)=(PSPEC(1,5))/det
cp(1,2)=(-NEWPARTICLE(1,5))/det
cp(2,1)=det*(-PSPEC(1,4))/det
cp(2,2)=det*(NEWPARTICLE(1,4))/det
p(1)=cp(1,1)*(-d1) + cp(1,2)*(-d2)
p(2)=cp(2,1)*(-d1) + cp(2,2)*(-d2)
p(3)=0

```

```

      c=0
    end if
    if (norm .GT. 0) then
      tmin1=(NEWPARTICLE(1,1)-p(1))*CL(1) + (NEWPARTICLE(1,2)-p(2))*CL(2) +
      (NEWPARTICLE(1,3)-p(3))*CL(3)
      tmin2=(PSPEC(1,1)-p(1))*CL(1) + (PSPEC(1,2)-p(2))*CL(2) + (PSPEC(1,3)-
      p(3))*CL(3)
      t1(1)=CL(1)*tmin1+p(1)
      t1(2)=CL(2)*tmin1+p(2)
      t1(3)=CL(3)*tmin1+p(3)
      ot1=sqrt( (NEWPARTICLE(1,1)-t1(1))**2 + (NEWPARTICLE(1,2)-t1(2))**2 +
      (NEWPARTICLE(1,3)-t1(3))**2 )
      t2(1)=CL(1)*tmin2+p(1)
      t2(2)=CL(2)*tmin2+p(2)
      t2(3)=CL(3)*tmin2+p(3)
      ot2=sqrt( (PSPEC(1,1)-t2(1))**2 + (PSPEC(1,2)-t2(2))**2 + (PSPEC(1,3)-
      t2(3))**2 )
      tt=sqrt( (t1(1)-t2(1))**2 + (t1(2)-t2(2))**2 + (t1(3)-t2(3))**2 )
      if (ot1.LT.R4.AND.ot2.LT.R4) then
        tt1=sqrt(R4**2 - ot1**2)
        tt2=sqrt(R4**2 - ot2**2)
        if (tt.LT.(tt1+tt2)) then
          CONP=0
        else
          CONP=1
        end if
      else
        CONP=1
      end if
    end if
  end subroutine
!*****
!***          End of the subroutine "DISKINT"          ****
!*****

```

```

!*** index=5
!*****
subroutine dist(dmin , NEWPARTICLE , PARTICLE1)
implicit none
real PARTICLE1(1,6),NEWPARTICLE(1,6),dmin,tk5,R5,L5,tun15,x1(1,3),x2(1,3),
x3(1,3),x4(1,3),dis1,dis2,w1(1,3),w2(1,3)

```

```

integer NMAX5 , NP5 , NB5 , MTSEED5
COMMON TUNL5 , R5 , L5 , tk5 , NMAX5 , NP5 , NB5 , MTSEED5
call pointdisk(x1,dis1,NEWPARTICLE(1,1:3),PARTICLE1)
call pointdisk(x2,dis2,PARTICLE1(1,1:3),NEWPARTICLE)
call pointdisk(x3,dis1,x2,PARTICLE1)
call pointdisk(x4,dis2,x1,NEWPARTICLE) !Distace btwn the center of the
NEWPARTICLE and disk PARTICLE1
if (dis1.LT.dis2) then
  dmin=dis1
  w1=x3
  w2=x2
else
  dmin=dis2
  w1=x1
  w2=x4
end if
end subroutine dist
!*****
!***          End of the subroutine "dist"          ****
!*****

```

```

!**          index=6
!*****
subroutine pointdisk(x2,dis,x1,PARTICLE)
implicit none
real
x2(1,3),dis,x1(1,3),PARTICLE(1,6),R6,L6,tunl6,tk6,d,dp,d21,pq,d3,tm,xs,ys,zs,di1,
di2,tt,v(3),dd
integer NMAX6 , NP6 , NB6 , MTSEED6
COMMON TUNL6 , R6 , L6 , tk6 , NMAX6 , NP6 , NB6 , MTSEED6
d=- ( PARTICLE(1,1)*PARTICLE(1,4) + PARTICLE(1,2)*PARTICLE(1,5) +
PARTICLE(1,3)*PARTICLE(1,6) )
dp=- ( x1(1,1)*PARTICLE(1,4) + x1(1,2)*PARTICLE(1,5) + x1(1,3)*PARTICLE(1,6) )
d21=abs(dp-d)
pq= sqrt((x1(1,1)-PARTICLE(1,1))**2 + (x1(1,2)-PARTICLE(1,2))**2 + (x1(1,3)-
PARTICLE(1,3))**2 )
d3=sqrt(pq**2 - d21**2)
tm=- ( d + ( x1(1,1)*PARTICLE(1,4) + x1(1,2)*PARTICLE(1,5) +
x1(1,3)*PARTICLE(1,6) ) )
xs=tm*PARTICLE(1,4)+x1(1,1)
ys=tm*PARTICLE(1,5)+x1(1,2)

```

```

zs=tm*PARTICLE(1,6)+x1(1,3)
if (d3.LE.R6) then
  x2(1,1)=xs
  x2(1,2)=ys
  x2(1,3)=zs
  dis=d21
else
  v(1)=PARTICLE(1,1)-xs
  v(2)=PARTICLE(1,2)-ys
  v(3)=PARTICLE(1,3)-zs
  dd=sqrt(v(1)**2 + v(2)**2 +v(3)**2 )
  v(1)=v(1)/dd
  v(2)=v(2)/dd
  v(3)=v(3)/dd
  tt=R6/sqrt(v(1)**2 + v(2)**2 +v(3)**2 )
di1=sqrt( ( v(1)*tt+PARTICLE(1,1)-x1(1,1) )**2 + ( v(2)*tt+PARTICLE(1,2)-x1(1,2)
)**2 +( v(3)*tt+PARTICLE(1,3)-x1(1,3) )**2 )
di2=sqrt( ( v(1)*(-tt)+PARTICLE(1,1)-x1(1,1) )**2 + ( v(2)*(-tt)+PARTICLE(1,2)-
x1(1,2) )**2 +( v(3)*(-tt)+PARTICLE(1,3)-x1(1,3) )**2 )
  if (di1.LT.di2) then
    dis=di1
    x2(1,1)=v(1)*tt+PARTICLE(1,1)
    x2(1,2)=v(2)*tt+PARTICLE(1,2)
    x2(1,3)=v(3)*tt+PARTICLE(1,3)
  else
    dis=di2
    x2(1,1)=v(1)*(-tt)+PARTICLE(1,1)
    x2(1,2)=v(2)*(-tt)+PARTICLE(1,2)
    x2(1,3)=v(3)*(-tt)+PARTICLE(1,3)
end if
end if
end subroutine pointdisk
!*****
!***          End of the subroutine "ponidisk"          ****
!*****



---


!** *** index=7
subroutine FACECHECK(F,NAP)
implicit none
integer CP , F(1,6) , NMAX7 , NP7 , NB7 , MTSEED7

```

```

real NAP(1,6) , PROJ(1,6) , tunl7,L7 , tk7 , R7 , d , CL(3)
common tunl7 , R7 , L7 , tk7 , NMAX7 , NP7 , NB7 , MTSEED7
F(1,1:6)=0
!d=- ( PARTICLE(1,4)*PARTICLE(1,1) + PARTICLE(1,5)*PARTICLE(1,2) +
PARTICLE(1,6)*PARTICLE(1,3) )
!*****
!*      Z=0      *
!*****
if (NAP(1,3).LE.(R7+tunl7)) then
  if ( abs(NAP(1,4)).EQ.0 .AND. NAP(1,5).EQ.0 ) then
    if ( NAP(1,3).LE.tunl7 ) then
      F(1,1)=1
    end if
  else
    PROJ(1,1)=NAP(1,1)
    PROJ(1,2)=NAP(1,2)
    PROJ(1,3)=tunl7
    PROJ(1,4)=0
    PROJ(1,5)=0
    PROJ(1,6)=1
    call DISKINT(CP,PROJ,NAP)
    F(1,1)=1-CP
  end if
end if
!*****
!*      Z=L      *
!*****
if ( NAP(1,3).GE.(L7-(R7+tunl7)) ) then
  if (abs(NAP(1,4)).EQ.0 .AND. NAP(1,5).EQ.0) then
    if (L7-NAP(1,3).LE.tunl7) then
      F(1,2)=1
    end if
  else
    PROJ(1,1)=NAP(1,1)
    PROJ(1,2)=NAP(1,2)
    PROJ(1,3)=L7-tunl7
    PROJ(1,4)=0
    PROJ(1,5)=0
    PROJ(1,6)=1
    call DISKINT(CP,PROJ,NAP)

```

```

        F(1,2)=1-CP
    end if
end if
!*****
!*    X=0    *
!*****
if (NAP(1,1).LE.(R7+tunl7)) then
    if (abs(NAP(1,5)).EQ.0 .AND. NAP(1,6).EQ.0) then
        if (NAP(1,1).LE.tunl7) then
            F(1,3)=1
        end if
    else
        PROJ(1,1)=tunl7
        PROJ(1,2)=NAP(1,2)
        PROJ(1,3)=NAP(1,3)
        PROJ(1,4)=1
        PROJ(1,5)=0
        PROJ(1,6)=0
        call DISKINT(CP,PROJ,NAP)
        F(1,3)=1-CP
    end if
end if
!*****
!*    X=L    *
!*****
if (NAP(1,1).GE.(L7-(R7+tunl7))) then
    if (abs(NAP(1,5)).EQ.0 .AND. NAP(1,6).EQ.0) then
        if ((L7-NAP(1,1)).LE.tunl7) then
            F(1,4)=1
        end if
    else
        PROJ(1,1)=L7-tunl7
        PROJ(1,2)=NAP(1,2)
        PROJ(1,3)=NAP(1,3)
        PROJ(1,4)=1
        PROJ(1,5)=0
        PROJ(1,6)=0
        call DISKINT(CP,PROJ,NAP)
        F(1,4)=1-CP
    end if

```

```

end if
!*****
!*   Y=0   *
!*****
if (NAP(1,2).LE.(R7+tunl7)) then
  if (abs(NAP(1,4)).EQ.0 .AND. NAP(1,6).EQ.0) then
    if( NAP(1,2).LE.tunl7) then
      F(1,5)=1
    end if
  else
    PROJ(1,1)=NAP(1,1)
    PROJ(1,2)=tunl7
    PROJ(1,3)=NAP(1,3)
    PROJ(1,4)=0
    PROJ(1,5)=1
    PROJ(1,6)=0
    call DISKINT(CP,PROJ,NAP)
    F(1,5)=1-CP
  end if
end if
!*****
!*   Y=L   *
!*****
if (NAP(1,2).GE.(L7-(R7+tunl7))) then
  if (abs(NAP(1,4)).EQ.0 .AND. NAP(1,6).EQ.0) then
    if ( (L7-NAP(1,2)).LE.tunl7) then
      F(1,6)=1
    end if
  else
    PROJ(1,1)=NAP(1,1)
    PROJ(1,2)=L7-tunl7
    PROJ(1,3)=NAP(1,3)
    PROJ(1,4)=0
    PROJ(1,5)=1
    PROJ(1,6)=0
    call DISKINT(CP,PROJ,NAP)
    F(1,6)=1-CP
  end if
end if
end if
end subroutine FACECHECK

```

```

!*****
!***          End of the subroutine "FACECHECK"          ****
!*****

!*****
!***This subroutine is developed by: Makoto Matsumoto and Takuji Nishimur
!** Copyright (C)1997-2002,Makoto Matsumoto and Takuji Nishimur **** index 8
!*****

      real function grnd()
      implicit integer(a-z)
      real TUNL8 , R8 , L8 , tk8
      integer NMAX8 , NP8 , NB8 , MTSEED8
      common TUNL8 , R8 , L8 , tk8 , NMAX8 , NP8 , NB8 , MTSEED8
!   Period parameters
      parameter(N      = 624)
      parameter(N1     = N+1)
      parameter(M      = 397)
      parameter(MATA   = -1727483681)
!
!               constant vector a
      integer, parameter :: k10=selected_int_kind(10)
      parameter(UMASK = -2147483648_k10)
!
!               most significant w-r bits
      parameter(LMASK = 2147483647)
!
!               least significant r bits
!   Tempering parameters
      parameter(TMASKB= -1658038656)
      parameter(TMASKC= -272236544)
      dimension mt(0:N-1)
!
!               the array for the state vector
      common /block/mti,mt
      save /block/
      data mti/N1/
!
!               mti==N+1 means mt[N] is not initialized
      dimension mag01(0:1)
      data mag01/0, MATA/
      save mag01
!
!               mag01(x) = x * MATA for x=0,1
      TSHFTU(y)=ishft(y,-11)
      TSHFTS(y)=ishft(y,7)

```

```

TSHFTT(y)=ishft(y,15)
TSHFTL(y)=ishft(y,-18)
if(mti.ge.N) then
!           generate N words at one time
  if(mti.eq.N+1) then
!           if sgrnd() has not been called,
    call sgrnd(MTSEED8) !Default for seed is 4357, MTSEED8: is set by the
user
!           a default initial seed is used
    endif
    do 1000 kk=0,N-M-1
      y=ior(iand(mt(kk),UMASK),iand(mt(kk+1),LMASK))
      mt(kk)=ieor(ieor(mt(kk+M),ishft(y,-1)),mag01(iand(y,1)))
1000  continue
    do 1100 kk=N-M,N-2
      y=ior(iand(mt(kk),UMASK),iand(mt(kk+1),LMASK))
      mt(kk)=ieor(ieor(mt(kk+(M-N)),ishft(y,-1)),mag01(iand(y,1)))
1100  continue
    y=ior(iand(mt(N-1),UMASK),iand(mt(0),LMASK))
    mt(N-1)=ieor(ieor(mt(M-1),ishft(y,-1)),mag01(iand(y,1)))
    mti = 0
  endif
  y=mt(mti)
  mti=mti+1
  y=ieor(y,TSHFTU(y))
  y=ieor(y,iand(TSHFTS(y),TMASKB))
  y=ieor(y,iand(TSHFTT(y),TMASKC))
  y=ieor(y,TSHFTL(y))
  if(y.lt.0) then
    grnd=(dble(y)+2.0d0**32)/(2.0d0**32-1.0d0)
  else
    grnd=dble(y)/(2.0d0**32-1.0d0)
  endif
  return
end
!*****
  subroutine sgrnd(seed)
  implicit integer(a-z)
!  Period parameters
  parameter(N      = 624)

```

```

dimension mt(0:N-1)
!           the array for the state vector
common /block/mti,mt
save  /block/
!   setting initial seeds to mt[N] using
!   the generator Line 25 of Table 1 in
!   [KNUTH 1981, The Art of Computer Programming
!   Vol. 2 (2nd Ed.), pp102]
mt(0)= iand(seed,-1)
do 1000 mti=1,N-1
    mt(mti) = iand(69069 * mt(mti-1),-1)
1000 continue
!
return
end

```

```

!*           .           *Index of common variables: 9
SUBROUTINE CONTACTCHECK( PARAMET , NEWPARTICLE , PARTICLE1 )
implicit none
!particle(1:3): coordiinate of origion , particle(3:6): orientation ,!!!
particle(7): diameter)
integer PARAMET, NMAX9 , NP9, NB9 , MTSEED9
real PARTICLE1(1,6), NEWPARTICLE(1,6), TUNL9, R9, L9, tk9, distance
COMMON TUNL9 , R9 , L9 , tk9 , NMAX9 , NP9, NB9 , MTSEED9
call diskdist( distance , NEWPARTICLE , PARTICLE1 )
if ((abs(distance)) .LT. TUNL9) then
PARAMET=1
else
PARAMET=0
end if
end subroutine CONTACTCHECK
!*****
!***           End of the subroutine "CONTACTCHECK"           ****
!*****

```

A.2 Finite Element Code Developed to Evaluate the Conductivity of the 3D Resistor Network

The following codes and routines are developed based on finite element method to evaluate the conductivity of a network of the CNT electrically connected by tunneling conductivity. The following codes are employed to investigate the conductivity behavior of CNT 3D network formed by Monte Carlo method.

```
function fem

load 'input1.txt'
load FRES.mat
%
tunl=input1(1,1);
R=input1(1,2);
L=input1(1,3);
Lf=input1(1,4);
Vfd=input1(1,7);
%
Clength=L;

% %
h=6.626068E-34;
e=1.60217646E-19;
m=9.10938188E-31;
%
%
%   if resistor(1,1)==0;
%       resistor(1,:)=[];
%       resistor(:,1)=[];
%% end
% if montecarlo(1,1)==0;
% %     montecarlo(1,:)=[];
% %     montecarlo(:,1)=[];
% % end
```

```

% % particle=montecarlo;
RES=FRES;
NR=size(FRES,1);
A=RES(:,1);
A=[A;RES(:,2)];
A(1,2)=1;
nodmax=1;
for i=2:2*NR
    AD=[];
    AD=A(1:i-1,1);
    AD=abs(AD-A(i));
    [m1,n1]=sort(AD);

    if m1(1)==0
        A(i,2)=A(n1(1),2);
    else
        nodmax=nodmax+1;
        A(i,2)=nodmax;
    end
end

AA=A(:,1);
[m1,n1]=sort(abs(AA-nright));
% %
if m1(1)==0
    NRIGHT=A(n1(1),2);
end
% %
[m1,n1]=sort(abs(AA-nleft));
% %
if m1(1)==0
    NLEFT=A(n1(1),2);
end
% %RESISTOR=RES(:,1);
RESISTOR=[A(1:NR,2)];
RESISTOR=[RESISTOR,A(NR+1:2*NR,2)];
RESISTOR=[RESISTOR,RES(:,3)];
RESISTOR=[RESISTOR,RES(:,4)];
% RESISTOR(:,1)=[];
EL1=min(NRIGHT,NLEFT);

```

```

EL2=max(NRIGHT,NLEFT);
% % % % % % % % % % % %
save('RES.mat','RESISTOR','nodmax','EL1','EL2','Ncnt')

```

```

function FEMCNT
% input: input1,NPNRES,resistor,montecarlo
% output:
% RESULT(1): The applied current,
% RESULT(2): the maximum of the voltage difference at the end of the resistor
% RESULT(3): The voltage at the second electrode.
% RESULT(4): Number of the resistors with voltage difference higher then
% "phi"
% RESULT(5): volume fraction
% RESULT(6): resistivity
%
prepare
fem
h=6.626068e-34;
m=9.10938188e-31;
RESULT=[];

load input1.txt
load RESULT.mat
strt=size(RESULT,1)+1;

for i=strt:1:size(input1,1)

    load RES.mat
    load input1.txt
    tunl=input1(i,1);
    R=input1(i,2);
    L=input1(i,3);
    Lf=input1(i,4);
    phi0=input1(i,5);
    Rho=input1(i,6);
    Vfd=input1(i,7);

```

```

Vapp=input1(i,8);
Temp=input1(i,9);
Clength=L;
Amp(1:nodmax,1)=0;
Amp(EL1,1)=-1;
Amp(EL2,1)=1;
KK(1:nodmax,1:nodmax)=0;
e=1.602176565e-19
phi=phi0*e;
sef=[];

for j=1:size(RESISTOR,1)
    n1=min(RESISTOR(j,1),RESISTOR(j,2));
    n2=max(RESISTOR(j,1),RESISTOR(j,2));
    if RESISTOR(j,4)==0 % The resistor is tunneling
        dtd=RESISTOR(j,3);
        if RESISTOR(j,3)<1 ; dtd=1 ; end % Unit is nm.
        dtd=dtd*1e-9;

        % Volt=abs(XD(n1)-XD(n2));
        Volt=0; % problem is simulated for lower voltage
        %
        Atunl=pi*R^2;

        Ke=simmontunl(dtd,R,phi,Temp);

    else
        Lcnt=RESISTOR(j,3)*1e-9; % units should be checked.
        Ke=(pi*R^2/(Lcnt*Rho));
    end

if Ke==0 ; sef=[sef;j]; end
    KK(n1,n1)=KK(n1,n1)+Ke;
    KK(n1,n2)=KK(n1,n2)-Ke;
    KK(n2,n1)=KK(n2,n1)-Ke;
    KK(n2,n2)=KK(n2,n2)+Ke;
end

Amp(EL1,:)=[];
KK(:,EL1)=[];

```

```

KK(EL1,:)=[];

Vnod=inv(KK)*Amp;
VEL2=Vnod(EL2-1,1);
res=VEL2*Clength;
sig=1/res;

RESULT=[RESULT;[R L Lf phi0 Rho Vfd Temp VEL2 res sig]];
save('RESULT.mat','RESULT')

end
end

```

```

function prepare
% ('output.mat','RTlist','CNTlist','Rlist','nodlist','nfc','stat')
%
load output.mat
load input1.txt
tunl=input1(1,1);
R=input1(1,2);
L=input1(1,3);
Lf=input1(1,4);
phi=input1(1,5);
Rho=input1(1,6);
Vfd=input1(1,7);
%
Clength=L;
%
cr=0;
i=1;
% % % stat=[stat; [nf , nfc , Nn , Rn , size(RTlist,1) , VFc]];
while cr==0
    if stat(i,6)>=Vfd
        Ncnt=stat(i,2);
        Nnd=stat(i,3);
        Nrd=stat(i,4);
        Nrtd=stat(i,5);
    %

```

```

        cr=1;
    end
    i=i+1;
end
% %
CNTlist=[];
for i=1:Nrd
    count=Rlist(i,1,1);
    Dn=Rlist(i,2:count+1,1);
    Dt=Rlist(i,2:count+1,2);
    [D1,D2]=sort(Dt);
    for j=1:count-1
        N1=Dn(D2(j));
        N2=Dn(D2(j+1));
        c1=nodlist(N1,:);
        c2=nodlist(N2,:);
        if norm(c1-c2)~=0
            CNTlist=[CNTlist;[ Dn(D2(j)) , Dn(D2(j+1))  norm(c1-c2)*1e9 ] ];
        end
    end
end
end

RTlist(:,4)=0;
CNTlist(:,4)=1;
%

TUNLlist=RTlist(1:Nrtd,:);
Ncntseg=size(CNTlist,1);
%
resistor=[TUNLlist;CNTlist];
NR=size(resistor,1);
SAME=[0];
si=0;
%
for iii=1:Nrd
%
    count=Rlist(iii,1,1);
    Dn=Rlist(iiii,2:count+1,1);
    Dt=Rlist(iiii,2:count+1,2);
    [D1,D2]=sort(Dt);

```

```

    tb=D1(1);
    si=si+1;
    SAME(si,1)=0;
%
    for kk=1:size(D1,2)

        if D1(kk)==tb
            SAME(si,1)=SAME(si,1)+1;
            SAME(si,SAME(si,1)+1)=Dn(D2(kk));

        else
            tb=D1(kk);
            si=si+1;
            SAME(si,1)=1;
            SAME(si,2)=Dn(D2(kk));
        end
    end
end
%
end
%
for k1=1:size(resistor,1)
    for k2=1:2
        for k3=1:size(SAME,1)
            for k4=2:SAME(k3,1)+1
                if resistor(k1,k2)==SAME(k3,k4)
                    resistor(k1,k2)=SAME(k3,2);
                end
            end
        end
    end
end
end
%
%
clst=resistor;
clst(1,5)=1;
clmax=0;
%
for i=2:NR
    DD=[];
    DD(1)=0;

```

```

    for j=1:i-1
        a1=resistor(i,1)-resistor(j,1);
        a2=resistor(i,1)-resistor(j,2);
        a3=resistor(i,2)-resistor(j,1);
        a4=resistor(i,2)-resistor(j,2);
        mm=a1*a2*a3*a4;
        if mm==0
            DD(1)=DD(1)+1;
            DD=[DD,clst(j,5)];
        end
    end
end
%
    clmax=clmax+1;
%
if DD(1)>0
    for j=1:i-1
        for k=2:DD(1)+1
            if clst(j,5)==DD(k)
                clst(j,5)=clmax;
            end
        end
    end
end
end

clst(i,5)=clmax;
end
D1=clst(:,5);
[m1,n1]=sort(D1);
clx=1;
% % % % s=1;
clst(n1(1),6)=clx;
AA=[clx];

for i=2:size(m1,1)
    if m1(i)==m1(i-1)
        clst(n1(i),6)=clx;
        AA=[AA,clx];
    else
        clx=clx+1;
    end
end

```

```

        clst(n1(i),6)=clx;
        AA=[AA,clx];
    end
end
%
PN=1:clx;
PN(2,1:clx)=0;
PN(3,1:clx)=0;
A=[];
B=[];

for j=1:NR
    for k=1:2
        nn=clst(j,k);
        xx1=nodlist(nn,1);
        dfr=(Clength-xx1);
        dfl=xx1;

        if dfl<1e-9
            PN(2,clst(j,6))=1;
        end
        if dfr<1e-9
            PN(3,clst(j,6))=1;
        end

    end
end

FRES=[];

for i=1:NR
    if PN(2,clst(i,6))*PN(3,clst(i,6))==1
        FRES=[FRES ; clst(i,:)];
        QQ=1;
    end
end
%
f1=0;
f2=0;
for j=1:size(FRES,1)

```

```

for k=1:2
    nn=FRES(j,k);
    xx1=nodelist(nn,1);
    dfr=(Clength-xx1);
    dfl=xx1;

    if dfl<1e-9 && f1==0
        nleft=nn;
        f1=1;
    end

    if dfr<1e-9 && f2==0
        nright=nn;
        f2=1;
    end

end

end
end
for j=1:size(FRES,1)
    for k=1:2
        nn=FRES(j,k);
        xx1=nodelist(nn,1);
        dfr=(Clength-xx1);
        dfl=xx1;
        if dfl<1e-9
            FRES(j,k)=nleft;
        end

        if dfr<1e-9
            FRES(j,k)=nright;
        end

    end

end
end

FRES=FRES(:,1:4);

save ('FRES.mat','FRES','nright','nleft','nodelist','Ncnt')

```